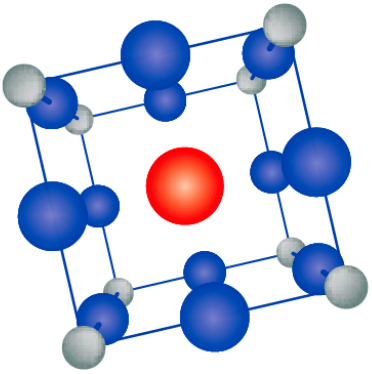

MaNEP
SWITZERLAND

Materials with Novel Electronic Properties

National Centre of Competence in Research

PROGRESS REPORT

Year 11

April 1st 2011 – March 31st 2012

FNSNF
Fonds national suisse
Schweizerischer Nationalfonds
Fondo nazionale svizzero
Swiss National Science Foundation

Die Nationalen Forschungsschwekpunkte (NFS) sind ein Förderinstrument des Schweizerischen Nationalfonds.
Les Pôles de recherche nationaux (PRN) sont un instrument d'encouragement du Fonds national suisse.
The National Centres of Competence in Research (NCCR) are a research instrument of the Swiss National Science Foundation.

FNSNF
SWISS NATIONAL SCIENCE FOUNDATION

www.snf.ch
Wildhainweg 3, P.O. Box 8232, CH-3001 Berne

Programmes division
National Centres of Competence in Research

NCCR: 11th Progress Report - Cover Sheet

Title of the NCCR	Materials with Novel Electronic Properties (MaNEP)
NCCR Director Name, first name Institution	 Prof. Øystein Fischer UNIVERSITE DE GENEVE, Faculté des Sciences Département de Physique de la Matière Condensée 24 quai Ernest-Ansermet, CH-1211 Genève 4 022 379 62 70 Oystein.Fischer@unige.ch

Contents

1 Executive summary

MaNEP is approaching its final year and will end on June 30, 2013. In addition to working intensely on MaNEP's various activities, management is also entering into the final stages for the preparation of what will happen afterwards. The MaNEP scientific committee is elaborating a plan to establish a Swiss association to continue its network. We are also preparing a detailed proposal to integrate MaNEP Geneva into the University.
Below is a summary of the year's main research results as well as other MaNEP projects.

Research

Project 1. In a collaboration between PSI and UniGE, the fundamental predictions of the polar catastrophe scenario were tested, conclusively identifying the polar catastrophe model as being the intrinsic origin of doping at the LAO/STO interface. In $LaNiO_3/LaMnO_3$ superlattices, it has been discovered that an exchange bias phenomenon takes place for short wavelength superlattices. This observation shows that a magnetic structure is induced in ultrathin films of otherwise (bulk) paramagnetic $LaNiO_3$, a result identified as an interfacial effect. It has been shown that electrical conduction takes place at ferroelectric domain walls in PZT thin films demonstrating that conduction at ferroelectric domain walls is not restricted to multiferroic $BiFeO_3$.

Project 2. Last year's activity resulted in considerable progress in improving the quality of the electronic systems investigated in this project. $LaAlO_3/SrTiO_3$ heterostructures with carrier mobility close to 10'000 cm^2/Vs can now be reproducibly fabricated, enabling the systematic investigation of Shubnikov-de Haas oscillations and the patterning of device structures in the submicron regime. Suspended graphene devices with very high mobility have been realized, and their investigation at temperatures below 1 K is ongoing; optical spectroscopy on graphene based systems has reached unprecedented accuracy. Theoretical work on systems with large spin-orbit interactions, where topological effects can emerge, has led to the prediction of new phenomena in combination with superconductivity, such as the experimental manifestation of a possible unconventional superconducting state in $LaAlO_3/SrTiO_3$ and the study of Majorana fermions.

Project 3. This project, which is dedicated to applied research that in several cases is carried out in close collaboration with industry, is steadily growing. This year our report covers twelve different subprojects on topics as varied as applied superconductivity, hydrogen sensors, supermirrors for neutron beams and marking technology for watches. Seven companies are collaborating with MaNEP presently. Among the highlights this year, we would like to mention the progress made in mechanical energy harvesters combining the knowledge on epitaxial ferroelectric films in Geneva and the knowledge on Si membranes developed in Neuchâtel.

Project 4. The three principle tasks of condensed matter research are (i) to develop new materials, either exhibiting entirely novel behavior, or with improved functional properties, (ii) to explore these properties by experimental means, and (iii) to provide theoretical understanding of the properties of these materials. The present project covers all these different aspects. In particular two main classes of materials have been targeted: the transition metal oxides, and the iron-pnictides and chalcogenides. This year, the MaNEP collaboration has made successful advances in the three aforementioned principle tasks. The appointment of Prof. Antoine Georges at UniGE will strengthen research in the field of strong correlations in transition metal oxides, improving the impact on the experimental studies of complex phase diagrams and intriguing prop-

erties of this class of materials.

Project 5. In the field of heavy fermion superconductivity, research has focussed on the Q-phase of $CeCoIn_5$, the role of valence fluctuation for the pairing mechanism, and the influence of non-centrosymmetricity on superconducting properties. A pseudogap phase has been discovered in URu_2Si_2 above the onset of the hidden order phase. Topological insulators have been a further important topic, on side of material synthesis as well as the experimental study of their transport and high magnetic field properties. Topological phases have also been a subject of theory and computational simulation, such as the chiral superconducting phase and the creation of specific models incorporating topological features.

Project 6. Both traditional and novel experimental techniques, as well as a variety of theoretical methods, were applied to studying correlations and phase transitions in quantum magnetic materials. Several important breakthroughs relied on tight collaborations between different groups, providing unique samples for experiments, complementary data, and theoretical tools for a new level of analysis and interpretation. These breakthroughs were spawned by a sustained buildup of effort and refinements over the previous few years, particularly in sample synthesis and technique development. The study of disorder in quantum magnets has evolved from a tentative subject to a rapidly maturing field. At the same time, there is a clear emphasis on the importance of dynamics and the study of excitations (as opposed to only static properties) in quantum materials.

Project 7. The subject of the project are low-dimensional conductors in which various ground states compete with each other. From this competition new, emergent phenomena may arise. The experimental approach consists of tuning the interactions between different ground states by temperature, chemical means (doping), or/and by applying external pressure. The major techniques are spectroscopic (optical, ARPES, STM) and electrical transport measurements. The theoretical modeling deals with the excitonic interactions and Luttinger liquid behavior in the low-dimensional systems studied experimentally.

Project 8. Cold atomic systems are constantly increasing their interconnection with the condensed matter community. As a particularly interesting result, lattices similar to those of graphene have been realized, paving the way for the study of interplay between Dirac points and interactions in these systems. Concerning the Hubbard model on square lattice, the hunt for antiferromagnetism is getting closer with improved probes. On the theoretical level, the very controlled realization of cold atomic gases forces us to sharpen our theoretical tools, both at the level of traditional methods such as density functional theory — with possible applications to other systems — but also with the perspective to understand more complex phenomena, such as some out of equilibrium physics effects.

Other aspects

Knowledge and technology transfer The last year saw an increase in our technology transfer activity. Collaboration with companies who were present from the beginning of Phase III are giving excellent results and we have developed new contacts with a number of other companies. The Geneva Creativity Center, a technology transfer structure initiated by MaNEP, has officially started its activity.

Education, training and advancement of women Our key activities, the doctoral school, the MaNEP winter school, the internship for female students, continued with great success. The PhysiScope initiated by MaNEP and run in collaboration with the Physics Section at UniGE continues its success with an attendance of 4'200 in 2011.

Communication The SUPRA100 events, celebrating 100 year's of superconductivity, were a major project in 2011. Attendance was high and the public showed enormous interest. All events were well covered by the media. The Swiss artist, Etienne Krähenbühl, inaugurated the world première of his work of art, featuring superconducting levitation

The future of MaNEP

This year preparations are on-going to ensure the future of MaNEP. The University of Geneva has set aside the necessary funds to continue these activities. Plans for a new Center for astronomical, physical and mathematical sciences, where MaNEP Geneva will be located, were presented to the cantonal authorities. Progress has been made regarding the future of the MaNEP network with the view of establishing an association, which will be a forum for Swiss researchers in this field.

2 Research

2.1 Structure of the NCCR and status of integration

2.1.1 Structure of the NCCR

This section provides an up-to-date summary of the organization of MaNEP, the Swiss National Centre of Competence in Research (NCCR) on Materials with Novel Electronic Properties.

Academic institutions members of MaNEP

- University of Geneva (UniGE), home institution
- University of Fribourg (UniFR)
- University of Berne (UniBE)
- University of Zurich (UniZH)
- Federal Institute of Technology, Lausanne (EPFL)
- Federal Institute of Technology, Zurich (ETHZ)
- Paul Scherrer Institute (PSI)
- Materials Science and Technology Research Institute (Empa)
- Haute école de paysage, d'ingénierie et d'architecture, Genève (Hepia)

Industrial Partners

- ABB, Baden
- AgieCharmilles, Meyrin
- Swatch Group R&D SA, Division Asulab, Marin
- Bruker BioSpin, Fällanden
- Phasis, Geneva
- Sécheron, Meyrin
- SwissNeutronics, Klingnau
- Vacheron Constantin, Geneva

Scientific Committee

- Leonardo Degiorgi, ETHZ
- Øystein Fischer, UniGE, director
- László Forró, EPFL
- Thierry Giamarchi, UniGE
- Dirk van der Marel, UniGE, deputy director
- Frédéric Mila, EPFL
- Alberto Morpurgo, UniGE
- Christoph Renner, UniGE, deputy director
- Manfred Sigrist, ETHZ
- Jean-Marc Triscone, UniGE
- Urs Staub, PSI
- Andrey Zheludev, ETHZ

MaNEP Forum

Full members:

- Markus Abplanalp, ABB
- Philipp Aebi, UniFR
- Dionys Baeriswyl, UniFR
- Bertram Batlogg, ETHZ
- Christian Bernhard, UniFR
- Gianni Blatter, ETHZ
- Markus Büttiker, UniGE
- Radovan Černý, UniGE
- Michel Decroux, UniGE
- Leonardo Degiorgi, ETHZ
- Daniel Eckert, Bruker BioSpin
- Tilman Esslinger, ETHZ
- Manfred Fiebig, ETHZ
- Øystein Fischer, UniGE
- René Flükiger, UniGE
- László Forró, EPFL
- Antoine Georges, UniGE
- Thierry Giamarchi, UniGE
- Enrico Giannini, UniGE
- Marco Grioni, EPFL
- Didier Jaccard, UniGE
- Janusz Karpinski, ETHZ
- Hugo Keller, UniZH
- Michel Kenzelmann, PSI
- Corinna Kollath, UniGE

- Dirk van der Marel, UniGE
- Joël Mesot, PSI and ETHZ
- Frédéric Mila, EPFL
- Elvezio Morenzoni, PSI
- Alberto Morpurgo, UniGE
- Christof Niedermayer, PSI
- Hans-Rudolf Ott, ETHZ
- Patrycja Paruch, UniGE
- Greta Patzke, UniZH
- Christoph Renner, UniGE
- T. Maurice Rice, ETHZ
- Nico de Rooij, EPFL
- Henrik M. Rønnow, EPFL
- Christian Rüegg, PSI
- Manfred Sigrist, ETHZ
- Nicola Spaldin, ETHZ
- Urs Staub, PSI
- Gilles Triscone, Hepia
- Jean-Marc Triscone, UniGE
- Matthias Troyer, ETHZ
- Anke Weidenkaff, Empa and UniBE
- Philipp Werner, UniFR
- Philip Willmott, PSI
- Klaus Yvon, UniGE
- Andrey Zheludev, ETHZ

Associate members:

- Christophe Berthod, UniGE
- Harald Brune, EPFL
- Kazimierz Conder, PSI
- Jorge Cors, UniGE and Phasis
- Bernard Delley, PSI
- Bertrand Dutoit, EPFL
- Vladimir Gritsev, UniFR
- Hans-Joseph Hug, Empa
- Jürg Hulliger, UniBE
- Ivan Maggio-Aprile, UniGE
- Reinhard Nesper, ETHZ
- Frithjof Nolting, PSI
- Davor Pavuna, EPFL
- Andreas Schilling, UniZH
- Louis Schlapbach
- Carmine Senatore, UniGE
- Oksana Zaharko, PSI

Advisory Board

- Dave Blank, University of Twente, Netherlands
- Robert J. Cava, Princeton University, USA
- Denis Jérôme, University Paris Sud, Orsay, France
- Andrew Millis, Columbia University, USA
- George Sawatzky, University of British Columbia, Canada

Management (UniGE)

- Øystein Fischer, director
- Dirk van der Marel, deputy director
- Christoph Renner, deputy director
- Marie Bagnoud, administrative manager
- Christophe Berthod, scientific manager, education and training
- Adriana Bonito Aleman, communication
- Jorge Cors, *ad interim*, knowledge and technology transfer
- Pascal Cugni, administrative assistant
- Lidia Favre-Quattropani, scientific manager, advancement of women
- Elizabeth Gueniat, executive assistant
- Mehregan Joseph, communication coordinator
- Ivan Maggio-Aprile, computer and internet resources
- Greg Manfrini, technical organization
- Christophe Schwarz, secretary

Collaborative projects

1. Novel phenomena at interfaces and in superlattices

Project leader:

- J.-M. Triscone (UniGE)

Members:

- Ph. Aebi (UniFR)
- C. Bernhard (UniFR)
- T. Giamarchi (UniGE)
- E. Morenzoni (PSI)
- A. Morpurgo (UniGE)
- C. Niedermayer (PSI)
- P. Paruch (UniGE)
- J.-M. Triscone (UniGE)
- Ph. Willmott (PSI)

2. Materials for future electronics

Project leader:

- A. Morpurgo (UniGE)

Members:

- M. Büttiker (UniGE)
- T. Giamarchi (UniGE)
- D. van der Marel (UniGE)
- A. Morpurgo (UniGE)
- P. Paruch (UniGE)
- M. Sigrist (ETHZ)
- J.-M. Triscone (UniGE)

3. Electronic materials for energy systems and other applications

Project leader:

- Ø. Fischer (UniGE)

Members:

- M. Abplanalp (ABB)
- Ph. Aebi (UniFR)
- J. Cors (UniGE and Phasis)
- M. Decroux (UniGE)
- D. Eckert (Bruker Biospin)
- Ø. Fischer (UniGE)
- R. Flükiger (UniGE)
- J. Hulliger (UniBE)
- M. Kenzelmann (PSI)
- G. Patzke (UniZH)
- C. Renner (UniGE)
- N. de Rooij (EPFL)
- C. Senatore (UniGE)
- G. Triscone (Hepia)
- J.-M. Triscone (UniGE)
- A. Weidenkaff (Empa and UniBE)
- K. Yvon (UniGE)
- This project is carried out with seven participating industries

4. Electronic properties of oxide superconductors and related materials

Project leader:

- D. van der Marel (UniGE)

Members:

- D. Baeriswyl (UniFR)
- B. Batlogg (ETHZ)
- L. Degiorgi (ETHZ)
- Ø. Fischer (UniGE)
- A. Georges (UniGE)
- T. Giamarchi (UniGE)
- E. Giannini (UniGE)
- J. Karpinski (ETHZ)
- H. Keller (UniZH)
- D. van der Marel (UniGE)
- J. Mesot (PSI)
- T. M. Rice (ETHZ)
- M. Sigrist (ETHZ)

5. Novel electronic phases in strongly correlated electron systems

Project leader:

- M. Sigrist (ETHZ)

Members:

- D. Baeriswyl (UniFR)
- G. Blatter (ETHZ)
- L. Forró (EPFL)
- E. Giannini (UniGE)
- D. Jaccard (UniGE)
- M. Kenzelmann (PSI)
- D. van der Marel (UniGE)
- M. Sigrist (ETHZ)
- M. Troyer (ETHZ)

6. Magnetism and competing interactions in bulk materials

Project leaders:

- F. Mila (EPFL)
- A. Zheludev (ETHZ)

Members:

- T. Giamarchi (UniGE)
- M. Kenzelmann (PSI)
- C. Kollath (UniGE)
- J. Mesot (PSI and ETHZ)
- F. Mila (EPFL)
- E. Morenzoni (PSI)
- H.-R. Ott (ETHZ)
- H. M. Rønnow (EPFL)
- C. Rüegg (PSI)
- U. Staub (PSI)
- M. Troyer (ETHZ)
- A. Zheludev (ETHZ)

7. Electronic materials with reduced dimensionality

Project leader:

- L. Forró (EPFL)

Members:

- Ph. Aebi (UniFR)
- L. Degiorgi (ETHZ)
- L. Forró (EPFL)
- T. Giamarchi (UniGE)
- M. Grioni (EPFL)
- C. Renner (UniGE)

8. Cold atomic gases as novel quantum simulators for condensed matter

Project leader:

- T. Giamarchi (UniGE)

Members:

- G. Blatter (ETHZ)
- T. Esslinger (ETHZ)
- T. Giamarchi (UniGE)
- V. Gritsev (UniFR)
- C. Kollath (UniGE)
- F. Mila (EPFL)
- M. Troyer (ETHZ)

2.1.2 Status of integration

At the beginning of the third phase, MaNEP had the choice between reducing the number of its members, give each an important financial support, and thus have a small but exclusive and outstanding network, or to reinforce its network by integrating a larger number of members who would necessarily then get less support each. The idea that prevailed was that in view of the long-term future, the integration of new and younger professors and researchers is crucial to the field. We thus opted for a broad network. The third phase thus began with a large number of full members (43) and since then we have added 7 new full members and 1 new associate member. MaNEP has thus been able to integrate young new professors and in this way to transmit the knowledge and enthusiasm from the senior to the younger generation. We judge that this approach has been successful and that MaNEP today represents, even more than before, a true national and integrated effort in the field of electronic materials.

During the last year, we have continued the various activities stimulating integration: internal workshops, Forum meeting with short scientific communications, topical meeting, the Swiss Workshop on Materials with Novel Electronic Properties (SWM 2011) in les Diablerets, summer internships, collaborative projects, outreach and technology transfer.

As described in chapter 6, we are now working on the plan to establish an association to continue this large network, allowing a long-term integration of the scientific activities in this field.

In Geneva, the planned establishment of a new Center for astronomical, physical and mathematical sciences is strongly inspired by MaNEP and this effort represents a strong integration of MaNEP in the University of Geneva.

2.2 Results since the last progress report

This section reports on the research performed in the eight MaNEP projects for the period from April 1st 2011 to March 31st 2012.

Project 1 Novel phenomena at interfaces and in superlattices

Project leader: J.-M. Triscone (UniGE)

Participating members: Ph. Aebi (UniFR), C. Bernhard (UniFR), T. Giamarchi (UniGE), E. Morenzoni (PSI), A. Morpurgo (UniGE), C. Niedermayer (PSI), P. Paruch (UniGE), J.-M. Triscone (UniGE), Ph. Willmott (PSI)

Introduction: The study of interface phenomena in oxide and novel compounds heterostructures is developing worldwide at an impressive pace. The hope is to achieve novel and complex functionalities in these artificial materials allowing possibly novel routes to design advanced devices. Our program has for goals to study interface systems and their fascinating properties.

Summary and highlights

In this short section, we describe in a few lines last year achievements in our studies of interface physics including studies of cuprate multilayers, conducting oxide interfaces, nickelate films, organic heterostructures, and domain walls in ferroelectric films and superlattices.

- Using polarised neutron reflectometry and resonant X-ray absorption and reflection techniques, we have obtained evidence that the magnetic proximity effect in cuprate/manganite superlattices is intrinsic in nature and controlled by the electronic (orbital) state of the manganite layers. We have also participated in low-energy muon-spin rotation experiments on $LaNiO_3/LaAlO_3$ superlattices which revealed a dimensionality controlled paramagnetic metal to antiferromagnetic insulator transition *(C. Bernhard)*.

- We report results of a search for spontaneous magnetization in the superconducting state of (110)-oriented $YBa_2Cu_3O_{7-\delta}$ (YBCO) films due to time reversal symmetry breaking currents that are theoretically predicted to develop in this geometry near the surface. We have studied optimally doped films near the surface using the low-energy muon-spin rotation technique. Zero field and weak transverse field measurements at depths from 5 to 120 nm in YBCO showed no apparent spontaneous magnetic fields below the superconducting temperature down to 2.9 K. Our results give an upper limit of 0.01 mT for the spontaneous internal field in these films *(E. Morenzoni)*.

- The complex magnetic structure of $LuMnO_3$ thin films was studied using polarized neutron reflectometry and neutron diffraction. Magnetic reflections at $(0\ 0.48\ 1)$ and $(1\ \pm 0.52\ 1)$ rule out the bulk E-type antiferromagnetic ground state observed in bulk samples but indicate the formation of an incommensurate spin spiral in strained thin films *(C. Niedermayer)*.

- The predictions of the polar catastrophe scenario were tested on thin films of the solid solution $(LaAlO_3)_x(SrTiO_3)_{1-x}$ (LASTO:x) grown on (001) $SrTiO_3$ substrates. The films change from being insulating to exhibiting a constant conductance above a critical thickness t_c, which is shown to scale with the strength of the internal electric field, thereby conclusively identifying the polar catastrophe model as being the intrinsic origin of doping at the $LaAlO_3/SrTiO_3$ interface *(Ph. Willmott)*.

- We have investigated the transport properties of $LaAlO_3/SrTiO_3$ interfaces grown at different temperatures. We observe a change of the electron mobility and carrier density, which we relate to the band struc-

ture and confinement of the electron gas *(J.-M. Triscone)*.

- During the course of the project period, we studied the temperature dependent electronic structure close to the Fermi level of $NdNiO_3$ thin films. We found both a temperature hysteresis in the gap intensity as well as a temperature dependent gap size in the insulating phase *(Ph. Aebi)*.

- In $LaNiO_3/LaMnO_3$ superlattices, we have shown that an exchange bias phenomenon takes place for short wavelength superlattices. This observation shows that a magnetic structure is induced in ultrathin films of otherwise (bulk) paramagnetic $LaNiO_3$. This amazing result is understood as an interfacial effect that arises in such artificial structures *(J.-M. Triscone)*.

- We have realized Schottky-gated organic charge transfer interfaces based on single-crystals of rubrene and PDIF-CN_2, and investigated the transport properties of the conducting layer that spontaneously forms at these interfaces as a function of gate voltage and temperature. We find that the conduction is mediated by electrons, whose mobility exhibits a band-like temperature dependence between room temperature and $\simeq 100-150$ K, remaining as high as 1 cm^2/Vs at 30 K in the best devices. The density of charge carriers shows an unexpected linear decrease with lowering temperature, that we can understand quantitatively in terms of the device band diagram *(A. Morpurgo)*.

- We have shown electrical conduction at ferroelectric domain walls in PZT thin films, and explored their geometrical fluctuations and thermal quench behavior in the framework of elastic disordered systems. We have also mapped out the phase diagram of $BiFeO_3/LaFeO_3$ superlattices *(P. Paruch)*.

- We have shown that controlling the depolarizing field in $SrTiO_3/PbTiO_3/SrTiO_3$ structures allows intrinsic ferroelectric domains to be imaged in thin $PbTiO_3$ layers. This approach allows several parameters to be individually controlled *(J.-M. Triscone)*.

- We have studied the effects of temperature on the roughness of an interface and shown the evidence of two different roughness regimes for the interface *(T. Giamarchi)*.

1 Magnetic proximity effect and dimensionality driven metal to insulator transitions in oxide multilayers (C. Bernhard)

1.1 Cuprate/manganite multilayers

We have grown high-quality $YBa_2Cu_3O_7/La_{1-x}Ca_xMnO_3$ superlattices on substrates different from $SrTiO_3$, like $NdGaO_3$ and $Sr_{0.7}La_{0.3}Al_{0.65}Ta_{0.35}O_3$ (LSAT), which provide a better lattice matching and do not undergo complicated structural phase transitions that strongly influence the physical properties of the film on top. Their high structural quality has been confirmed with various techniques as described in [1]. By changing the Ca concentration, we have also varied the electronic state of the manganite layers.

Subsequently, we investigated these superlattices with polarized neutron reflectometry (PNR) and magnetic resonant X-ray absorption and diffraction techniques. These studies provided detailed insight into the magnetic depth profiles of these superconductor/ferromagnet superlattices. They revealed that the magnetic proximity effect (MPE) which was previously identified [2, 3, 4] depends very strongly on the electronic (orbital) state of the ferromagnetic manganite layers [5]. For a superlattice with metallic, ferromagnetic $La_{2/3}Ca_{1/3}MnO_3$ (LCMO) layers, the MPE is very pronounced, whereas, for a corresponding superlattice with insulating, ferromagnetic $LaMnO_{3+\delta}$ (LMO) layers, the MPE is nearly absent. This can be seen in Fig. 1 which shows the PNR curves and the obtained profiles of the magnetic potentials.

With X-ray magnetic circular dichroism (XMCD) measurements, we have also investigated the ferromagnetic moments which are induced on the Cu ions. With additional X-ray resonant magnetic reflectometry (XRMR) measurements, we were able to show that these ferromagnetic Cu moments originate from the YBCO layers, i.e. they do not arise from Cu ions that are (unintentionally) incorporated in the manganite layers. Fig. 2 shows the corresponding XRMR data of the YBCO/LCMO superlattices which establish that the proximity-induced ferromagnetic Cu ions are periodically arranged and reside

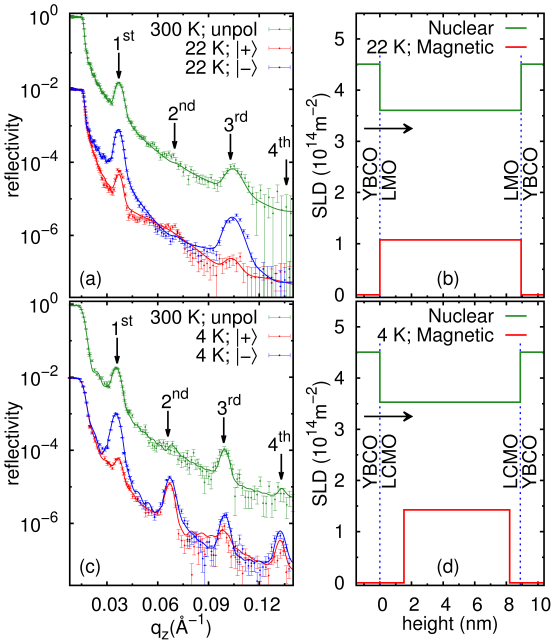

Figure 1: *Polarized neutron reflectrometry curves for spin-up $|+\rangle$ and spin-down $|-\rangle$ polarization of (a) [YBCO(10 nm)/LCMO(10 nm)]$_{10}$ and (c) [YBCO(10 nm)/LMO(10 nm)]$_{10}$ superlattices. Also shown are unpolarized curves at 300 K. The curves are vertically shifted for clarity. (b) and (d) Depth profiles of the nuclear (green) and magnetic (red) potentials obtained from fitting the data in (a) and (c).*

within the YBCO layers.
Our new studies establish that the magnetic proximity effect in these cuprate/manganite superlattices is intrinsic in nature. They also suggest that the depleted layer remains magnetic and hosts some kind of oscillatory magnetic order that persists well into the YBCO layers.

1.2 Nickelate/aluminate multilayers

In collaboration with the group of B. Keimer at the Max-Planck-Institut für Festkörperforschung in Stuttgart, we have also performed combined infrared ellipsometry and low-energy muon-spin rotation measurements on $LaNiO_3/LaAlO_3$ multilayers. Here we observed an unexpected transition from a paramagnetic metal to an antiferromagnetic insulator when the thickness of the individual $LaNiO_3$ layers was decreased below 4 unit cells [6]. This kind of dimensionality control of the electromagnetic properties might be very useful for the design of future oxide based sensors and devices and thus has obtained a great deal of attention.

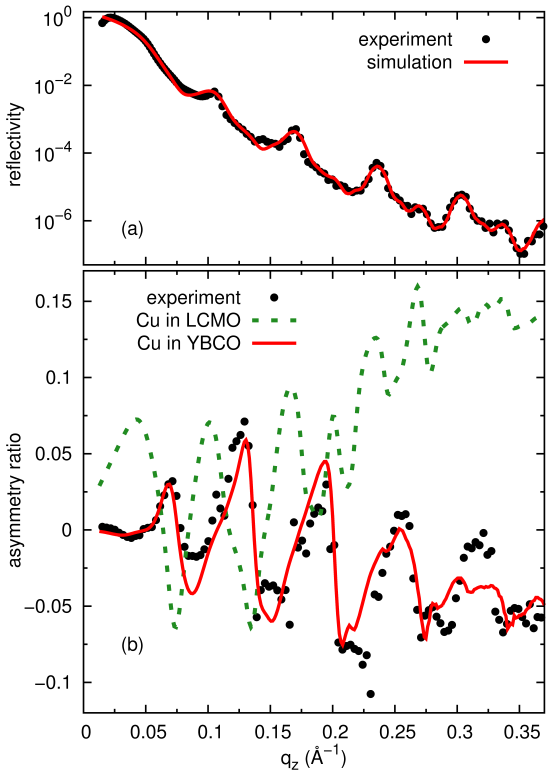

Figure 2: *(a) Resonant X-ray reflectometry curve at the Cu L_3 edge of YBCO/LCMO at 300 K. (b) Difference curve between positive and negative helicity at 40 K containing the information about the depth profile of the ferromagnetic Cu moments. The simulations have been performed for the cases where the Cu moments reside in the YBCO (red) and the LCMO layers (green), respectively.*

2 Search for spontaneous magnetism near the surface of (110)-oriented YBCO films (E. Morenzoni)

In unconventional superconductors, in addition to gauge symmetry, other symmetries may be broken. A widely debated scenario is broken time reversal symmetry (BTRS) with spontaneous magnetism as a signature [28]. Evidence of bulk spontaneous magnetism has been detected by zero field muon-spin relaxation (ZF-μSR) in very few systems such as UPt_3, Sr_2RuO_4, $PrOs_4Sb_{12}$, and $LaNiC_2$ [29, 30, 31, 32]. In cuprates, there are no evidence of bulk BTRS [33, 34]; but it has been suggested to occur at surfaces or interfaces where the shielding against magnetism is weaker [28]. In d-wave superconductors, scattering of the Cooper pairs from interfaces perpendicular to the CuO_2 planes such as (110) frustrates the bulk $d_{x^2-y^2}$-wave order parameter (OP) within a few coherence lengths from the interface [35]. This is predicted to lead to a BTRS complex order parameter such as $d_{x^2-y^2}+$ is or

$d_{x^2-y^2} + id_{xy}$ [35, 36]. Signatures of BTRS were detected in some tunneling junction experiments (below 10 K), while others did not [37].

The low-energy muon-spin rotation (LE-μSR) technique, in which low-energy spin polarized muons are stopped few nm near the surface, is very sensitive to small static fields and thus is ideally suitable to study directly BTRS near YBCO-(110) surface. In this experiment, we performed zero field and weak transverse field measurements on YBCO-(110) films. We find no evidence of static magnetic fields at depths from 5 to 120 nm, the region where BTRS due to surface scattering is expected in (110) films. We estimate an upper limit of 0.01 mT of the time reversal symmetry breaking fields.

The measurements were performed at the Swiss Muon Source on the μE4 beamline, at the Paul Scherrer Institute. The LE-μSR measurements were performed in a temperature range from 2.9 to 150 K, in zero field or small magnetic fields applied perpendicular to both the initial muon-spin polarization and beam direction, but parallel to the face of the substrates. The measurements presented here were carried out on (110) YBCO films grown by pulsed laser deposition on (110) $SrTiO_3$ (STO) single-crystal substrates measuring 5×5 mm^2. The YBCO films were grown on a 50 nm $PrBa_2Cu_3O_{7-x}$ buffer layer, and are optimally doped with a transition temperature of 88.5 (1.0) K. The (110) orientation of the films was confirmed by XRD measurements. The films have a typical rms surface roughness of less than 3 nm, and thickness $\sim$ 180 nm.

Typical asymmetry in the Meissner state in a magnetic field of $\sim$ 4.6 mT parallel to the surface is plotted in the inset of Fig. 3. The precession signal at a frequency of $\omega = \gamma_\mu B$, where the gyromagnetic ratio $\gamma_\mu = 0.85\ \mu s^{-1} mT^{-1}$ is a measure of the mean internal field which is equal to the applied field in the normal state. Upon cooling below T_c, we see a significant reduction in the precession frequency, i.e. internal field, as expected in the Meissner state. The mean internal field as a function of the beam energy at 5 K is plotted in Fig. 3 for an external field applied parallel to the c-axis. A fit of the data using a cosine hyperbolic function (valid for films) gives an estimate of $\lambda_{ab} \sim 155(7)$ nm. In a field perpendicular to the c-axis, we find $\lambda_c \sim 455(20)$ nm. The temperature dependence of the internal field (not given) is consistent with a single d-wave order parameter near the surface.

Typical zero field asymmetries in YBCO are presented in the inset of Fig. 4. The asymmetry is weakly dependent on temperature, and

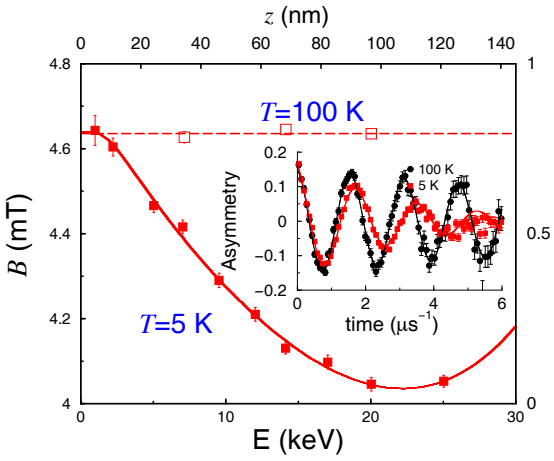

Figure 3: *The energy dependence of the average magnetic field in the Meissner state at 5 K fit by* $\frac{\cosh[(z-2d)/\lambda]}{\cosh(2d/\lambda)}$*, with* $\lambda = 155(5)$ *nm along the ab-direction, and* d *the thickness of the film. The applied field of 4.66 mT as measured in the normal state at 100 K (dashed line), is applied parallel to the c-axis direction of YBCO films. Inset: asymmetry in 14.2 keV at 100 and 5 K.*

decays with a small relaxation rate Λ. From single exponential fits with $e^{-\Lambda t}$ of the asymmetry, one extracts the relaxation rate which is proportional to the local magnetic field width, $\Lambda = \gamma_\mu \Delta B_{loc}$. The temperature variation of Λ at energies of 2 and 4 keV is plotted in Fig. 4. The damping rate in pure silver at 2 keV is also presented, as about half the muons stop in the Ag-covered backing plate. The measured relaxation is due to temperature-independent nuclear moments in YBCO+Ag. There is no noticeable increase of the relaxation rate be-

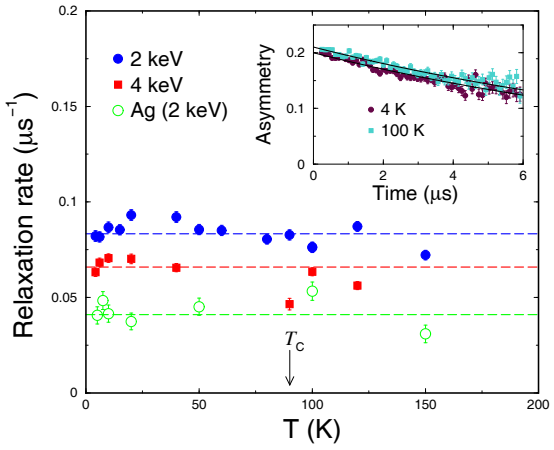

Figure 4: *The depolarization rate versus temperature at slow muon energies of 2 keV and 4 keV implanted in YBCO, and 2 keV muons implanted in control silver. Inset: typical asymmetry in ZF at 2 keV.*

low T_c or at very low temperature, as expected from onset of spontaneous magnetism in ZF-μSR [30].
From these results, we rule out the appearance of spontaneous magnetization below T_c down to 2.9 K, and at depths ranging from few nm below the surface up to 120 nm. From the average scatter of the data in Fig. 4, one can draw an upper limit of 0.008 μs^{-1}, corresponding to $\sim$ 0.01 mT of spontaneous magnetic fields. This upper limit is clearly much weaker than the one found by tunneling experiments in which much stronger magnetic fields are needed to cause the splitting of zero bias conductance peak [38].

3 Magnetic properties of RMnO$_3$ thin films (C. Niedermayer)

Single-crystalline orthorhombic (110) RMnO$_3$ films (R = rare earth element) on (110) YAlO$_3$ were grown by pulsed laser deposition. Due to the mismatch between the film and substrate unit cells, strain and lattice distortion can be induced in the epitaxial films. X-ray reciprocal mapping confirms that with increasing thickness the film lattice parameters relax towards bulk values [7]. This is consistent with the results of low-energy muon-spin relaxation measurements, which had shown that the film is magnetic throughout its volume, but that the magnetic properties change as a function of distance from the film substrate interface.
In 2011, the magnetic properties of a 5×8 mm^2 50 nm thin orthorhombic (110) LuMnO$_3$ film on (110) YAlO$_3$ were investigated using spin polarized neutron reflectometry (PNR) and neutron diffraction. While the PNR measurements are sensitive to the magnetization profile at the film substrate interface, the neutron diffraction experiments allow for the determination of the magnetic structure of the film.

3.1 Polarized neutron reflectometry

The PNR measurements were performed at the Paul Scherrer Institut at the time of flight reflectometer AMOR. A clear splitting of the reflectivity curves for spin-up and down neutrons is observed at low temperatures (10 K, 4 T, Fig. 5a). At approximately 40 K, the splitting is starting to close and above 100 K no difference in the q dependence between the two spin orientations can be observed (Fig. 5c). The data can successfully be described by a model, in which the difference in the two spin states arises from a 10 nm thin ferromagnetic phase at the substrate/film interface with an exponential magnetization profile (Fig. 5b). An homogeneous magnetization throughout the entire film volume or a ferromagnetic surface layer is not in agreement with the data. The data analysis matches well the assumption that a highly epitaxially and strained film has been grown over the first few nm. A subsequent strain relaxation is leading to a strong decay in the ferromagnetic properties. The observed ferromagnetism is consistent with magnetization measurements where a closing of the magnetic hysteresis loop takes place at around 100 K.

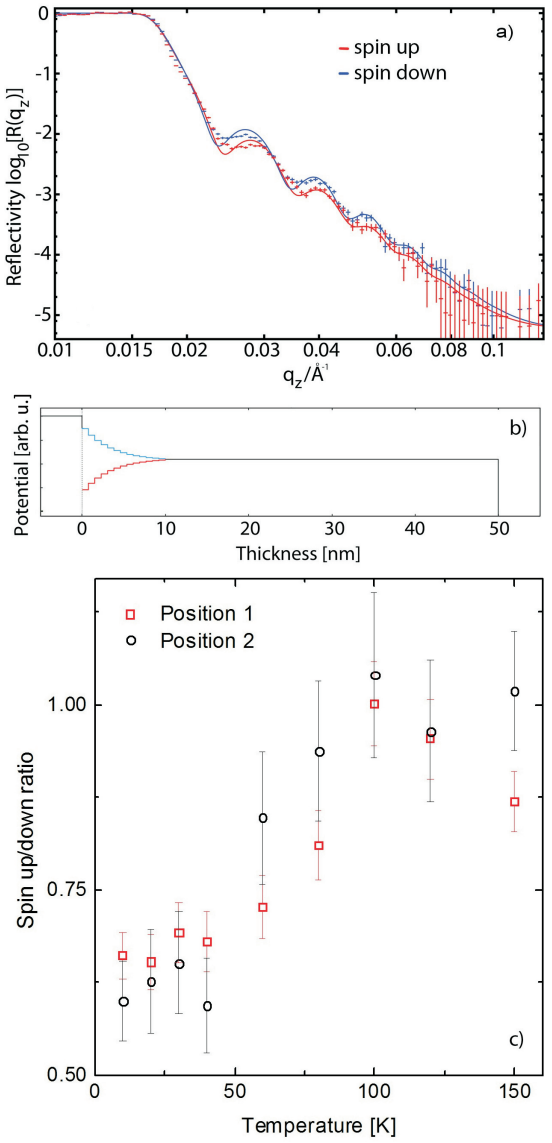

Figure 5: *(a) Neutron reflectivity for spin-up/down at 10 K, 4 T. (b) Simulated profile of the magnetic scattering potential. (c) Temperature dependence of the spin-up/down ratio at two distinct q positions.*

3.2 Neutron diffraction

Magnetic neutron diffraction measurement at the cold triple axis spectrometer RITA II at PSI

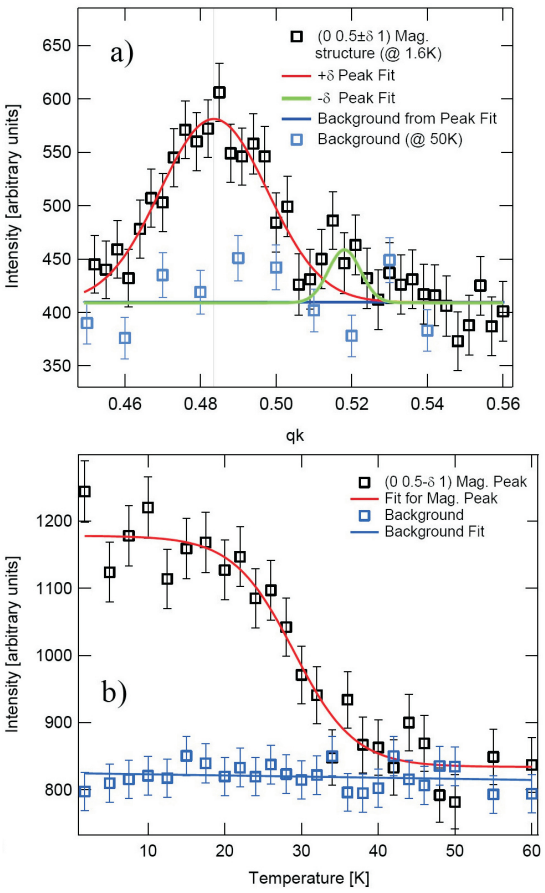

Figure 6: *(a) Magnetic Bragg peak at* $(0\ 0.48\ 1)$ *measured at 1.6 K. A second peak might be present at* $(0\ 0.52\ 1)$*. (b) Temperature dependence of the first peak between 1 and 60 K.*

of a single-crystalline orthorhombic 90 nm thin (110) $LuMnO_3$ film on (110) $YAlO_3$ revealed a magnetic Bragg peak at $(0\ 0.5 \pm \delta\ 1)$ with $\delta = 0.02$ (Fig. 6a). The position of the magnetic structure peak indicates a helical or cycloidal incommensurate structure. The second peak at $(0\ 0.5 + \delta\ 1)$ is considerably smaller leading to the assumption of differently populated magnetic domains. The suppression of the peak might be a result of anisotropic effects due to the growth-induced strain. The magnetic Bragg peak at $(0\ 0.5 \pm \delta\ 1)$ with $\delta = 0.02$ has been confirmed at the thermal diffractometer D10 at the ILL. In addition, five other magnetic structure peaks have been identified including $(1\ \pm qk\ 1)$, a peak position which is unique for spin spiral and therefore excludes the expected bulk E-type antiferromagnetic ground state in strained thin films. In a second step a full temperature scan of the magnetic structure was performed showing a decrease of the intensity in the range of $20 - 40$ K, with a complete disappearance above 40 K (Fig. 6b).

4 The intrinsic origin of the conducting interface between $LaAlO_3$ and $SrTiO_3$ (Ph. Willmott, J.-M. Triscone)

Although the conductivity at the $LaAlO_3/SrTiO_3$ (LAO/STO) interface was originally explained by the intrinsic polar catastrophe scenario, in which the presence of an electric field within the LAO [8, 9] caused by the polar discontinuity at the interface produces a Zener breakdown above a critical film thickness [39, 40, 41], models explaining the conductivity in terms of *extrinsic* effects caused by oxygen vacancies [42], or interfacial intermixing [10][43] have been suggested. By growing films of the solid solution $(LaAlO_3)_x(SrTiO_3)_{1-x}$ (LASTO:x), both the polar catastrophe and intermixing could be tested in the same system, and their electrical responses are predicted to be quite distinct from each other.

The intrinsic polar model can be elegantly formulated in the framework of the theory of polarization, such that the critical thickness t_c is proportional to ε_{film}, the dielectric constant of the polar film material, and inversely proportional to P^0_{film}, the formal polarization of the film unit cell. It can be simply shown that for LASTO:x films, $P^0_{\mathrm{LASTO}:x} = xP^0_{\mathrm{LAO}}$. First-principles calculations on bulk compounds of different LASTO compositions show that the dielectric constant of LASTO:x remains essentially constant between $x = 1$ and 0.5. This initially surprising result is explained by the fact that the large dielectric constant of pure STO, mainly produced by a low-frequency and highly polar phonon mode, is effectively suppressed by the atomic disorder of the solid solution. Hence, varying x allows one to tune the film's formal polarization while keeping all other quantities constant, that is,

$$t_c^{\mathrm{LASTO}:x} = t_c^{\mathrm{LAO}}/x. \qquad (2.1)$$

On the other hand, if interfacial intermixing were responsible for the conductivity, one would expect a film composed of this intermixed material to be conducting throughout its bulk, the film to be conducting at the surface and not just at the interface, and the conductance to increase with film thickness.

Sets of films for $x = 0.5, 0.75$, and 1 (pure LAO, to test reproducibility) were grown both at PSI and UniGE, and their conductances measured (Fig. 7) the central result of this study. The step in conductance for $x = 1.0$ is observed at 4 unit cells, as first observed by Thiel *et al.* [41] and reproduced by several groups. For $x = 0.75$ and 0.50, the data unambiguously demonstrate

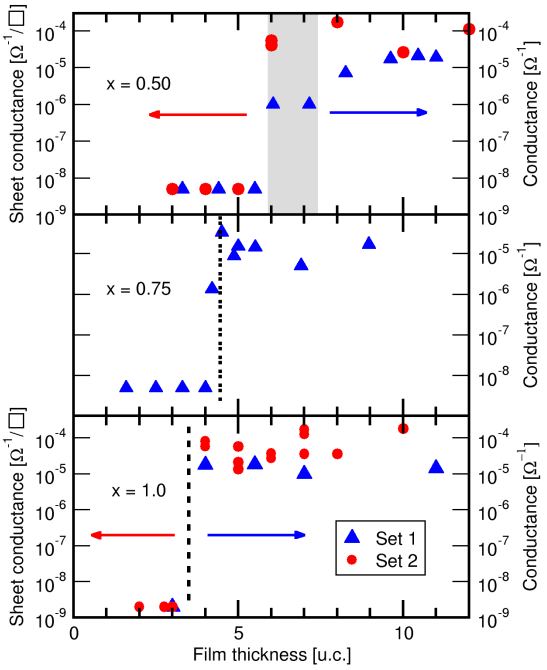

Figure 7: *Room temperature conductance of LASTO:x films for $x = 1, 0.75$ and 0.50. The dashed vertical lines for $x = 1.0$ and 0.75 indicate the experimentally determined threshold thicknesses t_c, which, for $x = 0.5$, is represented by a band for the more gradual transition. All values were obtained after ensuring that the samples had remained in dark conditions for a sufficiently long time to avoid any photoelectric contributions.*

that the critical thickness increases with STO-content in the solid solution, with $t_c^{\mathrm{LASTO:0.75}}$ close to 5 unit cells, and $t_c^{\mathrm{LASTO:0.5}}$ between 6 and 7 unit cells. This striking result demonstrates that the critical thickness depends on x, increasing as the formal polarization decreases. Although the critical thicknesses obtained from the experimental data are marginally smaller than predicted by theory, this can easily be attributed to the uncertainty in the dielectric constants of the solid solutions. The overall agreement, however, with the polar catastrophe model described by Eq. (2.1) is remarkable.

In conclusion, we have shown that in heterostructures of ultrathin films of the solid solution $(LaAlO_3)_x(SrTiO_3)_{1-x}$ grown on (001) $SrTiO_3$, the critical thickness at which conductivity is observed scales with the strength of the built-in electric field of the polar material. These results test the fundamental predictions of the polar catastrophe scenario and convincingly demonstrate the intrinsic origin of the doping at the LAO/STO interface [11].

5 High electron mobility at the $LaAlO_3/SrTiO_3$ interface (J.-M. Triscone)

Following recent *ab initio* calculations of the electronic band structure of the electron gas present at the $LaAlO_3/SrTiO_3$ (LAO/STO) interface [45], we have analyzed in detail the transport properties of this system. In heterostructures grown at 800°C, we observe, at low temperatures, carrier mobilities of 500-1000 cm^2/Vs (Fig. 8) and a two-dimensional carrier density of $2 - 5 \cdot 10^{13}$ cm^{-2}. The magnetic field dependence of the longitudinal and Hall resistance suggests a multi-channel conduction mechanism that we attribute to the fact that the Fermi level crosses electronic bands with different symmetries and different effec-

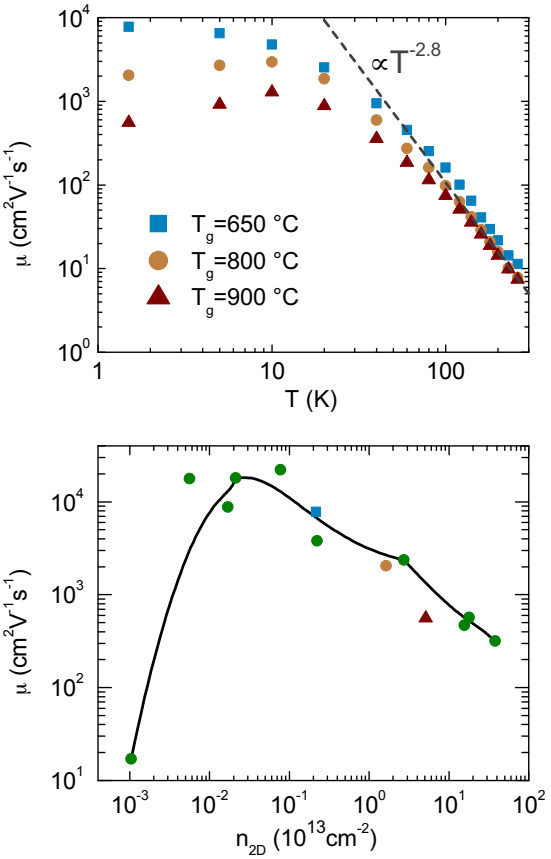

Figure 8: *Top: Hall mobility as a function of temperature for samples grown at 900°C (brown triangles), 800°C (gold dots) and 650°C (blue squares). The dashed line shows a fit assuming $\mu \propto T^{\alpha}$ with $\alpha = -2.8$. This temperature dependence is also observed in bulk doped STO. Bottom: comparison of $LaAlO_3/SrTiO_3$ interfaces and doped $SrTiO_3$ (green dots) showing the dependence of the low-temperature mobility on the carrier density (measured at 260 K) assuming a uniform gas thickness of 10 nm. The same color code is used in the top and bottom panels. Data for bulk STO are taken from [44].*

tive masses. Reducing the growth temperature to 650°C, we succeeded in producing samples with mobilities exceeding 5000 cm^2/Vs, as shown in Fig. 8. In these interfaces, the carrier density drops by about one order of magnitude reaching a few 10^{12} cm^{-2}. In magnetic fields, the magneto-resistance of such high-mobility samples displays 2D quantum oscillations. The evolution of the mobility with the carrier density of the interfaces shown in Fig. 8 resembles the behavior of bulk doped $SrTiO_3$, if we assume that the electron gas is confined within 10 nm from the interface.

6 $NdNiO_3$ thin films: a photoemission study (Ph. Aebi)

Nickel based rare earth (R) perovskite oxides $RNiO_3$ are a model system to study temperature driven metal to insulator phase transitions (MIT). In the case of $NdNiO_3$, multiple experiments tried to determine the nature and the width of the band gap in the insulating state. However optical and transport measurements lead to different results [46, 47, 48]. Ultraviolet photoelectron spectroscopy (UPS) is an ideal tool to probe the gap opening across the MIT and thereby paints a detailed picture of the evolution of the gap. An epitaxial 10 nm $NdNiO_3$ thin film was grown on an $LaAlO_3$ substrate following the procedure given in [12]. The *ex situ* transferred film was cleaned from adsorbates by applying an oxygen plasma to its surface. The surface cleanliness was checked using X-ray photoelectron spectroscopy of the O 1s and the C 1s core levels. UPS spectra were recorded using s-polarized monochromatic photons from the He I_α line ($h\nu = 21.2$ eV) of a helium discharge lamp.

UPS measurement on $NdNiO_3$ [49] report a loss of spectral weight not only close to the Fermi level, but over a broad binding energy range, once the system is cooled below T_{MIT}. This effect hinders a determination of the size and evolution of the gap. To circumvent this, we symmetrized our temperature dependent spectra with respect to the Fermi level. This not only made the presence of the gap evident (Fig. 9, inset), but also allowed us to subtract the above mentioned spectral loss. We then fitted the residuum using a gaussian profile.

The intensity of this gaussian is plotted in Fig. 9, top, as a function of sample temperature. It exhibits a temperature hysteresis with onsets comparable to the transition temperatures derived from transport data. This suggests that the gaussian profile describes the gap opening well and in turn validates the assumption that the width of the gaussian is directly correlated with the gap width.

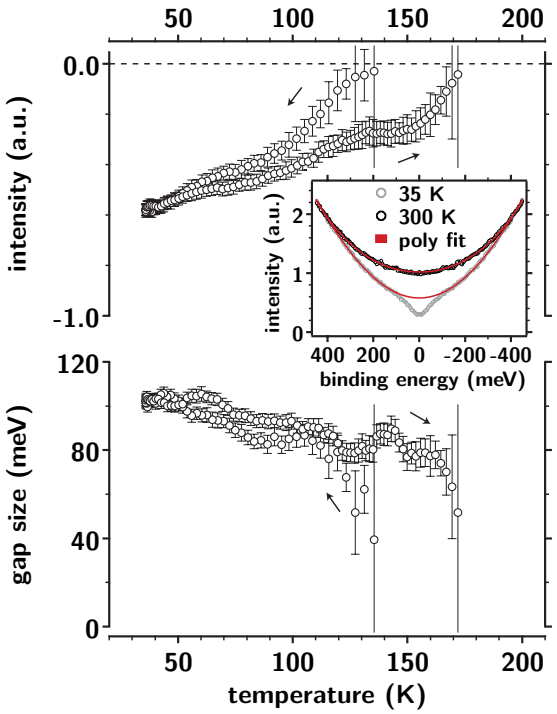

Figure 9: *Top: the intensity of the gap as a function of temperature. Bottom: the gap size as a function of temperature. Inset: two symmetrized spectra with the polynomial fit used as background for the determination of the gap.*

In Fig. 9, bottom, the gap size is plotted as a function of temperature. At the transition temperatures, the gap size has a value of $E_G(T_{MIT} \sim 150\ K) = (55 \pm 10)$ meV and it increases to $E_G(35\ \mathrm{K}) = (102 \pm 5)$ meV at low temperatures. It is interesting to note that the gap reaches around 80% of its 35 K limit in less than 20 K below the MIT. A similar behavior was found in the magnetic moments of the Ni atom in $NdNiO_3$ [49]. There it was attributed to the suppression of the magnetic transition due to the itinerant nature of the charge carriers above T_{MIT}. The similarity between both parameters suggests either that a coupling between the magnetic moment and the electronic gap size exists or that the MIT is suppressed in a similar way by an unknown order parameter as itself suppresses the magnetic transition.

7 Exchange bias in $LaNiO_3/LaMnO_3$ superlattices (J.-M. Triscone)

The wide spectrum of exotic properties exhibited by transition-metal oxides arises from the interplay between the spin, charge, orbital and lattice degrees of freedom [50]. In this con-

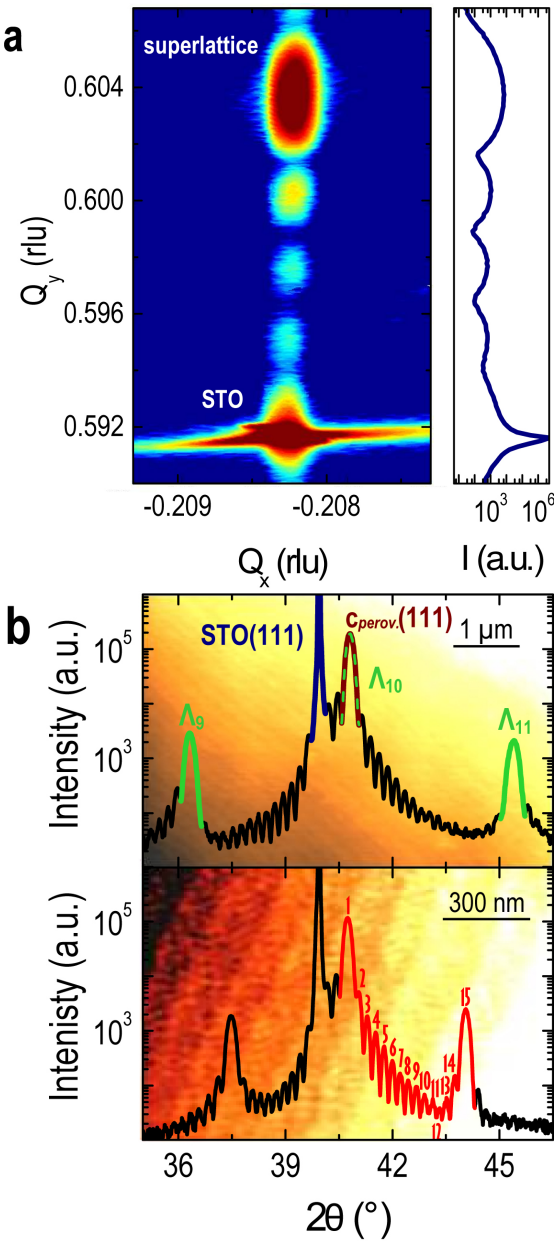

Figure 10: *(a) X-ray diffraction reciprocal space map and corresponding reciprocal space line-scan for a $(5/5)_{20}$ superlattice around the (1 1 2) reflection. (b) X-ray diffractograms for a $(5/5)_{20}$ (up) and $(7/7)_{15}$ (down) superlattices. Background: corresponding atomic force microscopy images showing the superlattices' topography.*

text, interface engineering in complex oxide heterostructures enables not only further tuning of the exceptional properties of these materials, but also gives access to hidden phases and emergent physical phenomena [13]. Following our previous work on nickelate-based heterostructures, we have shown that (111)-oriented $LaNiO_3/LaMnO_3$ (LNO/LMO) superlattices exhibit unexpected magnetic properties [14].

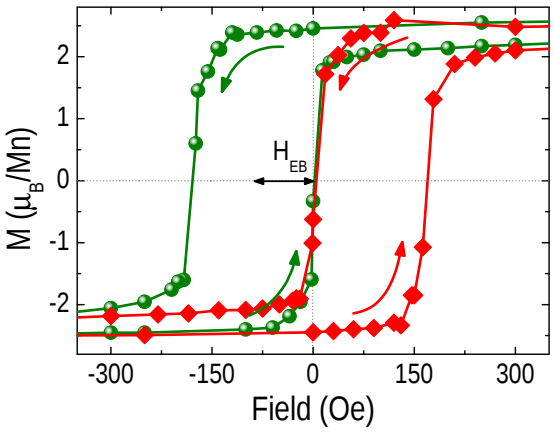

Figure 11: *Magnetization field loops at 5 K for a $(7/7)_{15}$ superlattice after field cooling from room temperature in +0.4 T (green circles) and in −0.4 T (red diamonds).*

Epitaxial $(n(\mathrm{LNO})/n(\mathrm{LMO}))_x$ superlattices have been grown by off-axis rf magnetron sputtering. As substrates, we use (111)-oriented $SrTiO_3$ single-crystals. The resulting superlattices grow coherently strained (Fig. 10a), with atomic force microscopy revealing that the surface preserves the step-like morphology of the substrate (background of Fig. 10b). The X-ray diffraction patterns of the artificially layered structure indicate excellent sample quality and good agreement with the designed layering (Fig. 10b).

LNO is the only member of the perovskite nickelate family lacking any magnetic order in its bulk form, whereas LMO is ferromagnetic when grown as a thin film. The temperature-dependence of the magnetization of the (111)-superlattices clearly resembles that of (111)-LMO thin films, suggesting that the overall magnetization is dominated by the inner ferromagnetic LMO layers. However, the low-temperature field-dependence of the magnetization in the (111)-heterostructures has been found to be strikingly different from that of the LMO films. After field-cooling from room temperature in the presence of a +0.4 T (−0.4 T) field, a shift of the centre of the magnetization-field loop along the magnetic field axis is observed toward negative (positive) fields, as illustrated in Fig. 11. This behavior reveals the surprising presence of exchange bias (EB) in (111)-oriented LNO/LMO superlattices at low temperatures, with the bias-field shift being a classic signature of unidirectional anisotropy [51]. The unexpected observation of EB provides key information about the magnetic properties and interactions within the heterostructure. First, the interfacial nature of EB effects implies a strong coupling between

LNO and LMO layers at the interface. Second, biasing effects hint at the development of magnetic order within the nominally paramagnetic material (LNO). First-principle calculations carried out for these specific heterostructures indicate that this interfacial interaction may give rise to an unusual spin order resembling a spin-density wave within the LNO layers, though development of antiferromagnetism or a spin glass behavior in the LNO layers cannot be excluded at present.

The observation of the EB phenomenon at the interface between a paramagnet and a ferromagnet highlights once more the potential of interface engineering for tailoring the properties of complex oxides and extending their functionalities towards new technological applications.

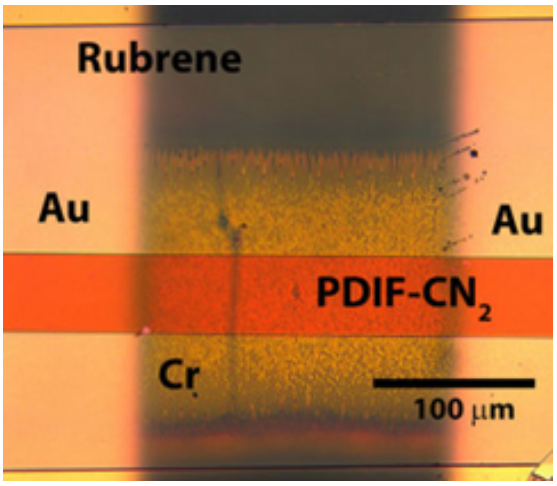

Figure 12: *Optical microscope image of a Schottky-gated rubrene-PDIF-CN_2 charge transfer interface used in our experiments.*

8 Electronic properties of organic charge transfer interfaces probed using Schottky-gated heterostructures (A. Morpurgo)

Organic semiconductors commonly have band-gaps in excess of 2 eV and — when undoped — are essentially insulators. Often, however, interfaces of two such materials exhibit high electrical conductivities, orders of magnitude larger than the bulk ones. Possibly the most striking example is provided by interfaces between crystals of TTF and TCNQ, where square resistances as low as a few kOhms have been observed down to low temperature [15]. There is consensus that the conductivity of organic-organic interfaces originates from charge transfer from the surface of one material to that of the other. However, the microscopic details of the process, as well as the nature of the charge carriers, are not known. The interpretation of experiments on organic interfaces realized using thin films of organic semiconductors — which have been carried out on gated devices — is complex, because the "bulk" of the films themselves have non-negligible conductance. Devices based on single-crystals do not suffer from this non-ideality, but only a few experiments have been performed so far, in no case on devices equipped with a gate electrode [15, 16]. In this project, we have studied the transport properties of organic charge transfer interfaces based on laminating together a rubrene and a PDIF-CN_2 crystal, the two organic molecules that give the highest carrier mobility values in organic single-crystal transistors (rubrene for holes and PDIF-CN_2 for electrons [17]). These charge transfer interfaces were assembled on Cr films (in contact with the rubrene crystal), acting as Schottky gates enabling the electrostatic modulation of the interfacial conductivity (Fig. 12). We have performed systematic investigations of gate-dependent conductivity in the temperature range between 300 and 30 K on many different devices and found that the charge carriers are electrons at the surface of PDIF-CN_2. The mobility of the carriers ranges between 1 and 3 cm^2/Vs at room temperature and it increases upon lowering temperature down to approximately 150 K, below which temperature it starts decreasing. In the best devices, however, the electron mobility remains as high as 1 cm^2/Vs at $T = 30$ K, which is orders of magnitude larger than in the best n-type organic transistor realized so far. The density of electrons is found to reproducibly decrease linearly with lowering temperature. This is an unexpected result, different from what has been found in other organic charge transfer interfaces where the carrier density is constant (e.g. in TTF-TCNQ exhibiting metallic conduction, due to a large overlap between the valence band of TTF and the conduction band of TCNQ) or decreases exponentially with lowering T, indicating the presence of an energy gap for interfacial charge transfer (which is the case for TMTSF-TCNQ interfaces) [15, 16]. The linear decrease of the carrier density indicates that the top of the valence band of rubrene is nearly perfectly aligned with the bottom of the conduction band of PDIF-CN_2, before charge transfer occurs. After charge transfer, an effective gap opens, entirely due to the electrostatic potential generated by the transferred charge itself. Taking this into account, we successfully reproduced the linear temper-

ature dependence of the electron density, and explained quantitatively the slope observed in the experiments.

9 Nanoscale PFM imaging of intrinsic domains in $PbTiO_3$ ultrathin films (J.-M. Triscone)

In ferroelectric ultrathin films, the depolarization field arising from bound charges on the surface of the film and at the interface with the substrate can be partially screened by free charges from metallic electrodes, ions from the atmosphere, or mobile charges from within the semiconducting ferroelectric itself. Even in structurally perfect metallic electrodes, the screening charges will spread over a small but finite length, giving rise to a non-zero effective screening length that will dramatically alter the properties of an ultrathin film. In the absence of sufficient free charges, a ferroelectric has several ways of minimizing its energy while preserving its polar state, e.g. by forming domains of opposite polarization, or rotating the polarization into the plane of the thin ferroelectric slab [18].

Using piezoresponse force microscopy (PFM), we investigated the intrinsic nanodomain pattern of $PbTiO_3$ ultrathin films at room temperature, focusing on the effect of the film thickness and the effective screening length. We clearly observe a decrease of the intrinsic domains size as the film thickness is reduced, in agreement with the Landau-Kittel law [52, 53, 54]. Interestingly, we also observe an evolution in the shape of the domains from nanodots for the thicker films to nanostripes for the thinner films. This may be the result of the competition between the elastic behavior of the domain walls and their pinning in a disorder potential. Our work also focuses on the study of domain wall motion and relaxation after the application of an electric field [19].

10 Interfaces, domain walls and disorder: pathways to multifunctionality and complex behavior (P. Paruch)

10.1 Conduction at ferroelectric domain walls

Domain walls are naturally-occurring, intrinsically nanoscale interfaces separating different orientations of spontaneous electric polarization, magnetization, or strain. They can present radically different properties from their parent materials, opening an alternative route towards unusual functionalities with enormous application potential [20]. Following the recent discovery of conduction at ferroelectric domain walls in insulating $BiFeO_3$ [55], different microscopic mechanisms were proposed, including band gap lowering [56], polarization discontinuity attracting charged defects [57], or dynamic conduction due to irreversible microscopic motion of the domain walls [58].

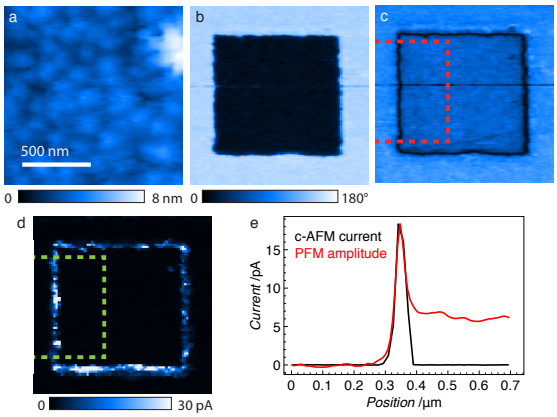

Figure 13: *Domain wall conduction in PZT. (a) Topography showing a rms roughness of 0.4 nm. (b) PFM phase and (c) amplitude images of a square domain written with a positive tip bias. (d) c-AFM measurement at −1.5 V tip bias, showing a 25 pA average current at the domain walls. (e) Line profiles of c-AFM current and inverse PFM amplitude averaged over the left domain wall, as indicated by the dashed lines in (c) and (d).*

We found that 180° domain walls in insulating epitaxial $Pb(Zr_{0.2}Ti_{0.8})O_3$ (PZT) thin films also present a current signal in conductive atomic force microscopy (c-AFM) measurements. At high voltages, dynamic displacement currents related to irreversible domain wall motion and polarization switching are observed, as demonstrated by concurrent piezoresponse force microscopy (PFM) imaging. However, at low voltages, small but stable static conductive currents with no changes in the domain configuration are observed, as shown in Fig. 13. The domain wall conduction is highly non-linear, with asymmetric current-voltage characteristics, and strong temperature dependence at higher temperatures. For more details, see [21].

10.2 Thermally quenched domain walls

Ferroic domain walls also provide an excellent model system for studying the static and dynamic behavior of elastic interfaces in disordered media [22]. Theoretically and experimentally, although equilibrium properties of such systems are relatively well understood, much less is know about their out-of-equilibrium behavior. A major challenge is understanding the non-steady slow dynamics as-

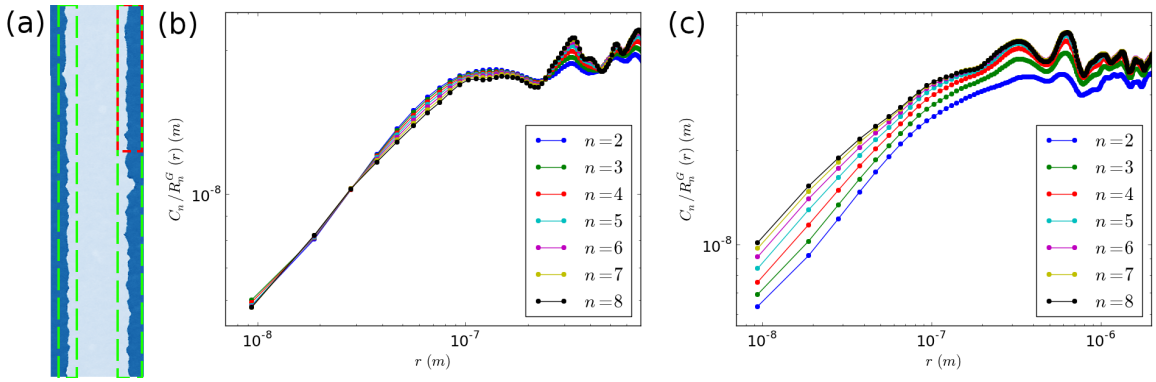

Figure 14: *(a) PFM phase map* $(1.2 \times 4.8\ \mu m^2)$ *of two domain walls. When the complete domain walls are considered (green boxes), the corresponding normalized correlation functions at different orders show either (b) collapse (Gaussian, self-affine behavior) or (c) fanning (non-Gaussian multi-affine behavior). Eliminating strong disorder fluctuations to consider only the upper part of the second wall (red box), however, returns to self-affine behavior.*

sociated with aging [59]. A specially interesting realization of such out-of-equilibrium phenomena is provided by quenches, in which a parameter is abruptly varied.
Using PFM, we measured the evolution of domain wall roughness in PZT thin films during heat-quench cycles up to 735°C, with the effective roughness exponent ζ changing from 0.25 to 0.5. Two possible mechanisms for the observed ζ increase can be considered: a quench from a thermal one-dimensional configuration, and from a locally-equilibrated pinned configuration with a crossover from a two- to one-dimensional regime. We find that the post-quench spatial structure of the metastable states, qualitatively consistent with the existence of a growing dynamical length scale whose ultraslow evolution is primarily controlled by the defect configuration and heating process parameters, makes the second scenario more plausible. This interpretation suggests that pinning is relevant in a wide range of temperatures. We also demonstrated the crucial effects of oxygen vacancies in stabilizing domain structures. For more details, see [23]

10.3 Multiscaling analysis of domain walls

A wealth of additional information about the static configuration of an elastic interface pinned by disorder can be obtained by a more complex multiscaling analysis investigating the higher moments of the probability distribution function (PDF) of the relative displacement from an elastically optimal flat configuration [22]. We carried parallel studies of these geometrical fluctuations in numerical one-dimensional interfaces pinned by random-bond disorder, and in ferroelectric domain walls in PZT thin films, allowing us to compare an ideal elastic line under weak collective pinning with a system in which complex local variation of disorder are observed [60, 61]. Following the multiscaling analysis developed in [62], we first showed that the numerical interfaces display Gaussian PDF behavior, as expected for a self-affine system, with slight deviations related to finite size effects at very small and very large length scales. Moreover, we observed an intrinsic spread of the roughness exponent between individual interfaces. On the ferroelectric domain walls, we showed that the multiscaling analysis is strongly sensitive to local disorder variations, displaying either self-affine or multi-affine behavior, as shown in Fig. 14. Using this analysis as a criterion to classify domain wall segments, we finally extracted the roughness exponent statistics for 30 self-affine domain walls, with an average value of 0.58 ± 0.05. For more details see [24].

11 Interfaces in disordered systems (T. Giamarchi)

We addressed different open questions in the field of classical disordered elastic systems (DES), i.e. the study of elastic interfaces or periodic systems embedded into a disordered medium. This class of models aims at describing, e.g., ferromagnetic or ferroelectric domain walls in thin films, or some spintronic materials in which domain walls can be manipulated by either an external magnetic field or an electrical current. The resulting competition between elasticity and disorder, blurred by thermal fluctuations at finite temperature, gives rise to metastability and glassy properties.

11.1 Thermal effects on the roughness of an interface

In a collaboration with V. Lecomte (LPMA, France) and S. Bustingorry (Centro Atomico Bariloche, Argentina), we focussed on the fluctuations of 1D interfaces. We had shown in [25] using a Gaussian variational method (GVM) approximation and complementary scaling arguments, the existence of two regimes in temperature: at high temperatures the thermal fluctuations define a thermal width ξ_{th} which completely erases the existence of the natural width of the interface $\xi > 0$, whereas at low temperatures the microscopic width ξ matters even for the macroscopic interface's geometrical fluctuations. We have pursued this analysis [22]. Exploiting the exact mapping between the static 1D interface and the directed polymer in random media (DPRM), we have extended analytical arguments and predictions known for $\xi = 0$ to the more general case with $\xi > 0$. Moreover, performing a numerical integration of the differential equations given by [63], we have measured the geometrical and free-energy fluctuations of the DPRM with a finite disorder correlation length ξ and at finite temperature. Investigating numerically the relation predicted analytically at large lengthscales between the amplitude of the geometrical fluctuations (one of the quantities accessible in experiments) and the effective strength of disorder $\widetilde{D}_\infty$, we have successfully pointed out the existence of the two temperature regimes predicted analytically (Fig. 15), supporting in particular that an experimental temperature-dependent measurement of the amplitude of an interface's roughness provides a way to determine quantitatively $T_c(\xi)$ and the microscopic disorder strength of its underlying medium.

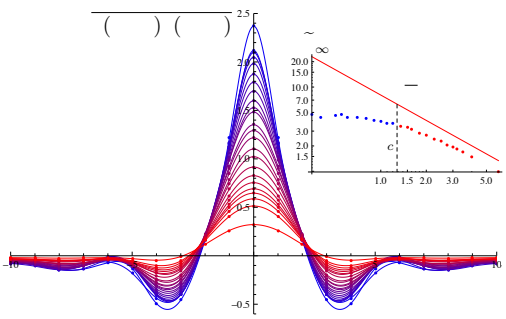

Figure 15: *Measured disorder correlator at large lengthscales, with increasing temperature from blue to red curves. Its amplitude $\widetilde{D}_\infty$ decreases at high temperatures in $\propto 1/T$, and tends to saturate below T_c.*

11.2 Interfaces with internal degrees of freedom

To address the question of spintronic materials, in which it is important to take into account the internal degrees of freedom of the domain wall, we have pursued, in collaboration with S. Barnes (Florida University, USA), J. P. Eckmann (UniGE) and V. Lecomte (LPMA, France), our analysis of domain walls with such internal degrees of freedom. In a previous report we had pointed out that such systems have depinning properties totally different than the normal walls. In a more theoretical approach we have developed the analysis of the properties of such systems and showed that they have interesting topological transitions [26].

11.3 Domain walls in ferroelectrics

In an ongoing collaboration with P. Paruch, we are investigating the roughness and more generally the distribution of the relative displacement of $Pb(Zr,Ti)O_3$ thin films domains walls, performing a multiscaling analysis of those measurements and comparing them to numerical simulations of 1D interfaces by S. Bustingorry.

11.4 Reviews for BKT transition

In addition to the above-mentioned research works, we have written, in collaboration with L. Benfatto and C. Castellani (Rome University, Italy), a mini-review of the Beresinskii-Kosterlitz-Thouless (BKT) transition and the effects of disorder, with special applications to superconducting films [27]. This review is part of a book on the 40 year anniversary of the BKT transition.

12 Collaborative efforts

This year, one can cite in particular the Willmott-Triscone collaboration on the testing of the fundamental prediction of the polar catastrophe scenario in the LAO/STO system, the Aebi-Triscone collaboration on the study of nickelate films, and the Paruch-Giamarchi ongoing collaboration on the study of the static and dynamic properties of ferrolectric domain walls.

MaNEP-related publications

- [1] V. K. Malik, I. Marozau, S. Das, B. Doggett, D. K. Satapathy, M. A. Uribe-Laverde, N. Biskup, M. Varela, C. W. Schneider, C. Marcelot, J. Stahn, and C. Bernhard, arXiv:1110.4173 (2011).

[2] J. Stahn, J. Chakhalian, C. Niedermayer, J. Hoppler, T. Gutberlet, J. Voigt, F. Treubel, H.-U. Habermeier, G. Cristiani, B. Keimer, and C. Bernhard, Physical Review B **71**, 140509(R) (2005).

[3] J. Chakhalian, J. W. Freeland, G. Srajer, J. Strempfer, G. Khaliullin, J. C. Cezar, T. Charlton, R. Dalgliesh, C. Bernhard, G. Cristiani, H.-U. Habermeier, and B. Keimer, Nature Physics **2**, 244 (2006).

[4] J. Hoppler, J. Stahn, C. Niedermayer, V. K. Malik, H. Bouyanfif, A. J. Drew, M. Rössle, A. Buzdin, G. Cristiani, H.-U. Habermeier, B. Keimer, and C. Bernhard, Nature Materials **8**, 315 (2009).

► [5] D. K. Satapathy, M. A. Uribe-Laverde, I. Marozau, V. K. Malik, S. Das, T. Wagner, C. Marcelot, J. Stahn, S. Brück, A. Rühm, S. Macke, T. Tietze, E. Goering, F. A., J. H. Kim, M. Wu, E. Benckiser, B. Keimer, A. Devishvili, B. P. Toperverg, M. Merz, P. Nagel, S. Schuppler, and C. Bernhard, arXiv:1111.5772 (2011).

► [6] A. V. Boris, Y. Matiks, E. Benckiser, A. Frano, P. Popovich, V. Hinkov, P. Wochner, M. Castro-Colin, E. Detemple, V. K. Malik, C. Bernhard, T. Prokscha, A. Suter, Z. Salman, E. Morenzoni, G. Cristiani, H.-U. Habermeier, and B. Keimer, Science **332**, 937 (2011).

► [7] Y. Hu, M. Bator, M. Kenzelmann, T. Lippert, C. Niedermayer, C. W. Schneider, and A. Wokaun, Applied Surface Science (2011), doi:10.1016/j.apsusc.2011.10.082.

► [8] S. A. Pauli, S. J. Leake, B. Delley, M. Björck, C. W. Schneider, C. M. Schlepütz, D. Martoccia, S. Paetel, J. Mannhart, and P. R. Willmott, Physical Review Letters **106**, 036101 (2011).

► [9] C. Cancellieri, D. Fontaine, S. Gariglio, N. Reyren, A. D. Caviglia, A. Fête, S. J. Leake, S. A. Pauli, P. R. Willmott, M. Stengel, P. Ghosez, and J.-M. Triscone, Physical Review Letters **107**, 056102 (2011).

[10] P. R. Willmott, S. A. Pauli, R. Herger, C. M. Schlepütz, D. Martoccia, B. D. Patterson, B. Delley, R. Clarke, D. Kumah, C. Cionca, and Y. Yacoby, Physical Review Letters **99**, 155502 (2007).

► [11] M. L. Reinle-Schmitt, C. Cancellieri, D. Li, D. Fontaine, M. Medarde, E. Pomjakushina, C. W. Schneider, S. Gariglio, P. Ghosez, J.-M. Triscone, and P. R. Willmott, arXiv:1112.3532 (2011).

[12] V. Scagnoli, U. Staub, M. Janousch, A. M. Mulders, M. Shi, G. I. Meijer, S. Rosenkranz, S. B. Wilkins, L. Paolasini, J. Karpinski, S. M. Kazakov, and S. W. Lovesey, Physical Review B **72**, 155111 (2005).

[13] P. Zubko, S. Gariglio, M. Gabay, P. Ghosez, and J.-M. Triscone, Annual Review of Condensed Matter Physics **2**, 141 (2011).

► [14] M. Gibert, P. Zubko, R. Scherwitzl, J. Íñiguez, and J.-M. Triscone, Nature Materials **11**, 195 (2012).

[15] H. Alves, A. S. Molinari, H. Xie, and A. F. Morpurgo, Nature Materials **7**, 574 (2008).

[16] M. Nakano, H. Alves, A. S. Molinari, S. Ono, N. Minder, and A. F. Morpurgo, Applied Physics Letters **96**, 232102 (2010).

► [17] N. A. Minder, S. Ono, Z. Chen, A. Facchetti, and A. F. Morpurgo, Advanced Materials **24**, 503 (2012).

[18] C. Lichtensteiger, P. Zubko, M. Stengel, P. Aguado-Puente, J.-M. Triscone, P. Ghosez, and J. Junquera, in *Oxide ultrathin films: science and technology*, G. Pacchioni and S. Valeri, eds. (Wiley, 2011), chap. 12.

[19] P. Paruch, T. Giamarchi, and J.-M. Triscone, in *Physics Of Ferroelectrics: A Modern Perspective*, K. M. Rabe, C. H. Ahn, and J.-M. Triscone, eds. (Springer, 2007), vol. 105 of *Topics in Applied Physics*, p. 339.

[20] H. Béa and P. Paruch, Nature Materials **8**, 168 (2009).

► [21] J. Guyonnet, I. Gaponenko, S. Gariglio, and P. Paruch, Advanced Materials **23**, 5377 (2011).

► [22] E. Agoritsas, V. Lecomte, and T. Giamarchi, Physica B (2012), doi:10.1016/j.physb.2012.01.017.

[23] P. Paruch, A. B. Kolton, X. Hong, C. H. Ahn, and T. Giamarchi, *submitted* (2012).

[24] J. Guyonnet, E. Agoritsas, S. Bustingorry, S. Gariglio, T. Giamarchi, and P. Paruch, *submitted* (2012).

[25] E. Agoritsas, V. Lecomte, and T. Giamarchi, Physical Review B **82**, 184207 (2010).

► [26] S. E. Barnes, J.-P. Eckmann, T. Giamarchi, and V. Lecomte, arxiv:1105.2219 (2011).

[27] L. Benfatto, C. Castellani, and T. Giamarchi, *to be published in Berezinskii-Kosterlitz-Thouless Transition*, J. V. José, ed. (World Scientific, 2012), arXiv:1201.2307.

Other references

[28] M. Sigrist and K. Ueda, Reviews of Modern Physics **63**, 239 (1991).

[29] G. M. Luke, A. Keren, L. P. Le, W. D. Wu, Y. J. Uemura, D. A. Bonn, L. Taillefer, and J. D. Garrett, Physical Review Letters **71**, 1466 (1993).

[30] G. M. Luke, Y. Fudamoto, K. M. Kojima, M. I. Larkin, J. Merrin, B. Nachumi, Y. J. Uemura, Y. Maeno, Z. Q. Mao, Y. Mori, H. Nakamura, and M. Sigrist, Nature **394**, 558 (1998).

[31] Y. Aoki, A. Tsuchiya, T. Kanayama, S. R. Saha, H. Sugawara, H. Sato, W. Higemoto, A. Koda, K. Ohishi, K. Nishiyama, and R. Kadono, Physical Review Letters **91**, 067003 (2003).

[32] A. D. Hillier, J. Quintanilla, and R. Cywinski, Physical Review Letters **102**, 117007 (2009).

[33] R. F. Kiefl, J. H. Brewer, I. Affleck, J. F. Carolan, P. Dosanjh, W. N. Hardy, T. Hsu, R. Kadono, J. R. Kempton, S. R. Kreitzman, Q. Li, A. H. O'Reilly, T. M. Riseman, P. Schleger, P. C. E. Stamp, H. Zhou, L. P. Le, G. M. Luke, B. Sternlieb, Y. J. Uemura, H. R. Hart, and K. W. Lay, Physical Review Letters **64**, 2082 (1990).

[34] G. J. MacDougall, A. A. Aczel, J. P. Carlo, T. Ito, J. Rodriguez, P. L. Russo, Y. J. Uemura, S. Wakimoto, and G. M. Luke, Physical Review Letters **101**, 017001 (2008).

[35] C.-R. Hu, Physical Review Letters **72**, 1526 (1994).

[36] M. Fogelström, D. Rainer, and J. A. Sauls, Physical Review Letters **79**, 281 (1997).

[37] G. Deutscher, Reviews of Modern Physics **77**, 109 (2005).

[38] M. Covington, M. Aprili, E. Paraoanu, L. H. Greene, F. Xu, J. Zhu, and C. A. Mirkin, Physical Review Letters **79**, 277 (1997).

[39] A. Ohtomo and H. Y. Hwang, Nature **427**, 423 (2004).

[40] N. Nakagawa, H. Y. Hwang, and D. A. Muller, Nature Materials **5**, 204 (2006).

[41] S. Thiel, G. Hammerl, A. Schmehl, C. W. Schneider, and J. Mannhart, Science **313**, 1942 (2006).

[42] W. Siemons, G. Koster, H. Yamamoto, W. A. Harrison, G. Lucovsky, T. H. Geballe, D. H. A. Blank, and M. R. Beasley, Physical Review Letters **98**, 196802 (2007).

[43] L. Qiao, T. C. Droubay, T. Varga, M. E. Bowden, V. Shutthanandan, Z. Zhu, T. C. Kaspar, and S. A. Chambers, Physical Review B **83**, 085408 (2011).

[44] A. Spinelli, M. A. Torija, C. Liu, C. Jan, and C. Leighton, Physical Review B **81**, 155110 (2010).

[45] P. Delugas, A. Filippetti, V. Fiorentini, D. I. Bilc, D. Fontaine, and P. Ghosez, Physical Review Letters **106**, 166807 (2011).

[46] T. Katsufuji, Y. Okimoto, T. Arima, Y. Tokura, and J. B. Torrance, Physical Review B **51**, 4830 (1995).

[47] X. Obradors, L. M. Paulius, M. B. Maple, J. B. Torrance, A. I. Nazzal, J. Fontcuberta, and X. Granados, Physical Review B **47**, 12353 (1993).

[48] J. Blasco, M. Castro, and J. García, Journal of Physics: Condensed Matter **6**, 5875 (1994).

[49] I. Vobornik, L. Perfetti, M. Zacchigna, M. Grioni, G. Margaritondo, J. Mesot, M. Medarde, and P. Lacorre, Physical Review B **60**, R8426 (1999).

[50] R. Ramesh and D. G. Schlom, eds., Materials Research Bulletin **33**, 1006 (2008), special issue.

[51] J. Nogués and I. K. Schuller, Journal of Magnetism and Magnetic Materials **192**, 203 (1999).

[52] L. Landau and E. Lifshitz, Physikalische Zeitschrift der Sowjetunion **8**, 153 (1935).

[53] C. Kittel, Physical Review **70**, 965 (1946).

[54] C. Kittel, Reviews of Modern Physics **21**, 541 (1949).

[55] J. Seidel, L. W. Martin, Q. He, Q. Zhan, Y.-H. Chu, A. Rother, M. E. Hawkridge, P. Maksymovych, P. Yu, M. Gajek, N. Balke, S. V. Kalinin, S. Gemming, F. Want, G. Catalan, J. F. Scott, N. A. Spaldin, J. Orenstein, and R. Ramesh, Nature Materials **8**, 229 (2009).

[56] A. Lubk, S. Gemming, and N. A. Spaldin, Physical Review B **80**, 104110 (2009).

[57] E. A. Eliseev, A. N. Morozovska, G. S. Svechnikov, V. Gopalan, and V. Y. Shur, Physical Review B **83**, 235313 (2011).

[58] P. Maksymovych, J. Seidel, Y. H. Chu, P. Wu, A. P. Baddorf, L.-Q. Chen, S. V. Kalinin, and R. Ramesh, Nano Letters **11**, 1906 (2011).

[59] L. F. Cugliandolo, J. Kurchan, J. P. Bouchaud, and M. Mezard, in *Spin Glasses and Random fields*, A. P. Young, ed. (World Scientific, Singapore, 1998).

[60] S. Jesse, B. J. Rodriguez, S. Choudhury, A. P. Baddorf, I. Vrejoiu, D. Hesse, M. Alexe, E. A. Eliseev, A. N. Morozovska, J. Zhang, L.-Q. Chen, and S. V. Kalinin, Nature Materials **7**, 209 (2008).

[61] S. V. Kalinin, S. Jesse, B. J. Rodriguez, Y. H. Chu, R. Ramesh, E. A. Eliseev, and A. N. Morozovska, Physical Review Letters **100**, 155703 (2008).

[62] S. Santucci, K. J. Måløy, A. Delaplace, J. Mathiesen, A. Hansen, J. Ø. H. Bakke, J. Schmittbuhl, L. Vanel, and P. Ray, Physical Review E **75**, 016104 (2007).

[63] D. A. Huse, C. L. Henley, and D. S. Fisher, Physical Review Letters **55**, 2924 (1985).

Project 2 Materials for future electronics

Project leader: A. Morpurgo (UniGE)

Participating members: M. Büttiker (UniGE), T. Giamarchi (UniGE), D. van der Marel (UniGE), A. Morpurgo (UniGE), P. Paruch (UniGE), M. Sigrist (ETHZ), J.-M. Triscone (UniGE)

Summary and highlights: Significant progress has been made in improving the quality of many of the electronic systems investigated in this project, and investigations of new systems have also started. The realization of $LaAlO_3/SrTiO_3$ heterostructures that reproducibly exhibit large mobility values ($\simeq 10'000$ cm^2/Vs) is enabling systematic investigations of Shubnikov-de Haas conductance oscillations as a function of gate voltage, as well as the study of nanopatterned devices in which effects due to the quantum coherence of electrons become visible. For graphene, the technology for realizing suspended devices has been established, resulting in a substantial decrease of the amount of disorder present: these devices are now enabling systematic studies of graphene close to the charge neutrality point, in the sub-Kelvin temperature range. The analysis of optical spectroscopy data on graphene and graphite has reached an unprecedented accuracy. The optical and transport properties of new systems — mainly based on thin layers of metal dichalcogenides, prepared using strategies developed for graphene — have also started to be investigated. Theoretical work has mainly concentrated on systems possessing large spin-orbit interaction and/or not trivial topological properties, focusing on the interplay with superconductivity, which leads to the emergence of new physical phenomena.

1 Devices based on oxide materials

Progress has been made in improving the quality of $LaAlO_3/SrTiO_3$ interfaces and developing new nanopatterning techniques. The higher carrier mobility values are now enabling a detailed investigation of Shubnikov-de Haas conductance oscillations as a function of gate voltage, which is essential to determine the low-energy band-structure of the interfacial electron gas present in these systems. Developments on nanopatterning show that small constrictions, with lateral dimensions of only a few hundreds nanometers, can be fabricated reliably without affecting the properties of the two-dimensional electron gas. In these devices, mesoscopic effects, such as universal conductance fluctuations, are observed in low-temperature transport measurements. Finally, considerable improvements in the fabrication of carbon nanotube tips for the nanoscale investigation of oxide structures have been made.

1.1 Gate-dependent Shubnikov-de Haas conductance oscillations at $SrTiO_3/LaAlO_3$ interfaces *(J.-M. Triscone)*

The electron gas discovered at the interface between $SrTiO_3$ and $LaAlO_3$ — two-band insulators — displays a variety of interesting electronic phenomena. We have recently succeeded in boosting the electron mobility μ by reducing the growth temperature of the $LaAlO_3$ layer, reaching μ values of $\sim$ 5′000 cm^2/Vs and enabling the observation of oscillatory effects in the magneto-resistance [1]. The study of the oscillations as a function of temperature and magnetic field orientation provides an estimate of the effective mass ($m^* \sim 1.5m_e$) of the interfacial carriers, as well as the first experimental confirmation of the two-dimensional character of the electronic states. In a series of recent experiments, we focused on the evolution of the oscillations upon modulation of the carrier density. For this purpose, we have realized field effect devices with samples exhibiting high mobility. Fig. 1 displays the evolution of the magneto-resistance measured at 30 mK for different gate voltages V_g. The analysis of the low-field data reveals that increasing the gate voltage increases the density of carriers and their mobility. For the state with the highest mobility and the largest carrier density that we could achieve during the experiment ($V_g = 10^7$ V), we clearly observe the presence of high and low-frequency oscillations in the magneto-resistance. When the temperature is raised to 800 mK, the high-frequency contribution is lost. As the gate voltage is lowered, hence reducing the doping and the charge mobility, we observe an evolution of the oscillation spectrum, with a progressive

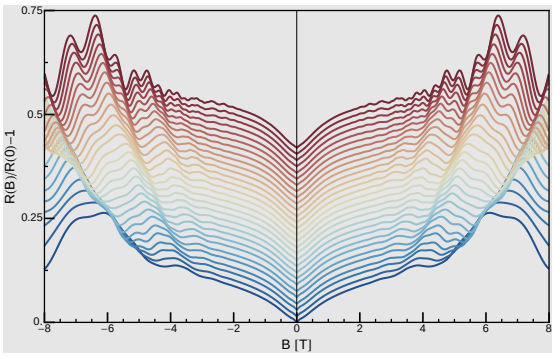

Figure 1: *Magneto-resistance of a $LaAlO_3/SrTiO_3$ interface modulated by an electric field. The data are acquired at 30 mK for gate voltages ranging from 80 V (blue curve) to 107 V (red curve). The curves are vertically displaced for clarity. We observe a complex Shubnikov-de Haas oscillation pattern which evolves as the mobility and carrier density are tuned by the gate voltage.*

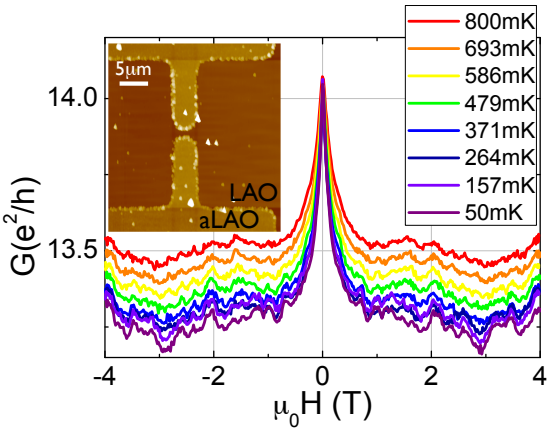

Figure 2: *Magneto-conductance of a 2 $\mu m \times 1\ \mu m$ bridge as a function of the temperature, obtained applying a back-gate voltage $V_g = 26$ V. In the inset, the device is revealed by a topography scan realized using an atomic force microscope.*

loss of the high-frequency component. Detailed modeling of the oscillation amplitude to elucidate the possible effects of Zeeman and Rashba spin-orbit interactions on the formation of Landau levels is ongoing.

1.2 Phase coherent effects in $LaAlO_3/SrTiO_3$ mesoscopic devices *(J.-M. Triscone, A. Morpurgo)*

The two-dimensional electron gas (2DEG) present at $LaAlO_3/SrTiO_3$ interface is emerging as a unique system in the panorama of oxide electronics for the variety of electronic states therein observed [2]. The possibility to tune its transport properties from superconductivity to weak localization using field effect makes this system particularly interesting for the investigation of quantum effects in transport devices. With the aim of studying mesoscopic phenomena in field effect devices, we have set up a nanofabrication procedure based on electron-beam lithography (EBL). After spinning a PMMA resist, we deposit a thin Cu layer to avoid charging effects at the insulating $SrTiO_3$ surface. Using EBL to define our patterns, we realize constrictions in the 100 nm range as shown in the inset of Fig. 2. An amorphous $SrTiO_3$ layer is deposited outside the conducting channel before the growth of the epitaxial $LaAlO_3$ layer. As a result a 2DEG is present only in the region where $LaAlO_3$ is directly in contact with the crystalline $SrTiO_3$ substrate, enabling the realization of laterally confined structures. Fig. 2 displays the magneto-conductance of a 2 μm $\times$ 1 μm bridge measured as a function of temperature. For small magnetic fields, we observe a peak in the conductance — a signature of weak antilocalization effects. At higher fields, fluctuations of the conductance are visible, whose amplitude decreases as the temperature is raised. We relate these fluctuations to phase coherent transport in a channel with dimensions comparable to (albeit still larger than) the phase coherence length. Analyzing these magneto-conductance fluctuations within the theory of the universal conductance fluctuations, we estimate a phase coherence length $L_\varphi \sim 130$ nm, in good agreement with the value calculated from the fit of the magneto-conductance curve using the weak localization theory in the presence of spin-orbit interaction.
These results provide clear evidence of the lateral confinement of the electron gas in our bridges exhibiting quantum coherent transport.

1.3 Atomic force microscopy tips based on carbon nanotubes *(P. Paruch)*

Nanoscale studies of (multi)ferroic thin films rely heavily on atomic force microscopy (AFM) techniques. These techniques are based on the varying interaction between the sample and the tip, whose geometry and material properties determine the performance and resolution of the instrument. A key challenge is therefore to improve the tip characteristics, and the outstanding mechanical and electrical properties of carbon nanotubes (CNT) allow them to be considered as ideal AFM topographical probes [9]. Further modification of the CNT can extend the areas of possible application. For instance, magnetic functionalization [10], or SiO_2-rigidification [11, 12] are important for

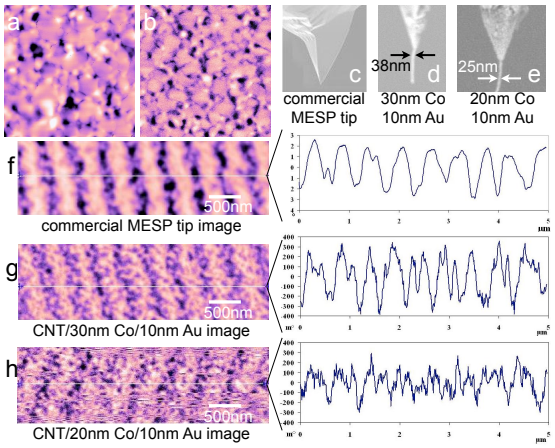

Figure 3: *MFM micrographs of multiferroic $BiFeO_3/CoFe_2O_4$ nanocomposites acquired with (a) commercial or (b) magnetically-coated CNT-AFM probes. Comparing such probes fabricated with different deposition parameters, using magnetic storage tape as a standard test medium, we can see that commercial MESP tips (c) show the highest signal levels, but the lowest resolution (f). All magnetically-coated CNT-AFM tips (d, e) show increased resolution (g, h), with better signal to noise ratios given by a thicker magnetic coating (indicated directly on the figures).*

magnetic (MFM) and piezoresponse force microscopy (PFM) measurements, respectively. The goal of our work is the fabrication of multifunctional CNT tips allowing high-resolution piezoelectric, magnetic and current imaging for the full spectrum of measurements, on ferroelectric and multiferroic thin films.

The tips are fabricated by chemical vapor deposition growth of $2-3$ μm long CNT projecting vertically from the AFM tip. Chemical vapor deposition uses an Fe-hydroxy polymer catalyst or an organic Mo and Fe salt based catalyst, electrophoretically deposited on the apex of standard doped Si probes. After the long CNT are shortened to $100-200$ nm by electrical etching, they show improved topographical resolution compared to standard AFM probes, with the ability to image small and deep structures due to their high aspect ratio. However, these simple CNT-AFM tips are the least stable in electrical measurements, as strong electrostatic effects lead to CNT vibration. For both electrostatic and magnetic measurements, the tips are therefore coated by a thin metal layer (Au, Al, Cr, Ti by e-beam at UniGE, Co and permalloy in collaboration with Jakoba Heidler and Mathias Klaui by molecular beam epitaxy at PSI), which increases the mass of the system, significantly improving its noise response. The tips show significantly better resolution than commercial magnetic (MESP) probes (Fig. 3). For additional protection against oxidation, a further Al or Au coating is applied. For contact measurements, e-beam evaporation of SiO_2 is used to rigidify the tip structure.

2 Carbon based electronics

The investigation of graphene has progressed in different directions. The fabrication of top quality devices, in which graphene is suspended on top of a gate electrode, has been demonstrated. These devices are now used for the investigation of transport in the so far unexplored regime of temperatures below 1 K. Optical spectroscopy studies have focused on large area materials, such as graphite — where agreement of unprecedented quality with band-structure calculations has been achieved — and on epitaxial graphene grown on SiC wafers. Large graphene layers have been grown using chemical vapor deposition techniques. With carbon nanotubes, devices with ferroelectric gates have been used both to investigate transport and to control the ferroelectric polarization on a scale of $\simeq 10$ nm. Finally, a new direction that has emerged is the investigation of the optical and transport properties of nanolayers exfoliated from different metal dichalcogenides, which are particularly suitable to be used in combination with ionic liquid gating techniques.

2.1 Suspended graphene devices *(A. Morpurgo)*

The electronic properties of graphene are strongly affected by the presence of the supporting substrate, which introduces electrostatic potential fluctuations in the material with a magnitude of several tens of meV. The presence of this substrate-induced disorder prevents accessing the physics of electrons at very low energy, close to the charge neutrality point, that is possibly the most interesting regime in graphene for the occurrence of new physical phenomena. Experiments reported over the past two-three years [13, 14, 15] have shown that it is possible to realize graphene devices, in which a graphene layer is suspended from the source and drain electrodes on top of a gate, without being in direct contact with any insulating material. In these suspended graphene devices, disorder is decreased substantially and the carrier mobility increased by over one order of magnitude (reaching values well above 100'000 cm^2/Vs).

During the last year, we have developed the technique to realize suspended graphene structures, and characterized the high quality of the resulting devices. Contrary to most previous

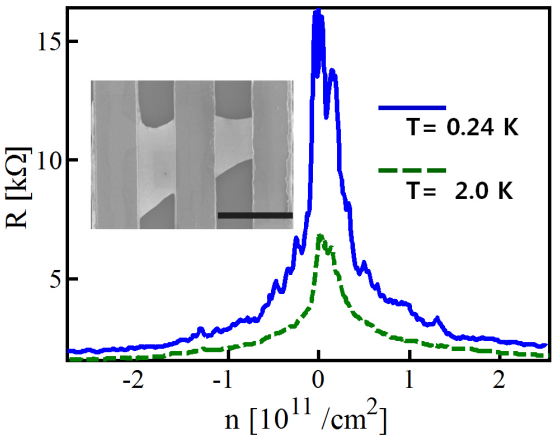

Figure 4: *Resistance of a suspended graphene device versus carrier density, measured at $T = 2$ K (green line) and at $T = 0.24$ K (blue line). The width of the peak is approximately 10^{10} carriers/cm^2, as can be found by plotting the resistance as a function of $\log(n)$. The inset shows a scanning electron micrograph of a suspended graphene device.*

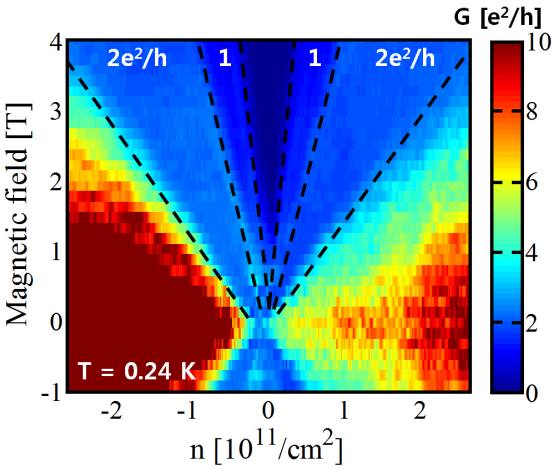

Figure 5: *Fan diagram of Landau level obtained by measuring the conductance of a suspended graphene device as a function of carrier density (i.e. gate voltage) and magnetic field (data taken at 240 mK).*

reports, which employed HF to remove a SiO_2 sacrificial layer, we have employed a technique based on polymeric layers, adapting a process developed at the University of Groningen [16]. In this technique, a graphene layer is placed on an electron sensitive resist (LOR), which can be lithographically patterned and developed away to achieve suspension. This process offers important advantages. First, the solvent used to remove LOR has a much lower surface tension than HF, so that graphene suspension does not require the use of a critical point drier (which is instead necessary when working with HF). Second, while HF rapidly etches many inorganic materials and prevents the use of most metal as contacts, the LOR developer is chemically inert and is compatible with all metal contacts. This is particularly important, for example, to realize suspended devices with superconducting or ferromagnetic electrodes. To achieve high-quality characteristics, the as fabricated devices are normally annealed by passing a large current at low temperature, inside the cryogenic insert used for their measurement (annealing removes residues adsorbed on the graphene surface). After this annealing step, the high quality is demonstrated by electrical measurements. A first indication is the narrow width of the resistance peaks around the charge neutrality point ("Dirac peak", Fig. 4), usually corresponding to 10^{10} carriers/cm^{-2} or better (nearly two orders of magnitude better than for graphene-on-SiO_2 devices). From these data, we can extract a carrier mobility well above 100'000 cm^2/Vs in our devices. Another indication is the observation of quantum Hall effect at magnetic field values as low as $B = 0.2$ T, which is limited by the physical dimensions of the graphene layer studied (normally the contact separation is 1 μm or smaller, to avoid bending of the suspended graphene layer). The high quality of the quantum Hall effect behavior is illustrated in Fig. 5, that shows a so-called fan diagram of the conductance measured in a two-terminal configuration. We are currently extending the fabrication techniques to realize disorder-free suspended graphene devices in combination with local electrostatic gates. In the future, these techniques will be applied also to graphene bilayers.

2.2 Magneto-conductance hysteresis in suspended graphene *(A. Morpurgo)*

Suspended single-layer graphene devices investigated in the course of the last two-three years have led to the observation of ballistic transport [13, 14], fractional quantum Hall effect at rather high temperature ($\simeq$ 10 K) [17, 18], and conductance quantization [19]. So far, the lowest temperature reached in these studies is 1.5 K, and the behavior at temperatures well below 1 K — readily reached using conventional dilution refrigerators or ^{3}He cryostats — remains unknown: the exploration of the transport properties of suspended graphene in this temperature range has been started in this project, using the devices discussed in the previous section. We found that, in a large fraction of the devices studied ($\simeq$ 70%), a clear hysteresis in the magneto-conductance appears below $\simeq$ 1 K (Fig. 6),

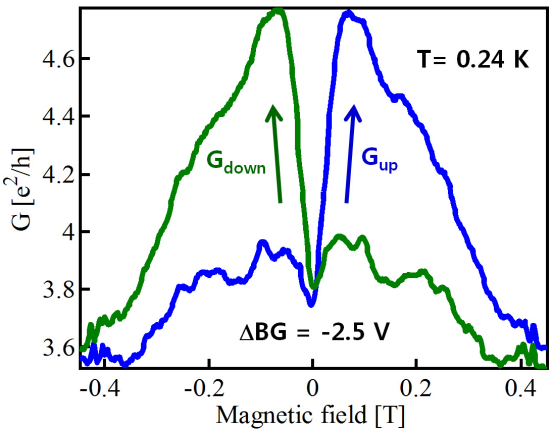

Figure 6: *Hysteresis in the magneto-conductance of a suspended graphene device, measured at 240 mK. The blue line is the result of the measurements performed while sweeping the magnetic field from negative to positive values; for the green line, the magnetic field is swept in the opposite direction.*

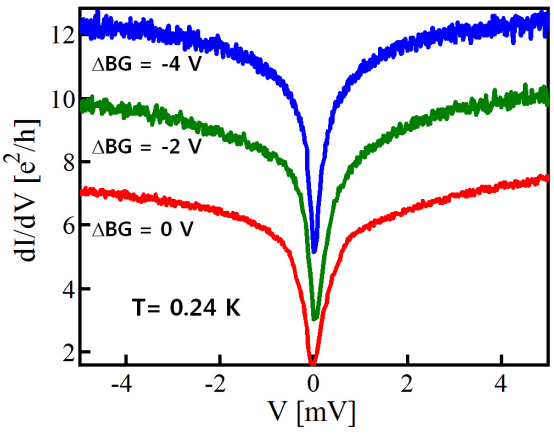

Figure 7: *Low-bias suppression of the differential conductance of suspended graphene devices measured at $T = 240$ mK, for different gate voltages.*

whose generic behavior (response to temperature, magnetic field, bias and gate voltage) is very reproducible whenever the phenomenon is observed. Specifically, the amplitude of the hysteresis ranges from 0.5 to about 1 e^2/h at $T = 240$ mK (depending on the sample), has a maximum at $B \simeq 0.1$ T and decays for larger magnetic fields. The hysteresis disappears above 1 K or when a bias of approximately 70 μeV (corresponding to an electron energy of 1 K) is applied, and it is nearly gate voltage independent, exhibiting a small suppression in the vicinity of the charge neutrality point. In all cases the hysteresis is time dependent, exhibiting an exponential decay with a very long time constant τ: $\tau \simeq 2$ minutes at 240 mK, increasing to $\tau \approx 10$ minutes at 30 mK). The presence of the hysteresis is accompanied by a suppression of the differential conductance at zero bias ($\approx 4\ e^2/h$ at 240 mK, Fig. 7) that occurs on a small bias scale ($\simeq 200 - 300$ μeV, depending on the sample), and that remains unaltered in the entire gate voltage range investigated (corresponding to values of carrier density extending up to $2 \cdot 10^{11}$ cm^{-2}).

Although we have not yet reached a full, detailed microscopic understanding of the phenomena observed, it seems that a most likely explanation — which captures the correct orders of magnitude observed — is related to the presence of rather large spin impurities ($S \simeq 5 - 10$) at edges. These spin-full impurities at the edge are theoretically predicted to form at sequences of zigzag bonds (approximately 3 zigzag bonds lead to a $S = 1/2$ edge spin, according to theory) [20, 21]. To account for the hysteresis, we need to consider that these edge impurities have a magnetic anisotropy due to the intrinsic spin-orbit interaction of graphene (whose magnitude is now theoretically agreed to be $20 - 40$ μeV [22]) that provides an energy barrier for spin-reversal upon inverting the applied magnetic field. This mechanism is similar in spirit to what happens in molecular magnets and the magnitude of the spin-orbit interaction is compatible with the characteristic energy scale of the phenomenon (< 1 K). Charge carriers are affected by the long-range exchange field generated by each of these edge magnetic impurities. The characteristic magnitude of exchange interaction for ≈ 1 μm samples is theoretically estimated to be ≈ 500 μeV [23]. At charge neutrality, this exchange interaction opens a gap, thereby lowering the conductance. We believe that at the carrier density in our experiments, exchange interaction would have a similar effect, thereby explaining the low-bias conductance suppression that we observe in the experiments (with the correct order of magnitude for the bias scale).

2.3 Magneto-optical conductivity of multilayer epitaxial graphene *(D. van der Marel)*

We extracted the diagonal and ac Hall conductivities of multilayer epitaxial graphene on the carbon terminated side of SiC from Faraday rotation and transmission spectra measured in magnetic fields up to 7 T [3]. Optical transitions between individual Landau levels in weakly doped graphene layers and, simultaneously, quasi-classical cyclotron resonance originating from highly doped layers close to the SiC substrate are observed. The Landau level transitions show the expected square root dependence on magnetic field, characteristic for

isolated monolayer graphene, while the quasi-classical cyclotron resonance reveals a linear dependence on B. The ac Hall conductivity additionally probes the sign of the charge carriers, delivering important information, such as the coexistence of electron and hole like charge carriers in weakly doped layers, which have different Fermi velocities. Different contributions to the magneto-optical conductivity are disentangled and analyzed using a phenomenological multi-component cyclotron resonance model revealing an unexpected broad optical absorption background. However, we found that the spectral weights of the Landau level transitions are several times smaller than predicted by theory. The existence of the unexpected optical absorption background is possibly related to this spectral weight anomaly.

2.4 Magneto-optical Kerr rotation spectroscopy in graphite *(D. van der Marel)*

Graphite attracts much attention nowadays as a reference 3D material for graphene. Despite numerous studies appeared after the first observation of the cyclotron effect more than fifty years ago [24], the line shapes and the intensities of the magneto-optical spectrum of graphite are not yet satisfactorily explained. We performed a specific magneto-optical study of graphite, consisting in measuring the infrared magneto-optical Kerr rotation and reflectivity spectra in graphite up to 7 T. This study allows the discrimination of transitions of different electron/hole symmetry. A classical scheme, based on a tight-binding Slonczewski-Weiss-McClure (SWMcC) band model of graphite [25, 26], describes accurately the cyclotron spectra in graphite in a broad range of magnetic fields. Our study reveals the importance to take rigorously into account the c-axis band dispersion and the trigonal warping, which describes the interplane next nearest neighbor hopping. Most importantly, it appears that the second- and the forth-order cyclotron harmonics are optically almost as strong as the fundamental cyclotron resonance even at high fields. This work suggests that same effects are expected to strongly influence the magneto-optical spectra of Bernal stacked multilayer graphene and therefore play a major role in the respective applications.

2.5 Chemical vapor deposition of graphene *(A. Morpurgo and P. Paruch)*

In the course of the past year, in a collaboration between the groups of A. Morpurgo and P. Paruch, we have developed a chemical vapor deposition (CVD) process to grow large graphene single-layers, and to transfer them onto substrates. The technique relies on the decomposition of methane at high temperature on a copper foil substrate acting as a catalyst. After optimization, uniform single-layer graphene can be grown over the entire copper substrate (which currently have a dimension of approximately 1 cm^2). The graphene layer can be transferred onto a substrate by using rather simple techniques involving a polymer support layer and chemical etching of the copper foil. This technique enables the transport properties to be measured to check the quality of the graphene layer. The mobility measured over large areas on devices with SiO_2 as gate insulator was found to reach 500 cm^2/Vs in the best devices (although values between 200 and 300 cm^2/Vs are more commonly found). These values are much smaller than what is seen in small area exfoliated graphene, but correspond to what is reported in the literature for CVD grown graphene of correspondingly large size (large values can be measured in some cases etching the layers to fabricate $\simeq 1$ μm devices). First results indicate that, using Cytop as a gate insulator, significant improvement in the large area mobility can be achieved, with values exceeding 1000 cm^2/Vs. Optimization of the graphene growth and of the device fabrication process is ongoing.

2.6 Nanodevices combining ferroelectric thin films and carbon nanotubes *(P. Paruch)*

Combining ferroelectric thin films with carbon nanotubes (CNT) in a field-effect-transistor-like geometry allows both the control of ferroelectric polarization by the application of highly local electric fields via the CNT, and the modulation of the CNT electronic properties via the ferroelectric field effect [4]. CNT-ferroelectric devices are realized by dispersion of single-walled CNT from suspension in aqueous solution onto $Pb(Zr_{0.2}Ti_{0.8})O_3$ thin films patterned with source and drain electrodes. The films are epitaxially grown on (001) oriented $SrTiO_3$, with $SrRuO_3$ as a back (gate) electrode. In these devices, concentrating on the nanoscale control of polarization switching, we measure domain growth as a function of voltage pulse duration in three different switching geometries, with the source/drain, the CNT, and the metallic AFM tip as electric field sources. The electric fields applied in each case are modeled using *Comsol Multiphysics*, showing an enhanced field intensity at

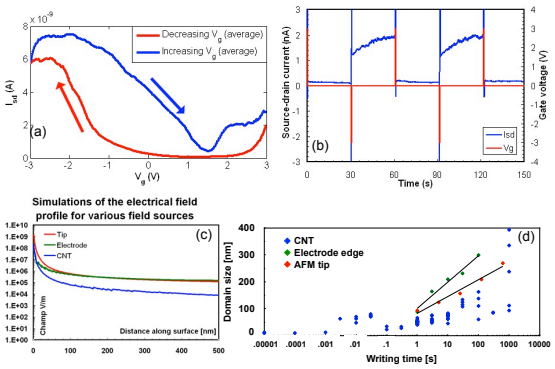

Figure 8: *(a) In devices combining CNT with epitaxial PZT thin films, transconductance measurements with source-drain current I_{SD} as a function of V_G sweeps show clockwise hysteresis. (b) Measurements of source-drain current at zero gate voltage after an applied switching pulse show clear ON and OFF state in the device, controlled by the polarization direction. (c) The out-of-plane component of the electric field, modeled in* Comsol Multiphysics, *for 10 V applied to the AFM tip (in red, opening angle: 40°, radius of apex: 50 nm, tip length: 20 μm), the CNT (in blue, diameter: 2 nm) and the patterned electrode (in red, height: 50 nm), each in contact with a 270 nm thick insulating film with a dielectric constant of 100, on top of a grounded metal electrode. (d) Comparison of domain size as a function of writing time for the three different electric field configurations.*

short distances for the CNT, with a rapid decrease, so that for distances $>$ 50 nm field intensities for the macroscopic electrodes and the AFM tip are higher (Fig. 8c). The observed growth of domains in the three cases shows good agreement with the modeled electric field (Fig. 8d). Importantly, the smallest stable domains observed to switch in the electrical fields applied via an overlying CNT, $\sim$ 20 nm wide in a 270 nm thick PZT film, are significantly smaller than minimum size predicted for stable domains in such films [12]. However, these predictions do not take into account the effects of microscopic disorder, which we have previously shown to pin domain walls, and thus stabilize domain structures in ferroelectric thin films [5].

We also carried out transconductance measurements clearly showing the clockwise hysteresis of the source-drain current as a function of the applied gate voltage (Fig. 8a). The width of the hysteresis window, and its onset in both directions, agree well with polarization-electric field hysteresis measurements in the same films. Additionally, quasi-static measurements of the source-drain current with zero gate voltage after a switching pulse of alternating polarity show the high remanence of the ON and OFF states of the device, in room temperature measurements (Fig. 8b).

2.7 Electric field effect on gated 2D crystals *(D. van der Marel)*

The rise of graphene precipitated a growing interest in two-dimensional or quasi-two-dimensional crystals. The possibility to gate such devices is also of major interest for technological application. The aim of this work is the investigation of exfoliated dichalcogenides and topological insulators by means of transport and optical spectroscopy, as a function of an applied external electric field. Dichalcogenides — such as $NbSe_2$, TaS_2 or WS_2 — are exfoliated using adhesive tape. The resulting flakes are then transferred to a silicon substrate with 300 nm SiO_2 layer on top. Our calculations in Fig. 9, left, show that even a monolayer has a sufficient contrast to be identified under an optical microscope. With standard electron-beam lithography techniques, gold contacts are written on the few layered sample and finally mounted on a chip carrier for resistivity and optical images. An example of a gated $NbSe_2$ quasi-2D crystal is shown in Fig. 9, right.

The main difficulty in the investigation of such kind of samples with infrared spectroscopy techniques is the diffraction limit imposed by light. Samples can be analyzed with help of a FTIR-spectrometer associated with an infrared microscope. Still, the challenge is to identify flakes which are thin enough to be sensible to a gate voltage and has a surface of at least 100 μm^2 to be measured at wave numbers down to 1000 cm^{-1} and carry gold contacts. An example of such a device is shown on Fig. 9, right, which presents one of the smallest measurable samples with this technique.

For transport, a particularly interesting direction that is being pursued is the use of ionic liquid gating techniques, which enable the accumulation of very large density of charge carriers at the surface of these materials. In WS_2 devices, for instance, we succeeded to observe

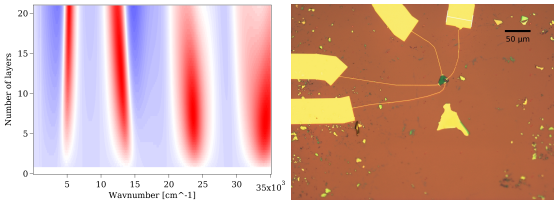

Figure 9: *Left: optical contrast calculations of $NbSe_2$ on a silicon/300 nm SiO_2 substrate over a spectral range. Right: few layered and gated $NbSe_2$ crystal.*

virtually ideal ambipolar transport characteristics, with the ionic liquid gate permitting shifting the position of the Fermi level from deep in the valence band to deep in the conduction gap. In these transistor devices, the excellent electrostatic coupling of the gate to the channel is manifested by the observation of the intrinsic value of the subthreshold slope ($\simeq$ 80 mV/decade, close to the ideal limit of 66 mV/decade at room temperature). As a result of this excellent coupling — and of the very high quality of the crystal used — we find that the shift in gate voltage that is necessary to bring the chemical potential from the top of the valence band to the bottom of the conduction band corresponds to the theoretically expected band-gap of the material with a 5% precision.

3 Theory

A new direction that has emerged — closely related to the work on topological insulators that was started earlier in this project — is the investigation of Majorana fermions. These are elusive particles whose properties have been investigated already long ago in the context of high-energy physics. Although no experimental evidence for the existence of Majorana fermions has been found so far in that context, there are now proposals for their realization in nanoelectronic devices based on superconductors combined with "spin-active" material systems. Also the effect of strong spin-orbit interaction on the superconducting state of two-dimensional superconductors has been investigated in some detail, leading to the prediction of new phenomena in devices where the strength of the spin-orbit interaction can be tuned locally. Finally, the role of dissipative effects on low-dimensional superconductors — which is particularly relevant for experiments — has been investigated in different regimes.

3.1 Scattering theory of chiral Majorana fermion interferometry *(M. Büttiker)*

Majorana fermions are their own antiparticles. They have been the subject of theories for more than seven decades without an experimental signature. However recently it has been suggested that these exotic particles can be discovered in condensed matters systems, in particular in topological superconductors [27, 28]. Topological superconductors are superconducting systems that admit exceptional boundary states — owing to nontrivial topology associated with bulk spectra — inside the

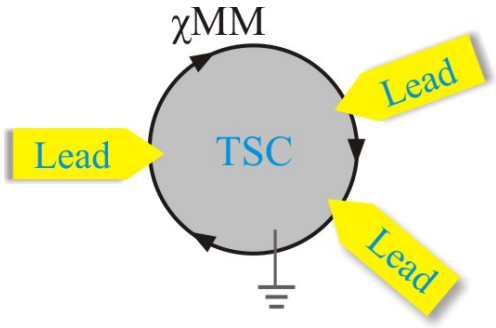

Figure 10: *Schematic picture of a typical chiral Majorana fermion interferometer composed of a chiral Majorana mode (χMM) coupled to one or several normal metal leads. The chiral Majorana mode lives at the edge of the underlying topological superconductor (TSC), which may accommodate a number of vortices in its interior. Majorana fermions traveling in the chiral Majorana mode pick up a phase that encodes (the parity of) the number of vortices, then scatter into normal leads. To generate charge current and noise, Majorana fermions interfere pairwise (after [6]).*

quasiparticle excitation gaps. These exceptional boundary states are coherent superpositions of electrons (particles) and holes (antiparticles) which, upon proper compositions, represent realizations of Majorana states. As one example of topological superconductors, two-dimensional chiral p-wave superconductors [29] are hosts for chiral Majorana modes, which are gapless, charge-neutral edge excitations. Chiral Majorana modes can serve as coherent transmission channels for Majorana fermions, and hence are ideal ingredients for building Majorana fermion interferometers [30, 31, 32, 33].

In order to detect Majorana fermions, to understand how they manifest themselves in laboratories, especially through transport, is a prior task. This question is particularly interesting, besides being important, in view of the peculiar nature of Majorana fermions as particles carrying zero energy and zero charge. In our recent paper [6], we address such a question by investigating the general features of charge transport with (chiral) Majorana fermions based on scattering theory. In particular, we focus on interferometers composed of chiral Majorana fermion modes coupled to normal metal leads (see, e.g., Fig. 10). By employing consistently the Majorana basis in the scattering problem, which treats the electron-hole modes in the normal leads as equivalent (up to a change of basis) Majorana modes, we find that the scattering of Majorana modes appears to be pairwise: only one lead Majorana mode couples to the intrinsic chi-

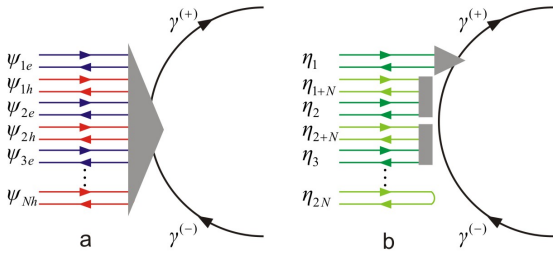

Figure 11: *Illustrations of the scattering at a junction between a multi-mode normal lead and a chiral Majorana mode, in the electron-hole basis for the normal lead (a), and in the properly-chosen Majorana basis (b). In the latter basis, only one Majorana mode in the normal lead is coupled to the chiral Majorana mode, the others are reflected in pairs and one is reflected with amplitude* 1 *(after [6]).*

ral Majorana mode, while the remaining lead Majorana modes are completely reflected but in general mix pairwise (Fig. 11). We further demonstrate that charge current can also be expressed in terms of interference between pairs of Majorana modes. We show through several examples that the above two basic facts lead to elegant treatments and in-depth understanding of current and noise signatures of chiral Majorana fermion interferometry.

Our work [6] emphasizes a scattering approach using a global Majorana basis. As a consequence, from a purely technical particle scattering point of view, Majorana scattering problems are rather similar to scattering problems in normal mesoscopic structures. However, Majorana modes are neutral and carry neither charge nor (electric) current. In contrast to normal scattering problems, the charge and current operators are not diagonal in the Majorana scattering states. Therefore, unlike in normal systems, current is not determined by transmission probabilities of Majorana fermions. We have shown that charge and current appear due to interference of pairs of Majorana modes. For averages of single-particle quantities, like charge and current, to be non-vanishing, interfering Majorana modes must necessarily have originated in the same contact. In contrast, in two-particle quantities, like the current noise, two-particle exchange permits interference of two Majorana particles even if they originate from different leads. The physics of neutral excitations is certainly an important field of future research. It can be expected that the theory of Majorana particles represents an instructive example of this development.

We have also worked in a wider area of mesoscopic physics, and especially renewed our work on the edge states of graphene systems. We have published a review paper on this topic in the Proceedings of the 2010 Nobel Symposium on Graphene and Quantum Matter [7].

3.2 Superconductor-insulator transition in the presence of a dissipative bath *(T. Giamarchi)*

Quantum phase transitions (QPT) and critical phenomena are at the heart of present research in condensed matter physics. One paradigmatic example of a QPT is the superconductor-to-insulator transition (SIT), observed in superconducting films, wires and Josephson-junction arrays, upon the increase of a parameter encoding charging or dissipative effects [34]. Although it has been the focus of intense investigations for more than 25 years, its complete theoretical understanding is still an open subject. In this research project we focus on the SIT occurring in one-dimensional Josephson arrays (1DJJA) [35, 36], and study the interplay between quantum fluctuations, originated in the effective low-dimensionality of the array, and quantum dissipation effects, which arise as a result of the capacitive coupling with a proximate two-dimensional diffusive electron gas (2DDEG) [8]. Physically, the presence of the 2DDEG modifies the electromagnetic environment of the 1DJJA, affecting the properties of the array and introducing dissipation in the dynamics of Cooper pairs. We clarify the role of dissipation in connection with the SIT, and predict a dissipation-tuned SIT, controlled by tuning the electronic density in the 2DDEG (i.e. through applied gate voltages). Interestingly, this idea has been recently confirmed experimentally [37]. Our work could also shed light on the understanding of other 1D superconducting systems (i.e. ultrathin superconducting wires) which have been recently shown to undergo a similar SIT [38].

3.3 Helical superconducting phase on $LaAlO_3/SrTiO_3$ interfaces *(M. Sigrist)*

$LaAlO_3/SrTiO_3$ interfaces provide non-centrosymmetric two-dimensional electron gases whose superconductivity can be tuned by an electric field. It has been shown that also spin-orbit coupling might be strongly field dependent. We model this system as a non-centrosymmetric superconductor including Rashba-type of spin-orbit coupling in order to elucidate the effect of in-plane magnetic fields on the superconducting phase. For such an in-plane magnetic field, superconductivity is limited through paramagnetic depairing as orbital depairing is suppressed by the

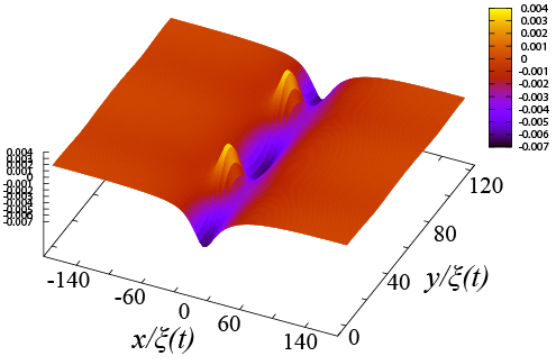

Figure 12: *Flux pattern at the boundary between two half-planes of different spin-orbit coupling strengths for a magnetic field along the x-direction. Positive flux lines compensate the negative magnetic flux on the boundary.*

two-dimensional confinement. The superconducting phase can, however, reduces the paramagnetic depairing effects considerably by escaping into a helical phase, similar to a Fulde-Ferrel state. We show that this leads to inhomogeneous nucleation of superconductivity in an in-plane magnetic field, if the strength of Rashba spin-orbit coupling is spatially modulated. Moreover, such modulations would generate phase frustration effects through inhomogeneous helical phase. One way to reduce frustration is to introduce a magnetic flux pattern inducing fields perpendicular to the applied in-plane field. However, for sufficiently large fields or low temperatures this flux pattern can be "screened" by introducing vortices of opposite field direction as depicted in Fig. 12. It is proposed that such kind of flux pattern might be observed for interfaces with specially designed inhomogeneity in the spin-orbit coupling. A publication of this study is in preparation.

4 Collaborative efforts

Many different collaborative efforts are ongoing. For example, J.-M. Triscone and A. Morpurgo work together to realize nanodevices based on $LaAlO_3/SrTiO_3$ heterostructures; A. Morpurgo and A. Kuzmenko (in van der Marel's group) are jointly developing new activities in the area of ionic liquid gated metal dichalcogenides; P. Paruch and A. Morpurgo have a common project on the chemical vapor deposition of graphene. Many other examples can be easily found. Next to these activities, work on systems with non-trivial topological electronic properties is continuing (the project is carried out by M. Sigrist, D. van der Marel, and A. Morpurgo). In this context, M. Sigrist has developed new theoretical concepts that are relevant for the experimental studies of $LaAlO_3/SrTiO_3$ heterostructures carried out in the group of J.-M. Triscone.

MaNEP-related publications

[1] A. D. Caviglia, S. Gariglio, C. Cancellieri, B. Sacépé, A. Fête, N. Reyren, M. Gabay, A. F. Morpurgo, and J.-M. Triscone, Physical Review Letters **105**, 236802 (2010).

[2] P. Zubko, S. Gariglio, M. Gabay, P. Ghosez, and J.-M. Triscone, Annual Review of Condensed Matter Physics **2**, 141 (2011).

► [3] I. Crassee, J. Levallois, D. van der Marel, A. L. Walter, T. Seyller, and A. B. Kuzmenko, Physical Review B **84**, 035103 (2011).

[4] P. Paruch, A.-B. Posadas, M. Dawber, C. H. Ahn, and P. L. McEuen, Applied Physics Letters **93**, 132901 (2008).

[5] P. Paruch, T. Giamarchi, T. Tybell, and J.-M. Triscone, Journal of Applied Physics **100**, 051608 (2006).

► [6] J. Li, G. Fleury, and M. Büttiker, arXiv:1202.1018 (2012).

► [7] J. Li, I. Martin, M. Büttiker, and A. F. Morpurgo, Physica Scripta **T146**, 014021 (2012).

► [8] A. M. Lobos and T. Giamarchi, Physical Review B **84**, 024523 (2011).

Other references

[9] H. Dai, J. H. Hafner, A. G. Rinzler, D. T. Colbert, and R. E. Smalley, Nature **384**, 147 (1996).

[10] H. Kuramochi, T. Uzumaki, M. Yasutake, A. Tanaka, H. Akinaga, and H. Yokoyama, Nanotechnology **16**, 24 (2005).

[11] N. Tayebi, Y. Narui, R. J. Chen, C. P. Collier, K. P. Giapis, and Y. Zhang, Applied Physics Letters **93**, 103112 (2008).

[12] N. Tayebi, Y. Narui, N. Franklin, C. P. Collier, K. P. Giapis, Y. Nishi, and Y. Zhang, Applied Physics Letters **96**, 023103 (2010).

[13] K. I. Bolotin, K. J. Sikes, Z. Jiang, K. M., G. Fudenberg, J. Hone, P. Kim, and H. L. Stormer, Solid State Communications **146**, 351 (2008).

[14] X. Du, I. Skachko, A. Barker, and E. Y. Andrei, Nature Nanotechnology **3**, 491 (2008).

[15] R. T. Weitz, M. T. Allen, B. E. Feldman, J. Martin, and A. Yacoby, Science **330**, 812 (2010).

[16] N. Tombros, A. Veligura, J. Junesch, J. J. van den Berg, P. J. Zomer, M. Wojtaszek, I. J. Vera Marun, H. T. Jonkman, and B. J. van Wees, Journal of Applied Physics **109**, 093702 (2011).

[17] K. I. Bolotin, F. Ghahari, M. D. Shulman, H. L. Stormer, and P. Kim, Nature **462**, 196 (2009).

[18] X. Du, I. Skachko, F. Duerr, A. Luican, and E. Y. Andrei, Nature **462**, 192 (2009).

[19] N. Tombros, A. Veligura, J. Junesch, M. H. Guimarães, I. J. Vera-Marun, H. T. Jonkman, and B. J. van Wees, Nature Physics **7**, 697 (2011).

[20] Y.-W. Son, M. L. Cohen, and S. G. Louie, Nature **444**, 347 (2006).

[21] M. Wimmer, I. Adagideli, S. Berber, D. Tománek, and K. Richter, Physical Review Letters **100**, 177207 (2008).

[22] S. Konschuh, M. Gmitra, and J. Fabian, Physical Review B **82**, 245412 (2010).

[23] Y.-W. Son, M. L. Cohen, and S. G. Louie, Physical Review Letters **97**, 216803 (2006).

[24] J. K. Galt, W. A. Yager, and H. W. Dail Jr., Physical Review **103**, 1586 (1956).

[25] J. W. McClure, Physical Review **108**, 612 (1957).

[26] J. C. Slonczewski and P. R. Weiss, Physical Review **109**, 272 (1958).

[27] A. Y. Kitaev, Uspekhi Fizicheskikh Nauk **44**, 131 (2001).

[28] X. Qi and S. Zhang, Reviews of Modern Physics **83**, 1057 (2011).

[29] N. Read and D. Green, Physical Review B **61**, 10267 (2000).

[30] L. Fu and C. L. Kane, Physical Review Letters **102**, 216403 (2009).

[31] A. R. Akhmerov, J. Nilsson, and C. W. J. Beenakker, Physical Review Letters **102**, 216404 (2009).

[32] K. T. Law, P. A. Lee, and T. K. Ng, Physical Review Letters **103**, 237001 (2009).

[33] G. Strübi, W. Belzig, M. Choi, and C. Bruder, Physical Review Letters **107**, 136403 (2011).

[34] D. B. Haviland, Y. Liu, and A. M. Goldman, Physical Review Letters **62**, 2180 (1989).

[35] E. Chow, P. Delsing, and D. B. Haviland, Physical Review Letters **81**, 204 (1998).

[36] Y. Takahide, R. Yagi, A. Kanda, Y. Ootuka, and S.-i. Kobayashi, Physical Review Letters **85**, 1974 (2000).

[37] I. L. Ho, W. Kuo, S. D. Lin, C. P. Lee, C. T. Liang, C. S. Wu, and C. D. Chen, Europhysics Letters **96**, 47004 (2001).

[38] A. Bezryadin, Journal of Physics: Condensed Matter **20**, 043202 (2008).

Project 3 Electronic materials for energy systems and other applications

Project leader: Ø. Fischer (UniGE)

Participating members: M. Abplanalp (ABB), Ph. Aebi (UniFR), J. Cors (UniGE and Phasis), M. Decroux (UniGE), D. Eckert (Bruker BioSpin), Ø. Fischer (UniGE), R. Flükiger (UniGE), J. Hulliger (UniBE), M. Kenzelmann (PSI), G. Patzke (UniZH), C. Renner (UniGE), N. de Rooij (EPFL), C. Senatore (UniGE), G. Triscone (Hepia), J.-M. Triscone (UniGE), A. Weidenkaff (Empa and UniBE), K. Yvon (UniGE)

Introduction: The long term vision of MaNEP is that research in this field shall have a key impact on the technological development in the 21st century. Because of the long-term view, most of MaNEP's research is of basic nature, but certain applications can already be developed. Over the years MaNEP's portfolio of applied projects has grown and Project 3 represents a broad approach to this end with twelve different subprojects and with the participation of seven companies.

Summary and highlights

Five areas are covered by this project.

1. Applied superconductivity

On a first side, in a collaboration with CERN and the company Bruker BioSpin, the group of R. Flükiger and C. Senatore (UniGE) is investigating superconducting materials and wires for high magnetic field applications. On another side, the group of M. Decroux (UniGE) has continued their collaboration with the company ABB in view of improving the performances of thin film coated conductors for superconducting fault current limiters.

Powder in tube (PIT) Nb_3Sn wires for high-field ($\geqslant$ 15 T) accelerator magnets Further developments of high-performance Nb_3Sn wires require a deep understanding of the interplay between heat treatment conditions and superconducting parameters (T_c, B_{c2}). To this purpose we determined the calorimetric T_c and B_{c2} distributions for PIT wires submitted to different heat treatments and related the results to the grain morphology of the Nb-Sn layer. Another subject of interest is the investigation of the electromechanical properties for PIT wires, in view of application to accelerator magnets. To this end we developed a new probe for measuring the critical current as a function of the transverse force, the objective being the simulation of the mechanical loads for wires operating in a Rutherford cable.

Densification of industrial lengths of in situ *MgB_2 wires and enhancement of J_c* The process for the densification of industrial lengths of MgB_2 wires was successfully implemented. Presently, up to 300 m can be densified in a day, but rates of $>$ 1 km/day appear as possible. Densification was also applied to multifilamentary MgB_2 wires, leading again to a strong enhancement of the transport J_c.

Vortex dynamics in $FeTe_{0.7}Se_{0.3}$ An extensive investigation of the vortex dynamics in single-crystals of $FeTe_{0.7}Se_{0.3}$ has been performed. We obtained new insights into the mechanisms behind the second peak in the magnetization curve (see Project 4).

Superconducting fault current limiters (SFCL) A new technique able to measure the thermal conductance of the superconducting layer/substrate interface in coated conductors has been set up. In this method a line is heated by an ac current and its temperature is measured as a function of the frequency. A theoretical model has been developed to simulate the experimental data. The data are very well fitted by the model with an interface thermal conductance of 280 W/Kcm^2. We have also developed a modeling of the quench propagation in coated conductors by an hybrid numerical and analytical approach.

2. Oxides for energy harvesting

In this subproject we follow two different routes. Part 1: mechanical energy transformed by piezoelectric devices (collaboration between the groups of N. de Rooij (EPFL) and J.-M. Triscone (UniGE)), and part 2: thermal energy harvested by thermoelectric materials (group of A. Weidenkaff, Empa, in collaboration with Ph. Aebi (UniFR) and J. Hulliger (UniBE)).

In the first part, the development of energy autonomous systems powered by piezoelectric

MEMS energy harvesters is in progress. Here we report on the advances made in implementing both resonant- and impact-type piezoelectric harvesters into system demonstrators.

In the second part, we have investigated transition metal oxides and half-Heusler intermetallics. This is of great importance in order to design improved thermoelectric materials. Tuning the band structure of $EuTiO_3$ by 2% Nb substitution at Ti site increased the density of states at the Fermi level. The maximum figure of merit obtained is $ZT \approx 0.4$ at 1040 K for $EuTi_{0.98}Nb_{0.02}O_3$. Fermi level band-structure and thermoelectric transport properties of layered cobaltites are strongly influenced by the oxygen excess in the lattice. A higher oxygen content significantly improves the electrical conductivity σ. Half-Heusler compounds are promising thermoelectrics. Investigations on TiNiSn-based materials show good results for $Hf_{0.26}Zr_{0.37}Ti_{0.37}NiSn$ with a ZT value of 1.0 at 700 K.

3. Applications of artificial superlattices

In this subproject we have worked on two different areas this year. On the one hand we have continued the collaboration between M. Kenzelmann (PSI) and the company SwissNeutronics to develop supermirrors and focusing devices for neutron beams. On the second hand we have been active is the one of ferroelectric superlattices, in the group of J.-M. Triscone.

Neutron focusing devices have been further developed in our research this year. The purpose of such devices is to focus intense neutron beams onto small areas, allowing the study of small samples using neutron scattering. We identified the most promising technology for this development and determined the precision requirements for the design of test devices which will be used in real experiments in the near future.

Ferroelectric materials have already numerous applications and they have the potential for much more. The basic idea of this project is to develop a method to tune the properties by making artificial multilayer. This is achieved by precise control of the thickness of the individual layers. We have demonstrated that in $PbTiO_3/SrTiO_3$ system a large range of permittivities can be obtained simply by changing the individual thicknesses of the ferroelectric and the paraelectric layers by a few unit cells. Such materials may find applications as variable capacitors, in voltage-controlled oscillators or in rf filters.

4. Hydrogen detectors and other sensors

We have here followed four different routes to develop new sensors based on materials with special properties: (a) selective hydrogen detectors based on the metal insulator transition occurring in intermetallic hydrides in a collaboration between Swatch Group R&D SA, Division Asulab and the groups of K. Yvon, J. Cors and Ø. Fischer (UniGE); (b) new Bi- and Mo- based sensor materials in the group of G. Patzke (UniZH); (c) electrochemical sensors in the group of J. Cors and Ø. Fischer (UniGE); (d) piezoresistive strain transducers in the group of Ch. Renner (UniGE).

The aim is to develop a cheap and selective hydrogen detector based on the hydrogen-induced metal insulator transition in the $LaMg_2PdH_x$ system. Thin films of intermetallic $LaMg_2Pd$ were deposited by sputtering and investigated with respect to their electric resistance response during exposure to hydrogen and other gases. The response of the films to hydrogen is relatively rapid, the reproducibility of the signal is good, and the drift is relatively small. The film's sensitivity to hydrogen meets the 0.5% target for detecting hydrogen. At higher hydrogen concentrations, both in oxygen and air, the resistance response is proportional to the partial hydrogen pressure, thus opening the way to a hydrogen sensor.

New Bi- and Mo-based sensor materials have been further investigated. We continued our structure-activity investigations into hydrothermally synthesized gas and humidity sensors. The promising ammonia sensing properties of a series of channel-based hexagonal molybdates with alkali cations incorporated as stabilizers are discussed for the K^+-containing representative, which excels through good operating temperature and high ammonia sensitivity in comparison with other reducing gases. Concerning humidity sensor development, we extended our investigations on Bi-based materials into the Bi/P/O-system. This brought forward the structurally flexible cubic sillenite-type of bismuth phosphate as a new and tuneable humidity sensor prototype.

Electrochemical sensors for the measurement of the oxygen content in liquids have been further improved and a record resolution of 0.2 ppb of oxygen partial pressure has been

achieved. A prototype sensor has been constructed. Tests are planned in brewing industry (liquids) and in a helium purification station (gas phase measurements).

Piezoresistive strain transducers have been thoroughly investigated. This project is aiming at developing a MEMS compatible piezoresistive strain transducer, capable of monitoring minute silicon cantilever bending as observed, for example, in atomic force microscopy. Our efforts have led to unexpected insight into the transport properties of strained silicon. We have not yet succeeded in building a MEMS compatible strain gauge, but will discuss another idea to obtain a strain transducer with sufficient sensitivity for MEMS applications.

5. New surface treatments for microcomponents

The basic idea of the research in this subproject is to exploit our technical knowledge in scanning tunneling microscopy and thin films to develop two new transfer projects: (a) marking technology for watch components as a collaboration between the watch manufacturers Vacheron Constantin, the start-up Phasis and the groups of J. Cors, Ø. Fischer and J.-M. Triscone (UniGE) and (b) Cut-and-coat process by wire-EDM as a collaboration between the company AGIECharmilles +GF+ and the group of J. Cors and Ø. Fischer (UniGE).

The marking technology is presently pursued, the precision of the marking process has been improved, and the team is presently developing a technique for an improved marking of the "Hallmark of Geneva" for high-quality watches.

The aim of the Cut-and-coat project is to provide AGIECharmilles with a technology to allow the company to enter the market for coated metal parts. Reliable coating technologies have been elaborated and target applications in the current AGIECharmilles market have been identified.

1 Applied superconductivity

1.1 High-performance Nb_3Sn for the next generation of accelerator magnets *(R. Flükiger, C. Senatore, D. Eckert; Bruker BioSpin)*

a) *Calorimetric T_c distribution* High-performance powder in tube (PIT) Nb_3Sn wires are among the most promising candidates for the next generation of high-field accelerator magnets at CERN. We have investigated the influence of the heat treatment conditions on the superconducting properties of these wires, focusing on the commonly used reaction schedule (675°C/84 h) and on an optimized heat treatment (625°C/320 h), which leads to a critical current increase of $\sim$ 10% [1]. The reaction process determines the morphology of the Nb_3Sn layer in PIT conductors, leading to a layer of large ($\sim$ 1 μm in size) Nb-Sn grains enclosed in a layer of fine (150 – 200 nm in size) Nb-Sn grains. From the field dependence of the T_c distribution we concluded that the competition between reaction kinetics and thermodynamic equilibrium induces marked differences in T_c and B_{c2} between the fine grain and the large grain regions. In particular, we showed that the wire reacted at 625°C/320 h exhibits two separated contributions in the T_c distribution directly related to the grain morphology of the Nb-Sn layer: a narrow peak, determined by the large grains, with a higher onset T_c and a broad peak due to the fine grains (Fig. 1) [2]. The two peaks tend to merge as the external magnetic field is increased. This indicates that a higher B_{c2} is achieved in the fine grain region, despite the lower average T_c.

b) *Critical current response under transverse stress* Modern high-performance Nb_3Sn wires are characterized by extremely high critical current I_c but also by reduced strain tolerance. In particular it is known that the critical current of PIT Nb_3Sn conductors shows

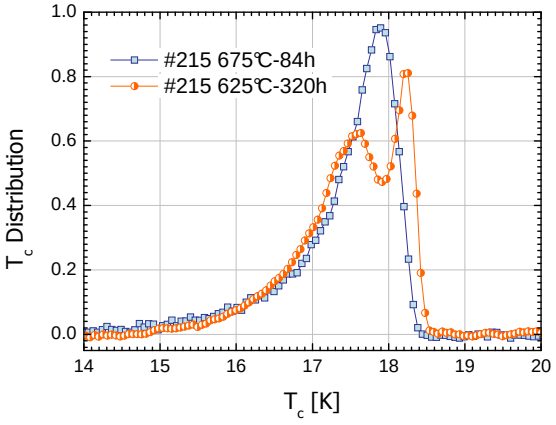

Figure 1: *Distribution of T_c for a PIT wire, after reaction at 675°C for 84 h (squares) and at 625°C for 320 h (circles). Two peaks are present in the T_c distribution of the wire reacted at 625°C/320 h.*

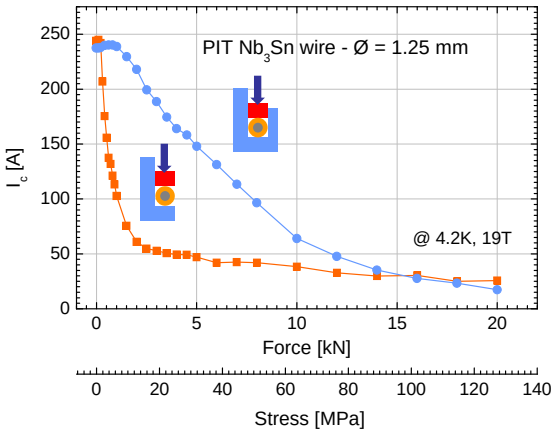

Figure 2: *Critical current as a function of the transverse stress for a PIT Nb_3Sn wire in the case of compression between two parallel plates (squares) and compression in a U-shaped anvil (circles).*

a dramatically decrease when a transverse compressive force is applied. In the past years we have developed a transverse compression probe that allows the measurement of I_c under a force perpendicular to the wire. In this probe, the sample is mounted between two parallel stainless steel plates and is free to move perpendicularly to the applied force. This condition is relatively far from reality in a superconducting cable, as it represents the extreme case of crossing wires (contact pressure) with no impregnation. In the meantime, we have developed a new measurement head: in the new geometry the wire fits into a groove and cannot move perpendicularly to the applied force (U-shaped anvil), the objective being to simulate the configuration of a wire in a Rutherford cable, geometrically confined by the neighboring wires. A comparison between the two different freedoms of deformation was performed for a multifilamentary PIT wire, developed by Bruker-EAS within the frame of the FP7 EuCARD project. The critical current was measured as a function of the transverse compressive force (up to 20 kN, $\sim$ 130 MPa) with an applied magnetic field of 19 T at 4.2 K. As shown in Fig. 2, the stress dependence of I_c is less pronounced when transverse compression is applied in a U-shaped anvil. In addition a higher limit for the irreversible I_c degradation is observed.

1.2 Densification of industrial lengths of *in situ* MgB_2 wires *(R. Flükiger, C. Senatore, D. Eckert; Bruker BioSpin)*

A new route for enhancing the mass density in the filaments of *in situ* MgB_2 wires has been developed during the last years at UniGE: the cold high pressure densification (CHPD). The CHPD technique has led to a strong improvement of the in-field critical current density (J_c), by a factor of $>$ 2 at 4.2 K and by $>$ 4 at 20 K. The enhancement at 20 K is of particular importance, since there is a market for cryogen-free applications at 20 K. Examples of such applications are a growing number of MRI systems, the link project for LHC upgrade at CERN, and possibly even eolic generators. The ultimate goal of the present project was the densification of industrial lengths of MgB_2 wires. This objective was achieved thanks to a new machine for sequential densification, which was built in collaboration with the company Heftec in Oberurnen. Presently, up to 300 m can be densified in a day, but rates of more than 1 km/day appear as possible. The positive effect of densification on J_c was also observed in multifilamentary MgB_2 wires [3]. It is remarkable that the filaments are still well separated from each other after densification, which is the most important requirement for the industrial use. This project was especially supported by the SNSF *economic stimulus packages*.

1.3 Vortex dynamics in $FeTe_{0.7}Se_{0.3}$ *(R. Flükiger, C. Senatore, D. Eckert; Bruker BioSpin)*

We explored the vortex phase diagram of $FeTe_{0.7}Se_{0.3}$ crystals prepared in the group of E. Giannini, with the purpose of investigating the basic physics of the vortex matter as well as for evaluating the perspectives of this new material for practical applications. Details about the results are presented in Project 4.

1.4 Superconducting fault current limiters *(M. Decroux, M. Abplanalp; ABB)*

a) *Measurement of the interface thermal conductance* To be able to simulate the quench propagation in coated conductors (CC) it is important to measure its thermal behavior. To measure the interface thermal conductance, we have developed a new technique in which a resistive line is heated by an ac current. The oscillation of the temperature, deduced from its resistance, is measured as a function of the frequency of the current. To fit the frequency dependence of this temperature, we have developed a theoretical model in which the CC is represented by three elements. The first element is the heater (heated by the ac current). The second is the part of the substrate which is penetrated by the heat. The third element is the unheated part of the substrate which is

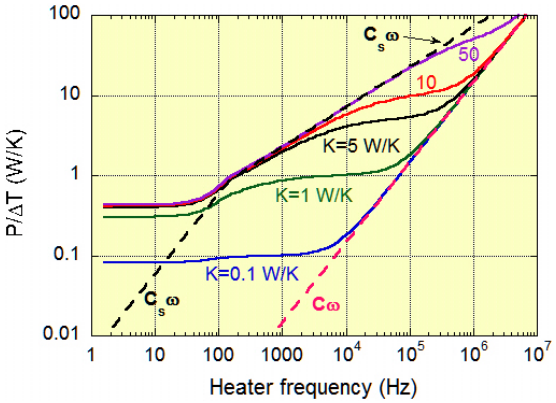

Figure 3: *Simulation of $P/\Delta T$ versus the heat frequency. P is the power generated in the resistive line.*

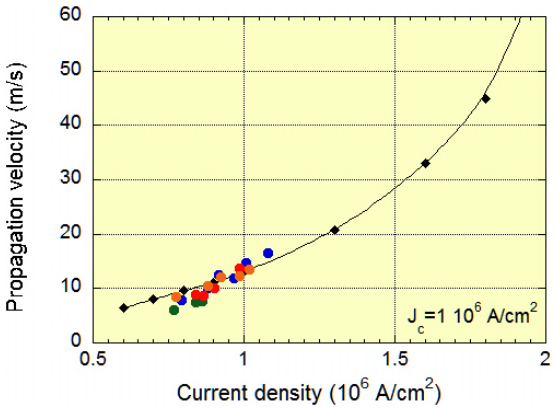

Figure 5: *Simulation and experimental data of the propagation velocities of the normal zone in coated conductors versus the current density.*

considered as a thermal bath. All the elements are connected by a thermal conductance K. The simulation of the temperature of the resistive line for different values of the interface thermal conductance is presented in Fig. 3.
Our simple theoretical model predicts that at low and high frequencies the temperature oscillation is related to the heat capacity C_s of the substrate and of the superconducting line C, respectively. However at intermediate frequencies a plateau is predicted which is related to the thermal conductance K of the superconducting/substrate interface. To measure the frequency dependence of the heater temperature we have built a dedicated probe. It allows measuring sample in vacuum from $T = 77$ K to room temperature. The experimental results and their simulation are shown on Fig. 4 [4].
The simulated curve fits very well the experimental data down to 130 Hz with the thermal conductance as the only free parameter. The best fit is obtained for $K = 280$ W/Kcm^2. This is the first report of the interface conductance in coated conductors. Below 130 Hz the experimental data follow $C_s\omega$. Indeed at these frequencies the thermal penetration depth is longer than the whole thickness of the substrate and the temperature of the heater is related to the heat capacity C_s of the Hastelloy.

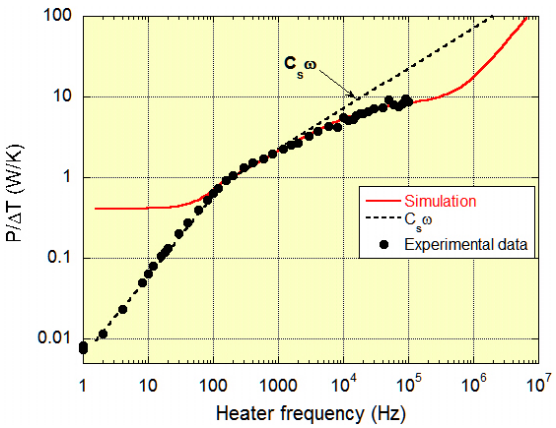

Figure 4: *$P/\Delta T$ versus the heat frequency.*

b) *Modeling of the quench propagation in coated conductors* We have developed a modeling of the quench propagation velocities in CC using our experimental values of the thermal conductance as an input parameter [5]. The calculations are performed by an hybrid numerical and analytical approach. A finite element method program is calculating the thermal behavior of the layers while an analytical function evaluates the local heat dissipation. Fig. 5 shows that the simulated quench propagation velocities versus the current density are in good agreement with the experimental data without using any adjustable parameter.
The better understanding of the CC behavior, based on our extensive characterization and modeling work, will lead to set up an adapted CC architecture for fault current limiter applications.

2 Oxides for energy harvesting

2.1 Realization of an energy harvesting demonstrator based on piezoelectric materials *(N. de Rooij, J.-M. Triscone, G. Triscone)*

a) *Autonomous wireless sensor node powered by piezoelectric energy harvesting* Within this report we demonstrate an autonomous wireless sensor system that is powered by piezoelectric energy harvesting. The wireless sensor node proposed in this work has been implemented by EPFL-ESPLAB to demonstrate the feasibility of UWB-IR technology applied to indoor positioning. It consists of three modules:

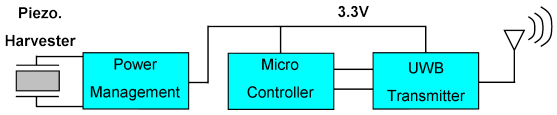

Figure 6: *System flow diagram of an autonomous wireless sensor node.*

a power management unit (PMU), a microcontroller unit (MCU) and an ultrawide band transmitter (UWB-Tx). To create an energy autonomous system, the piezoelectric harvester is directly connected to the sensor node through the PMU (Fig. 6) which is used to convert the ac input voltage from the piezoelectric transducer into a regulated dc voltage capable of powering both the MCU and the UWB-Tx module.
To reach the minimum power requirement of the PMU, an output voltage of 5.3 V_{rms} needs to be generated by the piezoelectric harvester. Our initial prototype of the piezoelectric harvester produced an open circuit voltage of 5.5 V_{rms} when excited at 4.4 ms^{-2} (0.45 g). A peak power of 54 μW was measured across an optimal load of 218 kΩ at 160 Hz. Our results demonstrate that the power generated from the piezoelectric harvester is sufficient to enable periodic transmission of the UWB transmitter.

b) *Proof of concept of an impact-type piezoelectric harvester in watches* The concept of the proposed system in this work consists of a piezoelectric harvester positioned above a gear driven by an inertial mass system in order to keep the system as compact as possible. The piezoelectric harvester is coupled to the gear through a point at the free end of the cantilever as shown in Fig. 7 (AFM-like design). The feasibility of this concept has been demonstrated using an electric motor in place of the inertial mass. As the gear rotates, the piezoelectric harvester is set into motion by the impact between the gear teeth and the tip of cantilever. Consequently, a portion of kinetic energy of the rotating gear is converted to electrical energy through the impact with the piezoelectric structure as demonstrated in [6].

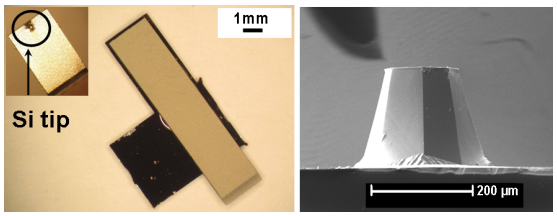

Figure 7: *Left: optical images of a PZT/Silicon cantilever. Right: SEM image obtained from the silicon tip (height of 240 μm.*

Further design and optimization of the MEMS harvester and system architecture are currently being investigated to increase the output power and reliability of the device, while optimizing its compactness. The next step will be to the implementation of this concept in an adapted watch mechanism with an oscillating mass-gear system in order to demonstrate a complete system.

2.2 Development and characterization of unconventional thermoelectric materials *(A. Weidenkaff, Ph. Aebi, J. Hulliger)*

The most extensively studied thermoelectric materials have been the chalcogenides due to their high power factor. However, there is a need of finding new families of materials which are naturally abundant, cheap and stable at high temperatures. Our interest has been focused on perovskite-type titanium oxides, layered cobalt oxides and half-Heusler intermetallics.

a) *Layered cobalt oxides* Among the transition-metal oxide materials, layered cobalt oxides (p-type) present unconventionally high values of thermoelectric power (Seebeck) coefficient S as compared to their electrical resistivity ρ. Typical values for the thermoelectric figure of merit ($ZT = (S^2T)/(\rho\kappa)$), with κ the thermal conductivity, range within $0.1 < ZT < 0.4$ [7]. However, some materials prepared with a high crystal alignment have been reported even with ZT approaching 0.9 [17] at high temperatures ($T > 1000$ K). The main reason for the high thermoelectric performance is understood as due to a "boost" in the charge-carrier entropy as a consequence of an elevated spin entropy, provided by a formally four-valent cobalt species embedded among essentially two-dimensional matrix of trivalent cobalt species [18].
The strong influence of the oxygen content on the thermoelectric properties of layered cobalt oxides was observed through a series of $Ca_{3-x}Bi_xCo_4O_{9+\delta}$ ($0 < x < 0.20$) samples, synthesized and post-annealed at 973 K in air and Ar atmospheres [8]. The annealing temperature was adjusted to be the highest where $Ca_{3-x}Bi_xCo_4O_{9+\delta}$ under Ar atmosphere still maintained it's original crystal phase. Oxygen-content analysis pointed out that the Ar-annealed samples contained less oxygen, and, unlike the air-annealed samples, showed a systematically decreasing total oxygen content with increasing x.
The thermoelectric properties were determined under the respective annealing atmospheres in

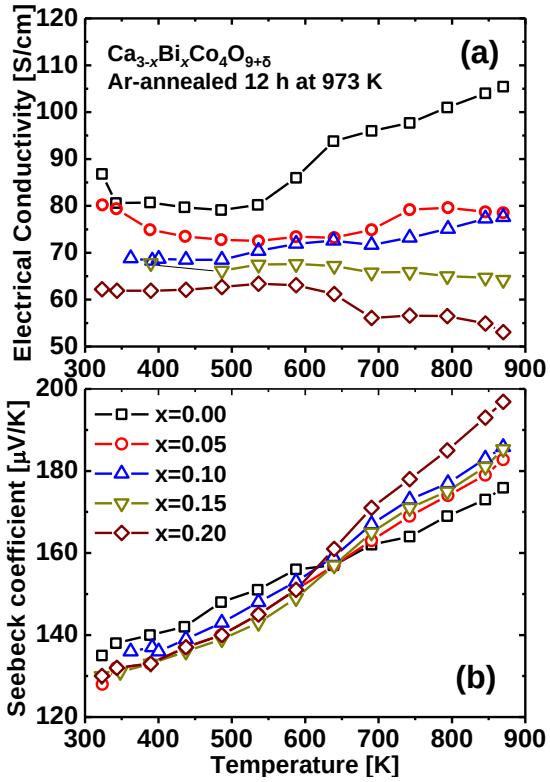

Figure 8: *(a) Electrical conductivity (b) Seebeck coefficient of $Ca_{3-x}Bi_xCo_4O_{9+\delta}$ samples pre-annealed and measured in argon atmosphere.*

order to discriminate between the influences of the Bi substitution and the oxygen content on the S (Fig. 8b) and the electrical conductivity σ (Fig. 8a). While no systematic evolution in the transport properties with substitution was observed with air-annealed samples, clear trends for both σ and S were found for the Ar-annealed samples. Oxygen has a strong influence on σ, which is strongly lowered by oxygen depletion. Bi-substitution reduces σ but also provides a semiconductor to metal transition into the $\sigma(T)$ behavior. The lowest values of ZT were obtained for $x = 0$, which showed no significant difference between the two preparation atmospheres, reaching $ZT_{870\ K} = 0.12$, whereas the Bi-substituted samples exhibit a pronounced dependence on the atmosphere throughout the measured temperature range. For $x = 0.20$ a $ZT_{870\ K} = 0.19$ (air) and $ZT_{870\ K} = 0.15$ (Ar) were obtained.

b) *$EuTiO_3$* The study of highly porous polycrystalline $EuTiO_3$ (n-type) has shown good thermoelectric performance with one of the highest power factors known for oxides (10^{-4} W/K^{2}m at 1000 K) and a low thermal conductivity κ. The valence band X-ray photoelectron (XPS) spectrum shows that the shape of the electron density of states is favorable for

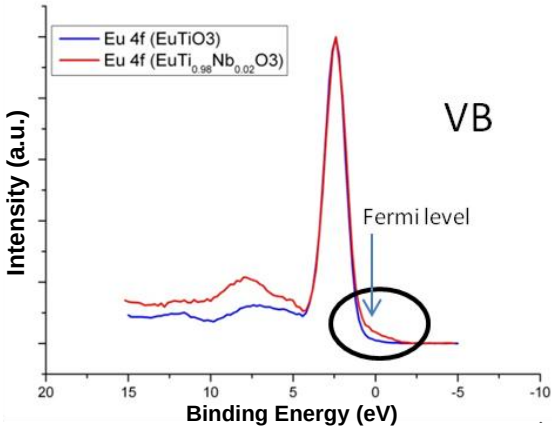

Figure 9: *XPS valence band spectra of $EuTiO_3$ and $EuTi_{0.98}Nb_{0.02}O_3$.*

a high S (Fig. 9) [19].
Substituting 2% Nb at Ti site introduces defect states at the Fermi level (Fig. 9) leading to a decrease in the ρ from $\rho(EuTiO_3)$ = 2.778 Ωm to $\rho(EuTi_{0.98}Nb_{0.02}O_3)$ = 0.084 Ωm, at room temperature. The calculated figure of merit for $EuTi_{0.98}Nb_{0.02}O_3$ is $ZT \approx 0.4$ at 1040 K, and $ZT \approx 0.3$ for $EuTiO_3$.
The study of a 100% dense sample, grown by floating zone method, has been performed for comparison and for a deeper understanding of the influence of porosity on the transport mechanism.

c) *Oxynitrides* Oxynitrides have a reduced band gap in comparison with the corresponding oxides. The N 2p levels are energetically higher than the O 2p levels, leading to a modified electronic structure at the valence band, with a decreased band gap [20]. The thermoelectric properties of polycrystalline $EuTiO_xN_y$ and $EuTi_{0.98}Nb_{0.02}O_xN_y$ have been investigated.

d) *Sample preparation for photoemission spectroscopy studies* Experimental data regarding the electronic band structures close to the Fermi level and their influence to the transport properties is desirable, in order to understand and improve the feasible properties. Photoemission spectroscopy (PES) is a technique of choice. With a probing depth of just few angstroms PES observation is highly surface sensitive. Therefore in order to retrieve bulk-related information, freshly cleaved and adsorbate-clean surfaces are required.
The as grown oxide crystals have appeared to suffer from carbonaceous surface contamination. Effective cleaning procedures are needed in order to produce surfaces for PES observations. By using O^+ plasma exposures,

the amorphous carbonaceous residual on the surface of the $Ca_3Co_4O_9$ crystal grown in a KCl/K_2CO_3-flux may be cleaned off to the point where the hexagonal atomic ordering of the sample surface is revealed. Furthermore, as was stated in our last year report, it turned out, that the band-structure near the Fermi level on the crystal surface may be reversibly shifted through subsequent O^+ and H^+ plasma exposures. This is in good correlation with our recent results on polycrystalline $Ca_{1-x}Bi_xCo_4O_{9+\delta}$ bulk materials [8].
Additionally, oxygen annealing has been tested for cleaning the surfaces of the KCl/K_2CO_3-flux-grown $K_{0.5}CoO_2$ [21] and traveling float zone grown $EuTiO_3$ [22] crystals. In the latter case a combination of sputtering with annealing was tried. Independent of the growth technique, both crystal surfaces appear to be heavily carbon contaminated. Few-hour treatments under several annealing pressures and temperatures were applied. It turned out that the carbon-free surface of an as annealed sample no more possesses a proper long-range order. Recently, we have also initiated experiments with carbon cleaning procedure based on O_3 (ozone) application.

e) *Half-Heusler intermetallics as thermoelectrics*
Half-Heusler compounds are ternary intermetallic materials with 1:1:1 stoichiometry. Their crystal structure resembles the non-centrosymmetric $MnCu_2Al$ ($L2_1$) type cubic Heusler structure with half of the Cu-site atoms missing. Heusler materials have drawn a huge attention due to their diverse properties and applications, namely half-metallic ferromagnetism, magneto-optic and magneto-mechanic applications, superconductivity, semiconductivity, heavy fermion behavior and topological insulator. Among these properties, half-Heusler semiconductors have been found to be good thermoelectric materials. To predict semiconductivity the 18-electron rule can be applied [23].
Typical values of $S \approx 300\ \mu V/K$ and $\rho \approx 10^{-4}\ \Omega m$. The only drawback is the relatively high thermal conductivity ($\kappa \approx 10\ W/Km$) [24].
The thermoelectric properties of n-type semiconductors based on TiNiSn have been studied. The phonon mean free path has been decreased by substitutions of Zr and Hf at the Ti position ($Hf_{0.5}Zr_{0.5}NiSn$ and $Hf_{0.26}Zr_{0.37}Ti_{0.37}NiSn$). The highest values for the Seebeck coefficient ($S_{max} \approx -300\ \mu V/K$) were found between 400 K and 500 K for $Hf_{0.26}Zr_{0.37}Ti_{0.37}NiSn$ corresponding to a ZT value of 1.0 at 700 K.

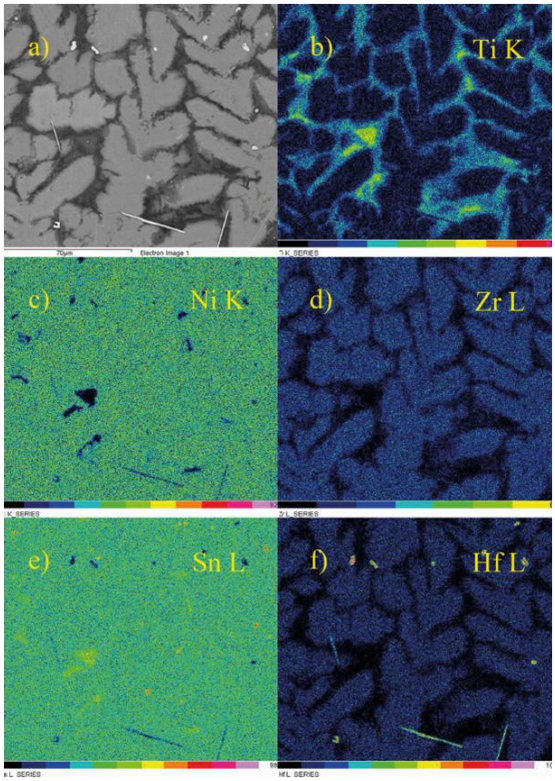

Figure 10: *SEM element mapping of $Hf_{0.26}Zr_{0.37}Ti_{0.37}NiSn$ shows the phase segregations.*

The thermal stability at temperatures higher than 700 K is critical and it has to be studied. The complex microstructure and demixing of phases of half-Heusler influence the transport properties; therefore a micro and nanostructural characterization has been performed by scanning electron microscopy (SEM) (Fig. 10) and transmission electron microscopy (TEM), and has been related to the electrical properties.

3 Applications of artificial superlattices

3.1 Development of adaptive focusing optics *(M. Kenzelmann; SwissNeutronics)*

Based on the preliminary earlier work on adaptive optics for neutrons, we developed three different concepts to realize an adaptive device using parabolic geometries. The testing of several different prototypes was crucial to identify the most promising technology for neutron optical focusing devices, and allowed us to gain important experience with this new technology and the determination of the precision requirements.

a) *Three prototypes of neutron focusing devices*
Prototype I: the neutron mirror is clamped at one end and a force is applied at the other

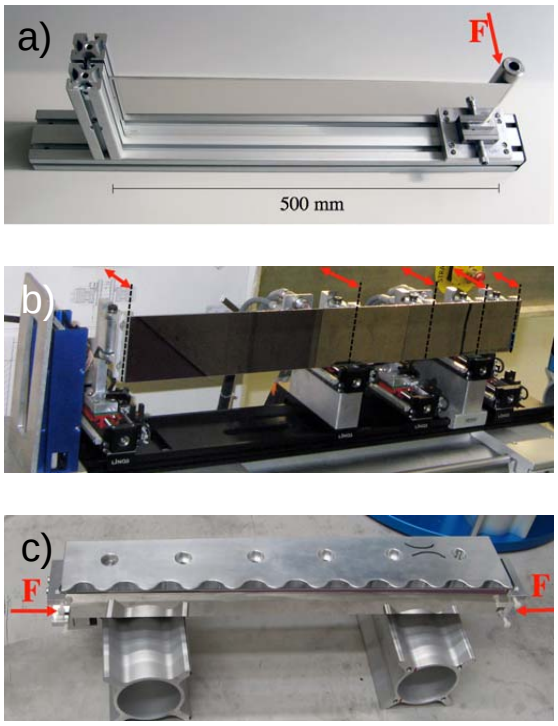

Figure 11: *(a) Prototype I, (b) prototype II and (c) prototype III. All prototypes are of the length of 500 mm.*

end with an actuator. To produce the correct parabolic curvature, the thickness $t(x)$ of the substrate is machined in an appropriate way. Prototype II: the basic idea of this concept is to fix five actuators on the back side of a uniform neutron mirror. To approximate the aimed parabolic geometry of the mirror, the actuators have to be activated accordingly. Prototype III: the profile of a 2 mm thick glass substrate is determined by an aluminium frame. The force is applied at the front edges of the glass-beam via two plastic cylinders. The aluminium unit is machined in such a way that the ten supporting points (lines) force the neutron mirror to attain a parabolic geometry. Pictures of the three prototypes are show in Fig. 11.

All prototypes were characterized by theodolite and neutron measurements (Fig. 12). The rms value of the waviness extracted from the deflection angle measurements of the theodolite experiments expresses the quality of the achieved parabolic approximation. The neutron measurements were performed at the cold beamline BOA at SINQ at PSI (max. flux at 3.5 Å). In a first measurement series all three prototypes were measured to compare their performances. In a second experiment, the influence of the beam properties on the focal point properties were studied for prototype III. The beam properties were adjusted by choosing different

#	p	f	n	w	g
I	0.2780	250	8.63	3.4	5.8
II	0.4464	200	11.64	8.6	5.5
III	0.4464	200	11.64	2.1	7.8

Table 2.1: *Summary of the performance experiments of the different prototypes. # indicates the number of the prototype, p is the geometry $y^2 = 2p(x_0 - x)$ parabola constant, f is the focal distance in mm, n is the projection in beam direction in mm, w is the waviness rms value in $1E^{-4}$ rad and g is the neutron gain factor (at focus point).*

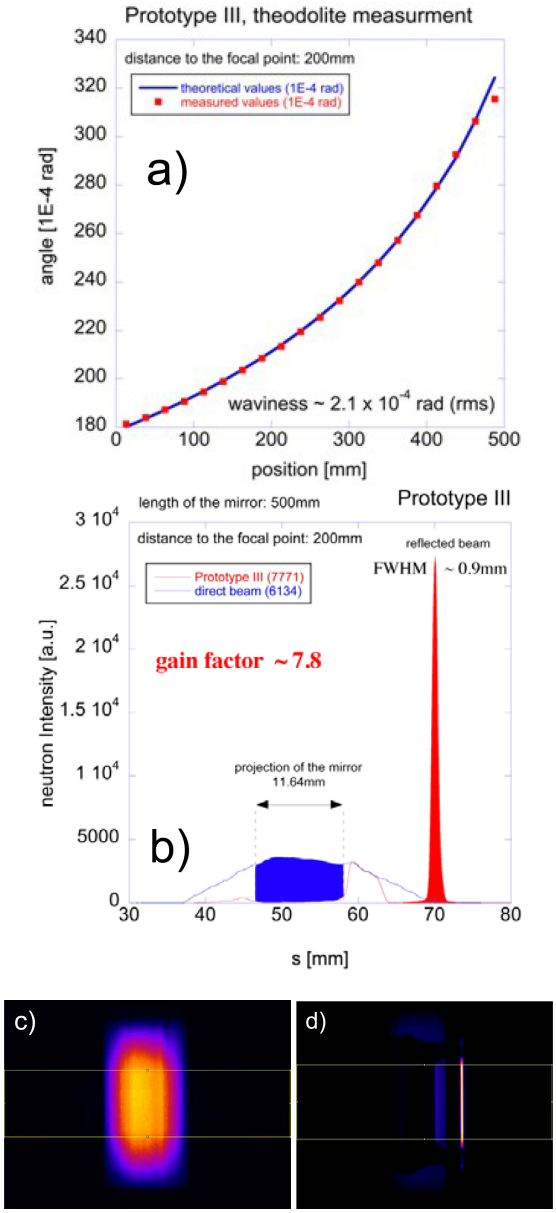

Figure 12: *(a) Results from theodolite measurements on prototype III. (b) Results of the neutron experiments with prototype III (first measurement series). (c-d) Raw data of the neutron measurements at BOA (top: direct beam, bottom: focused beam).*

A_S	B_d	I	I_N	g	ss
$0.8 \cdot 0.8$	$\pm$ 0.012	0.23	0.74	3.3	0.17
$2.0 \cdot 2.0$	$\pm$ 0.030	0.40	2.83	7.0	0.22
$5.5 \cdot 5.0$	$\pm$ 0.074	0.96	9.81	10.2	0.41
$10 \cdot 10$	$\pm$ 0.148	1.88	17.66	9.4	0.74

Table 2.2: *Influence of the beam properties on the spot size at the focal point (prototype III). A_S is the aperature setting in mm, B_d is the calculated beam divergence in degrees, I is the normalized intensities direct beam in arbitrary units (a.u.), I_N is the normalized intensity with optics in a.u. g is the neutron gain factor (at focal point), and ss is the spot size at focal point (FWHM) in mm.*

apertures. The results of all experiments are shown in Tables 2.1 and 2.2. In addition first tests of a focusing-defocusing geometry were performed at the BOA beamline. The results of this experiments are promising for future applications and allow to extract requirements to the adjustment of further devices.

The investigations of the three prototypes showed that the concept of prototype III provides the highest precision to form a parabolic shape. Therefore prototype III shows the best performance and was used for the extended investigation and experiments. From the focusing-defocusing experiments the following requirements for further experiments and technological developments were extracted: (1) the translation accuracy (Δx&Δy) has to be smaller than 0.1 mm; (2) the angle of impact needs to be adjustable with an accuracy of 0.01 degree; (3) the supporting points of prototype III need to be machined with a precision of $<$ 0.01 mm; (4) for the focusing-defocusing concept the angular accuracy for the second optic needs to be in the order of 0.001 degree.

In summary, using the developed adaptive focusing devices for neutrons it is possible to optimize the focal spot on small samples. We characterized three different prototype designs for neutron optical focusing devices, and identified the most promising technology. As a main result, we determined precision requirements for the key components of the device. With this knowledge, we will now plan to build a neutron focusing device for a test experiment. This project was especially supported by the SNSF *economic stimulus packages*.

3.2 Ferroelectric superlattices: tailored dielectric properties *(J.-M. Triscone)*

The functional properties of ferroelectric materials are intimately linked to the morphology and mobility of ferroelectric domains. These domains can emerge naturally in response to the presence of depolarizing fields that arise from the incomplete screening of the spontaneous polarization. Although such fields are generally detrimental to the stability of ferroelectric thin film memory devices, the accompanying domain formation can lead to significant enhancement of the dielectric permittivity that can be useful for other applications. Superlattices composed of alternating ultrathin ferroelectric and paraelectric layers offer a unique opportunity for engineering domain structures and hence tailoring the dielectric properties of these artificially layered materials.

Our studies on $PbTiO_3/SrTiO_3$ superlattices have shown that, by changing the thickness of the paraelectric $SrTiO_3$ layers, the degree of electrostatic coupling between the ferroelectric layers can be controlled. For $SrTiO_3$ layers thicker that about 3 unit cells (uc), the $PbTiO_3$ layers interact weakly and adopt a polydomain configuration. The regular ferroelectric domains in this regime are extremely small, with periods of just a few nanometers and scaling with the thickness of the $PbTiO_3$ layers according to the well known Kittel law. Due to the very large domain wall densities, even tiny displacements of domain walls under applied electric fields give rise to large changes in polarization and hence to very large and highly tunable dielectric responses [9]. The domain wall motion is also highly reversible, resulting in low dissipation.

Fig. 13 shows the field dependence of the dielectric permittivity for a series of superlattices with the same $PbTiO_3$ volume fraction (50%) but different periods. A very broad range of

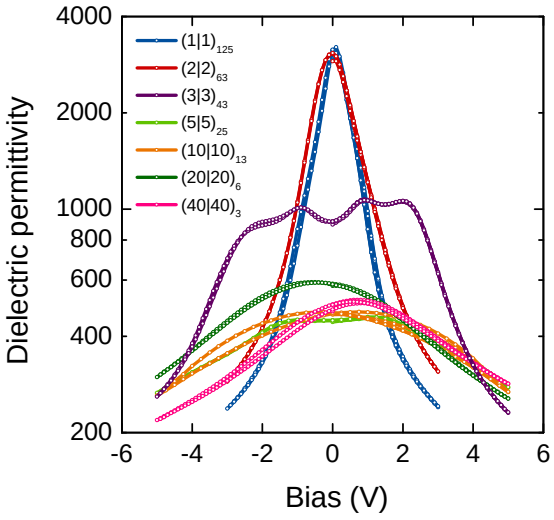

Figure 13: *Field dependent dielectric permittivities for a series of $(n_P|n_S)_m$ superlattices with n_P uc of $PbTiO_3$ and n_S uc of $SrTiO_3$ repeated m times.*

permittivities and tunability profiles is thus accessible by simply changing the individual thicknesses of the ferroelectric and paraelectric layers in the system. Moreover, by carefully choosing the superlattice composition, the temperature profile of the dielectric response can also be tailored. Such materials may thus find application as variable capacitors (varactors) in voltage controlled oscillators or rf filters, where the low-voltage operation of the superlattices may give them an advantage over existing devices. High frequency characterization is underway to assess the performance of the superlattice varactors in the GHz frequency domain.

4 Hydrogen detectors and other sensors

4.1 Progress towards a resistive thin-film hydrogen detector *(K. Yvon, J. Cors, Ø. Fischer; Swatch Group R&D SA, Division Asulab)*

Hydrogen fuel cells play a key role in future energy scenarios. Mass markets such as hydrogen powered vehicles and hydrogen production units for residential areas require hydrogen detectors and sensors on a very large scale. The devices must be cheap, sensitive and selective, and allow to detect hydrogen in various gases (e.g. oxygen) in the entire concentration range ($1.5 - 100\%$ H_2). This project aims at developing tailored sensing devices that are cheaper and more selective than those currently available, by using thin films and novel materials undergoing hydrogen-induced metal insulator transitions.

The intermetallic compound $LaMg_2Pd$ has been identified as a suitable candidate for detecting and sensing hydrogen. Measurements on the bulk have shown that a hydrogen-induced metal insulator transition occurs near room temperature and at relatively low hydrogen pressures between a partially charged phase of composition $LaMg_2PdH_{\sim 3}$ and a fully charged phase of composition $LaMg_2PdH_7$. Thus thin films were deposited by sputtering by using a single-target of $LaMg_2Pd$ and a $SrTiO_3$ substrate that was heated above 200°C under partial pressure of argon. No further annealing was necessary. X-ray diffraction confirmed the presence of the active phase $LaMg_2Pd$ and some lanthanum oxide La_2O_3.

As shown in the previous reporting period, the films were precharged with hydrogen and subjected to cycling experiments in pure hydrogen at room temperature in a self-made *in situ* chamber. The resistance of the films was monitored by using the four-point method while filling the chamber with 1 bar hydrogen during two minutes and subsequent pumping during two minutes. The resistance of the film increased by 1.5% during absorption and decreased by nearly the same amount during desorption. At room temperature the response was relatively rapid, the reproducibility of the signal was good, and the drift was relatively small. Most importantly, the film remained intact during cycling.

Next, various concentrations of hydrogen (0.5%, 1.5% and 3%) were added to 1 bar of argon. Interestingly, the lowest hydrogen concentration (0.5%) showed already a useful signal, thus meeting the 0.5% target for detecting hydrogen. The kinetics was relatively rapid and the changes in resistance scaled with partial hydrogen pressure. No significant degradation of the signal occurred during extended cycling experiments. Thus the device showed also promise for use as a hydrogen sensor.

Compared to the previous reporting period, the films were exposed to higher hydrogen concentrations in various H/Ar mixtures at room temperature (from 100 to 300 mbar H_2). The results showed that the resistance response was proportional to the partial pressure hydrogen, thus confirming the film's potential as hydrogen sensor. The resistance response was also measured in the presence of other gases such as oxygen and air. After a fixed exposure time (e.g. 30 s) the resistance response at constant hydrogen pressure was found to be practically independent of the admixture of these gases, thus proving the quasi-absence of cross-sensitivity to these gases. A patent application has been filed.

On a more fundamental side, attempts were made to understand better the effects of hydrogen insertion into a metallic matrix by a first principle study of the solid solution of hydrogen in metallic lanthanum [10]. If was found that the hydrogen atom distribution was not random but tended to aggregate into –H–La–H–La–H– chains.

In conclusion, thin films of intermetallic $LaMg_2Pd$ have been investigated with respect to their resistance response during exposure to hydrogen at various concentrations and in various gases. The sensitivity in pure hydrogen, and hydrogen/oxygen and hydrogen/air mixtures was sufficient for detecting 0.5% hydrogen, thus meeting the criterion for a hydrogen detection device. The resistance response was proportional to the partial hydrogen pressure in a large concentration interval, thus opening the way for sensing applications. Future work will concentrate on investigating the film's properties in potentially corrosive gases such as water vapor, sulphur or carbon

containing gases, and on finding low-cost substrates. In order to obtain a better understanding of the mechanism leading to the hydrogen-induced resistance changes, *in situ* synchrotron diffraction experiments will be performed.

4.2 Development of new Bi- and Mo-based sensor materials *(G. Patzke)*

a) *Mo-based gas sensors* Our research activities on the formation of new sensor materials are focused on structure-morphology-activity relationships among oxide-derived sensor materials with special emphasis on low-cost elements and tuneable syntheses.

Over the past years, we have garnered experience in the synthesis and analysis of hexagonal W- and Mo-oxides with a flexible channel structure motif [11]. We have now hydrothermally synthesized and characterized (e.g. powder X-Ray diffraction and electron microscopy) an isostructural series of hexagonal alkali molybdates with alkali cations (Na^+–Cs^+) as structural stabilizers within the channels. All members of the series are phase pure and exhibit a high degree of crystallinity after hydrothermal treatment. Gas sensing tests on these compounds were carried out on interdigitated Au electrodes using our in-house gas sensing facility in order to evaluate the influence of alkali cations on the gas sensing properties. The operating temperature was stepwise varied between 150 and 275°C.

The alkali cations were found to exert a significant effect on the sensing properties of the hexagonal molybdates, and representative results for the sensitivity of K^+-containing hexagonal molybdates towards ammonia [11] are shown in Fig. 14. Results are displayed for an optimized operating temperature of 225°C with maximum sensitivity towards NH_3.

Ammonia concentrations were gradually increased from 2 ppm to 100 ppm, and the response/recovery curves indicate a stable and reliable sensing behavior (Fig. 14a). A linear relationship between concentration and resistance could be clearly assigned. Moreover, we investigated the selectivity of K^+-stabilized hexagonal molybdate sensors towards other reducing gases (H_2, isopropanol, ethanol, methanol, acetone and CO) at the selected operating temperature to exclude interference effects (Fig. 14b). Concentrations of H_2 and CO were maintained at 100 ppm, those of isopropanol and ethanol at 500 ppm, and of methanol and aceton at 1000 ppm. The sensitivity S of the hexagonal molybdate towards 100 ppm ammonia gas was up to 130-

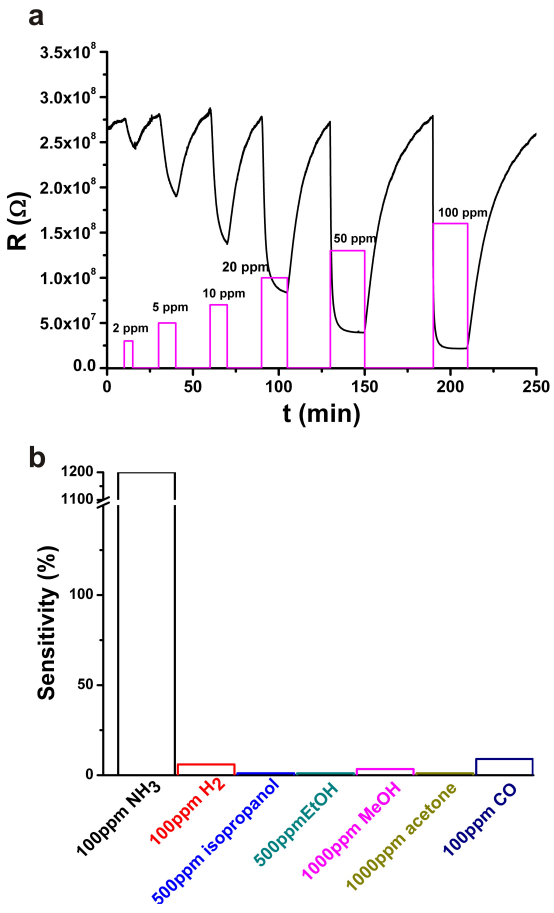

Figure 14: *(a) Sensitivity of K^+-containing hexagonal molybdate towards $2-100$ ppm NH_3. (b) High selectivity towards NH_3 in comparison with other reducing gases.*

fold higher than sensitivity values towards the other test gases ($S = (R_0 - R)/R$).

Whereas previous works pointed out the sensitivity of molybdenum oxides with Ti-based overlayers towards NH_3 [25], we open up a most direct one-step hydrothermal pathway to molybdenum oxide sensors with no need for doping, coating or other post-treatments.

b) *Bi-based humidity sensors* Following up on our structure-properties studies on Bi-containing humidity sensor materials [12, 13], we newly explored the Bi/P/O-system. Whereas our previous strategies were focused on the influence of W/Mo-substitution on the humidity sensing properties of the isostructural Aurivillius-type Bi_2MO_6 (M = W, Mo) phases, we now investigate the role of the structural motif whilst keeping the involved elements constant [14].

For this purpose, we hydrothermally synthesized monoclinic $BiPO_4$ (Fig. 15b) and sillenite-type cubic bismuth phosphate (Fig. 15a). The latter has a lower P content than $BiPO_4$, be-

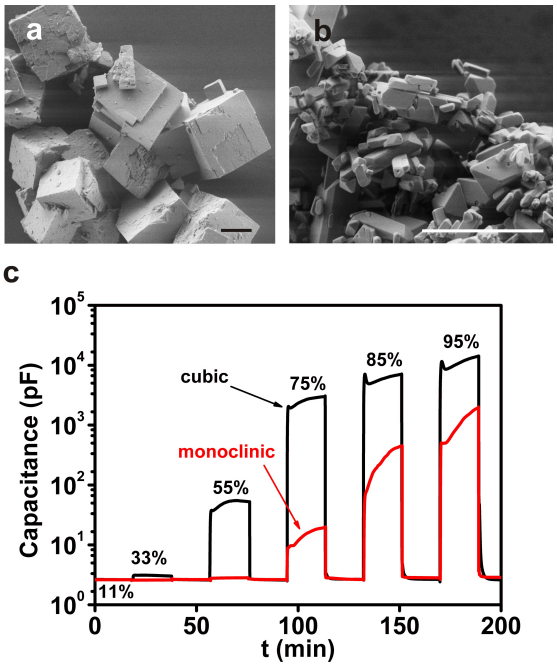

Figure 15: *SEM images of (a) cubic bismuth phosphate and (b) monoclinic $BiPO_4$. (c) Stable response and recovery curves for various RH for cubic and monoclinic bismuth phosphates.*

longing to the Bi_xPO_δ ($13 \leqslant x \leqslant 16$; $\delta \sim 17 - 20$) compound series. In addition, the 10-fold lower surface area of cubic bismuth phosphate suggests less favorable humidity sensing properties at first glance.

However, capacitance measurements over the entire range of relative humidity (RH) values clearly showed that cubic bismuth phosphate displays higher sensitivity than monoclinic $BiPO_4$. Additionally, the sillenite-type cubic form excels through a linear relationship between sensitivity and RH in combination with better response and recovery characteristics, especially at lower RH values (Fig. 15c). This renders the performance of cubic bismuth phosphate promising and comparable to our preceding results on Bi_2WO_6 [12]. Accordingly, we could assign a transition between "non-Debye" and "ion-transport" sensing mechanisms for cubic bismuth phosphate around 33% RH, i.e. at lower RH values than for monoclinic $BiPO_4$.

The favorable sensing properties of the Bi-rich phase point to a high degree of polarizability of the Bi^{3+} cations in the characteristic cubic framework of the sillenite structure type, which is the basis for a large family of mixed compounds derived from cubic Bi_2O_3. We thus opened up a new class of bismuth materials for humidity sensing which (a) leave plenty of room for sensitivity tuning with elements other than P, and (b) thus pave the way to novel humidity sensor design via new structure-activity relationships. According investigations are now in progress.

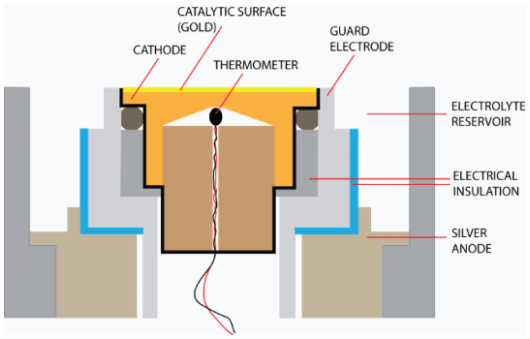

Figure 16: *Configuration of the developed electrochemical sensor. It consist of a stack of precise machined mechanical parts. Overall diameter of the sensor is 28 mm.*

4.3 Electrochemical sensors with higher resolution *(J. Cors, Ø. Fischer)*

This applied research project started in 2010 as part of the SNSF-supported *economic stimulus packages*. The goal of this project is the development of an electrochemical oxygen sensor with higher resolution than existing commercial devices. The sensing mechanism is based on the reduction of oxygen molecules on a gold surface (Clark cell). The idea is to adjust the surface properties of the gold electrode improving the transducing properties to obtain an enhanced signal. The main achievements in this project have been:

- a new concept of the sensor was developed, including better thermometry and modular design (Fig. 16);
- gold surfaces have been microstructured using different techniques, achieving positive effects on both sensing signal and electrolyte flow (life of the sensor) (Fig. 17);
- improvement of trace-level electronic signals based on STM current amplification design;

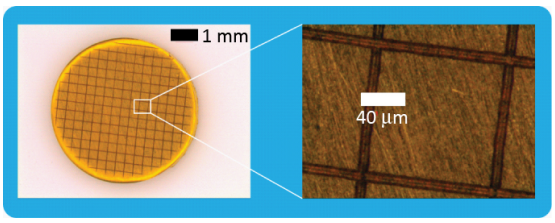

Figure 17: *Structured sensing gold surface.*

- a resolution of 0.2 ppb of oxygen partial pressure (trace level range) has been achieved; this level of detection is not achieved by the best commercial devices;
- two complete demonstration prototypes have been constructed; the systems are ready for field-testing.

Test are planned in both the brewing industry (for dissolved oxygen), and in a helium purification station (for gas phase measurements).

4.4 Piezoresistive strain transducer *(C. Renner)*

A host of applications exploiting the bending of tiny cantilevers, including atomic force microscopy (AFM) and biomechanical assays, are in need of an efficient, MEMS compatible, strain transducer. Existing schemes capable of detecting minute cantilever bending all suffer from severe loss of signal strength upon cantilever size reduction, with the exception of piezoresistive detection. The challenge with piezoresistive transducers is to design a detection scheme with sufficient accuracy and high sensitivity.

The key to piezoresistive monitoring of minute strain is to engineer a device with a gauge factor (GF) as large as possible. GF is defined as the relative change in resistance per unit strain $GF = \frac{\Delta R}{R_0} / \frac{\Delta \ell}{\ell_0}$. We have designed and tested different promising realizations over the past years. Unfortunately, they all turned out to be inadequate for the anticipated micromechanical applications.

Silicon nanowires had been reported to show extraordinarily large and non-linear piezoresistance [26]. In agreement with these findings, initial experiments we did indeed showed a very large resistance increase in a thin silicon slab subject to compressive strain. But upon closer inspection, this promising result turned out to be an experimental artefact [15], questioning the original results obtained by He and Yang [26]. In an earlier attempt [16], we had explored custom designed metal-semiconductor hybrid structures showing very large GF. Unfortunately, their fantastic gauge factor relied upon a four-terminal configuration with an intrinsic poor signal to noise ratio, rendering the device ineffective.

Both negative results above in terms of strain gauge applications have resulted in novel insight into the transport properties of silicon. They have also prompted us to search for other silicon based alternatives to achieve large gauge factors, with yet even more surprising findings about its electronic properties.

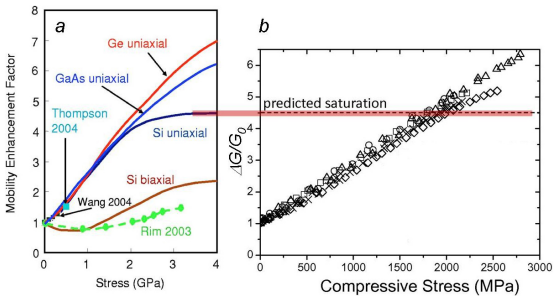

Figure 18: *(a) Selected model predictions of pressure dependent conductance of Silicon and Germanium. (b) Measured increase in relative conductance for p-type silicon compressed along ⟨110⟩, showing a nearly linear increase. Note the absence of saturation, in contradiction with theoretical predictions (manuscript in preparation).*

In a previous report, we had noted the possibility to exploit metal-semiconductor hybrid structures as a two terminal piezoresistive device, provided it would be heavily prestrained. Following up on this idea, we set out to measure the change in conductance of silicon under large uniaxial strain. We managed to measure the silicon conductance up to 3 GPa applied pressure. These experiments gave the unexpected result that the conductance, instead of saturating as predicted by existing models, keeps increasing (Fig. 18). This finding is again not going to help us designing a MEMS compatible strain transducer. But it offers the interesting collateral result that the information technology road map might be pursued for a little longer using the good old silicon technology by exploiting this enhanced mobility beyond the currently anticipated limit.

In parallel to the high-pressure conductance measurements of silicon, we have explored alternative routes to achieving large piezoresistive response to strain. One promising approach is the so-called stress concentration regions (SCR). It consists in a specific structuring

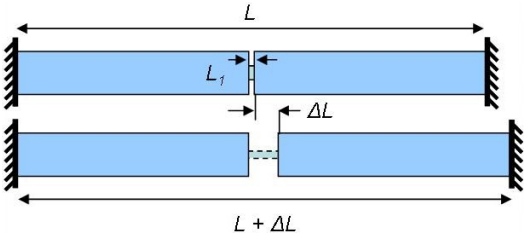

Figure 19: *Schematics of the stress concentration region (SCR) principle. The deformation of a beam forced to elongate by a length ΔL will concentrate on its weakest section, thereby enhancing the response to minute strain (unpublished).*

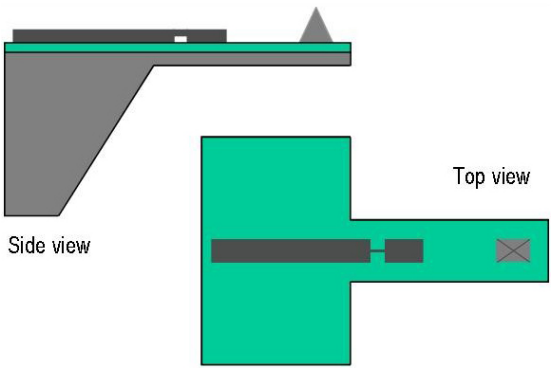

Figure 20: *Schematics of an AFM force sensor exploiting a stress concentration region for an all electric readout of the cantilever bending (unpublished).*

of a beam such as to concentrate the strain into a weakened region (Fig. 19). The idea is that upon applying stress, the weak section of the beam L_1 will deform more easily than the rest of the beam. The relative increase in the length of the SCR $(L_1 + \Delta L)/L_1$ becomes larger as its absolute length L_1 decreases compared to L. Conversely, the contribution of the SCR to the overall resistance decreases as L_1 decreases. It is thus possible to design an optimal length for a desired amplification of the piezoresistance effect.
Stress concentration is a well known and documented method, and therefore cannot be the subject of a new patent. However, SCR has not been applied to MEMS and NEMS configurations to the best of our knowledge. We are in the process of fabricating a first AFM cantilever with a SCR micromachined onto the surface of the cantilever beam (Fig. 20). If successful, this method holds promise to replace all functionalities of current optical detection schemes, including torsional motion of the cantilever. A feat that has so far eluded other non-optical cantilever motion detection schemes.

5 New surface treatments for microcomponents

5.1 Marking technology for watch components *(J. Cors, J.-M. Triscone, Ø. Fischer; Vacheron Constantin, Phasis)*

The aim of this project is the implementation of security and decorative features in watch components. Patterns of microscopic structures made of various surface alloys are "written" on the surface of metal parts. Such structures are produced by a STM-inspired device, comprising XYZ micromotors driven by a SERVO control, and power electronics[1]. This project

[1]International Patent Application WO 2008/010044 A3

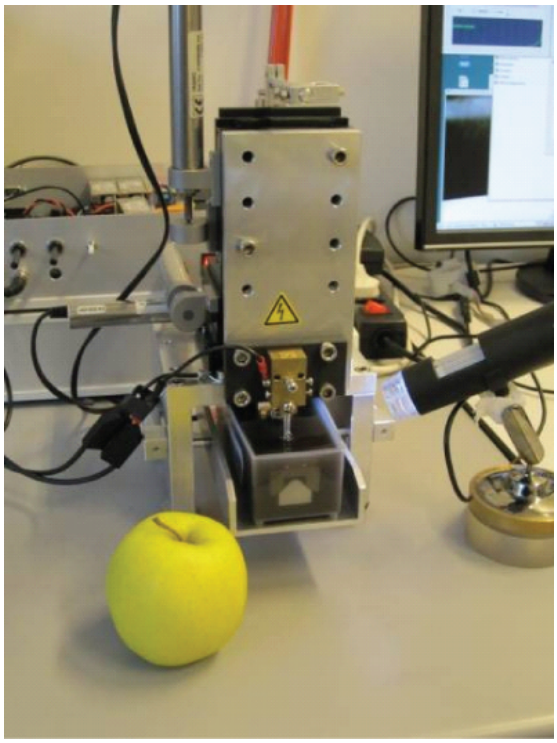

Figure 21: *Desktop marking system for watch components and other small mechanical parts.*

is supported by Vacheron Constantin in the framework of a regular CTI grant[2].The main achievements of the last twelve months are the following:

- the development of a versatile desktop marking machine (Fig. 21); the device supports automatic operation;
- deep-engraving of characters in fine brass parts; the process parameters related to the plasma power have been optimized to minimize wear of the electrode tip (Fig. 22);
- achieving the required surface condition on brass parts (roughness and integrity);
- improved accuracy in XY translation related to the design of specific patterns;

[2]CTI Project N° 10281.2

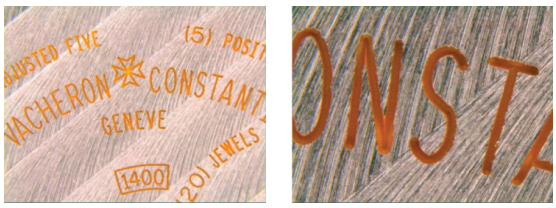

Figure 22: *Deep-engraved characters (75 µm deep) made by the marking process. The substrate is a decorated, rhodium-coated brass watch part.*

Figure 23: *Patterns written with surface alloys on medical steel (left) and silver (right).*

- feasibility tests for the "Hallmark of Geneva";
- synthesis of surface alloys on other substrates, as medical alloys and precious metals (Fig. 23).

The flexibility of the technology opens the door to applications in other fields, where the physical properties of the synthesized alloys give a clear advantage over the state-of-the-art. First successful tests have been performed on medical alloys, where the implementation of anti-corrosion marks has attracted considerable interest from industry.

5.2 Cut-and-coat process by wire-EDM *(J. Cors, Ø. Fischer; AgieCharmilles +GF+)*

This applied research project started also in 2010 as part of the SNSF-supported *economic stimulus packages*. The objective of the present project was to provide AGIECharmilles with the technology to enter the growing market of coated metal parts. The idea was to modify the traditional spark erosion setup. By changing the energy distribution of the machining sparks [27], and the metallurgical composition

Figure 24: *Iterative approach machining-analyzing.*

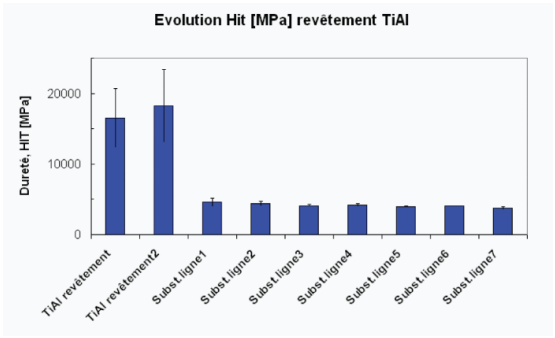

Figure 25: *Increased hardness at the surface.*

of the tool electrode, it has been possible to tune the process creating coatings with tailored properties. An iterative approach using X-ray fluorescence as analytic tool was implemented to optimize the coating process (Fig. 24). Main achievements have been:

- reliable, coating technologies have been elaborated, namely generator settings for a given couple of workpiece material and electrode alloy;
- elaboration of sets of coated parts, with full characterization of mechanical properties and added technical value (Fig. 25);
- identification of target applications in the current AGIECharmilles markets (Fig. 26);
- identification of a new application related to surface thermal shielding for parts submited to thermal stress.

6 Collaborative efforts

As explained in the previous report, this project is characterized by several close collaborations between researchers of MaNEP and our industry partners, and these collaborations have largely continued as last year. Below you find last year report slightly adapted to the situation today.
On superconductivity there is a long-standing collaboration between Bruker BioSpin and

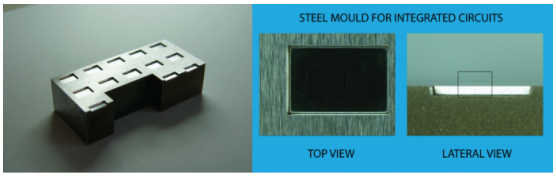

Figure 26: *Application of the technology: surface-engineered abrasion-resistant injection molds for integrated circuits (IC).*

Prof. René Flukiger. This collaboration is now taken over by Dr. Carmine Senatore on the MaNEP side. There is in addition a growing collaboration between MaNEP and CERN on the development for new superconducting wires for the future upgrade of LHC. As an extension of the work on new materials for applications, a collaboration between Carmine Senatore and Enrico Giannini has been established as a common effort between Projects 3 and 4 to measure the properties of $FeTe_{0.7}Se_{0.3}$. The collaboration between ABB and MaNEP on superconducting thin film fault current limiters has led to a proposal to develop a new type of superconducting tapes.

The search for mechanical energy harvesting devices is a close collaboration between three partners: the group of Jean-Marc Triscone (UniGE), the group of Nico de Rooij (EPFL, Neuchatel) and the group of Gilles Triscone (Hepia, Geneva). The collaboration between Philipp Aebi (UniFR), Jürg Hulliger (UniBE) and Anke Weidenkaff (Empa and UniBE) has continued in order to synthesize and characterize new materials for thermoelectric power.

The research on neutron supermirrors is a close collaboration between MaNEP researchers at PSI and the company SwissNeutronics with occasional collaboration with the group of Jean-Marc Triscone (UniGE).

The research on transition metal hydrogen detectors is a collaboration between the groups of Klaus Yvon, Øystein Fischer, Jorge Cors (UniGE) and Swatch Group R&D SA, Division Asulab. In particular we have combined the competence on hydrides of Klaus Yvon with the thin film synthesis competence in Øystein Fischer's group as well as Jorge Cors knowledge on the field of gas sensors and Asulab's experience in sensing devices. In this field a close collaboration has also developed between Greta Patzke (UniZH) and Jorge Cors (UniGE).

The projects on surface treatments consists of two close collaborations between the groups of Øystein Fischer and Jorge Cors on the one hand and two companies on the other hand, Vacheron Constantin and AgieCharmilles. In both these projects, we are now building a close collaboration between MaNEP and these companies. The MaNEP start-up Phasis is also part of these projects.

MaNEP-related publications

[1] T. Boutboul, L. Oberli, A. den Ouden, D. Pedrini, B. Seeber, and G. Volpini, IEEE Transactions on Applied Superconductivity **19**, 2564 (2009).

► [2] C. Senatore, G. Mondonico, F. Buta, B. Seeber, R. Flükiger, B. Bordini, P. Alknes, and L. Bottura, IEEE Transactions on Applied Superconductivity (2012), doi:10.1109/TASC.2011.2178992.

► [3] M. S. A. Hossain, C. Senatore, M. A. Rindfleisch, and R. Flükiger, Superconductor Science & Technology **24**, 075013 (2011).

[4] L. Antognazza, M. Decroux, A. Badel, C. Schacherer, and M. Abplanalp, *submitted to* Superconductor Science & Technology (2012).

[5] A. Badel, L. Antognazza, M. Therasse, M. Abplanalp, C. Schacherer, and M. Decroux, *submitted to* Superconductor Science & Technology (2012).

► [6] P. Janphuang, D. Isarakorn, D. Briand, and N. F. de Rooij, in *Proceedings of the 16th International Conference on Solid-State Sensors, Actuators and Microsystems (TRANSDUCERS'11)* (2011), p. 735.

[7] L. Karvonen, Tomeš, and A. Weidenkaff, Material Matters **6**, 92 (2011).

[8] D. Moser, L. Karvonen, S. Populoh, M. Trottmann, and A. Weidenkaff, Solid State Sciences **13**, 2160 (2011).

[9] P. Zubko, N. Stucki, C. Lichtensteiger, and J.-M. Triscone, Physical Review Letters **104**, 187601 (2010).

[10] G. Schöllhammer, P. Herzig, W. Wolf, P. Vajda, and K. Yvon, Physical Review B **84**, 094122 (2011).

► [11] Y. Zhou, K. Zheng, J.-D. Grunwaldt, T. Fox, L. Gu, X. Mo, G. Chen, and G. R. Patzke, The Journal of Physical Chemistry C **115**, 1134 (2011).

[12] K. Zheng, Y. Zhou, L. Gu, X. Mo, G. R. Patzke, and G. Chen, Sensors and Actuators B: Chemical **148**, 240 (2010).

[13] Y. Zhou, J.-D. Grunwaldt, F. Krumeich, K. Zheng, G. Chen, J. Stötzel, R. Frahm, and G. R. Patzke, Small **6**, 1173 (2010).

[14] M. Sheng, L. L. Gu, R. Kontic, Y. Zhou, K. Zheng, G. R. Chen, X. L. Mo, and G. R. Patzke, *submitted* (2012).

[15] J. S. Milne, A. C. H. Rowe, S. Arscott, and C. Renner, Physical Review Letters **105**, 226802 (2010).

[16] A. C. H. Rowe, A. Donoso-Barrera, C. Renner, and S. Arscott, Physical Review Letters **100**, 145501 (2008).

Other references

[17] M. Shikano and R. Funahashi, Applied Physics Letters **82**, 1851 (2003).

[18] W. Koshibae, K. Tsutsui, and S. Maekawa, Physical Review B **62**, 6869 (2000).

[19] D. M. Rowe, ed., *Thermoelectrics Handbook: Macro to Nano* (CRC Press, Taylor & Francis, Boca Raton, 2006).

[20] A. Kudo and Y. Miseki, Chemical Society Reviews **38**, 253 (2009).

[21] H. Usui, H. Iwasawa, M. Hirose, Y. Maeda, T. Saitoh, H. Osada, T. Kyômen, M. Hanaya, Y. Aiura, Y. Kotani, M. Kubota, and K. Ono, Physica C **470**, S758 (2010).

[22] E.-J. Cho, S.-J. Oh, S. Suga, T. Suzuki, and T. Kasuya, Journal of Electron Spectroscopy and Related Phenomena **77**, 173 (1996).

[23] D. Jung, H. J. Koo, and M. H. Whangbo, Journal of Molecular Structure: THEOCHEM **527**, 113 (2000).

[24] S. Sakurada and N. Shutoh, Applied Physics Letters **86**, 082105 (2005).

[25] C. Imawan, F. Solzbacher, H. Steffes, and E. Obermeier, Sensors and Actuators B: Chemical **64**, 193 (2000).

[26] R. He and P. Yang, Nature Nanotechnology **1**, 42 (2006).

[27] D. D. DiBitonto, P. T. Eubank, M. R. Patel, and M. A. Barrufet, Journal of Applied Physics **66**, 4095 (1989).

Project 4 Electronic properties of oxide superconductors and related materials

Project leader: D. van der Marel (UniGE)

Participating members: D. Baeriswyl (UniFR), B. Batlogg (ETHZ), L. Degiorgi (ETHZ), Ø. Fischer (UniGE), A. Georges (UniGE), T. Giamarchi (UniGE), E. Giannini (UniGE), J. Karpinski (ETHZ), H. Keller (UniZH), D. van der Marel (UniGE), J. Mesot (PSI and ETHZ), T. M. Rice (ETHZ), M. Sigrist (ETHZ)

Summary and highlights: The physics of oxide superconductors presents an arena of rich and exciting phenomena. It was shown hat the Hund's rule coupling leads to strong correlations in materials which are not close to a metal-to-Mott-insulator transition (such as oxides of the 4*d* transition metals), and a general physical view of these "Hund's coupled materials" was elaborated. Experimental indications were obtained that doped $SrTiO_3$ constitutes a Fermi liquid formed by polarons instead of conventional electrons. In the context of the Yang-Rice-Zhang theory of high-T_c superconductors, a theoretical framework has been developed for "hourglass" dispersion of the spin-fluctuations at the antiferromagnetic wave vector, a feature known to be common to high-T_c superconductors. A hitherto unknown pseudogap has been identified along the nodal directions in strongly underdoped La_2CuO_4 using angle-resolved photoemission spectroscopy (ARPES), at temperatures below 100 K. A new analysis of atomic resolution scanning tunneling microscopy (STM) spectra allows mapping out the spatial variation of the parameters describing the local band structure, showing striking correlation between particular features in the band structure (the second neighbor copper-copper hopping) and T_c. Using nuclear quadrupole resonance the local symmetry at the Ba-sites in $YBa_2Cu_3O_7$ was studied, allowing to establish that orbital currents are either absent or extremely weak in the ground state of this compound. Important advances have been made in the preparation of iron pnictides and iron selenides, for example *Ln*Fe*Pn*O, and the arsenic-free KFe_2Se_2. Optical studies of Co-doped $BaFe_2As_2$ has revealed pronounced pressure-induced anisotropy in the electronic structure of this material. Using advanced focussed ion etching techniques, microdevices of SmFeAsO were prepared, allowing the measurement and control of vortex pinning by defects within the FeAs layers, thus providing a pathway to improve the technological aspect of superconductivity in the Fe pnictides.

1 Electronic properties and high-T_c superconductivity in transition metal oxides

1.1 Strong correlations due to Hund's rule coupling *(A. Georges)*

In single-band metals, strong electronic correlations emerge close to the Mott-insulating state. Building on previous work [1][31], we have shown that in multiband metals the correlations are strongly affected by Hund's rule coupling [2]. The quasi-particle coherence and the proximity to a Mott-insulator are influenced distinctly and, away from single- and half-filling, in opposite ways. A strongly correlated bad metal far from a Mott-phase is found there. The Hund's rule coupling accounts for important material trends and we have proposed [2] a concise classification of 3*d* and 4*d* transition-metal oxides based on this observation (Fig. 1). In particular, the ubiquitous occurrence of strong correlations in Ru- and Cr-based oxides, as well as the recently observed [32] high Néel temperature in Tc-based perovskites are naturally explained [3].

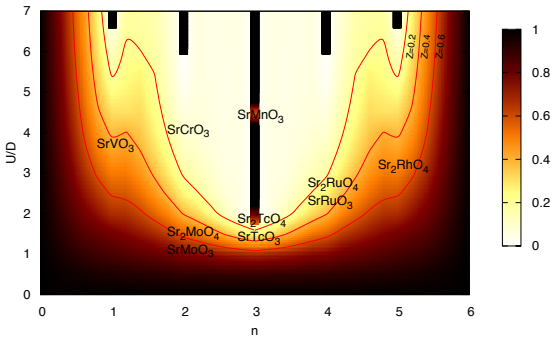

Figure 1: *Intensity plot of the quasi-particle weight for a three-orbital model with Hund's coupling. Darker regions correspond to good metals and lighter regions to bad metals. The black bars signal the Mott-insulating phases. Specific materials are schematically placed on the diagram (from [2]).*

1.2 Strong correlations induced by charge ordering in highly doped cobaltates *(A. Georges)*

Surprisingly, layered cobaltates (such as Na_xCoO_2) display spectral and transport properties suggestive of strong correlations close to the band-insulator limit (i.e for x close to unity). We have proposed an explanation for this [4], which relies on the key effect of charge ordering. Blocking a significant fraction of the lattice sites deeply modifies the electronic structure in a way which we found to be quantitatively consistent with photoemission experiments. It also makes the system highly sensitive to interactions (especially to intersite ones), hence accounting for the strong correlation effects observed in this regime, such as the high-effective mass and quasi-particle scattering rate. These conclusions are supported by a theoretical study of an extended Hubbard model with a realistic band structure on an effective kagome lattice.

1.3 Electronic structure and photoemission spectrum of $LaNiO_3$ *(A. Georges)*

Recent angular-resolved photoemission experiments on $LaNiO_3$ reported a renormalization of the Fermi velocity of e_g quasi-particles, a kink in their dispersion at ~ -0.2 eV and a large broadening and weakened dispersion of the occupied t_{2g} states [33]. We have shown that all these features result from electronic correlations and are quantitatively reproduced by calculations combining density-functional theory and dynamical mean-field theory [5]. Furthermore, we proposed a general explanation of the observed broadening of filled bands as due to interorbital interactions inducing electron-hole excitations in the partially-filled bands when the photoemission hole is created.

1.4 Common Fermi liquid origin of T^2 resistivity and superconductivity in n-type $SrTiO_3$ *(D. van der Marel)*

$SrTiO_3$ is a semiconductor which, when doped with a low density of electrons, becomes a good conductor with relatively high mobility and strong temperature dependence of the electrical resistivity and the infrared optical conductivity. At low temperatures the material becomes superconducting [34] with a maximum reported T_c of 1.2 K [35], although superconductivity is usually reported below 0.7 K with a dome-shaped doping dependence of T_c [36, 37]. Superconductivity is also observed below 0.3 K in the two-dimensional electron gas formed at the interface between $SrTiO_3$ and $LaAlO_3$ [6] where the carrier-concentration dependence of T_c has also a dome shape [7]. The dc resistivity below 100 K has a T^2 temperature dependence, which has been attributed to electron-electron scattering by some groups [38, 39, 40].

By comparing the density of states (DOS) obtained from the optical free carrier spectral weight, from the linear term in the specific heat and from angle-resolved photoemission spectroscopy (ARPES) data to state-of-the-art local density approximation (LDA) *ab initio* values, we have determined the quasi-particle effective mass as a function of doping [8], shown in Fig. 2. The verdict is clear: there is a fac-

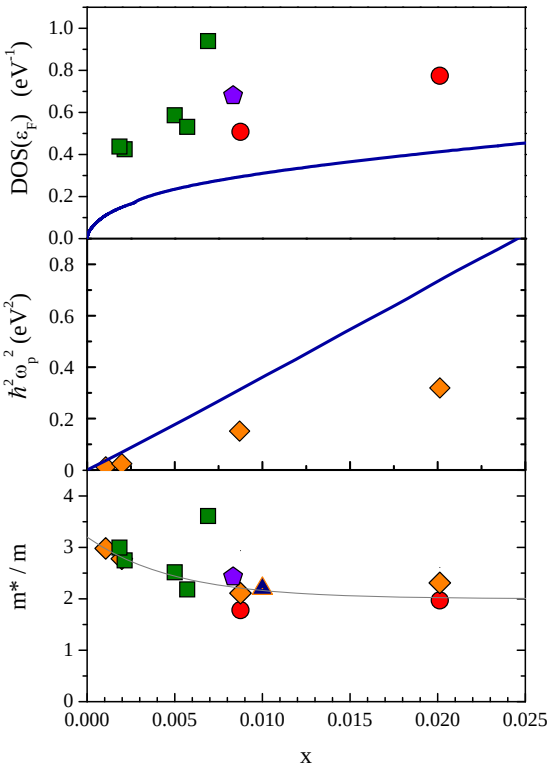

Figure 2: *Top panel: doping dependence of the density of states (DOS) at the Fermi energy. The solid curve corresponds to the WIEN2k band structure. Squares [41], circles (this work [8]), pentagon [42]: density of states obtained from the linear term in the specific heat. Middle panel: doping dependence of the Drude spectral weight, ω_p^2. The solid curve corresponds to the band structure results. Diamonds are the experimental values [9]. Bottom panel: (i) ratio of experimental DOS over band structure DOS (experimental and theoretical values taken from top panel, the meaning of the symbols is the same). (ii) Ratio of band structure over experimental ω_p^2 (values taken from middle panel). (iii) Ratio of bare and experimental (dressed) Fermi-velocity, $v_{F,b}/v_{F,e}$ (triangle, data from Ref. [10]). The grey curve is a smooth interpolation.*

tor of 2 to 3 mass enhancement with a tendency to become smaller for higher doping. Electron-phonon coupling is the only plausible suspect for the enhancement. Indeed, recent calculations confirm this [11]: based on the Fröhlich interaction, the essential characteristics of the observed optical conductivity spectra of $SrTi_{1-x}Nb_xO_3$, in particular intensity, lineshape and energy of a peak at 130 meV, was explained without any adjustment of material parameters. The electron-phonon coupling constant was found to be of intermediate strength.
We carried out a detailed analysis of the T^2 term in the resistivity, using Fermi liquid theory for the T^2 term in the resistivity of common metals, and combined this with expressions for T_c and with the Brinkman-Platzman-Rice (BPR) sum-rule [43] to obtain Landau parameters of n-type $SrTiO_3$. These parameters are comparable to those of liquid ^{3}He, indicating interesting parallels between these Fermi liquids despite the differences between the composite fermions from which they are formed.

1.5 Phenomenological approach to the anomalous pseudogap phase *(T. M. Rice)*

The pseudogap phase that appears in the underdoped cuprates has long been considered a key to the understanding of the physics of these high-temperature superconductors. Although there has been continued progress in refining the experimental characterization, progress on a comprehensive theory has been slow. Some years ago, we have put forward a phenomenological theory which described the pseudogap phase as a precursor to the Mott-insulating phase at stoichiometry with local singlet pairing as in the Anderson's RVB model. The key step in this approach is a simple but novel ansatz for the single-particle propagator which partially truncates the Fermi surface by an insulating gap in the antinodal regions. Considerable progress has been made in explaining a series of the anomalous properties in a consistent way in this theory. We have now written a detailed review describing the successes of this phenomenological approach in tying together the puzzling anomalies that characterize the pseudogap phase [12].

1.6 Magnetic response in the underdoped cuprates *(T. M. Rice)*

The magnetic spectrum of the underdoped cuprate superconductors measured in numerous neutron scattering experiments takes an unusual form, generally referred to as the

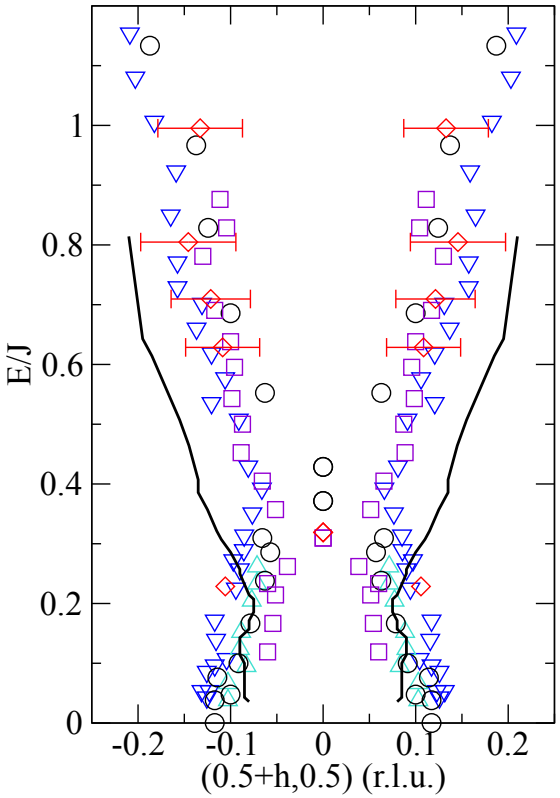

Figure 3: *Hourglass dispersion of the resonance near (π,π). The thick black line is the position of the maximum intensity peak after integrating the numerical data over a strip of width $2\pi/25$ along the parallel direction, averaged over sections of length $2\pi/33$. Experimental data are taken from various groups (see [13]).*

"hourglass" spectrum centered around the (π,π)-point in the Brillouin zone. Recently we showed that this hourglass form can be obtained in a RPA analysis of the spin spectrum within the Yang-Rice-Zhang (YRZ) phenomenological theory (Fig. 3) [13]. The low-energy incommensurate legs of the hourglass spectrum arise through particle-hole transitions between the nodal pockets and the waist is a resonance at (π,π) which comes from transitions between the antinodal gapped regions. The loss of spectral weight in the low-energy legs at the transition from normal to superconducting phase appears naturally in these calculation.

1.7 Adiabatic continuity of Gutzwiller-type wave functions *(D. Baeriswyl)*

In a first step, we have chosen a reference state $|\Psi_0\rangle$ without broken symmetry. Any indication of order should then appear in the long-distance behavior of certain correlation functions. We did not find any evidence for long-range order, even for antiferromagnetism at

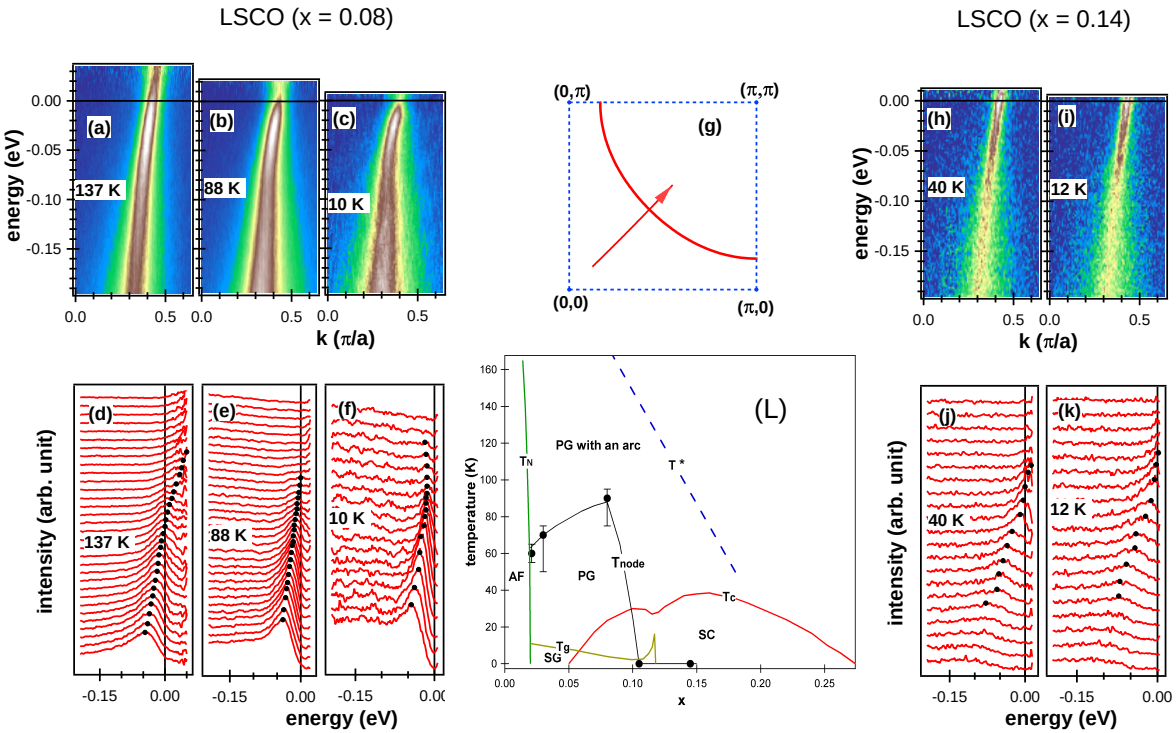

Figure 4: *ARPES spectra for underdoped superconducting LSCO samples ($x = 0.08$, $T_c = 20$ K and $x = 0.145$, $T_c = 33$ K). (a-c) Intensities along zone diagonal cut marked with the arrow in (g) at $T = 137$ K, 88 K and 10 K for LSCO ($x = 0.08$). The spectra were obtained by deconvolution Fermi function division method. (d-f) The energy distribution curves (EDC) from (a-c) in the vicinity of k_F. (g) The first quarter of Brillouin zone. The red curve is the Fermi surface (FS) of LSCO ($x = 0.08$) obtained from tight-binding fits to experimental data. The arrow indicates the cut along which the ARPES data were taken. (h-i) The same as (a-c) but for LSCO ($x = 0.145$) at $T = 40$ K and 12 K. (j-k) EDC from (h-i) in the vicinity of k_F. (L) The schematic phase diagram of LSCO. The lines are the superconducting transition temperature (T_c), the pseudogap temperature (T^*), the Néel temperature (T_N) and the temperatures at which a node appears (T_{node}). SC (PG, SG, AF) stands for superconducting (pseudogap, spin glass, antiferromagnetic) phase.*

half-filling and for lattice sizes up to 60×60. This somewhat disappointing result can be traced back to the "adiabatic continuity" of Gutzwiller-type wave functions. In fact, for a simple soluble model, the anisotropic quantum XY chain, it can be shown explicitly that a variational ground state à la Gutzwiller is perfectly smooth at the critical point where long-range order appears in the exact ground state [14]. Nevertheless these calculations gave useful insight for the origin of an effective electron-electron attraction.

1.8 Trial state with broken symmetry *(D. Baeriswyl)*

The failure of our attempt to produce long-range order without including it in the reference state of our variational ansatz indicates that possible broken symmetries should be explicitly admitted. Therefore we have turned our attention to the trial state

$$|\Psi\rangle = e^{-h\hat{H}_0} e^{-g\hat{D}} |\Psi_0\rangle\,, \qquad (2.1)$$

where $\hat{H}_0$ is a mean-field Hamiltonian including both antiferromagnetic and superconducting order parameters, $|\Psi_0\rangle$ is the ground state of $\hat{H}_0$ and g, h are variational parameters. With this form the expectation value of the energy, $E[\Psi] = \langle\Psi|\hat{H}|\Psi\rangle / \langle\Psi|\Psi\rangle$, can be expanded in powers of g using the linked-cluster theorem. We have calculated the lowest-order terms analytically and are currently attacking the minimization with respect to the four variational parameters (g, h as well as the two symmetry-breaking fields).

1.9 The gap profile in the electronic excitation spectra of underdoped $La_{2-x}Sr_xCuO_4$ (LSCO) *(J. Mesot)*

Using high-resolution angle-resolved photoemission spectroscopy (ARPES), we performed a systematic study of electronic excitations of underdoped $La_{2-x}Sr_xCuO_4$ (LSCO) as a function of temperature and doping [15]. The main experimental findings are: (1) for highly underdoped superconducting LSCO ($x = 0.08$), in

the superconducting state, the electronic excitations are gaped along the entire underlying Fermi surface (FS), and the gap function deviates from the pure $d_{x^2-y^2}$-wave form, (2) the gap structure persists into the normal state either by increasing temperature or by reducing the hole-concentration all the way to a non-superconducting LSCO ($x = 0.03$) sample, (3) while the antinodal gap remains constant in the temperature range up to 150 K, the diagonal gap is temperature-dependent (Fig. 4a-f), it closes at different temperatures (T_{node}) for superconducting and non-superconducting samples (Fig. 4L), but both temperatures are well below the pseudogap temperature (T^*), (4) when the gap at k_F on the zone diagonal decreases to zero a pure $d_{x^2-y^2}$-wave form of energy gap appears, beyond this temperature a Fermi arc occurs and its length increases with temperature.

1.10 Analysis of the tunneling spectra of $Bi_2Sr_2CuO_{6+\delta}$ *(Ø. Fischer)*

We have continued the analysis of the tunneling spectra of $Bi_2Sr_2CuO_{6+\delta}$. We showed in 2010 that the tunneling spectra unambiguously exhibit the signature of a strong Van Hove singularity (VHS) [16]. Taking advantage of the intrinsic inhomogeneities of the cuprate's high-T_c superconductors (HTS), we could spatially map the local superconducting gap (Fig. 5a) and correlate its values with other relevant parameters like the VHS position. Since it is routinely admitted that the local doping level controls both the position of the VHS and the opening of the superconducting gap, the correlation at the local scale between these two parameters is thus of great interest. In most of the area where the VHS is measured at negative energies, the VHS shifts towards higher energies when the gap magnitude decreases. This trend is in agreement with an increase of the local doping level (overdoping), well seen in Fig. 5b, where the spectra have been sorted according to the VHS position. However, this classification strikingly reveals that the gap opens again when the VHS approaches the Fermi level. A more quantitative analysis was achieved by fitting all the 17000 spectra acquired in the map (14×14 nm^2) with a numerical model which includes a d-wave BCS spectral function and a realistic three-orders tight binding-based band structure (in $Bi_2Sr_2CuO_{6+\delta}$ the coupling of the quasi-particle with the spin fluctuations is weak and can be neglected, see [16]). With such an analysis, the spatial maps for each

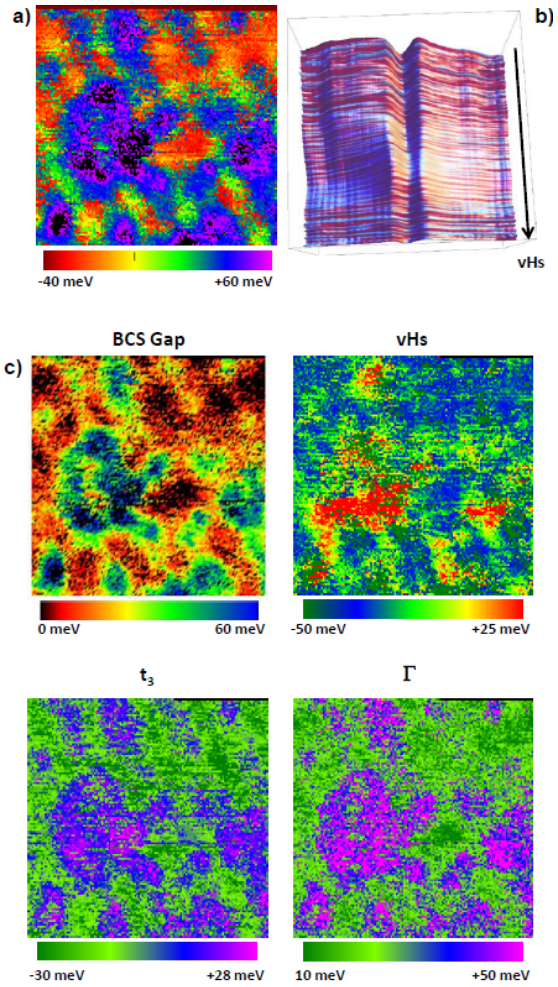

Figure 5: *Analysis of scanning tunneling microscopy (STM) data acquired in $Bi_2Sr_2CuO_{6+\delta}$ ($T_c = 11$ K). (a) Map of the gap magnitude (b) Tunneling spectra sorted according to the VHS position. (c) Maps of the various parameters extracted from the BCS fit of the spectra [16]: BCS gap value, VHS position, tight-binding parameter t_3 and scattering rate* Γ.

of the fitted parameters can be reconstructed (Fig. 5c). Similarly to the gap map (Fig. 5a), all the parameters are locally correlated with the superstructure of the material. We also find the expected correlation of the gap with the scattering parameter Γ, as reported in [16]. Moreover we observe an interesting correlation between the gap and the tight-binding parameter t_3 maps. Since t_3 is relevant of the second neighbor along the a/b-axis in the Copper planes, this could provide crucial keys to argue that it plays an unexpected role in the opening of the gap and thus in how superconductivity appears in cuprates. All our observations show that local doping variations only are not sufficient to explain the evolution of the whole body of tunneling spectra observed on the surface of Bi-based cuprates.

1.11 Revealing the high-energy electronic excitations underlying the onset of high-temperature superconductivity in cuprates *(D. van der Marel)*

In strongly correlated systems the electronic properties at the Fermi energy E_F are intertwined with those at high-energy scales. One of the pivotal challenges in the field of high-temperature superconductivity (HTS) is to understand whether and how the high-energy scale physics associated with Mott-like excitations ($|E - E_F| > 1$ eV) is involved in the condensate formation. We have investigated the interplay between the many-body high-energy CuO_2 excitations at 1.5 and 2 eV, and the onset of HTS. This is revealed by a novel optical pump-supercontinuum probe technique that provides access to the dynamics of the dielectric function in $Bi_2Sr_2Ca_{0.92}Y_{0.08}Cu_2O_8$ over an extended energy range, after the photoinduced suppression of the superconducting pairing. These results unveil an unconventional mechanism at the base of HTS both below and above the optimal hole concentration required to attain the maximum T_c. Our results [17] indicate that most of the superconductivity-induced modifications of the excitation spectrum and optical properties at the low-energy scale are compensated by a variation of the in-plane electronic excitations at 1.5 and 2 eV, demonstrating that these excitations are at the base of an unconventional superconductive mechanism both in the underdoped and overdoped sides of the superconducting dome. When moving from below to above the optimal hole doping, the spectral weight variation of these features entirely accounts for a crossover from a superconductivity-induced gain to a BCS-like loss of the carrier kinetic energy [18, 19][44]. Superconductivity-induced changes of the optical properties at high-energy scales seem to be a universal feature of high-temperature superconductors, indicating that the comprehension of the interplay between low-energy excitations and the high-energy scale physics, associated with Mott-like excitations, will be decisive in understanding high-temperature superconductivity.

1.12 Electronically driven disordering of the vortex lattice in $La_{2-x}Sr_xCuO_4$ *(J. Mesot)*

A commonality across the cuprates, heavy fermion and organic superconductors, and ferro-pnictides is the coexistence of magnetism and superconductivity. The corresponding order parameters typically compete and often a small perturbation is sufficient to tip the balance between the two. Magnetic field-induced vortices may, for example, permit enhanced magnetic correlations in the core regions where the superconducting order parameter is suppressed [46]. This idea was proposed to explain field-induced and -enhanced magnetic correlations observed in the cuprate superconductor $La_{2-x}Sr_xCuO_4$ (LSCO) [47].

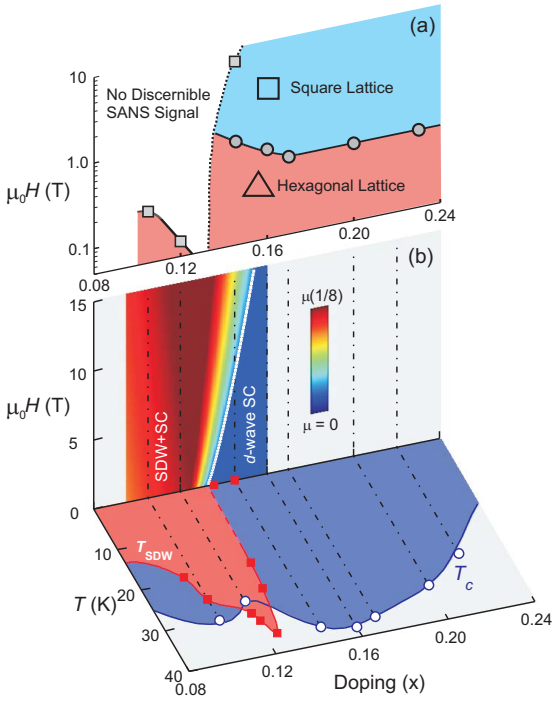

Figure 6: *Phase diagram of (a) the ($T < 3$ K) vortex lattice structure and (b) the magnetism in $La_{2-x}Sr_xCuO_4$, both revealed by neutron diffraction. Circular points are defined by the onset of a square VL coordination. The field – doping plane in (b), adapted from [20], shows schematically the ordered spin-density wave (SDW) moment normalized to that at the 1/8-doping. The temperature – doping plane shows the superconducting dome together with the onset of static incommensurate SDW order T_{SDW} as seen by neutron diffraction [20][45]. The dashed lines indicate the samples studied [21].*

Little is known, however, about the reverse connection: how does the presence of magnetic correlations affect the arrangement of vortices? When magnetism and superconductivity coexist there are at least three relevant length scales: the vortex core size ξ, the vortex spacing a_0, and the magnetic correlation length ζ. Using small angle neutron scattering (SANS) we have studied two different regimes (Fig. 6): (i) far away from the magnetic ordering where $\xi, \zeta \ll a_0$ and (ii) entering the magnetic phase where $\zeta \sim a_0$. In the first regime, where static magnetism is absent, the vortex lattice (VL) structure and core size are understood from pure fermiological considerations.

In the second regime with static long-range magnetism, the vortex arrangement exhibits increasing disorder. We find these regimes to be well-described within the topical "Bragg glass" paradigm [48]. Disordering of the vortex lattice is usually driven by effects extrinsic to superconductivity such as sample impurities, crystalline defects or rare earth magnetism. In contrast, magnetic and superconducting (SC) order parameters are intertwined in LSCO; we show that this provides a novel and tunable source of VL disorder.

As shown in Fig. 6, the appearance of magnetism is, in essence, concomitant with the suppression of SANS intensity with field and underdoping. Drawing upon results from the literature and new observations (see Ref. [21]), we are able to plot the vortex lattice structure at low temperature T versus magnetic field H and doping x.

1.13 Identification of subgap features in the tunneling spectra of $YBa_2Cu_3O_{7-\delta}$ *(Ø. Fischer)*

Contrary to the easy-cleavable Bi-based cuprates, $YBa_2Cu_3O_{7-\delta}$ (YBCO) has been less intensively studied by scanning tunneling spectroscopy (STS). In early STS studies, one of the most striking and still unexplained observation is the existence of finite-energy states in the center of the vortex cores in YBCO [49]. These states were also detected in the vortex cores of Bi-2212 compounds, and appeared to be energy-scaled with the superconducting gap [50]. Subgap features in the same energy ranges were observed outside the vortex cores, and even in zero magnetic field. In recent STS investigations on as grown YBCO surfaces, spectroscopic maps acquired in a 7 T magnetic field revealed a distribution of tunneling spectra with very different characteristics (Fig. 7a), indicating doping inhomogeneities attributed to sample aging. All spectra show a feature located in the $5-6$ meV range. Some of the spectra exhibit sharp coherence peaks at $15-20$ meV with faint subgap kinks, reminiscent of the spectra acquired outside the cores. Although a direct imaging of individual flux lines was hampered by the inhomogeneities of the spectral features, some other spectra reveal the very sharp low-energy peaks reported earlier, and a broad pseudogap-like feature emerging at energies slightly higher than the superconducting gap.

Tunneling spectra acquired over a similar area in zero field reveal only low-energy kinks and no sharp peaks. We also acquired zero-field

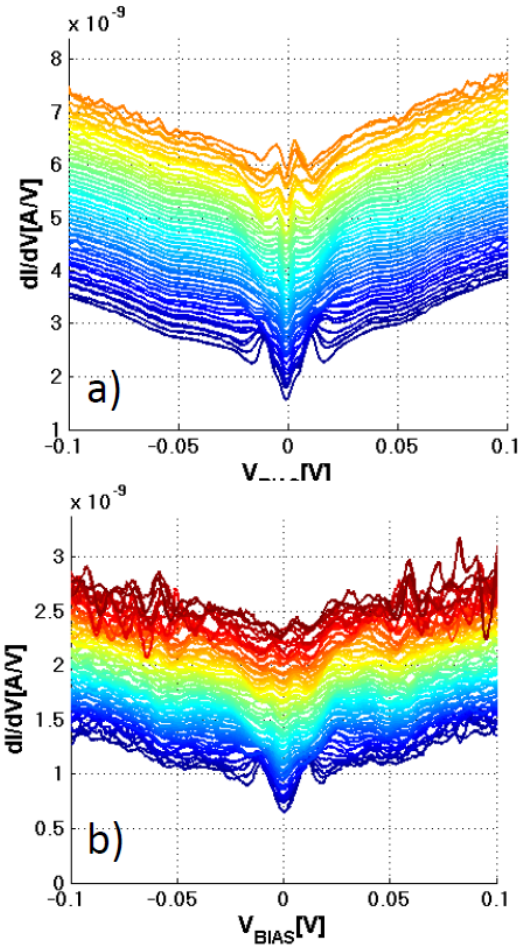

Figure 7: *Distribution of tunneling spectra in $YBa_2Cu_3O_{7-\delta}$ ($T_c = 91$ K) (a) in a 7 T field, revealing the core finite-energy states, (b) on a cleaved single-crystal in zero-field.*

spectroscopic maps on crystals fractured in air (Fig. 7b); while most of the spectra exhibit subgap kinks and quite developed coherence peaks, we also detect spectra exhibiting very sharp low-energy peaks (with broad kinks at higher energy), similar to the ones observed in the vortex cores. All these observations raise the question of the origin and of the links between these subgap features. The fact that sharp peaks appear in the vortex cores and are flanked by broad high-energy kinks suggests that these states are somewhat associated with the pseudogap. On the other hand, YBCO-specific structural features (like the CuO chains) might also play a role in the evanescence of these states, and the identification of the mechanisms behind these peculiar spectroscopic signatures is the challenging goal of our investigations.

1.14 Search for orbital currents in $YBa_2Cu_4O_8$ *(H. Keller)*

The concept of orbital currents (OC) was proposed to explain the pseudogap of the cuprate superconductors [51]. However, the present state of knowledge about OC is contradictory both in theory and experiment. No evidence for local fields was found, i.e. in a Yttrium nuclear magnetic resonance (NMR) investigation by our group [22].

Recently, Zeeman perturbed nuclear quadrupole resonance was applied to evaluate weak magnetic fields in the context of OC in cuprate superconductors [23]. The magnetic environment of the Barium atom in *c*-axis oriented powder samples of $YBa_2Cu_4O_8$ was investigated in the pseudogap phase at 90 K. The Ba atom is of particular interest since it is situated outside, but close to the copper oxide bilayer, at a position where the combined fields from the two neighboring layers would be enhanced because of the suggested ferromagnetic order within the bilayer. Zeeman perturbed nuclear resonance utilizes the fact that the Ba atom has both a quadrupolar and a nuclear magnetic moment. This technique is a rarely implemented variant of nuclear quadrupole resonance (NQR), which utilizes the local electric field gradient to lift the nuclear degeneracy. The Zeeman perturbation is introduced by means of an external coil as a weak static magnetic field (of the order of mT). For a typical ^{137}Ba NQR resonance line of a few hundred kHz width (inset of Fig. 8), the resonance line split caused by a field of the order of mT would not be directly observable. The principle of the measurement is to detect a weak local magnetic field through a beat oscillation superposed on the Gaussian shaped decay of the spin echo intensity, caused by homonuclear dipolar fields (Fig. 8). In order to demonstrate the sensitivity of the technique for weak local magnetic fields, the Ba nucleus was studied at 300 K, where no OC are expected. The result of this measurement is presented in Fig. 8, revealing the expected dominating Gaussian decay of the spin echo intensity with pulse separation time τ. This curve is our zero-field reference. The measurement procedure was calibrated using applied Zeeman fields of known strength. Fields calculated from the response were found to deviate less than 0.07 mT from the Zeeman fields actually applied with the calibrated external coil. In all experiments, background contributions, including Earth's magnetic field, were shielded. In conclusion, the NQR results [23] do not indicate the presence of local fields at the Ba site in the pseudogap phase of *c*-axis oriented $YBa_2Cu_4O_8$. The detection limit of our method excludes static or dynamic field larger than 0.07 mT and 0.7 mT, respectively [23].

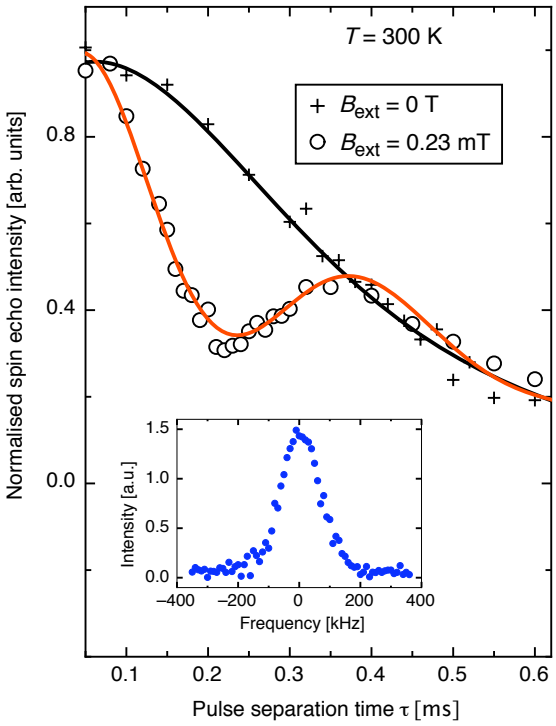

Figure 8: *Dependence of the normalized ^{137}Ba spin echo intensity as a function of the pulse separation time τ at 300 K for B_{ext} parallel to the c-axis of $YBa_2Cu_4O_8$. Results are shown for $B_{ext} = 0$ T and $B_{ext} = 0.23$ mT. The inset shows the ^{137}Ba resonance line at 300 K in zero external field.*

1.15 μSR studies of novel superconductors under pressure *(H. Keller)*

One of the most unique techniques for studying magnetic and superconducting properties of solid is muon-spin rotation (μSR). Recent studies showed that most of the novel superconductors (e.g. iron-based, heavy fermion, cuprates) exhibit quite a strong and interesting evolution of the superconducting and magnetic properties with pressure. In order to use μSR also in high transverse fields for magnetic materials, the μSR data analysis methods should be refined to account for the fields induced by the sample in the pressure cell volume.

We studied this problem experimentally for the case of $YBa_2Cu_3O_x$ [24]. Modeling of the field distribution induced by a homogeneously magnetized sample showed that there is indeed a substantial induced magnetic field at the muon stopping sites (Fig. 9). This leads to additional contribution to the pressure cell re-

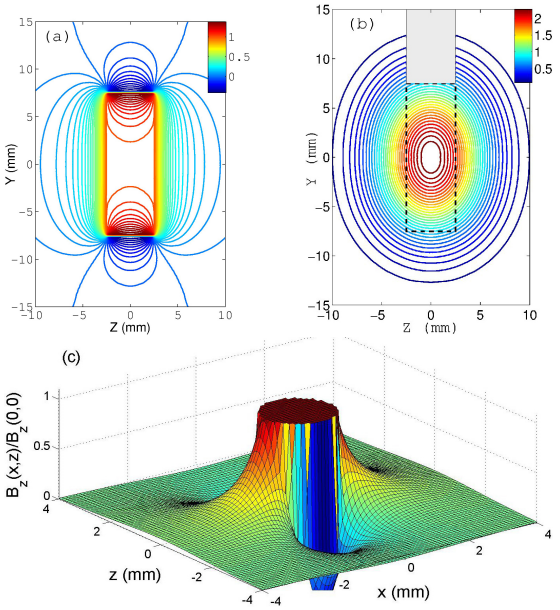

Figure 9: *(a) Contour plot of the field distribution $B_z(y,z)$ along the sample. (b) Contour plot of the muon stopping distribution in the pressure cell. The dashed line indicates the cylindrical sample space (radius $R = 2.5$ mm and height $H = 15$ mm). (c) Plot of the field distribution $B_z(y,z)$ across the sample.*

laxation rate proportional to the magnetization of the sample. The simulated μSR response of the pressure cell is in good agreement with that obtained experimentally [24].

1.16 Band structure and properties of cuprates, oxides and metallic systems *(T. Giamarchi)*

First-principle density functional calculations on Nd_2CuO_4 were carried out by T. Jarlborg (UniGE), showing that the f-band is partially occupied at the Fermi energy. From excited state calculations, with an electron removed from an occupied band and put into an itinerant state at high energy, it is possible to simulate the photoemission process. The relaxation energy for excitations from the f-state is negative and larger than from itinerant states. The effect is opposite in the inverse process. Calculation for the wide Cu-d band is such that the band seems to be narrower than the true ground state because of excitation relaxation. The method is applied to elementary hcp and bcc rare earth elements where local density approximation (LDA) f-levels also can be fully occupied and below the Fermi energy. The electronic heat capacities are consistent with the positions of the f-levels and the excitation relaxations go in the same directions as in Nd_2CuO_4, but with varying amplitudes. In Ce-doped Nd_2CuO_4, it is possible to interpret photoemission from very weak electron doping. Signatures of f-bands at the Fermi surface are deduced from Compton profiles. Results from calculations on $La_2CuO_{4-\delta}$ and $Ba_2CuO_{4-\delta}$ with oxygen vacancies within CuO planes or within apical positions are very different. The latter acts as electron dopants in the Cu-d band, so that apical O-vacancies in the SrCuO system will approach the situation of strongly hole-doped LaCuO.
It is shown that observations of coexisting Fermi surface arcs and closed Fermi surface pockets in ARPES in hole-doped La_2CuO_4 are consistent with modulated spin fluctuations of varying wave lengths. This result makes a link to what is seen from neutron scattering and suggests that spin-phonon coupling is an important mechanism in the cuprates.

2 Electronic properties and high-T_c superconductivity in iron chalcogenides and iron pnictides

2.1 Improved crystal growth $Ln1111$ *(J. Karpinski)*

The LnFePnO ($Ln1111$. Ln: lanthanide, Pn: pnicogen) crystals up to 300 μm and $T_c \approx 53$ K were reproducibly obtained from NaCl/KCl flux. Using NaAs and KAs fluxes crystal size has been increased up to 1 mm, but phase formation and F doping control are more difficult (Fig. 10).

2.2 Pressure-induced superconductivity in $SmFeAs_{1-x}P_xO_{1-y}$ *(J. Karpinski)*

Single-crystals of $SmFeAs_{1-x}P_xO_{1-y}$ with various T_c have been grown under high pressure, and their structural and superconducting properties were investigated. The upper critical field deduced from resistance measurements is anisotropic with slopes of $\sim$ 5.7 T/K ($H \parallel ab$-plane) and $\sim$ 1.3 T/K ($H \parallel c$-axis) sufficiently far below T_c [25].

2.3 Magnetism and superconductivity in $LaFeAsO_{0.945}F_{0.055}$ *(J. Karpinski)*

We show that the application of hydrostatic pressure on $LaFeAsO_{0.945}F_{0.055}$, which is at the

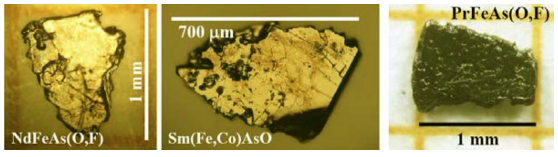

Figure 10: *Single-crystals of $Ln1111$.*

border to the superconducting state but still magnetic, leads to a substantial decrease of T_N and a reduction of the magnetic phase volume and, at the same time, to a strong increase of T_c and the diamagnetic susceptibility. From magnetic history dependent zero field muon-spin relaxation (ZF-μSR) measurements it can be concluded that superconductivity most probably develops in the areas of the sample that are non-magnetic down to the lowest temperatures. This shows that in $LaFeAsO_{1-x}F_x$ magnetism and superconductivity are competing order parameters [26].

2.4 Specific heat measurements on $SmFeAsO_{1-x}F_x$ single-crystals *(J. Karpinski)*

In zero-field, a clear cusp-like anomaly in C/T with a height of $\Delta C/T_c = 24$ mJ/mole K^2 appears at $T_c = 49.5$ K. In magnetic fields applied along the c-axis, pronounced superconducting fluctuations induce strong broadening and suppression of the specific heat anomaly

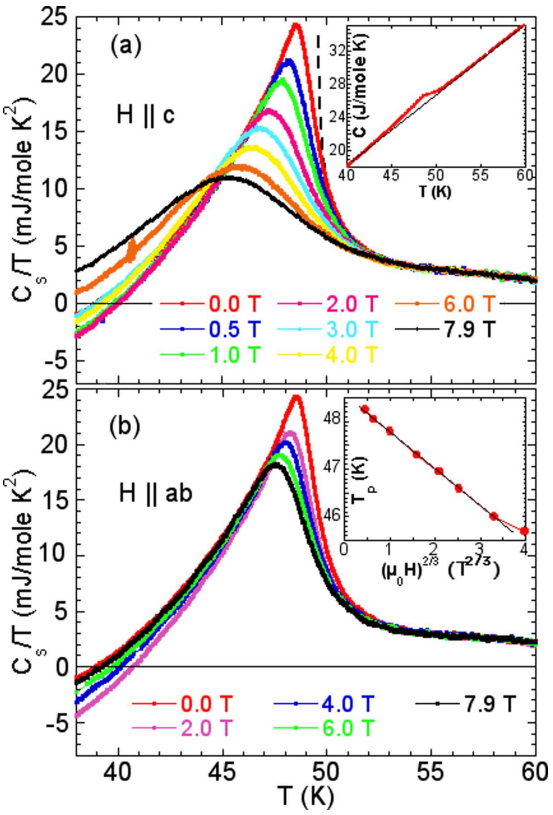

Figure 11: *Temperature dependence of the superconducting specific heat plotted as C_s/T in various magnetic fields applied (a) along the c-axis and (b) along the ab-planes. The inset in (a) shows the total specific heat with the solid line indicating the linear background. The inset in (b) shows the peak temperature of C_s/T plotted versus $H^{2/3}$.*

(Fig. 11). Upper critical field slope is 3.5 T/K and anisotropy $\Gamma = 8$. The small value of $\Delta C/T_c$ implies a modest value of the Sommerfeld coefficient $\gamma \sim 8$ mJ/mole K^2 indicating that $SmFeAsO_{1-x}F_x$ is characterized by a modest density of states and a strong coupling [27].

2.5 Structure modifications due to substitution of P for As *(J. Karpinski)*

We have investigated the structural response to P substitution after ambient (AP) and high-pressure (HP) treatment. After HP treatment $SmFeAs_{1-x}P_xO_{1-y}$ samples are O deficient which moves the Sm-O layer closer to the As-Fe-As block and facilitates electron transfer, while P substitution in AP samples (without O deficiency) is a pure geometrical lattice effect without charge carrier transfer. Oxygen deficiency make more electrons available for transfer to the Fe-As/P layer, modifying the bonding geometry in $Fe(As,P)_4$ and shifting the Fermi level to higher energies [25].

2.6 $K_xFe_{2-y}Se_2$ *(E. Giannini)*

Alkali-intercalated superconducting chalcogenides were thought to be isostructural to the "122" ferropnictides, but actually exhibit a large amount of vacancies that form an ordered pattern in the crystal structure. The vacancy sublattice is likely to play a key role in the superconductivity of this system [52], which is reported to occur below 33 K. We have grown crystals of $K_xFe_{2-y}Se_2$ by the self-flux in a vacuum sealed quartz reactor, starting from a stoichiometric admixture of alkaline elements, Fe and Se, instead of pre-forming FeSe as commonly reported. As grown samples are not single-phase and crystals of various compositions around the nominal one are cleaved out. A record $T_{c,onset}$ of $\sim$ 42 K has been observed both in transport and magnetic measurements in a sample made from a nominal atomic ratio 0.55:1.65:2. In contrast, no superconductivity is obtained when Te substitutes for Se; this is likely to alter the ordered vacancy pattern, and element segregation and phase separation are observed.

2.7 Fe-tuning in $Fe_{1+x}Te_{1-y}Se_y$ *(E. Giannini, H. Rønnow)*

In superconducting Fe-based pnictides and chalcogenides, an antiferromagnetic (AF) order is suppressed either by chemical substitution or pressure, while the material enters a superconducting state. In superconducting Fe-chalcogenides $Fe_{1+x}Te_{1-y}Se_y$, we have shown

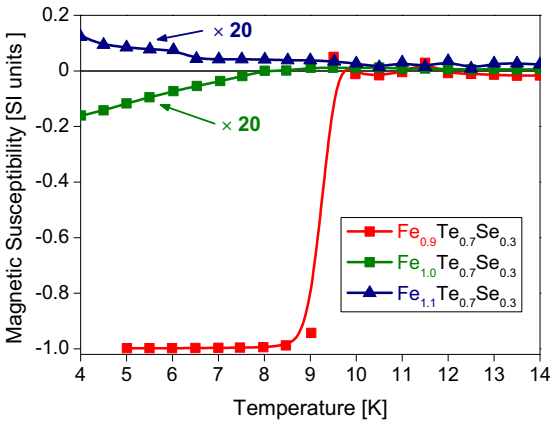

Figure 12: *Magnetic susceptibility at low field (10 Oe) at three different nominal Fe contents. Values of the Fe formula units 1 (green) and 1.1 (blue) are enhanced by a factor 20 to be shown on the same scale as Fe = 0.9 (red).*

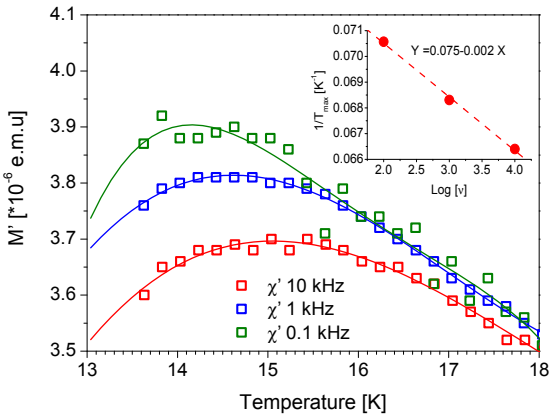

Figure 13: *$\chi_{ac}(T)$ of $Fe_{1.05}Te_{0.73}Se_{0.27}$ at three different frequencies. The maximum shifts following the ν-dependence expected for metallic spin glass systems (inset).*

that both the Fe excess and the Se substitutions modify the FeCh_4 tetrahedron and tune the magnetic and electronic properties, thus drawing a 3D phase diagram T versus (x, y) [28]. We have prepared crystals of $Fe_{1+x}Te_{1-y}Se_y$ in the composition range $x \in (0, 0.1)$ and $y \in (0.1, 0.3)$, which corresponds to the intermediate region of the phase diagram in which either non-bulk superconductivity or coexistence of superconductivity and magnetic order are often invoked. Magnetic susceptibility clearly shows the strong effect of Fe excess on the superconducting state (Fig. 12): lowering the occupation of the additional Fe site enhances superconductivity.

The ability of growing sizeable crystal with a controlled composition and tuned electronic properties has allowed us to carry out various experiments that prove the interplay between spin fluctuations and superconductivity. The most striking result has been obtained in an inelastic neutron scattering study conducted in collaboration with the group of H. Rønnow at EPFL (see Project 6). It has been proven that "hourglass" dispersing (π, π) spin fluctuations are a necessary condition for superconductivity, in a mechanism that is reminiscent of what is observed in $YBa_2Cu_3O_{7-\delta}$.

2.8 Fe-tuning in $Fe_{1+x}Te_{1-y}Se_y$ *(E. Giannini, L. Forró)*

We have performed a systematic study of transport properties as a function of pressure ($\leqslant$ 2.3 GPa) and Fe content ($x = 0.2$, 0.5 and $y = 0$, 0.2, 0.3). Structural effects can be induced in $Fe_{1+x}Te$ [29] either by applying mechanical pressure or by Se substitution.

We have also demonstrated that pressure is a clean control parameter to drive the system with high Fe-excess through the metal-insulator (MI) transition, in analogy with increasing the Se-doping or reducing the Fe-excess. Pressure is found to suppress the low-T magnetic contributions to the resistivity and thermopower, due to Fe-excess. Below a critical pressure $P_c = 0.8$ GPa, the observed behavior is compatible with a Kondo-like scenario due to diluted magnetic impurities. The existence of disordered magnetic moments or clusters, ascribable to compositional fluctuations and phase separation in the region between the AF and SC states, is responsible for a spin glass behavior observed above T_c and marked by the frequency dependence of the $\chi_{ac}(T)$ (Fig. 13).

2.9 Vortex dynamics in $Fe_{1+x}Te_{1-y}Se_y$ *(E. Giannini, C. Senatore)*

We have investigated the magnetic properties of $Fe_{1+x}Te_{1-y}Se_y$ in the superconducting state. Field-, temperature-, and time-dependence of the magnetization in $Fe_{1.02}Te_{0.7}Se_{0.3}$ have shown that a weak collective pinning acts in this material, originating from spatial variations of the charge carrier mean free path (δl-pinning). Our results are compatible with a 10 nm-scale phase separation reported by direct scanning transmission electron microscopy (STEM) and electron energy-loss spectroscopy (EELS) observations [53], which would act as pinning centers. This leaves the question about intrinsic coexistence of magnetism and superconductivity in Fe-chalcogenides still controversial. Vortices are found to move in the single-vortex regime up to fields as high as 8 T in Fe(Te,Se) materials,

in agreement with what is found in other Fe-pnictides. A temperature- and time-dependent second peak effect is observed, which is reminiscent of the behavior of YBCO high-T_c superconductor. Our findings point to a unique vortex configuration, at the origin of the peak effect, determined by T independent vortex-vortex and vortex-defect interactions over a wide range of T. Such an unexpected finding deserves further investigations in other superconductors.

2.10 Anisotropic in-plane optical conductivity in detwinned $Ba(Fe_{1-x}Co_x)_2As_2$ *(L. Degiorgi)*

We studied the anisotropic in-plane optical conductivity of detwinned $Ba(Fe_{1-x}Co_x)_2As_2$ single-crystals for $x = 0$, 2.5% and 4.5% in a broad energy range (3 meV – 5 eV) across their structural and magnetic transitions. Detwinned, single-domain specimens were achieved with the crystal held under uniaxial pressure. Fig. 14 shows the real part $\sigma_1(\omega)$ of the optical conductivity of detwinned $Ba(Fe_{1-x}Co_x)_2As_2$ for different temperatures along both polarization directions. In the visible and UV energy interval $\sigma_1(\omega)$ is characterized by polarization independent broad absorption bands which overlap with a dominant near-infrared (NIR) contribution peaked at about 5000 cm^{-1}. The temperature and doping dependent optical anisotropy in $\sigma_1(\omega)$ is mainly evident in the far-infrared (FIR) and mid-infrared (MIR) regions. In the FIR region, there is a strong polarization dependence of the itinerant charge carriers contribution to $\sigma_1(\omega)$. Along the a-axis $\sigma_1(\omega)$ shows a more pronounced metallic behavior which gets enhanced below the magnetic phase transition at T_N ($\leq T_s$), leading to the stripe-like spin order pointed out above. Along the b-axis $\sigma_1(\omega)$ below T_N is depleted due to the formation of a pseudogap, prior to displaying a metallic-like upturn for $\omega \to 0$. The strong absorption peak dominating $\sigma_1(\omega)$ at about 5000 cm^{-1} develops into a pronounced shoulder on its MIR frequency tail at about 1500 cm^{-1}. This latter MIR-band in $\sigma_1(\omega)$ shows a strong polarization and doping dependence, as highlighted in Fig. 14 (bottom panels). Interestingly enough, for increasing doping the maximum of the MIR-band shifts to lower frequencies indicating that the MIR-band is significantly affected by the doping.

It is especially interesting to compare the temperature dependence of the dc ($\Delta\rho$) and optical ($\Delta\sigma_1(\omega)$) anisotropy. Two characteristic frequencies, identifying the position of the peaks in $\sigma_1(\omega)$ (Fig. 14), are selected in order to follow the temperature dependence of $\Delta\sigma_1(\omega)$; namely, $\omega_1 = 1320$ cm^{-1} and $\omega_2 = 5740$ cm^{-1} for $x = 0.025$. It is remarkable that the temperature dependence of $\Delta\sigma_1(\omega)$ at ω_1 and ω_2 follows the temperature dependence of $\frac{\Delta\rho}{\rho}$ in all compounds, extracted from the dc properties and from the metallic contribution in $\sigma_1(\omega)$, saturates at constant values well above T_s and then displays a variation for $T < 2T_s$ (Fig. 15). We underscore that the rather pronounced optical anisotropy, extending up to temperatures higher than T_s for the stressed crystals, clearly implies an important pressure-induced anisotropy in the electronic structure, which is also revealed by ARPES measurements.

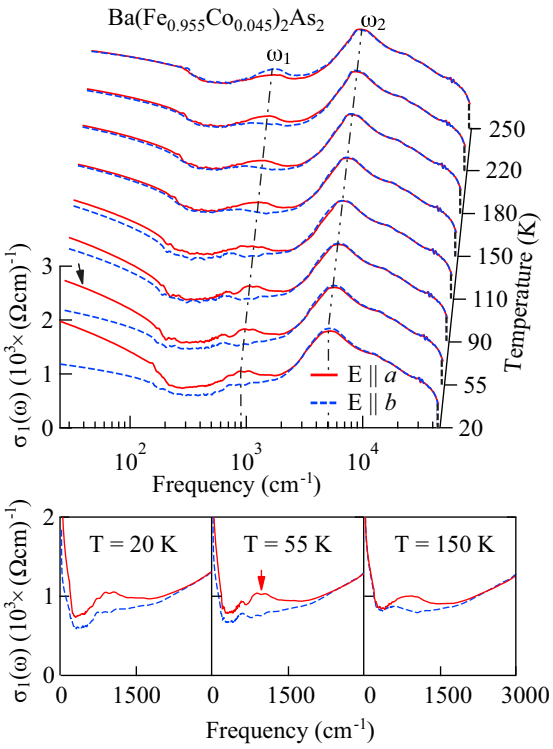

Figure 14: *Temperature dependence of the optical conductivity of $Ba(Fe_{1-x}Co_x)_2As_2$ ($x = 0.045$) in the whole measured spectral range for two polarizations, parallel to the a-axis direction ($E \parallel a$, red solid line) or perpendicular to it ($E \parallel b$, blue dashed line). The black arrow indicates $\sigma_1(\omega)$ at the temperature close to the structural phase transition at T_s, while the red arrow (bottom panels) indicates the center of the MIR-band close to T_N. The dashed-dotted and dashed double-dotted lines (top panel) mark the frequency ω_1 and ω_2 (see text).*

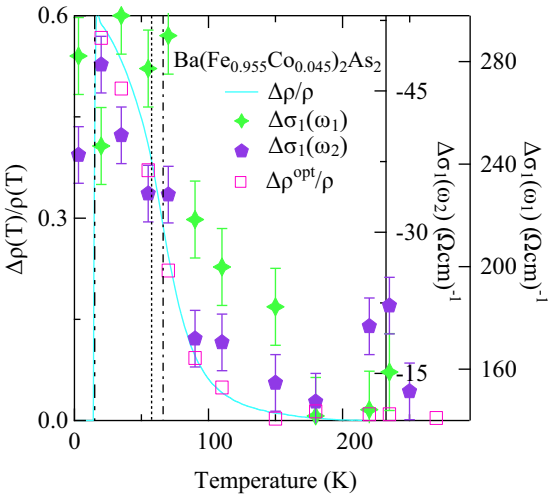

Figure 15: *Temperature dependence of the dichroism $\Delta\sigma_1(\omega)$ of $Ba(Fe_{1-x}Co_x)_2As_2$ ($x = 0.045$) at ω_1 and ω_2 (Fig. 14) compared to $\frac{\Delta\rho}{\rho}$ obtained from the dc transport data, as well as from the metallic (Drude) contribution in $\sigma_1(\omega)$ ($\Delta\rho^{opt}/\rho$). The vertical dotted-dashed, dotted and double-dotted-dashed lines mark the structural, magnetic and superconducting phase transitions at T_s, T_N and T_c, respectively.*

2.11 The electronic structure of $LaRu_2P_2$ *(J. Mesot)*

$LaRu_2P_2$ is a stoichiometric pnictide with a superconducting transition temperature $T_c \sim 4$ K [54]. It is isostructural to "122" high-temperature Fe-pnictide superconductors (e.g. doped $BaFe_2As_2$) [55]. Using the newly developed soft X-ray angle-resolved photoemission spectroscopy (SX-ARPES) at ADRESS beamline of SLS at PSI, we revealed the electronic structure of $LaRu_2P_2$ in the normal state. The observed Fermi surface (FS) is highly three-dimensional (Fig. 16), and is very different from the quasi-2D FS cylinders of high-temperature superconducting Fe-pnictides. The mapped Fermi surface is in good agreement with density functional theory (DFT) calculations. We also found that, in contrast to Fe-pnictide superconductors for which their bandwidths are renormalized by a factor of $2-3$, the measured dispersions of $LaRu_2P_2$ can be reproduced by DFT calculation without notable renormalization (Fig. 16). By comparing with ultraviolet(UV)-ARPES spectra, we illustrate that the increased probing depth of SX-ARPES is essential for the determination of bulk electronic structure in our experiments [30].

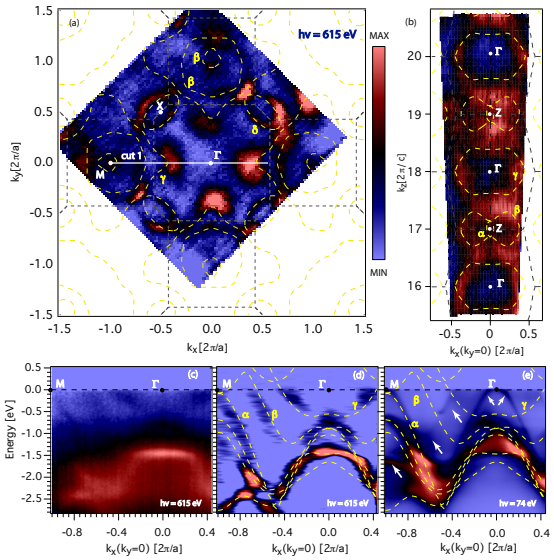

Figure 16: *ARPES spectra for $LaRu_2P_2$. (a) Fermi surface (FS) map in $(k_x, k_y, 22\pi/c)$- plane, taken with $h\nu = 615$ eV. (b) FS map in $(k_x, 0, k_z)$- plane, taken with $h\nu = 300-550$ eV in steps of 5 eV. The maps in (a) and (b) are obtained by integrating ARPES spectral weight in an energy window of $E_F \pm 50$ meV. The superimposed dashed lines are the FS from DFT calculation. (c) ARPES spectrum along $M-\Gamma$ direction (cut 1 in (a)) taken with $h\nu = 615$ eV. (d) The second derivative of momentum distribution curves (MDC) of the ARPES data in (c). (e) UV-ARPES spectrum along $M-\Gamma$ direction taken with $h\nu = 74$ eV. The superimposed dashed lines are the band structure from DFT calculation.*

2.12 Critical currents and geometrical vortex transition in Fe-pnictide superconductors *(B. Batlogg)*

Fe-pnictide superconductors pose conceptual challenges, particularly concerning the pairing interaction and symmetry, and they are also of interest for potential applications because of the extremely high critical fields and high critical current densities. The FeAs layers host the essential electrons for high-temperature superconductivity, and these layers may be separated by various structural blocks resulting in a large family of layered superconductors.

To gain insight into the rich vortex physics on a microscopic scale and to further improve j_c, it is highly desirable to locate the pinning sites. To this end we create a particular vortex arrangement by aligning the magnetic field along the superconducting planes in SmFeAs(O,F) with $T_c \sim 50-48$ K, and passing the current perpendicular to them. The single-crystal bars are microcut with a focused ion beam into samples with various geometries and contact arrangements (Fig. 17a, b).

An overview of the dissipation as a func-

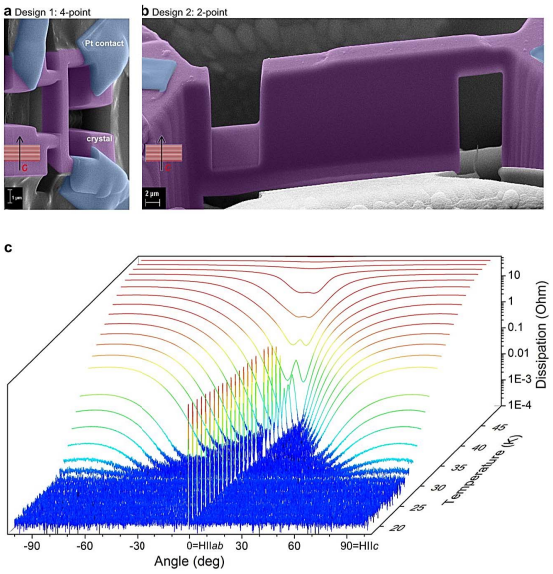

Figure 17: *(a), (b) SEM images of sample in four-point and in two-point contact design to measure the c-axis resistivity. The crystal (purple) was cut into shape by three-dimensional cutting and electrically contacted (blue) using a focused ion beam technique. The resistivity anisotropy at T_c is around 15, thus homogenizing the current profile in the two-point sample. (c) Dissipation as a function of angle between the magnetic field ($H = 12$ T) and the crystallographic ab-plane for several temperatures. Starting at high temperatures, the typical V-shaped angle dependence originating from the electronic anisotropy turns into a more camel-toe like feature exhibiting a broad peak when the field lies exactly parallel to the FeAs planes. Upon further cooling below $T^* \sim 41$ K, the feature sharpens significantly and increases in height. The FWHM of the peaks is below 0.3° at low temperatures. T^* is identified as the crossover temperature separating larger from smaller, completely locked-in vortices.*

tion of angle between applied field (12 T) and FeAs layers at various temperatures is shown in Fig. 17c. We have discovered a distinct vortex matter transition upon cooling below $T^* \sim 41$ K into a unique configuration of highly mobile vortices. Below T^*, in agreement with $\xi_c(T^*) \sim c/2$, the vortex core is confined in-between two adjacent FeAs planes by the periodic modulations along c of the superconducting order parameter, but are nearly free to slide between adjacent planes. This motion parallel to the FeAs layers is even more pronounced at lowest temperatures, well below T_c and H_{c2}, as the vortex cores avoid the highly effective pinning sites located in the FeAs layers. For fields slightly out-of-plane ($< 0.3°$) the vortices are again completely immobile as they cross the planes and hence are strongly pinned by defects within the FeAs layers. Our results indicate a strong and highly effective pinning mechanism localized in the FeAs layers, thus suggest a pathway to improve the technological prospect of the Fe pnictides superconductors.

3 Collaborative efforts

Collaborative efforts are of essential importance for the success of Project 4. Numerous collaborations between all crystal growers and other experimental groups have taken place: the cuprates, transition metal oxides, iron pnictides and iron selenides that were grown in the laboratories at ETHZ, EPFL, UniGE and PSI have been analyzed by at least two other groups at different institutions. Theory groups at the ETHZ, UniGE, UniFR have modeled the results obtained with ARPES, STM, optical spectroscopy, inelastic neutron scattering(INS), and provide theoretical feedback and ideas for further materials development as well as novel experiments. Experimental groups at EPFL, UniGE, ETHZ have ongoing projects with experiments carried out jointly at the three complementary probes of synchrotron X-rays, neutrons and muons at PSI.

MaNEP-related publications

[1] P. Werner, E. Gull, M. Troyer, and A. J. Millis, Physical Review Letters **101**, 166405 (2008).

► [2] L. de' Medici, J. Mravlje, and A. Georges, Physical Review Letters **107**, 256401 (2011).

► [3] J. Mravlje, M. Aichhorn, and A. Georges, arXiv:1108.1168 (2011).

► [4] O. E. Peil, A. Georges, and F. Lechermann, Physical Review Letters **107**, 236404 (2011).

► [5] X. Deng, M. Ferrero, J. Mravlje, M. Aichhorn, and A. Georges, arXiv:1107.5920 (2011).

[6] N. Reyren, S. Thiel, A. D. Caviglia, L. F. Kourkoutis, G. Hammerl, C. Richter, C. W. Schneider, T. Kopp, A.-S. Ruetschi, D. Jaccard, M. Gabay, D. A. Muller, J.-M. Triscone, and J. Mannhart, Science **317**, 1196 (2007).

[7] A. D. Caviglia, S. Gariglio, N. Reyren, D. Jaccard, T. Schneider, M. Gabay, S. Thiel, G. Hammerl, J. Mannhart, and J.-M. Triscone, Nature **456**, 624 (2008).

[8] D. van der Marel, J. L. M. van Mechelen, and I. I. Mazin, Physical Review B **84**, 205111 (2011).

[9] J. L. M. van Mechelen, D. van der Marel, C. Grimaldi, A. B. Kuzmenko, N. P. Armitage, N. Reyren, H. Hagemann, and I. I. Mazin, Physical Review Letters **100**, 226403 (2008).

[10] W. Meevasana, X. J. Zhou, B. Moritz, C.-C. Chen, R. H. He, S.-I. Fujimori, D. H. Lu, S.-K. Mo, R. G. Moore, F. Baumberger, T. P. Devereaux, D. van der Marel, N. Nagaosa, J. Zaanen, and Z.-X. Shen, New Journal of Physics **12**, 023004 (2010).

[11] J. T. Devreese, S. N. Klimin, J. L. M. van Mechelen, and D. van der Marel, Physical Review B **81**, 125119 (2010).

► [12] T. M. Rice, K.-Y. Yang, and F. C. Zhang, Reports on Progress in Physics **75**, 016502 (2012).

[13] A. J. A. James, R. M. Konik, and T. M. Rice, arXiv:1112.2676 (2011).

[14] D. Baeriswyl, Annalen der Physik (Leipzig) **523**, 724 (2011).

[15] E. Razzoli, G. Drachuck, A. Keren, M. Radovic, J. Chang, J. Mesot, and M. Shi, *in preparation* (2012).

► [16] A. Piriou, N. Jenkins, C. Berthod, I. Maggio-Aprile, and Ø. Fischer, Nature Communications **2**, 221 (2011).

► [17] C. Giannetti, F. Cilento, S. Dal Conte, G. Coslovich, G. Ferrini, H. Molegraaf, M. Raichle, R. Liang, H. Eisaki, M. Greven, A. Damascelli, D. van der Marel, and F. Parmigiani, Nature Communications **2**, 353 (2011).

[18] H. J. A. Molegraaf, C. Presura, D. van der Marel, P. H. Kes, and M. Li, Science **295**, 2239 (2002).

[19] F. Carbone, A. B. Kuzmenko, H. J. A. Molegraaf, E. van Heumen, V. Lukovac, F. Marsiglio, D. van der Marel, K. Haule, G. Kotliar, H. Berger, S. Courjault, P. H. Kes, and M. Li, Physical Review B **74**, 064510 (2006).

[20] J. Chang, C. Niedermayer, R. Gilardi, N. B. Christensen, H. M. Rønnow, D. F. McMorrow, M. Ay, J. Stahn, O. Sobolev, A. Hiess, S. Pailhes, C. Baines, N. Momono, M. Oda, M. Ido, and J. Mesot, Physical Review B **78**, 104525 (2008).

[21] J. Chang, J. S. White, M. Laver, C. J. Bowell, S. P. Brown, A. T. Holmes, L. Maechler, S. Strassle, R. Gilardi, S. Gerber, T. Kurosawa, N. Momono, M. Oda, M. Ido, O. J. Lipscombe, S. M. Hayden, C. D. Dewhurst, R. Vavrin, J. Gavilano, J. Kohlbrecher, E. M. Forgan, and J. Mesot, *submitted* (2012).

[22] S. Strässle, J. Roos, M. Mali, H. Keller, and T. Ohno, Physical Review Letters **101**, 237001 (2008).

► [23] S. Strässle, B. Graneli, M. Mali, J. Roos, and H. Keller, Physical Review Letters **106**, 097003 (2011).

► [24] A. Maisuradze, A. Shengelaya, A. Amato, E. Pomjakushina, and H. Keller, Physical Review B **84**, 184523 (2011).

[25] N. D. Zhigadlo, S. Katrych, M. Bendele, P. J. W. Moll, M. Tortello, S. Weyeneth, V. Y. Pomjakushin, J. Kanter, R. Puzniak, Z. Bukowski, H. Keller, R. S. Gonnelli, R. Khasanov, J. Karpinski, and B. Batlogg, Physical Review B **84**, 134526 (2011).

[26] R. Khasanov, S. Sanna, G. Prando, Z. Shermadini, M. Bendele, A. Amato, P. Carretta, R. De Renzi, J. Karpinski, S. Katrych, H. Luetkens, and N. D. Zhigadlo, Physical Review B **84**, 100501 (2011).

[27] U. Welp, C. Chaparro, A. E. Koshelev, W. K. Kwok, A. Rydh, N. D. Zhigadlo, J. Karpinski, and S. Weyeneth, Physical Review B **83**, 100513 (2011).

[28] R. Viennois, E. Giannini, D. van der Marel, and R. Černý, Journal of Solid State Chemistry **183**, 769 (2010).

[29] E. Giannini, R. Viennois, R. Černý, and M. Hanfland, Chemistry of Metals and Alloys **3**, 63 (2010).

[30] E. Razzoli, M. Kobayashi, V. N. Strocov, B. Delley, Z. Bukowski, J. Karpinski, N. C. Plumb, M. Radovic, J. Chang, T. Schmitt, L. Patthey, J. Mesot, and M. Shi, *submitted* (2012).

Other references

[31] K. Haule and G. Kotliar, New Journal of Physics **11**, 025021 (2009).

[32] E. E. Rodriguez, F. Poineau, A. Llobet, B. J. Kennedy, M. Avdeev, G. J. Thorogood, M. L. Carter, R. Seshadri, D. J. Singh, and A. K. Cheetham, Physical Review Letters **106**, 067201 (2011).

[33] R. Eguchi, A. Chainani, M. Taguchi, M. Matsunami, Y. Ishida, K. Horiba, Y. Senba, H. Ohashi, and S. Shin, Physical Review B **79**, 115122 (2009).

[34] J. F. Schooley, W. R. Hosler, and M. L. Cohen, Physical Review Letters **12**, 474 (1964).

[35] J. G. Bednorz and K. A. Müller, Reviews of Modern Physics **60**, 585 (1988).

[36] C. S. Koonce, M. L. Cohen, J. F. Schooley, W. R. Hosler, and E. R. Pfeiffer, Physical Review **163**, 380 (1967).

[37] G. Binnig, A. Baratoff, H. E. Hoenig, and J. G. Bednorz, Physical Review Letters **45**, 1352 (1980).

[38] Y. Tokura, Y. Taguchi, Y. Okada, Y. Fujishima, T. Arima, K. Kumagai, and Y. Iye, Physical Review Letters **70**, 2126 (1993).

[39] T. Okuda, K. Nakanishi, S. Miyasaka, and Y. Tokura, Physical Review B **63**, 113104 (2001).

[40] N. E. Hussey, Journal of the Physical Society of Japan **74**, 1107 (2005).

[41] N. E. Phillips, B. B. Triplett, R. D. Clear, H. E. Simon, J. K. Hulm, C. K. Jones, and R. Mazelsky, Physica **55**, 571 (1971).

[42] E. Ambler, J. H. Colwell, W. R. Hosler, and J. F. Schooley, Physical Review **148**, 280 (1966).

[43] W. F. Brinkman, P. M. Platzman, and T. M. Rice, Physical Review **174**, 495 (1968).

[44] G. Deutscher, A. F. Santander-Syro, and N. Bontemps, Physical Review B **72**, 092504 (2005).

[45] M. Kofu, S.-H. Lee, M. Fujita, H.-J. Kang, H. Eisaki, and K. Yamada, Physical Review Letters **102**, 047001 (2009).

[46] S. Sachdev, Reviews of Modern Physics **75**, 913 (2003).

[47] B. Lake, H. M. Rønnow, N. B. Christensen, G. Aeppli, K. Lefmann, D. F. McMorrow, P. Vorderwisch, P. Smeibidl, N. Mangkorntong, T. Sasagawa, M. Nohara, H. Takagi, and T. E. Mason, Nature **415**, 299 (2002).

[48] T. Giamarchi and P. Le Doussal, Physical Review B **52**, 1242 (1995).

[49] I. Maggio-Aprile, C. Renner, A. Erb, E. Walker, and Ø. Fischer, Physical Review Letters **75**, 2754 (1995).

[50] B. W. Hoogenboom, C. Renner, B. Revaz, I. Maggio-Aprile, and Ø. Fischer, Physica C **332**, 440 (2000).

[51] S. Chakravarty, R. B. Laughlin, D. K. Morr, and C. Nayak, Physical Review B **63**, 094503 (2001).

[52] W. Bao, G. N. Li, Q. Huang, G. F. Chen, J. B. He, M. A. Green, Y. Qiu, D. M. Wang, J. L. Luo, and M. M. Wu, arXiv:1102.3674 (2011).

[53] H. Hu, J.-M. Zuo, J. Wen, Z. Xu, Z. Lin, Q. Li, G. Gu, W. K. Park, and L. H. Green, New Journal of Physics **13**, 053031 (2011).

[54] W. Jeitschko, R. Glaum, and L. Boonk, Journal of Solid State Chemistry **69**, 93 (1987).

[55] J. Paglione and R. L. Greene, Nature Physics **6**, 645 (2010).

Project 5 Novel electronic phases in strongly correlated electron systems

Project leader: M. Sigrist (ETHZ)

Participating members: D. Baeriswyl (UniFR), G. Blatter (ETHZ), L. Forró (EPFL), E. Giannini (UniGE), D. Jaccard (UniGE), M. Kenzelmann (PSI), D. van der Marel (UniGE), M. Sigrist (ETHZ), M. Troyer (ETHZ)

Summary and highlights: We report progress in the field of heavy fermion superconductors, covering the Q-phase of $CeCoIn_5$ and the properties of superlattices of (Ce/Yb)$CoIn_5$, the role of valence fluctuations in $CeCu_2Si_2$ and aspects non-centrosymmetric superconductors. A pseudogap feature has been discovered for URu_2Si_2 which sets in above the transition to the hidden order phase. In the field of vortex matter dynamical properties of strong flux line pinning have been further examined. Various topological insulators, in particular, in the Pn_2Ch_3 class have been synthesized and experimentally investigated. We also report progress in the theoretical discussion of various topological phases.

1 Heavy fermion superconductor $CeCoIn_5$ (M. Kenzelmann, M. Sigrist)

The symmetry of unconventional superconductors and their interplay with magnetism and other strong correlations lead to an amazing diversity of novel phenomena and are the subject of many studies in condensed matter physics. The widely spread believe is that magnetism and superconductivity would mainly compete. In several unconventional superconductors, however, magnetism and magnetic fluctuations seems to be necessary for superconductivity to emerge. Therefore we may ask under which circumstances superconductivity and magnetism compete or support each other, as discussed here prominently for $CeCoIn_5$. Valence fluctuations represent another feature which can play a crucial role for the superconductivity, as the case of $CeCu_2Si_2$ shown in section 3.

1.1 Neutron diffraction study of the Q-phase

$CeCoIn_5$ is an excellent model system to study unconventional superconductivity. It is a d-wave superconductor that can be made as an ultraclean material. The energy scale is such that the field-temperature phase diagram of the superconducting phase is readily accessible with a number of experimental techniques that are important for the development of a microscopic understanding of the magnetism and the superconductivity in this material. Among the unique properties of $CeCoIn_5$ is the observation of a second superconducting phase where magnetic order and superconductivity exist, although magnetic order does not exist otherwise, not even in the normal phase. Magnetic order thus only exists in the superconducting phase, and its existence appears to require the presence of superconductivity.

Using neutron diffraction, the Kenzelmann group measured the magnetic Bragg peaks as a function of field direction and field strength. One important new result is that only one magnetic domain is observed in this material, even for the case where the magnetic field is along the [1 0 0] direction and both $\boldsymbol{Q}_1 = (q,\ q,\ 1/2)$ and $\boldsymbol{Q}_2 = (q,\ -q,\ 1/2)$ are identical by symmetry. This suggests an extreme sensitivity to the magnetic field direction, or a monodomain formation under cooling into the phase.

For fields along the [1 1 0] direction, only the $\boldsymbol{Q}_2 = (q,\ -q,\ 1/2)$ is populated, as had been previously known. The field was applied along the [1 −1 0] direction and il was observed that, in this case, only the $\boldsymbol{Q}_1 = (q,\ q,\ 1/2)$ is populated. This represents a direct observation of the switching of the magnetic domain using a magnetic field.

Recent theoretical and NMR studies have proposed that the Q-phase consists of at least two phases: one phase at high fields that is a single Q-phase, where a magnetic domain is described by one ordering wave vector $\boldsymbol{Q}$, and a double Q domain where the magnetic structure is described by a superposition of two ordering wave vectors. The experiment of Kenzelmann and coworkers allowed to distinguish these two cases. Fig. 1 shows at $H = 10$ T the magnetic Bragg peak of one domain, but no second Bragg peak associated with the second ordering wave-vector has been seen. This magnetic field lies in the range where the NMR

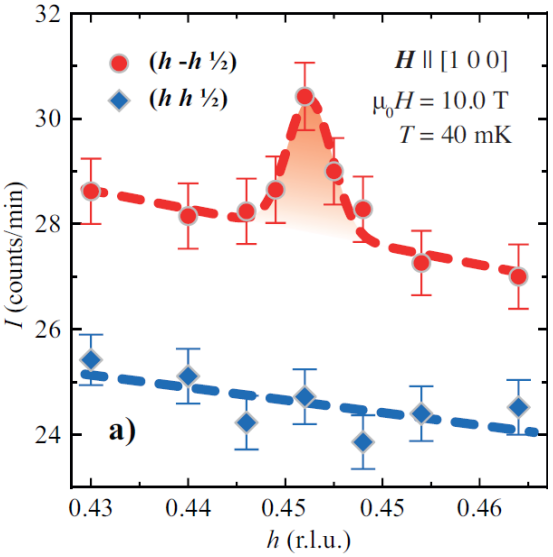

Figure 1: *Single-domain spin-density wave order is observed close to the lower Q-phase boundary at $H = 10$ T and $T = 40$ mK, where strong spin fluctuations and absent static order as well as a double Q magnetic structure were suggested.*

study found a double-Q phase. However, this study allows to exclude the realization of a double-Q phase with certainty.
In all experiments, Kenzelmann and coworkers have so far always observed only one magnetic ordering wave vector. They are presently considering several ways how such a monodomain formation can occur. A tendency for monodomain formation is not uncommon, and has been observed in some ferroelectrics. A possibility is that a monodomain formation is associated with the nature of d-wave superconductivity and they are planning further experiments to test this possibility.

1.2 Artificially layered $CeCoIn_5$

Recently Mizukami *et al.* succeeded to fabricate artificial superstructures of several layers of $CeCoIn_5$ alternating with always five layers of metallic $YbCoIn_5$ [29]. For $CeCoIn_5$ thicknesses of three layers and more, the system is superconducting with an upper critical field which is surprisingly high, in view of the low T_c. This prompted these authors to declare these superlattices a strong-coupling superconductor based on a straightforward approach to paramagnetic limiting effects. On the other hand, Murakami, Yanase and Sigrist demonstrated that taking into account that the superstructure incorporates local non-centrosymmetricity could lead to an enhancement of paramagnetic limiting fields through van Vleck contributions to the spin susceptibility [1, 2]. This proposal suggests that the unusually high critical fields are not necessarily a sign for strong-coupling effects but rather a consequence of superstructure-induced spin-orbit coupling.

2 Non-centrosymmetric superconductivity (M. Sigrist)

Several new aspects of unconventional non-centrosymmetric superconductors have been investigated in Sigrist's group.

2.1 Magnetism at twin boundaries

It has been shown by Iniotakis *et al.* that the mixed-parity phase (Cooper pairs with both parities as realized in superconductors without inversion symmetry) can generate superconducting states with broken time reversal symmetry at twin boundaries (between domains of different crystalline non-centrosymmetricity) [3]. Similar to helical states in topological insulators, here twin boundaries support states which carry spin currents. In contrast to common expectation, this time reversal symmetry breaking superconducting phase does not induce any magnetic features, such as spontaneous supercurrents. A recent study in Sigrist's group shows the short-coming of the earlier work. Indeed a magnetic phase can occur through the combination of supercurrent and spin polarization. This is a phenomenon which could be called a "spontaneous spin Hall effect", because the supercurrent in combination with spin current induces a spin accumulation on the twin boundary. Calculations both based on Bogolyubov-de Gennes approximation and generalized Ginzburg-Landau theory have been applied. It can be speculated that this finding is relevant in connection with $LaNiC_2$ which has been identified as a time reversal symmetry breaking non-centrosymmetric superconductor [30]. This work is in progress and a publication is in preparation.

2.2 Locally non-centrosymmetric superconductors

Together with time reversal, inversion represents a key symmetry for Cooper pairing. In this context it is interesting to analyze the effect of staggered forms of non-centrosymmetry on Cooper pairing symmetries which may be viewed as the analog of an antiferromagnet in relation to a ferromagnet for time reversal violating systems. This local non-centrosymmetricity means that the crystal lattice possesses an inversion center, but anal-

ogous to the antiferromagnetic state there is an antisymmetric spin-orbit coupling doubling the unit cell by imposing a sublattice structure. It is found that there are two basic types of systems distinguished through the topology of spin-orbit coupling, whether it is active in intra- or inter-sublattice hopping processes. The stability of several pairing states and their spin symmetry has been discussed in this context [4]. An extension of this work is in progress, taking the effect of magnetic fields into account.

3 Proximity to valence transition in heavy fermion superconductor $CeCu_2Si_2$ under pressure (D. Jaccard)

Numerous studies on Ce-based heavy fermion compounds focus on the magnetic instability as a driving force for exotic behaviors such as unconventional superconductivity. However, it is also known that the Ce valence changes with pressure (delocalization of the $4f$ electron) and that this effect may also play a major role in determining of electronic properties. In this respect, the first heavy fermion superconductor $CeCu_2Si_2$ may be a good candidate to help to disentangle the contributions from the spin and charge degrees of freedom, more intricated in other Ce systems (like the 115-family). In particular, the pressure – temperature ($p - T$) phase diagram of $CeCu_2Si_2$ (Fig. 2) deviates from the "generic" one in which superconductivity (SC) emerges more or less close to a magnetic instability, presumably mediated by critical spin fluctuations. Instead, in $CeCu_2Si_2$, the superconducting region extends far beyond the magnetic quantum critical point (located at $p_c \approx 0$ GPa), and exhibits an enhanced transition temperature (T_c) culminating at $\sim$ 2.4 K around 4 GPa [5]. The most elaborate scenario [31] invokes critical charge or valence fluctuations (VF) associated with the delocalization of the Ce $4f$ electron when tuning p across the critical region (p_V). In elementary Ce (inset of Fig. 2, Ce data from [32]), the first-order valence transition (FOVT) line ($\gamma - \alpha$ transition), the location of its critical end point (CEP) and the valence crossover (VCO) line have been unambiguously identified. In $CeCu_2Si_2$, despite compelling indications for the presence of critical VF in proximity to a CEP [5], the precise location of that point and the corresponding transition or crossover line have so far not been identified quantitatively. On this footing, Jaccard and coworkers have carried out a multiprobe experiment up to 7 GPa [6, 7, 8] on a very high-quality single-

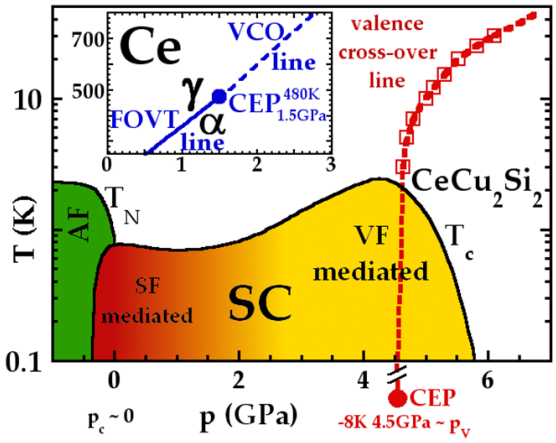

Figure 2: *Updated $p - T$ phase diagram of $CeCu_2Si_2$ with its superconducting phase extending far beyond the magnetic instability at p_c. The maximum T_c roughly coincides with the position of the critical end point (CEP); the valence crossover (VCO) line (red) is obtained from $\rho(p)$ data. Inset: $p - T$ plane of elementary Ce in vicinity of the CEP (data from [32]).*

crystal. The following analysis is restricted to resistivity ρ.

All major characteristics in the $\rho(T, p)$ data are in line with previous reports [5], namely the extracted p-dependence of the parameters ρ_0, A and n, obtained from simple fits to $\rho(T \leqslant 4.2\text{ K}, H = 0) = \rho_0 + A \cdot T^n$. The VF theory [31] predicts, for a $4f$ electron delocalization realized at $p = p_V$, a maximum in the associated fluctuations at slightly lower p ($p \lesssim p_V$), coupled to $n \sim 1$ and an enhancement in A and T_c. Right at $p = p_V$, the impurity scattering cross section should rise strongly, leading to a maximum in $\rho_0(p)$. Beyond the delocalization ($p > p_V$), obviously a deep loss of correlation effects is expected. These features are all in good agreement with the experiment: while $A(p)$ and $T_c(p)$ culminate around 4 GPa, the extremum in $\rho_0(p)$ points to a slightly higher p_V.

Next, Jaccard and coworkers have extracted the p dependence $\rho^*(p) = \rho - \rho_0$ for several $T \leqslant 30$ K [6, 7]. Strikingly, $\rho^*(p)$ drops significantly above 4 GPa, indicating the Ce $4f$ electron delocalization. This resistance loss takes place over a $\sim$ 4 times wider p range at 30 K compared to 3 K. The observed broadening of $\rho(p)$ with increasing T is reminiscent of elementary Ce [33]. However, in $CeCu_2Si_2$ below 30 K, the situation is less straightforward: the effect of delocalization is combined with a strongly T-dependent scattering rate. This "artifact" can be eliminated by a normalization $\rho_{\text{norm}} = (\rho^* - \rho^*(p_{\text{VCO}}))/\rho^*(p_{\text{VCO}})$, where p_{VCO} designates for each T the 50%-

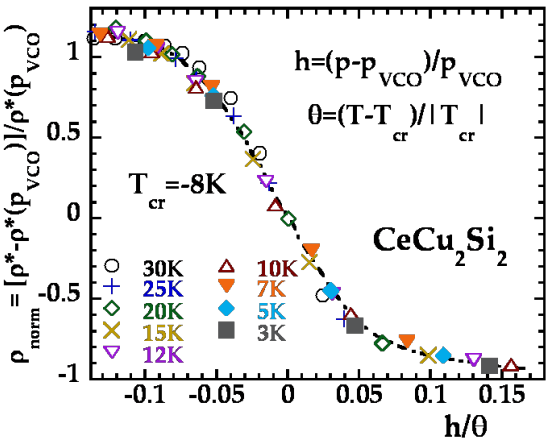

Figure 3: *Best collapse of all normalized $\rho_{\rm norm}(p)$ data as a function of the generalized "distance" h/θ from the CEP ($T_{cr} \sim -8$ K, $p \geqslant 3.6$ GPa, dashed line: guide to the eye).*

midpoint of the $\rho^*(p)$-drop compared to the "initial" value at 4 GPa. In order to locate the CEP, the steepness of the resistance drop was quantified through its slope χ at the midpoint and its divergence $\chi(T \rightarrow T_{cr})$ was analyzed. A simple fit of the type $\propto (T - T_{cr})^{-\gamma}$ yields $T_{cr}^{CeCu_2Si_2} \cong -8 \pm 3$ K and $\gamma \cong 1$, and a similar treatment of the Ce data [33] $T_{cr}^{Ce} \cong 465$ K. Furthermore, joining these midpoints of the resistivity drop leads to the VCO line represented in Fig. 2.

An additional feature reveals that resistivity is governed by the existence of an underlying CEP. It is namely possible to collapse all the $\rho_{\rm norm}(p)$ data on a single curve in vicinity to $p_{\rm VCO}$. Introducing the dimensionless variables $h = (p - p_{\rm VCO})/p_{\rm VCO}$ and $\theta = (T - T_{cr})/|T_{cr}|$, a collapse of excellent quality is obtained according to $\rho_{\rm norm} = f(h/\theta)$ (f: scaling function) with $T_{cr} \cong -8 \pm 5$ K, as shown in Fig. 3 for $p \geqslant 3.6$ GPa. This means that for a generalized "distance" h/θ from the CEP, the $\rho_{\rm norm}$ data behave in a unique manner.

In conclusion, the resistivity analysis unveils that the complete $\rho(p)$ data at low T around p_V are governed by the proximity to a CEP. For the first time, its location could be estimated experimentally: $T_{cr} \sim -8$ K and $p_{cr} \sim 4.5$ GPa. This means that $CeCu_2Si_2$ entirely lies within the VCO regime, but very close to the CEP of the valence transition. Hence its low-T properties are likely to be strongly influenced by the associated critical VF. Moreover, the VCO line could be added to the $p - T$ phase diagram of $CeCu_2Si_2$, and a data collapse has been found. This brings the scenario of SC mediated by VF to the front in heavy fermion physics, and further studies may reveal its widespread relevance, even in the more common case where p_c and p_V are not well separated.

4 Sr_2RuO_4 — Chiral p-wave pairing (M. Sigrist)

Recently, Nakamura *et al.* reported intriguing properties of the Josephson effect between a Pb-film on Sr_2RuO_4 contacted through Ru-metal inclusions [9]. The critical current I_c shows a non-monotonous temperature dependence with an anomalous drop of I_c immediately below T_c of Sr_2RuO_4. Sigrist and collaborators interpret this behavior in terms of a change in topology between the superconducting phase nucleating at the Ru-Sr_2RuO_4 interface at $T^* \sim 3$ K and the chiral p-wave phase of Sr_2RuO_4 below $T_c = 1.5$ K. While the so-called "3 K-phase" matches well with the conventional pairing state proximity-induced from Pb in Ru, there occurs a phase frustration for chiral p-wave superconductor. The latter diminishes the Josephson effect dramatically. Interestingly, the frustration is released to some extend through the creation of spontaneous magnetic flux [10] which is important for limiting the Josephson critical current. Indeed Sigrist and coworkers show that, under such circumstances, the critical current is determined by a pinning-depinning transition of the sponta-

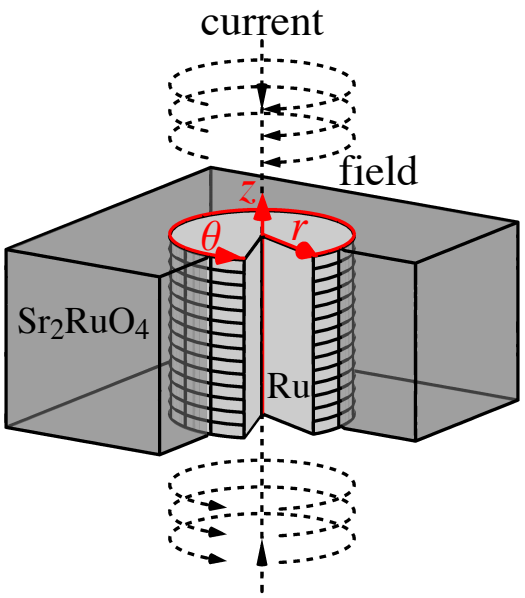

Figure 4: *Geometry studied for the pinning-depinning transition for the Josephson contact between a Ru-inclusion and Sr_2RuO_4. The cylindrical inclusion is superconducting with s-wave symmetry, while the surrounding Sr_2RuO_4 has chiral p-wave superconductivity. The circular currents at the ends of the cylinder allow to impose the desired boundary conditions.*

neous flux pattern in a finite current, in a geometry as shown in Fig. 4. This work is in progress and a publication is in preparation.

5 Dynamic aspects of strong pinning (G. Blatter)

The defining property of a (type II) superconductor is its ability to carry electric current without dissipation. This superflow is destroyed when the magnetic induction B enters the material in the form of vortices. It is the material defects immobilizing vortices which reestablish the superflow of current, eventually rendering the superconductor amenable to technological applications. An elementary distinction is made in the design and action of pinning defects: *strong* pins with $\kappa > 1$ act individually and generate large (plastic) deformations and metastable vortex states, while *weak* defects with $\kappa < 1$ are unable to pin vortices alone and thus act collectively. The Labusch parameter $\kappa = f_p'/\bar{C}$ is given by the ratio of the pin curvature $f_p' = -e_p''$ and the effective elastic constant $\bar{C}$. Blatter and coworkers have determined the generic force – velocity (or current – voltage) characteristic of vortices driven by a current j and subject to a small density n_p of strong pins [11].

The velocity – force characteristic derives from the dynamical equation for vortex motion

$$\eta v = F_{\rm L}(j) - \langle F_p\rangle(v) \qquad (2.1)$$

with the viscosity η and the velocity dependent average pinning force density $\langle F_p\rangle(v)$,

$$\langle F_p\rangle = n_p\langle f_p\rangle = -n_p\Big\langle \int_{-\infty}^{\infty}\frac{dx}{a} f_p[u(x)]\Big\rangle,$$

where a is the distance between vortices and $f_p(x)$ the bare pinning force of a defect. The displacement field $u(x)$ has to be found from the self-consistent equation

$$u(x) = x + \int_{-\infty}^{x}\frac{dx'}{v}\, G[0,(x-x')/v]\, f_p[u(x')],$$

with $G(x/v = t)$ the Green's function of the vortex system. The resulting average pinning force density for a Lorentzian shaped pin is shown in Fig. 5.

Inserting the result for $\langle F_p\rangle(v)$ into Eq. (2.1) and solving for v at given j provide us with the current – voltage or force – velocity characteristic (Fig. 6). Rewriting (2.1) in the form

$$\frac{F_{\rm L}}{F_c} = \frac{v}{v_c} + \frac{\langle f_p\rangle(v/\kappa v_{\rm th})}{f_c}$$

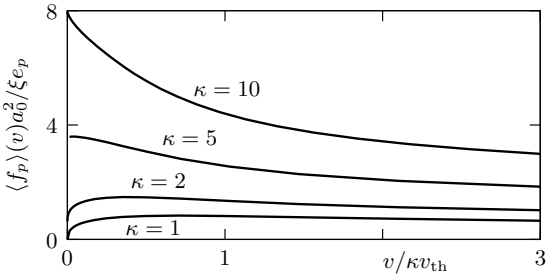

Figure 5: *Average pinning force $\langle f_p\rangle$ for a Lorentzian shaped pinning potential of various strengths. For strong pinning $\kappa \gg 1$, the critical force f_c is large and the pinning force decays monotonously. On approaching the Labusch point $\kappa \to 1$, the critical force f_c vanishes and the pinning force is non-monotonic, first increasing $\propto \sqrt{v}$ and then decaying $\propto 1/\sqrt{v}$.*

unveils two velocity scales, $v_c = F_c/\eta \propto n_p$ and $\kappa v_{\rm th}$, characterizing the homogeneous flow of the vortex system and the vortex velocity in the depinning process. In the small density limit, the two scales separate, $v_c/\kappa v_{\rm th} \sim n_p a_0 \xi^2(\kappa-1)^2/\kappa \ll 1$, implying that $\langle f_p\rangle(v) \approx f_c$ for velocities $v \sim v_c \ll \kappa v_{\rm th}$. Blatter and coworkers find a characteristic that takes the generic form of a shifted (by F_c) linear (flux-flow) curve, $v \approx (F_{\rm L} - F_c)/\eta$ (Fig. 6); the free dissipative flow $v = F_{\rm L}/\eta$ is approached only at very high velocities $v \gg \kappa v_{\rm th} \gg v_c$. The behavior near onset is determined by the small-velocity behavior $\propto \pm\sqrt{v}$ of the pinning force density $\langle F_p\rangle$.

Comparing these results to typical measured

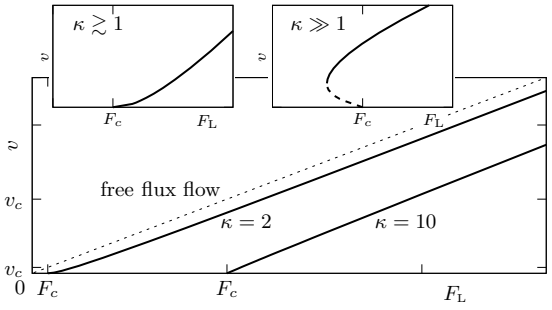

Figure 6: *Force-velocity characteristic for a Lorentzian shaped pinning potential. For small defect densities $n_p a_0 \xi^2 \kappa = 0.05$, one finds an excess-current characteristic, a shifted (by $F_c \propto n_p$) linear curve with a slope reflecting flux-flow behavior and approaching the true (unshifted) flux-flow behavior only at high velocities $\kappa v_{\rm th} \gg v_c$. The insets sketch the behavior near critical force, with a hysteretic jump of order $v_{\rm nl} \propto n_p^2$ appearing at strong pinning $\kappa \gg 1$ and a smooth onset $v \propto v_{\rm th}(\kappa - 1)^4 (F_{\rm L}/F_c - 1)^2$ on approaching the Labusch point $\kappa \to 1$.*

current – voltage characteristics, good agreement with experimental results is found [34, 35].

6 Pseudogap in URu_2Si_2 (D. van der Marel)

A long standing mystery encountered in the cuprate high-T_c superconductors is formed by the pseudogap: well above the critical temperature, where the Cooper-pairs form, a partial gap in the density of states is observed by low-energy spectroscopic probes including tunneling, ARPES and optical spectroscopy. This partial suppression of density of states is commonly referred to as the pseudogap. No change of specific heat has been observed at the temperature where the pseudogap forms. While various different models have been proposed for the exact nature of the pseudogap, it is universally regarded as a key dowel to the puzzle of high-T_c superconducting materials.
The recent studies of the heavy fermion compound URu_2Si_2 by the van der Marel group have revealed a similar pseudogap in the optical conductivity [12]. This compound is fascinating because it presents (at least) two phase transitions: one occurs at ~ 1.5 K and is associated to a superconducting transition, the other takes place at $T_{HO} = 17.5$ K and is attributed to a hidden order transition whose order parameter, despite numerous theoretical and experimental efforts, is still unidentified.
Van der Marel and coworkers measured the optical conductivity $\sigma_1(\omega)$ for both axis of the tetragonal structure (Fig. 7a). It appears that $\sigma_1(\omega)$ exhibits a partial suppression of spectral weight around 12 meV and below 30 K, that is to say well above the transition at 17.5 K. This suppression is very clear in the temperature dependence of the reflectivity in the energy range $20 - 30$ meV (Fig. 7b), which presents an abrupt suppression when the temperature is lowered below 30 K. After the first diffusion of this work, the presence of a pseudogap in URu_2Si_2 has been confirmed by a number of other experimental groups. Understanding the pseudogap in URu_2Si_2 may help to identify the nature of similar phenomenona in other materials, including high-T_c superconductors.

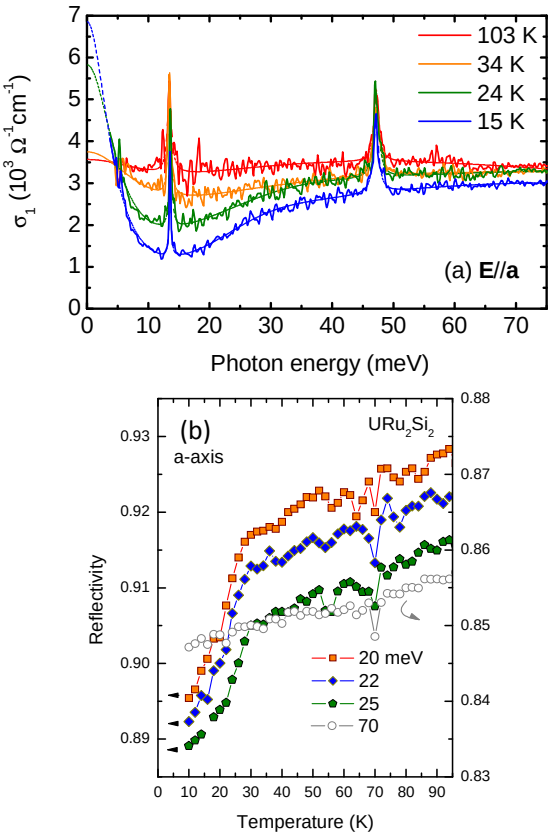

Figure 7: *(a) Real part of the optical conductivity along the a-axis as a function of frequency at different temperatures. The thin dashed lines which extend to zero frequency are Drude-Lorentz fits. The measurements were performed down to 4 meV. (b) Temperature dependence of the a-axis reflectivity for selected energies.*

7 Topological insulators and topologically ordered phases (D. van der Marel, E. Giannini, D. Baeriswyl, M. Troyer)

The discovery of a quantum phase transition in semiconductors, separating the topologically trivial materials like Bi and CdTe from their topologically non-trivial counterparts like Sb and HgTe, has invigorated research activity in a broad class of materials. The importance of spin-orbit coupling to transport in these materials is central, as the propagation of electrons is affected by the rotational properties of spin-1/2 in the extreme limit. A symptom of the novel bulk conduction is the manifestation of Dirac-dispersing helical states localized to the sample surface. These have been detected and studied extensively by magneto-resistance [13] and angle-resolved photoemission.

7.1 High-field magneto-transport measurements

The simplest class of topological insulators which have a large nominal gap and single Dirac cone on the surface includes the three highest-Z members of the class Pn_2Ch_3 (Pn = Bi, Sb; Ch = Se, Te). Single-crystals of this class and variants have been successfully synthesized and characterized in the van der Marel group using a variety of methods. These crystals showed clear early signatures of the Dirac cones dispersing on the surface in

magneto-resistance measurements carried out in the Morpurgo group [13].

7.2 Cyclotron resonance experiments

The impetus for much study in the area of topological insulators arises from the discovery of the quantum spin Hall effect (QSHE), now understood to be a two-dimensional topological insulator. This effect manifested in CdTe-HgTe-CdTe heterostructures, where advanced synthesis and high mobility allowed the observation of the QSHE. In bulk, HgTe is gapless, but a thin 70 nm film of HgTe grown on a CdTe opens a gap of order 10 meV of the appropriate type to establish 3D topological insulating phase with high mobility and very low bulk conduction. The non-trivial character of these surface states was first detected as a quantum Hall effect of surface states [36].
In similar samples, and in collaboration with the Molenkamp group in Würzburg, van der Marel's group observed the first cyclotron resonance of topological surface states [14]. This was accomplished through accurate measurement of the Kerr angle using a commercial time-domain terahertz spectrometer, polarizers, and a home-wound superconducting magnet. This technique has strong promise for future studies in this class of materials, where a looming prediction of the topological magneto-electric effect awaits direct observation [37].

7.3 Crystal growth and characterization of topological insulators: Bi_2Se_3

Zone melting growth of bismuth-chalcogenides inside vacuum-sealed quartz tubes allows minimizing the losses of volatile elements, and better keeping under control a homogeneous composition throughout the sample. Precursors are melted, stirred and re-mixed several times before zone-melting in a mirror furnace. Nevertheless, as grown Bi_2Ch_3 (Ch = Se, Te) always exhibit bulk-metallic conductivity due to intrinsic chemical defects, like vacancies and internal doping. The Fermi level lies either in the valence or in the conduction band and the carrier concentration is high. This means that the bulk contribution to the physical properties can not be neglected and the surface states can be hidden to most of probes. The good crystalline quality of the samples obtained is shown in Fig. 8. No composition fluctuations are observed at the scale of SEM/EDX analysis. Crystals of these materials are being used in various experiments, conducted in both internal and external collaborations.

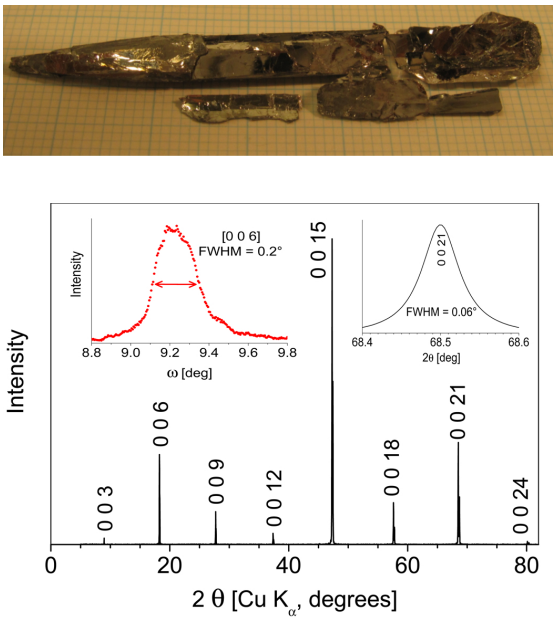

Figure 8: *Bi_2Se_3 crystal (top panel) and XRD characterization of the crystalline quality. The two insets show the (0 0 6) rocking curve (left) and the (0 0 21) $I(2\theta)$ peak profile (right).*

The Dirac surface fermions have been investigated by A. Morpurgo (see Project 2) by means of a gate-tuning of carriers, in thin flakes exfoliated from these crystals [13]. The surface states in Bi_2Se_3 are found to be metastable and *in situ* K deposition is found to homogenize and stabilize topological surface states. This study has been carried out by the group of A. Damascelli at the UBC, Canada [15]. In this uniform and stable electronic surface structure, Rashba-like states have been clearly observed to emerge from bulk states. STM/STS investigations of the surface electronic structure as well as optical spectroscopy studies are in progress at UniGE, in the groups of Ø. Fischer and D. van der Marel, respectively.

7.4 $Bi_2(Se_{1-x}Te_x)_3$ solid solution

Instead of shifting the Fermi level into the band gap by chemical doping (as successfully done in $(Bi_{1-x}Ca_x)_2Te_3$ [38]), Giannini and coworkers have investigated the possibility of tuning the charge carrier density by isovalent substitutions of Te for Se. As a matter of fact, pure Bi_2Se_3 is thought to be n-doped, because of Se-vacancies, and pure Bi_2Te_3 can be p-doped, because of possible Bi-Te substitutions. In the solid solution $Bi_2(Se_{1-x}Te_x)_3$, one expects to compensate chemical defects for each other. The whole solid solution can be grown single-crystalline by the zone melting technique. Thanks to this growth technique,

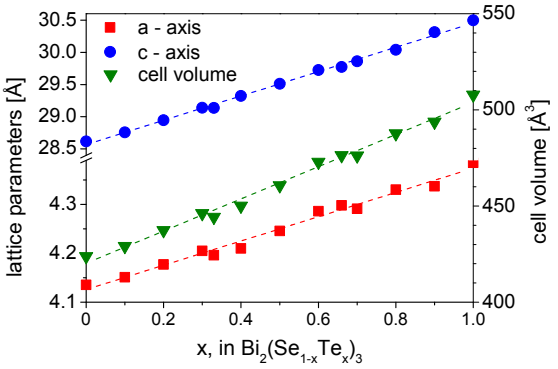

Figure 9: *Lattice parameters of the $Bi_2(Se_{1-x}Te_x)_3$ $(0 \leqslant x \leqslant 1)$ solid solution.*

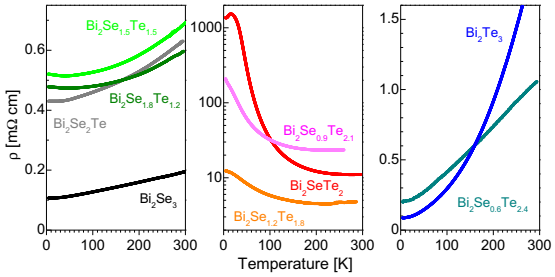

Figure 10: *Electrical resistivity of the $Bi_2(Se_{1-x}Te_x)_3$ $(0 \leqslant x \leqslant 1)$ solid solution. The three panels show the three different conducting regimes as a function of the Te:Se ratio (see text).*

the composition gradients and phase separations are avoided, and macroscopic homogeneous crystals with a composition close to the nominal one are obtained. The lattice parameters follow a Vegard's law as a function of Te-substitutions (Fig. 9). The transport properties reveal a charge compensation as a function of Te-substitutions and three regimes can be identified in the solid solution (Fig. 10). In the Se-rich region ($x \leqslant 0.5$), the behavior is metallic with a very low residual resistivity ratio and a slight upturn at low T, as Te increases. On the Te-rich side ($x \geqslant 0.8$), the behavior is again metallic, but with a strongly different T-dependence. At intermediate compositions ($0.6 \leqslant x \leqslant 0.7$), the resistivity rises by more than three orders of magnitude and exhibits a semiconducting behavior, thus indicating a sudden drop of the carrier density due to a defect compensation.

Raman spectroscopy studies have confirmed the homogeneity of the samples of the whole solid solution and proven that no structural transition occurs. The almost linear Raman shift dependence on x is compatible with the increase of the c-axis and the weakening of the van der Waals bonds. Four vibration modes are active in the structure of the end-compounds Bi_2Te_3 and Bi_2Se_3. A fifth mode appears at intermediate compositions, due to local mixing of the two anions on an equivalent site. The study of the T-dependence of these modes has interestingly shown that, only for the insulating composition Be_2SeTe_2, all modes follow a non-monotonic trend, with a softening at $T \sim 50$ K. This exotic behavior is being further investigated.

7.5 Superconductivity in intercalated Bi_2Ch_3

The $Cu_xBi_2Se_3$ and $Pd_yBi_2Te_3$ intercalated compounds are found to be superconducting below 3.5 K and 5.5 K, respectively. Whereas $0.05 - 0.45$ at% of Cu actually intercalates the Bi-Se block layers, Pd is never found to be present, and plays an indirect role in driving Bi_2Te_3 to superconductivity. Pd-rich secondary phases precipitate, and off-stoichiometric Bi_2Te_3 becomes superconducting. Both compounds exhibit a very weak diamagnetic signal in the Meissner state.

7.6 Topological phases and anyonic models

Troyer's group has extended his previous simulations for interacting anyon chains to two-dimensional arrays of anyons, generalizing the physics of spin-ladders to anyons [16, 17]. The resulting models describe the edge states of non-Abelian quantum Hall systems in two dimensions.

Troyer and coworkers have investigated whether it is possible to construct topological models for topological phases, dropping local physics from the models. The approach runs into problems related to the difficulties of obtaining flat space-time in microscopic Lagrangians for quantum gravity, and they find that geometry and the distinction between local and macroscopic scales are essential for topological protection in topological models [18].

Making anyons mobile, they arrive at anyonic generalizations of the Hubbard and t-J models. In one dimension they discover a generalized version of fermionic spin-charge separation, i.e. the U(1)-electric charge and anyonic charge separate, leading to different velocities for U(1) and anyonic charges in quantum Hall edge states [19].

They have finally also simulated generalizations of previously studied models of non-Abelian anyons to non-unitary anyonic theories [20], which might describe the edge states of hypothetical non-unitary quantum Hall states, but could later prove that such exotic quantum Hall states cannot appear in

physical Hamiltonians with quasi-local interactions [21].

7.7 Quantum XY chain as a toy model for an interface

In the framework of his master thesis in the group of Baeriswyl, Gabriel Ferraz studied the quantum XY chain consisting of two pieces with different parameters, both numerically and analytically. It can be considered as a simplified model of an interface. In fact, several characteristic features of interfaces between different electronic systems, for instance between a semiconductor and a metal, can readily be reproduced by this model. Specifically, the case of two different values of the transverse field, $+h$ in one segment, $-h$ in the other, has been investigated. For the equivalent fermion system, a metal-insulator transition occurs, if h reaches the value of the exchange constant J, but in contrast to the homogeneous chain where the spectrum consists of a single band, which is either full or empty above the critical point, in the present case a gap opens in the middle of the band, separating a filled valence band from an empty conduction band. Ferraz *et al.* have also studied interfaces between metallic and insulating segments. In this case, pronounced Friedel oscillations are found in the metallic part of the chain. A paper on their results is in preparation.

Interestingly, for an odd number of sites and $|h| > |J|$, a single level with a wave function localized at the interface is found essentially in the middle of the gap. Its energy depends on the level occupation (due to the term $e^{i\pi N}$ generated by the Jordan-Wigner transformation, N being the total number of fermions). Nevertheless, the total energy of the ground state is found to be the same in the two cases. Therefore the ground state for an odd-numbered chain is doubly degenerate. One may speculate that localized Majorana fermions emerge at specific interfaces of this model. These exotic quasi-particles are intensively studied in the context of topological insulators [39].

Generalizations of the model, for instance by including interactions between the z components of the spin (XXZ model), are also worth being investigated. In this case, the fermionic counterpart in the weak-coupling limit ($|J_z| \ll |J_x|$) is given by two spinless Luttinger liquids, separated by an interface. Instead of the two chain segments, one can introduce a pseudospin describing even and odd combinations of fermions to the right and left of the interface, respectively, and map the problem onto a single chain of fermions with spin, scattered by an impurity. This fermionic model has been studied extensively since about two decades [22], and its established properties are expected to yield relevant predictions for the interface in the XXZ chain.

8 Simulations of fermions (M. Troyer)

Using their recently developed dynamical mean field theory (DMFT) solvers [23], Troyer and coworkers consider two problems: the local magnetism of Cerium [24], and the Kondo physics of Co impurities in bulk Cu and on Cu surfaces [25]. For the latter, they clearly see that a Kondo model is not sufficient to describe the materials but that an Anderson model is needed since the f state is not occupied with exactly one electron. Using quantum Monte Carlo (QMC) simulations of cluster dynamical mean field theory, they have calculated the spectral properties of the 3D Hubbard model [26]. They have developed a new diagrammatic QMC algorithm and used it to simulate the Cooperon model for high-temperature superconductors [27].

Finally, they have performed the first accurate simulations of the two-dimensional $t-J$ model using infinite projected entangled pair states (iPEPS). Using this variational method, they get lower energies than any other variational approach (such as fixed node QMC or density matrix renormalization group (DMRG) simulations) and find evidence for the formation of stripe phases in the 2D $t-J$ model [28].

9 High-pressure and low-temperature infrared setup (D. van der Marel, L. Forró)

On one hand, applying pressure modifies the interatomic distances (if not the crystal structure of the material) and can therefore be seen as a "knob" of the electronic band structure of materials. On the other hand, temperature-dependent optical infrared spectroscopy allows to probe low-energy vibrational, electronic and magnetic excitations present in a large variety of systems.

For these reasons, a vacuum horizontal infrared microscope, based on a pair of reflective objectives surrounding a diamond anvil cell attached to a cryostat was developed in the van der Marel group (Fig. 11), in order to perform at the same time both low-temperature and high-pressure infrared measurements. The small sample's size required the enhanced brilliance of a synchrotron light source to counterbalance the important signal loss.

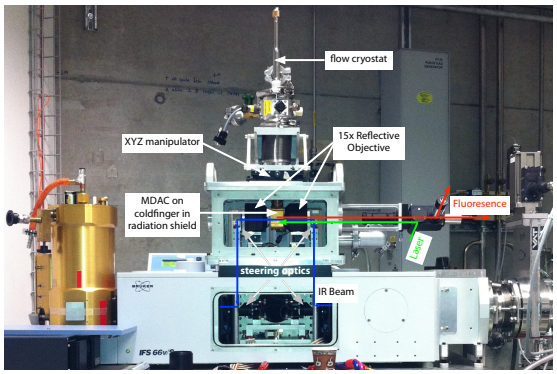

Figure 11: *Vacuum horizontal microscope mounted on the 66 v/s FTIR spectrometer at the infrared beamline of SLS.*

This setup was successfully tested at the infrared beamline of the Swiss Light Source (SLS) of the Paul Scherrer Institute, were pressure up to 16 GPa and temperature down to 20 K were reached. Preliminary results were obtained on power form samples as well as in crystal form.

10 Collaborative efforts

Several of projects reported here profit from the collaborations within MaNEP. The prime example within Project 5 is the study of the heavy fermion superconductor $CeCoIn_5$. Here the close contact of the two groups of Kenzelmann and Sigrist brings together experimental and theoretical expertise and has resulted in a number of prominent publications. A further important area is represented by the topological electronic states which include topological insulators as well as topologically ordered phases. This topic has been additionally fostered by the collaborative project "Topomatter" which is running since about three years initiated by A. Morpurgo, D. van der Marel and M. Sigrist, and includes several further groups, both experimental and theoretical. While the materials and phases investigated are rather diverse, the common concepts and classification schemes underlying these systems have proven most fruitful for the exchange of ideas. Research efforts in this area reported under Project 5 include experiments on and sample growth of topological insulators by the groups of van der Marel and Giannini, the discussion of topological phases in unconventional superconductors by the group of Sigrist and the computational simulation of topological phases by Troyer's group. Further related aspects have also been reported under Project 2. Since January 2011 a collaboration of the groups of van der Marel, Forró and Phillippe Lerch (PSI, infrared beam line) studies the optical spectra of materials under pressure, among other things tuning and closing the gap in topological insulators by pressure. Several collaborative projects of recent years, such as work on FeSi – FeGe and related materials, are pursued with a lower priority at present and have not been reported this year. General aspects of unconventional superconductivity, in particular for heavy fermion systems, also benefit from the large experience in the field within MaNEP, and there is a strong collaborative overlap with Project 4.

MaNEP-related publications

[1] D. Maruyama, M. Sigrist, and Y. Yanase, Journal of the Physical Society of Japan **81**, 034702 (2012).

[2] D. Maruyama, M. Sigrist, and Y. Yanase, arXiv:1110.6000 (2011).

[3] C. Iniotakis, S. Fujimoto, and M. Sigrist, Journal of the Physical Society of Japan **77**, 083701 (2008).

▶ [4] M. H. Fischer, F. Loder, and M. Sigrist, Physical Review B **84**, 184533 (2011).

[5] A. T. Holmes, D. Jaccard, and K. Miyake, Journal of the Physical Society of Japan **76**, 051002 (2007).

▶ [6] G. Seyfarth, A.-S. Rüetschi, K. Sengupta, A. Georges, S. Watanabe, A. Miyake, and D. Jaccard, *to be published in* Journal of the Physical Society of Japan (2012).

▶ [7] G. Seyfarth, A.-S. Rüetschi, K. Sengupta, A. Georges, and D. Jaccard, arXiv:1111.4873 (2011).

▶ [8] A.-S. Rüetschi, K. Sengupta, G. Seyfarth, and D. Jaccard, Journal of Physics: Conference Series **273**, 012052 (2011).

[9] T. Nakamura, R. Nakagawa, T. Yamagishi, T. Terashima, S. Yonezawa, M. Sigrist, and Y. Maeno, Physical Review B **84**, 060512 (2011).

[10] H. Kaneyasu and M. Sigrist, Journal of the Physical Society of Japan **79**, 053706 (2010).

▶ [11] A. U. Thomann, V. B. Geshkenbein, and G. Blatter, arXiv:1110.4247 (2011).

▶ [12] J. Levallois, F. Lévy-Bertrand, M. K. Tran, D. Stricker, J. A. Mydosh, Y.-K. Huang, and D. van der Marel, Physical Review B **84**, 184420 (2011).

▶ [13] B. Sacépé, J. B. Oostinga, J. Li, A. Ubaldini, N. J. G. Couto, E. Giannini, and A. F. Morpurgo, Nature Communications **2**, 575 (2011).

▶ [14] J. N. Hancock, J. L. M. van Mechelen, A. B. Kuzmenko, D. van der Marel, C. Brüne, E. G. Novik, G. V. Astakhov, H. Buhmann, and L. W. Molenkamp, Physical Review Letters **107**, 136803 (2011).

▶ [15] Z.-H. Zhu, G. Levy, B. Ludbrook, C. N. Veenstra, J. A. Rosen, R. Comin, D. Wong, P. Dosanjh, A. Ubaldini, P. Syers, N. P. Butch, J. Paglione, I. S. Elfimov, and A. Damascelli, Physical Review Letters **107**, 186405 (2011).

[16] A. W. W. Ludwig, D. Poilblanc, S. Trebst, and M. Troyer, New Journal of Physics **13**, 045014 (2011).

[17] D. Poilblanc, A. W. W. Ludwig, S. Trebst, and M. Troyer, Physical Review B **83**, 134439 (2011).

[18] M. H. Freedman, L. Gamper, C. Gils, S. V. Isakov, S. Trebst, and M. Troyer, Annals of Physics (N.Y.) **326**, 2108 (2011).

[19] D. Poilblanc, M. Troyer, E. Ardonne, and P. Bonderson, arXiv:1112.5950 (2011).

[20] E. Ardonne, J. Gukelberger, A. W. W. Ludwig, S. Trebst, and M. Troyer, New Journal of Physics **13**, 045006 (2011).

[21] M. H. Freedman, J. Gukelberger, M. B. Hastings, S. Trebst, M. Troyer, and Z. Wang, Physical Review B **85**, 045414 (2012).

[22] T. Giamarchi, *Quantum Physics in One Dimension* (Oxford University Press, Oxford, 2004).

► [23] E. Gull, A. J. Millis, A. I. Lichtenstein, A. N. Rubtsov, M. Troyer, and P. Werner, Reviews of Modern Physics **83**, 349 (2011).

[24] S. V. Streltsov, E. Gull, A. O. Shorikov, M. Troyer, V. I. Anisimov, and P. Werner, arXiv:1106.3470 (2011).

[25] B. Surer, M. Troyer, P. Werner, A. M. Läuchli, T. O. Wehling, A. Wilhelm, and A. I. Lichtenstein, Physical Review B **85**, 085114 (2011).

[26] S. Fuchs, E. Gull, M. Troyer, M. Jarrell, and T. Pruschke, Physical Review B **83**, 235113 (2011).

[27] K.-Y. Yang, E. Kozik, X. Wang, and M. Troyer, Physical Review B **83**, 214516 (2011).

► [28] P. Corboz, S. R. White, G. Vidal, and M. Troyer, Physical Review B **84**, 041108 (2011).

Other references

[29] Y. Mizukami, H. Shishido, T. Shibauchi, M. Shimozawa, S. Yasumoto, D. Watanabe, M. Yamashita, H. Ikeda, T. Terashima, H. Kontani, and Y. Matsuda, Nature Physics **7**, 849 (2011).

[30] A. D. Hillier, J. Quintanilla, and R. Cywinski, Physical Review Letters **102**, 117007 (2009).

[31] S. Watanabe and K. Miyake, Journal of Physics: Condensed Matter **23**, 094217 (2011).

[32] M. Lipp, D. Jackson, H. Cynn, C. Aracne, W. J. Evans, and A. K. McMahan, Physical Review Letters **101**, 165703 (2008).

[33] A. Jayaraman, Physical Review **137**, A179 (1965).

[34] A. R. Strnad, C. F. Hempstead, and Y. B. Kim, Physical Review Letters **13**, 794 (1964).

[35] Y. B. Kim, C. F. Hempstead, and A. R. Strnad, Physical Review **139**, 1163 (1965).

[36] C. Brüne, C. X. Liu, E. G. Novik, E. M. Hankiewicz, H. Buhmann, Y. L. Chen, X. L. Qi, Z. X. Shen, S. C. Zhang, and L. W. Molenkamp, Physical Review Letters **106**, 126803 (2011).

[37] X.-L. Qi, T. L. Hughes, and S.-C. Zhang, Physical Review B **78**, 195424 (2008).

[38] Y. L. Chen, J. G. Analytis, J.-H. Chu, Z. K. Liu, S.-K. Mo, X. L. Qi, H. J. Zhang, D. H. Lu, X. Dai, Z. Fang, S. C. Zhang, I. R. Fisher, Z. Hussain, and Z.-X. Shen, Science **325**, 178 (2009).

[39] M. Z. Hasan and C. L. Kane, Reviews of Modern Physics **82**, 3045 (2010).

Project 6 Magnetism and competing interactions in bulk materials

Project leaders: F. Mila (EPFL), A. Zheludev (ETHZ)

Participating members: T. Giamarchi (UniGE), M. Kenzelmann (PSI), C. Kollath (UniGE), J. Mesot (PSI and ETHZ), F. Mila (EPFL), E. Morenzoni (PSI), H.-R. Ott (ETHZ), H. Rønnow (EPFL), C. Rüegg (PSI), U. Staub (PSI), M. Troyer (ETHZ), A. Zheludev (ETHZ)

Introduction: With two notable exceptions discussed below, much of the progress made in year 11 followed a sustained built up over the past two years. The latter includes sample synthesis and characterization, preliminary experiments, refinements of measurement techniques, and theoretical approaches. These past efforts provided a foundation for new accurate experiments and calculations and resulted in several significant breakthroughs.

Summary and highlights

The study of novel quantum phases in antiferromagnets with competing interactions was and remains the central theme of Project 6. In this area, on the theoretical side, we have shown the possibility of a condensate-free spin superfluid, that may be realized in the spin dimer system $BaCuSi_2O_6$. Here, a unique proximity effect is caused by fully frustrated exchange interactions between magnetic bilayers. We also investigated how a more subtle competition between two types of Dzyaloshinskii-Moriya interactions in $Ba_2CuGe_2O_7$ leads to a most peculiar phase diagram and numerous incommensurate phases in this material in applied fields.

The use of extreme sample environments and advanced measurement techniques has become increasingly important in the study of materials which show novel emergent behavior. We used high pressure and a series of neutron diffraction techniques, including 3D polarization analysis, to study novel materials. We were able to identify a new ferromagnetic ferroelectric in which the ferroelectric polarization can be switched using a magnetic field. Using neutron diffraction, we developed a microscopic understanding for the origin of the ferroelectricity and ferromagnetism, and also their coupling. Further, we improved our capabilities to perform high-pressure magnetization measurements at EPFL and we performed a series of high-pressure diffraction experiments at PSI.

With a focus on fluctuations, excitations in several magnetic systems were probed in both the frequency and time domains. Novel probes such as resonant inelastic X-ray scattering (RIXS), applied to cuprate chain systems, and femtosecond diffraction, applied to cupric oxide, played a very important role. For the latter material it was possible to follow a commensurate-incommensurate phase transition *in real time*. What was also notable is the level to which the analysis of experimental data has become entwined with theoretical input. A case in point is the discovery of long lived bound states in the quantum spin-ladder DIMPY. Here, density matrix renormalization group (DMRG) calculations, semi-analytical computations of instrumental resolution functions, and fitting to measured scans were combined in a single procedure, setting a new standard for the interpretation of inelastic neutron data. Also in relation to novel light scattering techniques, progress was made in the theoretical understanding of Raman scattering from *quadrupolar* order in $S = 1$ systems.

Two sets of very complementary studies focused on the effect of disorder on quantum magnets. Bulk measurements, electron spin resonance (ESR) and neutron experiments on the *bond*-disordered organic spin liquids piperazinium hexacopper chloride (PHCX) and Sul-$Cu_2(Cl_{1-x}Br_x)_4$ were performed in addition to nuclear magnetic resonance (NMR) and neutron investigations of the *site*-disordered ladder $Bi(Cu_{1-x}Zn_x)_2PO_6$. At the same time, muon spectroscopy, which was previously used to study ordering in weakly-coupled random singlet (RS) spin-chains in the organic compound $(NC_5H_5)_2Cu(Cl_{1-x}Br_x)_2$ (CPX), was applied to a conceptually similar inorganic material $BaCu_2(Si_{1-x}Ge_x)_2O_7$. The result is the observation of an inhomogeneous order that appears to be a universal feature of weakly-coupled RS systems.

One of the entirely new thrusts is the study of

spin excitations in pnictide superconductors. It illustrates how expertise accumulated in one project of the NCCR (magnetism, Project 6) can directly influence a core topic of another project (superconductors, Project 4). The most important achievements in this direction is the first observation of the so-called "hourglass" excitation spectrum in $Fe_{1+x}Te_{0.7}Se_{0.3}$, previously only seen in hole-doped cuprates.
On the pure theory side, an interesting result has been obtained on exact ground states in arbitrary-S spin-chains. To date, such dimerized states were only known for the special case of $S = 1/2$. This result adds to our "treasury" of exactly solved problems in quantum magnetism. Exotic quantum phase transitions, SU(3) and SU(4) quantum antiferromagnets, and anyonic generalizations of spin-ladders have also been simulated, with a number of important new results, and version 2.0 of the ALPS libraries and applications has been released.

1 Magnetic excitations and quantum spin correlations

Most magnetic phenomena of current interest involve strongly fluctuating quantum spins and other degrees of freedom. In these cases, static properties are but a small part of the whole picture. The most relevant information is contained in excitations and dynamics. In our work we have applied traditional (neutron scattering, ESR) and novel (RIXS, femtosecond diffraction) probes to investigate magnetic excitations in several classes of quantum materials.

1.1 Bound states in a strong-leg ladder *(A. Zheludev, T. Giamarchi)*

A series of neutron scattering experiments, bulk measurements and density matrix renormalization group (DMRG) first principle calculation on the compound $(DmpyD)_2CuCl_4$ revealed qualitative differences in the properties of *strong-leg* quantum spin-ladders, as compared to the widely previously studied strong-rung case [1]. Long-lived magnons were observed in the antisymmetric excitation channel. Their stability across the entire Brillouin zone supports the symmetric-ladder model for this compound [2]. A totally new result is the observation of a long-lived magnon bound state in the symmetric spectrum [3]. A combination of both spectral components can be seen in the projection yet to be analyzed time of flight data measured on the CNCS spectrometer at Oak Ridge National Laboratory, shown in Fig. 1. Further specific features of the strong-leg ladders were revealed in numerical studies of Tomonaga-Luttinger liquid parameters for the magnetized phase induced by strong applied fields. The numerical DMRG predictions [3] are in spectacular agreement with bulk measurements and inelastic neutron studies. In addition, we have discovered that weak interladder interactions produce long-range magnetic order, previously overlooked by other authors. Our measurements of the phase diagram are also in good agreement with DMRG results.

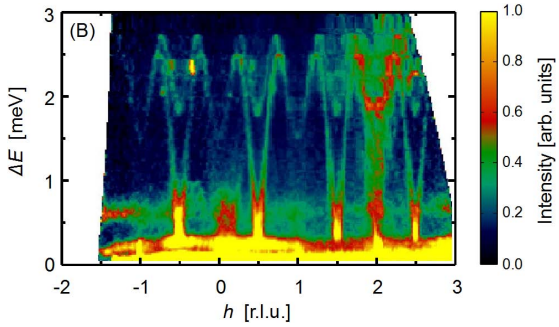

Figure 1: *Time of flight spectrum of magnetic excitations in DIMPY in projection onto the ladder axis. Both single-magnon excitations and two-magnon bound states are visible.*

1.2 ESR in spin-ladders *(T. Giamarchi)*

In the continuity of our investigations of spin-1/2 ladders, we explored the effects of the anisotropies on such a system. In particular, we investigated the influence of these anisotropies on the electron spin resonance (ESR) shift [4]. This study was a collaboration with S. Furuya and M. Oshikawa (ISSP, Japan). Using density matrix renormalization group (DMRG) computations, we have shown that the ESR technique can be used to distinguish the origin of different anisotropies. As an experimental example, we determined the anisotropies in the spin-1/2 ladder compound $(C_5H_{12}N)_2CuBr_4$ (BPCB) and predicted its ESR shift in a full range of temperatures and magnetic field. The latter is in very good agreement with recent measurements (Fig. 2).

1.3 Real time spin dynamics in CuO *(U. Staub)*

The ability to manipulate magnetic order has become vital to modern data storage and processing technology. Here we investigated how fast magnetic moments can be manipulated in a coherent way [5]. For that purpose we have chosen CuO, the building block for cuprates and an interesting material by its own means.

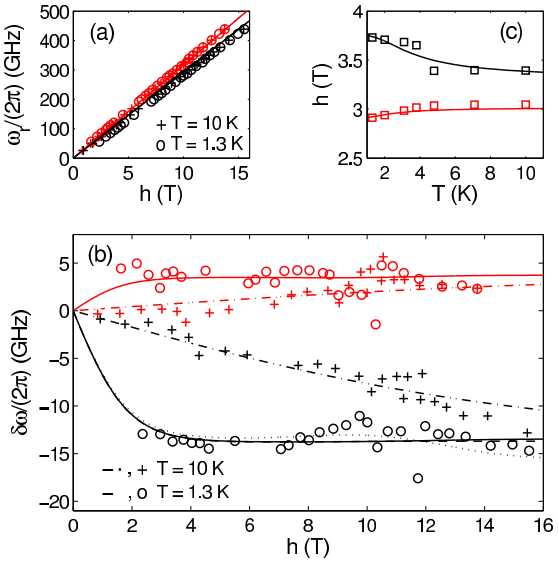

Figure 2: *Magnetic field dependence of (a) the ESR paramagnetic resonance frequency, (b) the ESR resonance frequency shift. (c) Temperature dependence of the magnetic field at which the ESR paramagnetic resonance at $\omega_r = 2\pi \cdot 96$ GHz occurs. Symbols denote experimental on BPCB and lines theoretical predictions.*

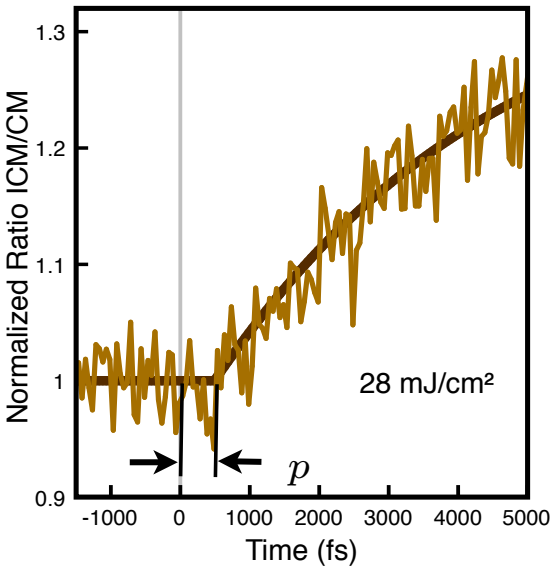

Figure 4: *Time-dependent normalized diffracted intensity representing the elative phase population. t_p represents the time for a 1/4 period of a long-wavelength magnetic excitation in the CM phase (400 fs).*

CuO exhibits a commensurate (CM) to incommensurate (ICM) phase transition at approximately 213 K (Fig. 3), which can be easily studied by resonant X-ray diffraction [6]. Correspondingly cupric oxide is ideally suited for an ultrafast pump probe experiment with ultrashort fs X-ray probe pulses, which were created by the X-ray free electron laser facility LCLS at Stanford University.

To induce the phase transition, an ultrafast optical laser pulse of 50 fs duration was used to excite the crystal and create electronic (magnetic) disorder. Disorder is the basic ingredient to understand the static phase transition. This transition is caused by the competing

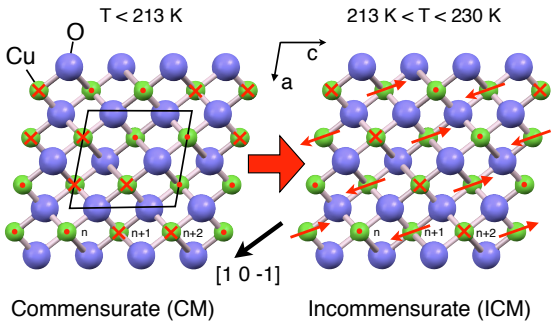

Figure 3: *Magnetic structures in CuO, projected onto the (010) plane. Left: the magnetic structure of the CM phase; right: that of the ICM phase. Red arrows indicate the orientation of the magnetic dipoles.*

interactions of the superexchange interactions with a small balancing biquadratic exchange term, which is responsible for the stability of the different phases. Displaying the normalized ratio of the magnetic reflections of these two phases in the vicinity of the phase transition as a function of time difference between pump and probe pulses (Fig. 4), a clear delay between the optical excitation and the beginning of the change of the phase fractions are observed. We found that there is a minimal time delay before the phase transition can occur, which is approximately 400 fs. Such a delay can be understood in terms of time required for the spin-system to perform a coherent motion (spin wave excitation) to transform to the new magnetic structure. This time, we propose, is directly related to 1/4 of the wave of the low lying magnetic excitation connecting these two phases. This is consistent with the size of the spin wave gap observed by inelastic neutron scattering (1.6 ps).

1.4 Theory of inelastic light scattering in spin-1 systems *(F. Mila)*

Motivated by the lack of an obvious spectroscopic probe to investigate non-conventional order such as quadrupolar orders in spin-$S > 1/2$ systems, we have investigated the theory of inelastic light scattering for spin-1 quantum magnets in the context of a two-band Hubbard model [7]. In contrast to the $S = 1/2$ case, where the only type

of local excited state is a doubly occupied state of energy U, several local excited states with occupation up to 4 electrons are present. As a consequence, we have shown that two distinct resonating scattering regimes can be accessed depending on the incident photon energy. For $\hbar\omega_{in} \lesssim U$, the standard Loudon-Fleury operator remains the leading term of the expansion as in the spin-1/2 case. For $\hbar\omega_{in} \lesssim 4U$, a second resonant regime is found with a leading term that takes the form of a biquadratic coupling $\sim \left(\boldsymbol{S}_i \cdot \boldsymbol{S}_j\right)^2$. Finally, we have shown that combining both resonant regimes makes Raman scattering a powerful probe to distinguish between magnetic and quadrupolar order in spin-1 antiferromagnets.

1.5 SU(N) quantum magnets *(M. Troyer)*

Using infinite projected entangled pair states (iPEPS) and density matrix renormalization group (DMRG), SU(3) and SU(4) generalizations of quantum Heisenberg antiferromagnets have been simulated. In the context of quantum magnetism, the SU(3) model describes spin-1 antiferromagnets with equal bilinear and biquadratic couplings, while the SU(4) model is equivalent to the symmetric Kugel-Khomskii spin-orbital model. In the SU(3) case, the presence of a generalization of Néel order has been demonstrated [8], while the SU(4) model on the square lattice has been shown to undergo a spontaneous dimerization [9].

1.6 Spin excitations and phase transitions in pnictides *(H. Rønnow)*

High-temperature superconductivity remains arguably the largest outstanding enigma of condensed matter physics, with renewed importance since the discovery of iron-based high-temperature superconductors, which intriguingly show magnetic fluctuations reminiscent of the superconducting (SC) cuprates. We obtained inelastic neutron scattering data on $Fe_{1+x}Te_{0.7}Se_{0.3}$ crystals, prepared in the group of E. Giannini at UniGE (see Project 4), using excess iron concentration to tune between SC ($x = 0.02$) and non-SC ($x = 0.05$) (Fig. 5). Both samples display incommensurate spectra, but the one that becomes SC develops a constriction towards a commensurate "hourglass" shape well above T_c. Our results imply that the hourglass shaped dispersion is a pre-requisite for superconductivity, whereas the spin gap and shift of spectral weight appearing below T_c are consequences of superconductivity. We explain this observation by pointing out that

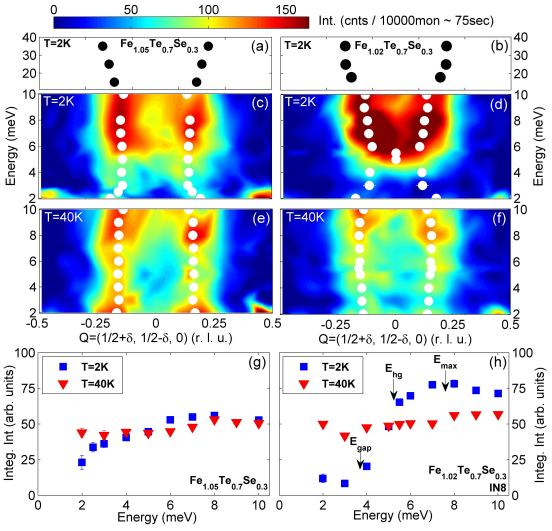

Figure 5: *Magnetic spectrum and dispersion along* $(1/2+\delta, 1/2-\delta, 0)$ *in* $x = 0.05$ *(a, c, e) and* $x = 0.02$ *(b, d, f), from Q-scans at a series of energies. Colormaps represent intensity with a Q-independent background subtracted. Below 2 meV, incoherent elastic background becomes dominant. Data above* $E = 10$ *meV were measured in different configuration and intensities are not directly comparable. Each scan was fitted by two symmetric Gaussians, yielding the dispersion (circles) and integrated intensity, which is shown in (g, h) as a function of energy. Blue and red circles correspond to* $T = 2$ *K and at* $T = 40$ *K, respectively.*

an inwards dispersion towards the commensurate wave vector is needed for the opening of a spin gap to lower the magnetic exchange energy and hence provide the necessary condensation energy for the SC state to emerge. Somewhat related to this effort was our discovery and study of a cascade of magnetic and structural phase transitions in the pnictide parent compound $Fe_{1+x}Te$ [10]. We concluded that these transitions are driven by weak instabilities, as compared to the strength of the underlying interactions, and that the impact of the Fe interstitials can be treated with random-field models.

1.7 Directly coupled ferromagnetism and ferroelectricity in Mn_2GeO_4 *(M. Kenzelmann)*

The low-temperature properties of the olivine compound Mn_2GeO_4 were investigated by both bulk measurement and neutron scattering techniques [11]. In zero magnetic field, Mn_2GeO_4 was found to undergo a sequence of magnetic structure phase transitions as a function of decreasing temperature, culminating in a final transition into a magnetically-driven multiferroic (MF) phase. The properties of the multiferroic phase were found to

be extremely rich, and provide a rare case where both magnetization and ferroelectric orders emerge spontaneously along the crystal *c*-axis. The microscopic details of the magnetism and magnetic symmetry underpinning the MF phase were unraveled by neutron diffraction. The magnetic order was found to consist of two modulations; a simple commensurate order was found to coexist with a doubly incommensurate spin spiral order. The magnetic symmetry shows the commensurate order to be responsible for the magnetization, and the incommensurate spin spiral order to be the cause for the emergence of ferroelectricity.

The direct coupling between the magnetization and ferroelectric orders was demonstrated directly by the concomitant switching of the ferromagnetic and ferroelectric domains by sweeping magnetic fields. Therefore, the commensurate and incommensurate magnetic orders are shown to be coherently superposed in order to form a single magnetic structure, and thus by necessity the magnetization and ferroelectricity are directly coupled. We introduced a model based on microscopic Dzyaloshinskii-Moriya interactions in order to describe the coupling mechanism. The model makes solid predictions about the multiferroic domain structure expected under proper poling electric and magnetic fields, these predictions are currently under scrutiny using polarized neutron diffraction under poling fields. Our reported results are an important, and thus far unique, demonstration of the increasingly rich variety of magneto-electric coupling phenomena that may be found in frustrated magnets such as Mn_2GeO_4.

1.8 Local spin fluctuations in cuprate chains *(U. Staub)*

The quasi-one-dimensional cuprates Li_2CuO_2 and $CuGeO_3$ are prototype edge-sharing chain compounds. The Cu^{2+} ions in these strongly correlated materials give rise to one spin-1/2 per CuO_4 plaquette with a nearest neighbor Cu-O-Cu bond angle close to 90°, implying weak superexchange coupling between Cu spins. For Li_2CuO_2, below $T_N \sim 9$ K, antiferromagnetic and ferromagnetic correlations are dominating between and within the chains, respectively. For $CuGeO_3$ short range antiferromagnetism coexists with frustrated magnetic interactions, and for low temperatures ($T_{SP} \sim 14$ K) the presence of strong fluctuations drives the system into a spin Peierls phase.

We have performed resonant inelastic X-ray scattering (RIXS) at Cu L_3 and O K resonances

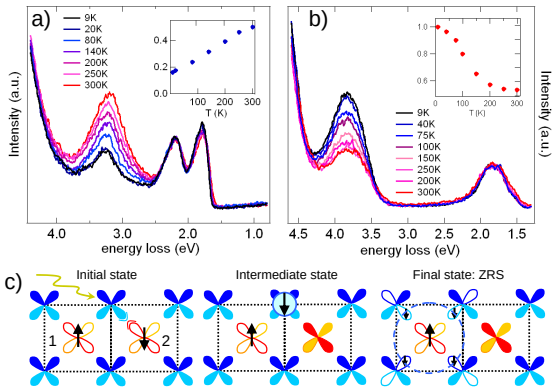

Figure 6: *RIXS spectra measured as a function of temperature at the upper Hubbard band of the O K edge of (a) Li_2CuO_2 and of (b) $CuGeO_3$. The spectra are plotted in an energy loss scale. These spectra show the strong opposite temperature dependence of the Zhang-Rice singlet excitons in these two compounds, which are directly related to the temperature evolution of the antiferromagnetic correlations. (c) Schematic picture illustrating the creation of a Zhang-Rice singlet exciton during the RIXS process, as a non-local charge-transfer excitation.*

at the ADRESS beamline of the Swiss Light Source. We discuss charge transfer related spectral components in the scenario of exotic Zhang-Rice (ZR) singlet (Fig. 6c) and triplet excitons which can be created in the final state with O K edge RIXS. For $CuGeO_3$ ZR singlet excitons are observed with increasing intensity when cooling towards T_{SP} (Fig. 6b). In contrast to this, temperature dependent measurements for Li_2CuO_2 evidence clear opposite temperature behavior for ZR singlet (Fig. 6a) and ZR triplet spectral components, in good agreement with *pd*-Hamiltonian cluster calculations. Comparing the energy of both ZR excitons from the spectra allows determining the binding energy of the Zhang-Rice singlet in Li_2CuO_2 (Fig. 6). Furthermore, the intensity development of the ZR excitons can be analyzed in terms of the thermodynamics of domain walls in one dimension. This study establishes RIXS as an excellent probe for investigating local spin correlations in quasi-one-dimensional cuprates and other systems [12].

2 Quantum phases and phase transitions in spin-systems

Spin-systems are the favorite testing ground for the study of exotic order parameters, phase transitions, geometric frustration, scaling and quantum criticality. Excellent well-characterized realizations of important spin-models are available and amenable to experimental investigation. At the same time, the

theorist has access to an extraordinary toolbox to address the problem analytically or numerically.

2.1 Antiferromagnetic spin-S chains with an exactly dimerized ground state *(F. Mila)*

We have shown that spin-S Heisenberg spin-chains with an additional three-body interaction of the form $(\boldsymbol{S}_{i-1}\cdot\boldsymbol{S}_i)(\boldsymbol{S}_i\cdot\boldsymbol{S}_{i+1})+h.c.$ possess fully dimerized ground states if the ratio of the three-body interaction to the bilinear one is equal to $1/(4S(S+1)-2)$. This result generalizes the Majumdar-Ghosh point of the J_1-J_2 chain, to which the present model reduces for $S=1/2$. For $S=1$, we have used the density matrix renormalization group method (DMRG) to show that the transition between the Haldane and the dimerized phases is continuous with central charge $c=3/2$. Finally, we have shown that such a three-body interaction appears naturally in a strong-coupling expansion of the Hubbard model, thus proving that this mechanism is a realistic one to induce spontaneous dimerization in spin-chains [13].

2.2 Complete field phase diagram of $Ba_2CuGe_2O_7$ *(A. Zheludev)*

In this well-studied material we have identified and characterized a novel two-k phase [14] and performed comprehensive studies in canted magnetic fields (Fig. 7). Small-angle neutron scattering experiments revealed strong *even*-order harmonics of magnetic Bragg reflections. These were attributed to staggered Dzyaloshinskii-Moriya (DM) interactions, which may prevent the formation of the much sought after "skirmyon lattice" topological phase in this compound. We are currently looking at several similar materials where staggered DM coupling is prohibited by symmetry, and skyrmions may be stable after all.

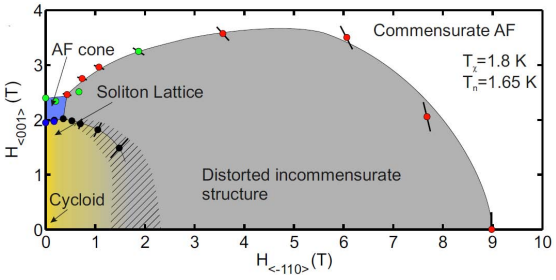

Figure 7: *Magnetic phase diagram of $Ba_2CuGe_2O_7$ measured in fields applied at an angle to the tetragonal unique axis.*

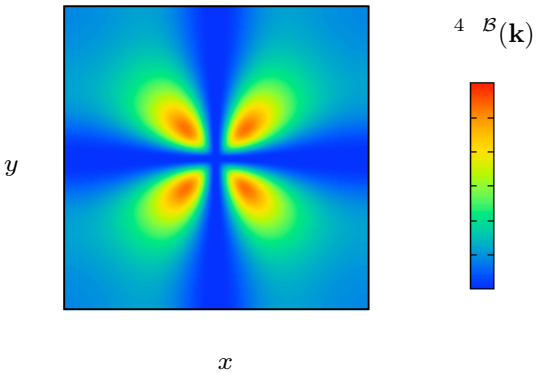

Figure 8: *Color intensity plot of the incommensurate structure factor of the less polarized bilayer between the first two critical fields in the two-bilayer model of $BaCuSi_2O_6$.*

2.3 Condensate-free superfluid and frustrated proximity effect *(F. Mila)*

Motivated by the properties of $BaCuSi_2O_6$, a system of inequivalent spin-1/2 bilayers coupled by a fully frustrated antiferromagnetic interaction, we have investigated the intermediate regime between the first critical fields of the two types of layers [15]. We have shown that, while standard Bose-Einstein condensation (BEC) is present in the bilayer with the smallest critical field, no condensate is present in the second bilayer, although it has a small but finite polarization and a stiffness of its own. We have shown that this property is best understood in the context of an analogy with the physics of bosons, the population in the layer with the highest critical field being the consequence of a frustrated proximity effect that allows uncondensed particles to hop from the layer with the smallest critical field but prevents the condensate from leaking out of it. This condensate-free bosonic fluid has been further shown to be a superfluid with incommensurate correlations (Fig. 8), a proposal that could be checked with nuclear magnetic resonance (NMR) or neutron scattering.

2.4 Quantum phase transitions *(M. Troyer)*

Ground states of certain materials can have topological order and no conventional order. As an example of such a state, we have found a topologically ordered Z_2 spin liquid in a Bose-Hubbard boson model on the kagome lattice. We have identified its topological order directly by measuring the topological entanglement entropy in quantum Monte Carlo simulations [16].

We have then shown that the superfluid to spin liquid quantum phase transition in a Bose-

Hubbard model on the kagome lattice was driven by the condensation of fractionalized particles. We have confirmed this by measuring a highly non-classical critical exponent $\eta = 1.49$, and by constructing a universal scaling function of winding number distributions that directly demonstrated the existence of the fractional charge [17].
We have also studied the Néel to dimer quantum phase transition driven by interlayer exchange coupling in spin-S Heisenberg antiferromagnets on bilayer square and honeycomb lattices for $S = 1/2,\ 1,\ 3/2$. We have compared bond operator mean field theory with quantum Monte Carlo simulations and found that the agreement was better when the high-energy quintet modes in the bond operator theory were taken into account [18].
We have finally studied the dynamical critical behavior at conformal quantum critical points and found that — in contrast to expectations and common belief — the dynamical critical exponent is not $z = 2$ but non-universal and $z \geq 2$ unless a U(1) symmetry is present in a model [19].

2.5 Frustrated spin-chains *(A. Zheludev)*

Several new materials, both oxides and organometallic complexes, are being investigated as possible realizations of the quintessential model in frustrated magnetism, namely the antiferromagnetic spin-chain with next nearest neighbor interactions. In particular, we have found that the compound $Cu(py)_2Cl_2$ targeted on our μSR experiments actually orders in an incommensurate structure. This exploratory work is complementary to our studies of well-established frustrated spin-chain systems such as $LiCu_2O_2$ [20].

3 Disorder in quantum magnets

A growing thrust within Project 6 is the study of intrinsically disordered quantum magnets. It is a natural extension of our focus on spin-systems, as we pay specific attention to the localization of magnetic quasi-particles on site or bond defects. In the quantum case, this often results in qualitatively new collective phases and distinct critical points.

3.1 Bose glass in spin liquids with disorder *(A. Zheludev)*

The goal of this study was to test the "$z = d$" scaling hypothesis for the Bose glass to BEC transition [30]. We employed neutron diffraction and calorimetry to measure the critical indexes β and ϕ for the field-induced BEC of magnons in the disordered spin liquid $(C_4D_12N_2)Cu_2(Cl_{1-x}Br_x)_6$. It was found that the crossover exponent ϕ is slightly increased by the randomness of exchange interactions, while β remains practically unchanged [21]. The measured values are far smaller than those predicted for $z = d$. Our results are consistent with recent theoretical and numerical work that debunked that conjecture, but not with less accurate measurements by other authors [22]. Similar studies were performed for the disordered spin-ladder system $Cu(quinoxaline)(Cl_{1-x}Br_x)_2$ [23]. At the same time, studies of another ladder compound, namely $Sul\text{-}Cu_2(Cl_{1-x}Br_x)_4$ revealed that disorder can have a more dramatic effect in the presence of geometric frustration. In our case it totally suppresses the BEC transition due to a "random phase" effect [24].

3.2 Site-diluted spin-ladders *(H.-R. Ott)*

An excellent model compound for studying the physics of disordered antiferromagnets is the recently synthesized spin-1/2 zigzag ladder $Bi(Cu_{1-x}Zn_x)_2PO_6$ (BCPO) [25]. Our previous preliminary ^{31}P nuclear magnetic resonance (NMR) study at the high-magnetic-field laboratory LNCMI in Grenoble has revealed the onset of a field-induced ordered (FIO) phase at $H_c \simeq 20.9$ T for $x = 0$ and $H \parallel b$. Replacing Cu with Zn at the few percent level leads to impurity-induced order (IIO) which, however, may be quenched by external magnetic fields $H_0(T)$. Recent neutron scattering data indicate that the IIO phase for $x = 0.01$ and $x = 0.05$ is suppressed at $H_0 \approx 4$ and 14 T, respectively. Consequently, the IIO and the expected FIO phases are separated by a region with unexplored magnetic features.
Our current project aimed to explore in detail the regime $\mu_0 H \geqslant 11$ T by means of ^{31}P NMR, in particular at fields $H \geqslant H_c$. The NMR lineshapes for pure BCPO, measured with H along the crystalline b-axis, reveal a distinct change in character with increasing H. While narrow at low fields, their growing widths at $H > H_c$ indicate a continuous distribution of the local magnetic field, typical of an incommensurate magnetic structure. In spite of the presence of defect-induced satellites, similar features of the lineshapes are observed for the doped compound. The variation of the ^{31}P NMR lineshapes across the covered field range (11 – 31 T) provided the boundaries of the FIO phase in the pure and doped BCPO, with extrapolated

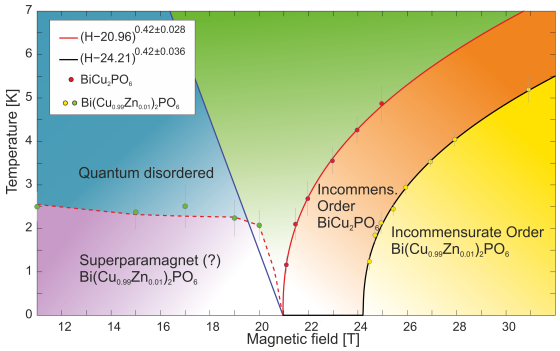

Figure 9: *$H-T$ phase diagram for both pure and 1% Zn-doped $Bi(Cu_{1-x}Zn_x)_2PO_6$. Doping at the 1% level introduces a 3 T shift of the phase boundary to $H_c \sim 24$ T.*

$T = 0$ K critical-field values $H_c = 20.96$ T and $H_c = 24.2$ T, respectively (Fig. 9).

At high fields T_c may be obtained from distinct maxima in $T_1^{-1}(T)$ in a constant field H. For H close to H_c, however, the relaxation rates decrease dramatically overall and, therefore, measurements of $T_1^{-1}(H)$ at a constant temperature are more suitable for observing the maxima in $T_1^{-1}(H)$, which were then used to identify the transition (Fig. 10). The phase boundaries, obtained by fits to the experimental data, are in both cases well represented by a power law of the form $T_c \propto (H - H_c)^{0.42}$. The exponent 0.42 is significantly lower than the expected value of 2/3 for 3D magnetic BEC transitions [26].

3.3 Temperature and impurity effects on magnons in spin liquids *(A. Zheludev)*

In 2010 we have succeeded in growing very large single-crystal samples of the quasi-2D spin liquid compound $(C_4D_12N_2)Cu_2Cl_6$ with a varying concentration of Br substitutes on the Cl site [27]. These samples were used in detailed spectroscopic experiments. Finite-T broadening and blue shift of excitations were studied using neutron spectroscopy [21], resonant neutron spin echo spectroscopy and electron spin resonance (ESR) [28]. These effects are due to magnon collisions. Unlike in $d = 1$ [31] they are non-universal in $d = 2$. The non-universal behavior is revealed by comparing the effect of temperature to that of impurity substitution. This study is complementary to a similar one that employed neutron spin echo to probe excitations in the spin-ladder compound IPA-$CuCl_3$ [29].

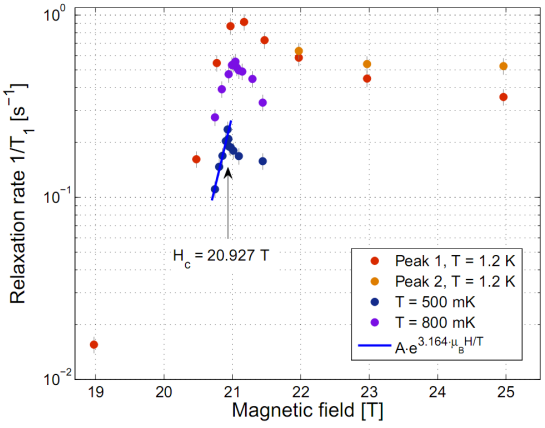

Figure 10: *Maxima in NMR relaxation rates $T_1^{-1}(H)$ at constant temperatures for pure BCPO. The peaks indicate $H_c(T)$.*

3.4 Weakly coupled random singlet chains *(A. Zheludev)*

Random exchange in gapless spin-chains qualitatively changes the nature of the ground state and therefore has a profound impact on long-range magnetic ordering in the quasi-1D case. We have performed μSR experiments to probe this effect in two classes of materials, namely $(NC_5H_5)_2Cu(Cl_{1-x}Br_x)_2$ (CPX), where disorder is introduced by a random substitution on the halogen site, and $BaCu_2(Si_xGe_{1-x})_2O_7$, where randomness is due to Si/Ge disorder. In both cases, disorder-free compounds undergo rather conventional ordering at low temperatures, which gives rise to typical muon polarization oscillations. As randomness is introduced, the oscillations are no longer observed (Fig. 11). Instead, one gets a broad decay of polarization that resembles a stretched exponential law. Such behavior is a hallmark of a *distri-*

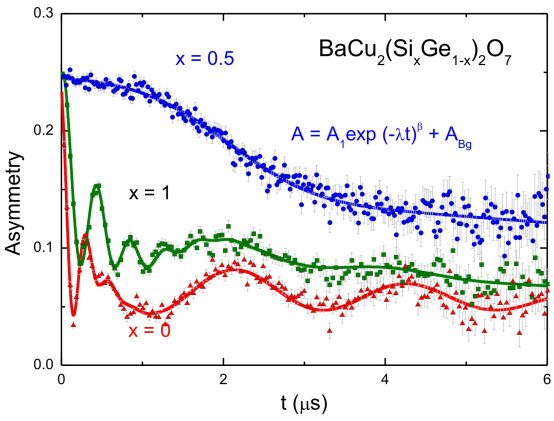

Figure 11: *Muon relaxation spectra measured in $BaCu_2(Si_xGe_{1-x})_2O_7$ for $x = 0$, $x = 0.5$ and $x = 1$ at $T = 20$ mK.*

bution of relaxation rates, as expected for coupled random chains.

4 Collaborative efforts

Much of the progress made in year 11 is a direct result of collaborations supported by MANEP. The NMR studies of low-D spin-systems profit from collaborations within the project, including the groups of H.-R. Ott, Ch. Rüegg, H. Rønnow and A. Zheludev, as well as the materials preparation group at PSI, headed by K. Conder. The latter group also provided samples for neutron experiments on $Ba_2CuGe_2O_7$. Extremely tight intraproject collaboration between the groups of T. Giamarchi and A. Zheludev was at the heart of the studies on strong-leg spin-ladders. A collaboration between the groups of F. Mila and M. Troyer produced important results on the SU(4) symmetric Kugel-Khomskii model on the square lattice. The entire μSR effort is party on the MaNEP collaborative project between the groups of E. Morenzoni and A. Zheludev.

In the context of a collaboration between PSI and EPFL, we improved our capabilities to perform high-pressure magnetization measurements at EPFL, and we performed a series of high-pressure diffraction experiments at PSI. Temperature-dependent measurements of the dc susceptibility in the $S = 1/2$ even-leg spin-ladder system $BiCu_2PO_6$ were performed with the sample under hydrostatic pressure. The problem of deconvolving the weak sample signal from the large paramagnetic signal of the commercial pressure cell was approached using a numerical method incorporated into newly developed software. The software was used to demonstrate the now routine capability for analyzing such data, as shown in our study of $BiCu_2PO_6$ where the spin gap was found to increase slightly with increasing pressure.

Hydrostatic pressure has also been used in recent neutron scattering experiments at the SINQ neutron source at PSI. The Paris-Edinburgh press has been operated routinely at temperatures as low as 5 K, where new research projects in both crystallography and magnetically-driven multiferroics have been initiated. Piston cylinder cells have also been implemented at low temperatures in order to begin new studies of the pressure-dependent magnetic order in a range of superconducting systems.

Between projects (with Project 1), the group of U. Staub started a collaboration with the group of J.-M. Triscone on the multiferroic pervoskite nickelates $RNiO_3$. That group provided epitaxial films of sufficient magnetic quality to perform synchrotron experiments in applied electric fields/currents, as proposed for the next year.

MaNEP-related publications

- [1] P. Bouillot, K. Corinna, A. M. Läuchli, M. Zvonarev, B. Thielemann, C. Rüegg, E. Orignac, R. Citro, M. Horvatić, C. Berthier, M. Klanjšek, , and T. Giamarchi, Physical Review B **83**, 054407 (2011).
- [2] D. Schmidiger, S. Mühlbauer, S. N. Gvasaliya, T. Yankova, and A. Zheludev, Physical Review B **84**, 144421 (2011).
- [3] D. Schmidiger, P. Bouillot, S. Mühlbauer, S. Gvasaliya, C. Kollath, T. Giamarchi, and A. Zheludev, arXiv:1112.4307 (2011).
- [4] S. C. Furuya, P. Bouillot, C. Kollath, M. Oshikawa, and T. Giamarchi, Physical Review Letters **108**, 037204 (2012).
- [5] S. L. Johnson, R. A. de Souza, U. Staub, P. Beaud, E. Möhr-Vorobeva, G. Ingold, A. Caviezel, V. Scagnoli, W. F. Schlotter, J. J. Turner, O. Krupin, W.-S. Lee, Y.-D. Chuang, L. Patthey, R. G. Moore, D. Lu, M. Yi, P. S. Kirchmann, M. Trigo, P. Denes, D. Doering, Z. Hussain, Z.-X. Shen, D. Prabhakaran, and A. T. Boothroyd, Physical Review Letters **108**, 037203 (2012).
- [6] V. Scagnoli, U. Staub, Y. Bodenthin, R. A. de Souza, M. García-Fernández, M. Garganourakis, A. T. Boothroyd, D. Prabhakaran, and S. W. Lovesey, Science **332**, 696 (2011).
- [7] F. Michaud, F. Vernay, and F. Mila, Physical Review B **84**, 184424 (2011).
- [8] B. Bauer, P. Corboz, A. M. Läuchli, L. Messio, K. Penc, M. Troyer, and F. Mila, Physical Review B **85**, 125116 (2012).
- [9] P. Corboz, A. M. Läuchli, K. Penc, M. Troyer, and F. Mila, Physical Review Letters **107**, 215301 (2011).
- [10] I. A. Zaliznyak, Z. J. Xu, J. S. Wen, J. M. Tranquada, G. D. Gu, V. Solovyov, V. N. Glazkov, A. I. Zheludev, V. O. Garlea, and M. B. Stone, Physical Review B **85**, 085105 (2012).
- [11] J. S. White, T. Honda, K. Kimura, T. Kimura, C. Niedermayer, O. Zaharko, A. Poole, B. Roessli, and M. Kenzelmann, Physical Review Letters **108**, 077204 (2012).
- [12] K.-J. Zhou, M. Radovic, J. Schlappa, V. Strocov, R. Frison, J. Mesot, L. Patthey, and T. Schmitt, Physical Review B **83**, 201402 (2011).
- [13] F. Michaud, F. Vernay, S. Manmana, and F. Mila, Physical Review Letters **108**, 127202 (2012).
- [14] S. Mühlbauer, S. N. Gvasaliya, E. Pomjakushina, and A. Zheludev, Physical Review B **84**, 180406 (2011).
- [15] N. Laflorencie and F. Mila, Physical Review Letters **107**, 037203 (2011).
- [16] S. V. Isakov, M. B. Hastings, and R. G. Melko, Nature Physics **7**, 772 (2011).
- [17] S. V. Isakov, R. G. Melko, and M. B. Hastings, Science **335**, 193 (2012).
- [18] R. Ganesh, S. V. Isakov, and A. Paramekanti, Physical Review B **84**, 214412 (2011).
- [19] S. V. Isakov, P. Fendley, A. W. W. Ludwig, S. Trebst, and M. Troyer, Physical Review B **83**, 125114 (2011).

[20] A. A. Bush, V. N. Glazkov, M. Hagiwara, T. Kashiwagi, S. Kimura, K. Omura, L. A. Prozorova, L. E. Svistov, A. M. Vasiliev, and A. Zheludev, Physical Review B **85**, 054421 (2012).

► [21] D. Hüvonen, S. Zhao, M. Månsson, T. Yankova, E. Ressouche, C. Niedermayer, M. Laver, S. Gvasaliya, and A. Zheludev, arXiv:1201.6143 (2012).

[22] A. Zheludev and D. Hüvonen, Physical Review B **83**, 216401 (2011).

[23] B. C. Keith, F. Xiao, C. P. Landee, M. M. Turnbull, and A. Zheludev, Polyhedron **30**, 3006 (2012).

► [24] E. Wulf, S. Mühlbauer, T. Yankova, and A. Zheludev, Physical Review B **84**, 174414 (2011).

[25] S. Wang, E. Pomjakushina, T. Shiroka, G. Deng, N. Nikseresht, C. Rüegg, H. M. Rønnow, and K. Conder, Journal of Crystal Growth **313**, 51 (2010).

[26] T. Giamarchi, C. Rüegg, and O. Tchernyshyov, Nature Physics **4**, 198 (2008).

[27] T. Yankova, D. Hüvonen, S. Mühlbauer, D. Schmidiger, E. Wulf, S. Zhao, A. Zheludev, T. Hong, V. O. Garlea, R. Custelcean, and G. Ehlers, arXiv:1110.6375 (2011).

[28] V. N. Glazkov, T. S. Yankova, J. Sichelschmidt, D. Hüvonen, and A. Zheludev, Physical Review B **85**, 054415 (2012).

► [29] B. Náfrádi, T. Keller, H. Manaka, A. Zheludev, and B. Keimer, Physical Review Letters **106**, 177202 (2011).

Other references

[30] M. P. A. Fisher, P. B. Weichman, G. Grinstein, and D. S. Fisher, Physical Review B **40**, 546 (1989).

[31] S. Sachdev and K. Damle, Physical Review Letters **78**, 943 (1997).

Project 7 Electronic materials with reduced dimensionality

Project leader: L. Forró (EPFL)

Participating members: Ph. Aebi (UniFR), L. Degiorgi (ETHZ), L. Forró (EPFL), T. Giamarchi (UniGE), M. Grioni (EPFL), C. Renner (UniGE),

Summary and highlights: The program of the project is to study various electronic instabilities in low-dimensional materials and their competition in the stabilization of the ground state of the system. The highlighted topics of our in-debt studies are: the the influence of an exciton condensate on the lattice and the stripe formation in the pristine and the Cu intercalated $1T$-$TiSe_2$ dichalcogenide compound; a large spin-orbit interaction in a quantum confined geometry of $BiAg_2$ which yields a complex and tunable spin-polarized gap structure; the long-range incommensurate magnetic order in $TbTe_3$ charge density wave (CDW) compound; the Luttinger liquid features of the purple bronze compound and the unusual metallic phase of an organic kagome system.

1 Exciton condensation driving the periodic lattice distortion of $1T$-$TiSe_2$ (Ph. Aebi)

We studied the lattice deformation of $1T$-$TiSe_2$ within the exciton condensate phase. At low temperature, the condensed excitons influence the lattice through electron-phonon interaction. The theoretically found ionic displacement is comparable in amplitude to the value measured experimentally. This is the first quantitative estimation of the amplitude of the periodic lattice distortion as a consequence of the exciton condensate phase.

In a semimetallic or semiconducting system exhibiting a small electronic band overlap or gap, the Coulomb interaction, when poorly screened, leads to the formation of bound states of holes and electrons, called excitons. If their binding energy E_B is larger than the gap, they may *spontaneously* condense at low temperature and drive the system into a new ground state with exotic properties.

This new ground state, called the excitonic insulator phase, has been theoretically predicted in the 1960s [9]. Recently, we investigated the charge density wave (CDW) system $1T$-$TiSe_2$ with angle-resolved photoemission spectroscopy (ARPES), favoring the excitonic insulator phase scenario as the origin of the CDW phase [1, 2].

The quasi-two-dimensional $1T$-$TiSe_2$ undergoes a phase transition towards a commensurate $2 \times 2 \times 2$ CDW phase below the critical temperature $T_c \simeq 200$ K. A weak periodic lattice distortion (PLD) accompanying the CDW (which requires only electronic degrees of freedom) has been measured, involving small ionic displacements < 0.1 Å [10]. The occurrence of this PLD lead Hughes to suggest a band Jahn-Teller effect as the driving force of the CDW in $1T$-$TiSe_2$ [11].

In this perspective, it is crucial to know whether ionic displacements of a reasonable amplitude may appear at all as a consequence of exciton condensation in the low-temperature phase. We addressed this question and studied the influence of an exciton condensate on the lattice.

To do so, the electron-phonon coupling is derived in the framework of the tight binding (TB) formalism. The transfer integrals for the TB band structure were derived from a fit to a band structure of $1T$-$TiSe_2$ calculated with density functional theory (Fig. 1).

The role of excitons is expressed within this TB approach through an anomalous Green's function in a similar way as used for the BCS-like

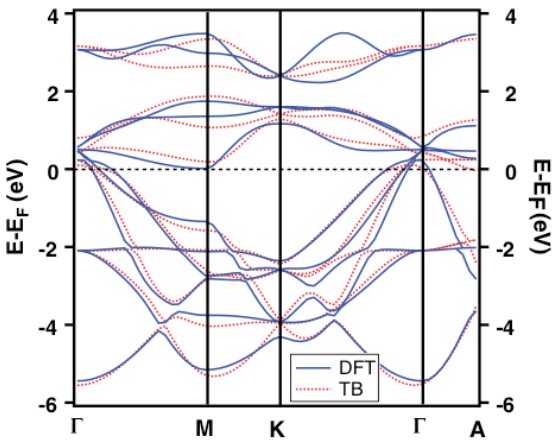

Figure 1: *Comparison of the band structure of $1T$-$TiSe_2$ calculated with density functional theory (DFT) and its fit within a tight binding (TB) approach.*

formalism of the exciton model. This results in an exciton-phonon Hamiltonian. Minimizing the sum of the bare, harmonic lattice and the exciton-phonon energy results in an equilibrium displacement amplitude of the ions. The values found are similar to those obtained from experiment [3]. This demonstrates that the exciton condensate phase, as a possible origin of the CDW phase of $1T$-$TiSe_2$, can also account for the PLD.

2 Scanning tunneling microscopy of Cu-doped $1T$-$TiSe_2$ (Ch. Renner)

Charge and spin segregation into stripe domains is ubiquitous in copper oxide high-temperature superconductors (HTS) and colossal magneto-resistance (CMR) manganese oxides. The precise role of these stripes in the occurrence of HTS and CMR remains matter of heated debates. Last year, we have reported the observation of stripes by scanning tunneling microscopy (STM) in stage I calcium intercalated graphite [4]. CaC_6 becomes superconducting below $T_c = 11.6$ K, the largest superconducting transition temperature for any graphite intercalated compound to date.
The new observation of a striped phase by STM at the surface of $1T$-Cu_xTiSe_2, again a compound with the largest T_c in its class, holds promise to shed new light on the interplay between superconductivity and such a one-dimensional ordered electronic phase. Here we show first STM results obtained at 78 K on pristine and $\sim 6\%$ copper doped $1T$-$TiSe_2$.
In summer 2011, we have started an effort to grow high-quality $1T$-Cu_xTiSe_2 single-crystals, with x in the range of 0 to 0.1. The pristine phase ($x = 0$) undergoes a phase transition into a $2a_0 \times 2a_0$ charge density wave (CDW) near 218 K [12]. Single-crystals with $0.04 < x < 0.10$ become superconducting at low temperature, with a maximum T_c of about 4 K for $x \simeq 0.08$.

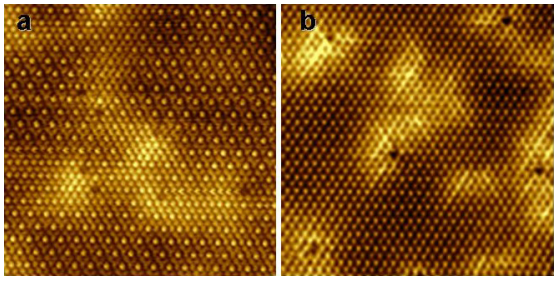

Figure 2: *STM micrographs of $1T$-Cu_xTiSe_2 measured at 78 K. (a) $2a_0 \times 2a_0$ CDW observed in pure $1T$-$TiSe_2$. (b) Charge stripes running horizontally through the image observed on $\sim 6\%$ copper intercalated sample (unpublished).*

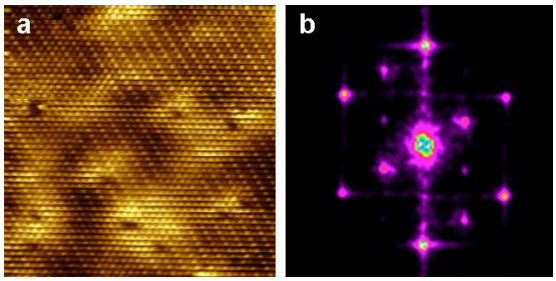

Figure 3: *(a) STM micrograph of $1T$-Cu_xTiSe_2 ($x \simeq 0.06$) at $T = 78$ K showing $\sqrt{3}a_0$ stripes running diagonally through the image. (b) Fourier transform of the STM micrograph shown in (a) (unpublished).*

Our current STM setup is limited to temperatures above 3 K, insufficient for a detailed investigation of the superconducting phase.
Here we report on a first set of STM micrographs obtained on $1T$-Cu_xTiSe_2 (for $x = 0$ and $x \simeq 0.06$) at $T = 78$ K. Fig. 2a reveals the $2a_0 \times 2a_0$ CDW also reported in the literature for pristine $1T$-$TiSe_2$. STM micrographs of $1T$-Cu_xTiSe_2 cleaved surfaces with $x \simeq 0.06$ (Figs. 2b and 3a) reveal a very different texture: the $2a_0 \times 2a_0$ CDW is replaced with a commensurate stripe modulation of periodicity $\sqrt{3}a_0$ running along the principal lattice directions in the ab-plane. The Fourier transform of the STM micrograph (Fig. 3b) reveals the stripe as two enhanced diffraction spots.
Figs. 2b and 3a reveal several other interesting features of the striped surface. There is a distinct electronic inhomogeneity, that seems correlated with black single-atom defects. The nature of these defects has not yet been determined. The stripe contrast is much weaker, if not absent, in the bright regions, corresponding to domains of locally larger density of states. But the bright regions do not affect the long range order and registry of the stripes. We observe stripes oriented along either of the three possible lattice directions. Another interesting feature are the bright, three branch star-shaped defects observed in the bright regions.
These experiments have just started, and we have not performed detailed spectroscopy yet. This will be our next step, alongside cooling the crystals below their superconducting transition temperature to investigate the interplay between stripes and superconductivity.

3 High-resolution ARPES of 2D and 1D electron systems (M. Grioni)

We have exploited high-resolution angle-resolved photoemission (ARPES) to study the electronic structure of two-dimensional spin-split surface states. We have found that a

large spin-orbit interaction in a quantum confined geometry yields a complex and tunable spin-polarized gap structure. We have also exploited synchrotron radiation to quantify the transverse coupling in the quasi-one-dimensional Peierls system $(TaSe_4)_2I$.

3.1 Spin-splitting in two-dimensional surface states

States of opposite spin are usually degenerate in non-magnetic systems (Kramers degeneracy) as a consequence of two general symmetry properties: time-reversal and space inversion symmetry. However, at a surface or at an interface between two different solids, inversion symmetry is broken and the degeneracy is lifted under the influence of spin-orbit interaction. The corresponding two-dimensional (2D) surface or interface states are split in energy and momentum depending on their spin. This offers an attractive mean of manipulating spin-polarized currents without magnetic fields. Device concepts based on this Rashba effect have been proposed, but operation at practical temperatures is hindered by the small energy splitting (< 1 meV) typically achieved in semiconductor heterostructures.

We have shown that very large energy splittings, up to two orders of magnitude larger than in semiconductors, can be achieved in monolayer(ML)-thin metallic surface alloys based on high-Z elements like Bismuth [5]. We have now explored the possibility of transferring such *giant* Rashba effect onto a silicon substrate, in a Si(111)-Ag-Bi trilayer structure. We have found that an epitaxial $BiAg_2$ surface alloy can indeed be grown on top of the Ag buffer layer, and that it supports a large spin separation. When the Ag layer is only a few monolayers thin, vertical quantum confinement gives rise to very peculiar band structure properties, which are well characterized by high-resolution angle-resolved photoemission (ARPES) [6]. The ARPES intensity map of Fig. 4a shows the dispersion of 2D quantum-well states (QWS) confined in a 19 ML Ag buffer layer.

These QWS exhibit a nearly free-electron parabolic dispersion along the surface, but are quantized by confinement in the perpendicular direction, in a particle-in-the-box fashion. When the $BiAg_2$ alloy is formed at the Ag surface, characteristic spin-split surface states (SS) with negative effective mass appear. The spin selective hybridization of the SS and QWS yields a complex gap structure, illustrated in Fig. 4b. The hybrid bands display constant-energy contours with a marked hexagonal symmetry (not shown), reminiscent of the case of the spin-split surface states of the related topological insulator compounds, and can be similarly analyzed [13]. We find that the QWS are also polarized, and that the spin polarization is large within the SS gaps. Large changes of the polarization at the Fermi level E_F are possible by sweeping E_F through the gap structure. This can be achieved over ~ 250 meV by electron doping, when Na is evaporated on the surface at sub-ML coverage.

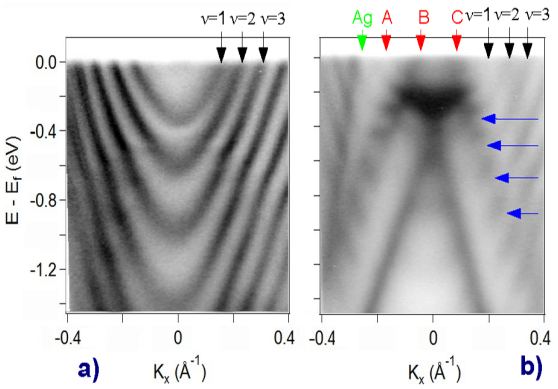

Figure 4: *(a) In-plane dispersion of the quantum-well states (QWS) of a 19 ML Ag buffer layer grown on Si(111). (b) Hybrid Bi-Ag spin-split states of a $BiAg_2$ surface alloy grown on the Ag buffer layer, showing the complex gap structure.*

3.2 Transverse coupling in 1D $(TaSe_4)_2I$

The charge density wave (CDW) — a periodic spatial modulation of the electronic charge density and of the ionic positions — is a characteristic electronic instability of low- and especially one-dimensional solids. According to the standard Peierls model, the CDW is a consequence of the good nesting properties of the Fermi surface (FS), i.e. of the good overlap of the FS with a replica translated by a nesting vector $\boldsymbol{Q}_{CDW}$. The same vector determines the spatial periodicity of the CDW. Strictly in 1D the Fermi surface consists of parallel planes, and nesting is perfect with wave vector $Q_{CDW} = 2k_F$. In real, chainlike quasi-1D materials, transverse interactions modify the FS and the nesting condition. Moreover, the electrostatic interaction between CDWs on different chains often influences 2D or 3D order, so that $\boldsymbol{Q}_{CDW}$ in general has non-zero transverse components.

The quasi-1D compound $(TaSe_4)_2I$ exhibits below $T_P = 263$ K a transition to an incommensurate CDW, corresponding to a near tetramerization of the Ta atoms along the chains.

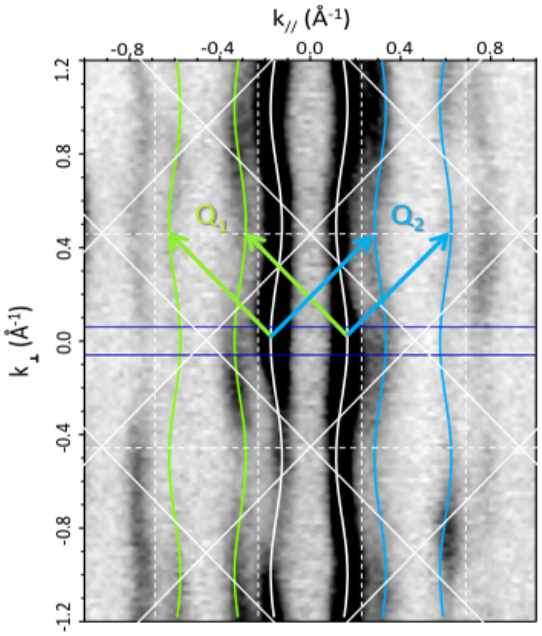

Figure 5: *ARPES constant energy map measured 0.6 eV below E_F in the CDW phase in $(TaSe_4)_2I$, with photon energy $h\nu = 95$ eV. It shows open contours running perpendicular to the chains direction. Transverse coupling is illustrated by their warping and by the replicas spanned by the equivalent 2D nesting vectors $\boldsymbol{Q_1}$ and $\boldsymbol{Q_2}$.*

Diffraction shows that the CDW orders with opposite phases on adjacent chains, but cannot establish if the transverse order has an electrostatic origin or if it is rather due to coherent interchain hopping. ARPES can discriminate between the two scenarios. Fig. 5 shows an ARPES constant energy (CE) cut through the band structure, measured 0.6 eV below E_F in the CDW phase. The open CE contours run perpendicular to the chain direction, as expected for a 1D material. However, unlike the ideal 1D case, the contours are warped, revealing a finite perpendicular coupling. A fit of the whole dispersion with a cosine band yields a sizeable interchain hopping parameter $t_\perp \sim 50$ meV. As a result of this transverse coupling, the most favorable nesting condition corresponds to a transverse $\boldsymbol{Q}_{CDW}$, in agreement with diffraction data. The Brillouin zones (BZ) corresponding to the CDW periodicity are superposed on the data, drawn as solid lines. Interestingly, shadow band contours, highlighted by blue and green lines, are well reproduced by folding the main band with the $\boldsymbol{Q}_{CDW}$ periodicity, but not by a mere symmetry around the 1D BZ boundary (dashed vertical lines).

4 Incommensurate magnetic order in $TbTe_3$ (L. Degiorgi)

The RTe_3 family of compounds (R = rare earth) has recently attracted renewed interest as a model system for layered (two-dimensional) charge density wave (CDW) materials. RTe_3 crystallizes in an orthorhombic structure, composed of double layers of planar Te-sheets separated by corrugated R-Te layers. The average chemical structure can be described using the $Cmcm$ space group (in this setting the lattice parameters a and c are close to each other, whereas b is approximately 6 times longer). A CDW state with modulations along the c-axis is present in all RTe_3 materials. However, the members with the heaviest rare earth elements exhibit a second CDW phase transition at lower temperatures that is characterized by a modulation wave vector $q_a \sim 2/3a^*$. The critical temperatures of these two CDW transitions show opposite trends as a function of the R-atom mass. Whereas T_{CDW1} decreases towards heavier members of the family (i.e. going from La to Tm), the T_{CDW2} associated with the a-axis incommensurability is higher for heavier compounds. For the specific composition addressed in our study, $TbTe_3$, transport and diffraction experiments yield $T_{CDW1} = 336$ K. Although transport measurements do not clearly reveal the presence of a second CDW transition, STM measurements performed at 6 K do show an ordering pattern that is associated with the wave vector $\sim 2/3a^*$. More recent high-resolution X-ray diffraction measurements confirm the presence of a transverse CDW at low temperatures, with wave vector $\sim 0.683a^*$, though T_{CDW2} is at present unknown.

In addition to hosting an incommensurate CDW, RTe_3 also hosts long range antiferromagnetic order at low temperatures for magnetic rare earth ions. The nature of the long-range magnetic order in this family of compounds has not yet been studied by diffraction techniques, and the effect of the incommensurate lattice modulation on the magnetic structure is unknown. To bridge this gap, we have performed neutron scattering experiments in $TbTe_3$, which exhibits three closely located magnetic phase transitions at $T_{mag1} = 5.78$ K, $T_{mag2} = 5.56$ K and $T_{mag3} = 5.38$ K.

Fig. 6 shows the magnetic diffraction pattern measured in $TbTe_3$ at 2 K. Some of the magnetic peaks could be indexed in terms of the average chemical cell and are labeled in Fig. 6. Clearly, most of the magnetic Bragg peaks are at positions incommensurate with the average chemical structure of the material.

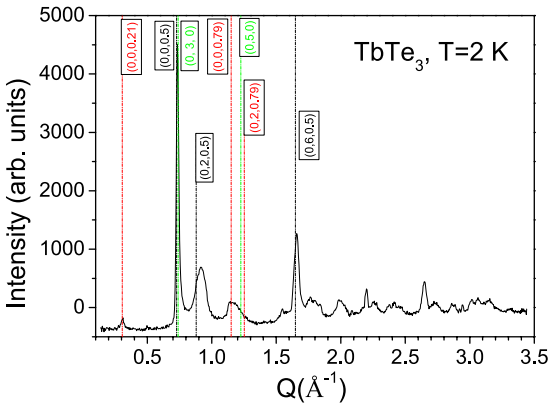

Figure 6: *Indexed magnetic reflections for $TbTe_3$ at 2 K in a powder diffraction pattern (the contribution from the chemical structure is eliminated by subtracting the powder spectrum taken at $T = 60$ K). The peaks that are associated with the magnetic propagation vector $\boldsymbol{q}_{mag1} = (0,\ 0,\ 0.21)$ are labeled in red, those associated with the magnetic propagation vector $\boldsymbol{q}_{mag2} = (0,\ 0,\ 0.5)$ are shown in black, and finally, with $\boldsymbol{q}_{mag3} = (0,\ 1,\ 0)$, in green.*

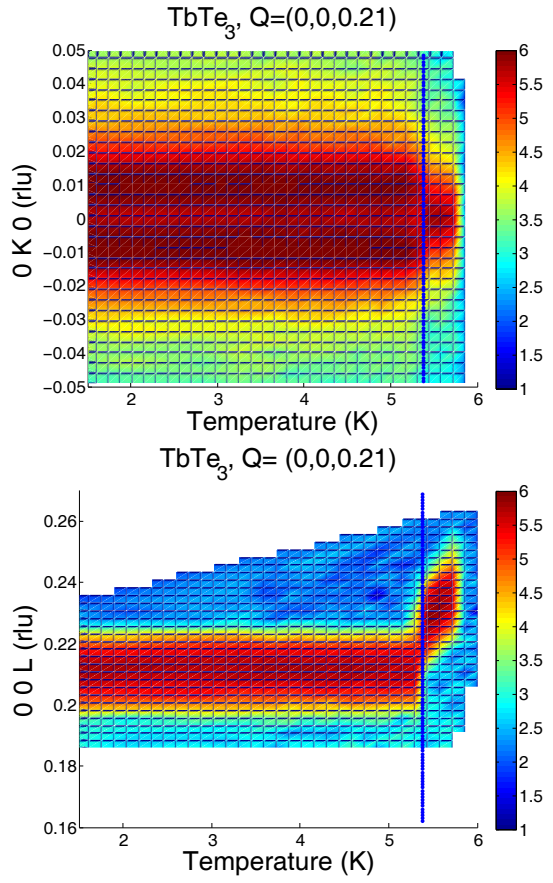

Figure 7: *The temperature evolution of the intensity distribution taken in the vicinity of the $(0,\ 0,\ 0.21)$ position of $TbTe_3$. Vertical solid lines on both plots denote $T_{mag3} = 5.38$ K. Note that below T_{mag3} the reflection is incommensurate in both $< 0,\ K,\ 0 >$ and $< 0,\ 0,\ L >$ directions.*

Fig. 7 shows false-color maps of neutron intensities taken in a close vicinity of the $(0,\ 0,\ 0.21)$ incommensurate magnetic reflection in the temperature range $1.5 - 6$ K. At the base temperature this reflection has incommensurate components both along the $< 0,\ K,\ 0 >$ and $< 0,\ 0,\ L >$ directions. However, the incommensurate component along the $< 0,\ K,\ 0 >$ direction appears to be small and diminishes above T_{mag3} in a step-like way. Above T_{mag3} the incommensurate components along the $< 0, 0, L >$ direction is also temperature-dependent. For a more quantitative analysis the scans for each temperature are fitted assuming a Gaussian shape for a Bragg reflection. The resulting temperature dependence of the position and intensity of the peak $(0,\ 0,\ 0.21)$ is shown in Fig. 8. The modulation vector along the $< 0,\ 0,\ L >$ direction stays constant within the precision of the measurements below T_{mag3}. Above T_{mag3} the propagation vector increases smoothly and reaches the value of $(0,\ 0,\ 0.242 \pm 0.001)$ at T_{mag1}. The modulation vector along the $< 0,\ K,\ 0 >$ direction is also constant $(0,\ 0.01 \pm 0.001,\ 0)$ below T_{mag3}, while above this temperature the component of the modulation vanishes. The intensity measured around the $(0,\ 0,\ 0.21)$ position appears to be nearly temperature-independent below T_{mag3}. Above this temperature however, the overall intensity observed in the vicinity of the $(0,\ 0,\ 0.21)$ position drops by a factor of 2, as can be deduced from Fig. 8b and d. Further the intensity gradually decreases and above T_{mag1} we could not detect any scattering above the background level around that posi-

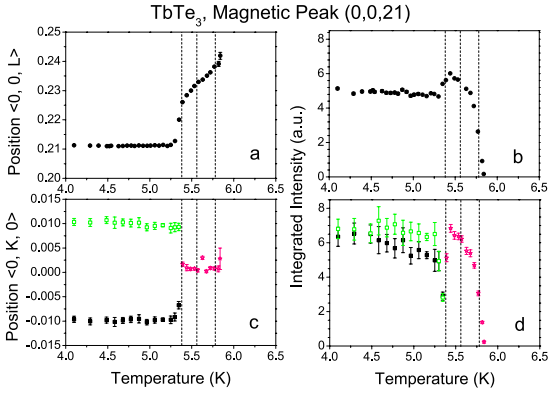

Figure 8: *The temperature evolution of the propagation vectors (left column) and of the intensity (right column) measured around the position $(0,\ 0,\ 21)$. Green symbols denote the position and the intensity of the $(0,\ 0+\delta,\ 0.21)$ satellite, whereas black squares stand for the $(0,\ 0-\delta,\ 0.21)$. Vertical dashed lines denote the temperatures of the magnetic phase transitions.*

tion. Gradual decrease of the Bragg intensity suggests a continuous character of the phase transition that the crystal undergoes at T_{mag1}, whereas an abrupt change in magnetic intensity at T_{mag3} points to a first order phase transition.

5 Properties of purple bronze (T. Giamarchi)

The compound $Li_{0.9}Mo_6O_{17}$ (purple bronze) shows very unusual behavior (for example see [7] and references therein). On one hand it shows properties, such as ARPES or STM, which would be consistent with Luttinger liquid ones, on the other hands some of the scalings between temperature and frequency do not obey the canonical picture of a Luttinger liquid.
We have thus started to analyze the properties of this system. We have used density functional theory (DFT) techniques to confirm the bandstructure properties of this systems, in particular that there are two very close bands crossing the Fermi surface, and also to study precisely the band dispersion perpendicular to the main conducting axis of the system. The DFT study was also used to analyze the effects of the thermal displacements of the atoms. Indeed such a disorder could have been a reason for the unusual behavior of the compound. Our analysis shows that thermal fluctuations alone cannot account for the observed behavior. We have also derived, in a spirit similar to studies performed for the cuprates, an effective hamiltonian which should allow the study of the strong correlation properties. The key issue was to marry the results of DFT valid at the electronvolts energy scale with the low-energy effective field theory. The aim was to explain the experimentally observed features, which at energy scale 20 meV fit very well with expectations from the Luttinger liquid physics.

6 Pressure effect on the electronic properties of an organic metallic kagome compound (L. Forró)

We have studied the first organic kagome system, which has highly unusual properties. It has metallic resistivity well above the Ioffe-Regel limit, and its response to hydrostatic pressure is opposite to the expectations. We suspect that this behavior is linked to a dense polaronic system. The kagome network, composed of corner-sharing interlaced triangles is nowadays at the heart of intense research due to the possibility to generate, in frustrated magnets, new and original electronic ground states. Many studies were devoted to the case of systems with localized moments and antiferromagnetic correlations, for which the geometry of the lattice highly frustrates the spin interactions and induces a fluctuating behavior without long-range order down to $T = 0$.

Since the initial proposal of a resonating valence bond state by Anderson [14], the field was intensively investigated from the theoretical point of view. On the experimental side, systems with a kagome topology such as Volborthite [15], SCGO [16], and Herbertsmithite [17] are the subject of many studies. A kagome geometry based on organic molecules was realized for the first time in (EDT-TTF-$CONH_2)_6[Re_6Se_8(CN)_6]$ [18] (Fig. 9), which is the subject of our investigation. The kagome geometry persists down to 180 K where the system undergoes a structural phase transition into an insulating chain-like structure. This report focuses on the kagome phase. Our transport data show metallic behavior at ambient pressure (Fig. 10) with a strong two-dimensional character, in coherence with the kagome lattice. Surprisingly, this metallicity is present much above the Ioffe-Regel limit, at $\rho = 0.2\ \Omega$cm. A further peculiarity is the pressure dependence of the resistivity. Instead of becoming a better metal with pressure, its resistivity increases and changes character: from the metallic it switches gradually to a semiconducting behavior. The ingredients of the theoretical modeling are a dense polaronic system with strong Coulomb interactions [8].

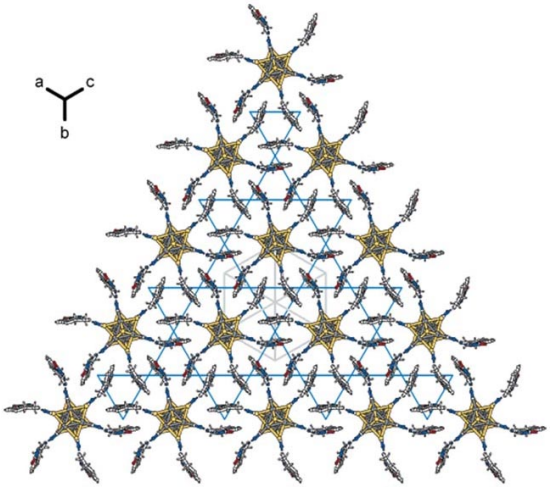

Figure 9: *This projection of one single hybrid slab down to [1 1 1]. The red lines connecting the centers of [EDT-TTF-$CONH_2$]$_2$ dimers realize the kagome lattice.*

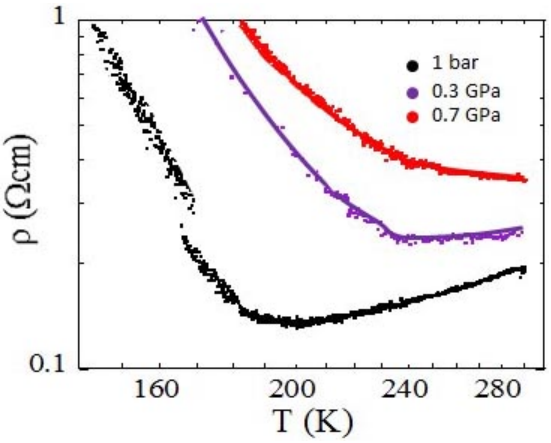

Figure 10: *Electrical resistivity at three representative pressures. The structural phase transition increases with pressure, but surprisingly the ambient pressure metallic resistivity is lost with increasing pressure.*

7 Collaborative efforts

Within the project, among the experimentalists, there is a focused research on the layered dichalcogenide $TiSe_2$ and $BaVS_3$, a quasi-one-dimensional material. These systems are studied by a variety of experimental methods which helps the theoretical description. There is an excellent collaboration with other MaNEP projects (namely Projects 2, 4 and 5) on the study of graphene or other two-dimensional superconductors.

MaNEP-related publications

[1] H. Cercellier, C. Monney, F. Clerc, C. Battaglia, L. Despont, M. G. Garnier, H. Beck, P. Aebi, L. Patthey, H. Berger, and L. Forró, Physical Review Letters **99**, 146403 (2007).

[2] C. Monney, H. Cercellier, F. Clerc, C. Battaglia, E. F. Schwier, C. Didiot, M. G. Garnier, H. Beck, P. Aebi, H. Berger, L. Forró, and L. Patthey, Physical Review B **79**, 045116 (2009).

► [3] C. Monney, C. Battaglia, H. Cercellier, P. Aebi, and H. Beck, Physical Review Letters **106**, 106404 (2011).

► [4] K. C. Rahnejat, C. A. Howard, N. E. Shuttleworth, S. R. Schofield, K. Iwaya, C. F. Hirjibehedin, C. Renner, G. Aeppli, and M. Ellerby, Nature Communications **2**, 558 (2011).

Other references

[5] C. R. Ast, J. Henk, A. Ernst, L. Moreschini, M. C. Falub, D. Pacilé, P. Bruno, K. Kern, and M. Grioni, Physical Review Letters **98**, 186807 (2007).

[6] A. Crepaldi, S. Pons, E. Frantzeskakis, K. Kern, and M. Grioni, Physical Review B **85**, 075411 (2012).

[7] T. Giamarchi, Physics **2**, 78 (2009).

[8] J. Jaćimović, D. Djokic, A. Olariu, P. Batail, B. Náfrádi, E. Tutiš, and L. Forró, *submitted to* Physical Review B (2012).

[9] D. Jérome, T. M. Rice, and W. Kohn, Physical Review **158**, 462 (1967).

[10] F. J. Di Salvo, D. E. Moncton, and J. V. Waszczak, Physical Review B **14**, 4321 (1976).

[11] H. P. Hughes, Journal of Physics: Condensed Matter **10**, L319 (1977).

[12] E. Morosan, H. W. Zandbergen, B. S. Dennis, J. W. G. Bos, Y. Onose, T. Klimczuk, A. P. Ramirez, N. P. Ong, and R. J. Cava, Nature Physics **2**, 544 (2006).

[13] L. Fu, Physical Review Letters **103**, 266801 (2009).

[14] P. W. Anderson, Materials Research Bulletin **8**, 153 (1973).

[15] M. P. Shores, E. A. Nytko, B. M. Bartlett, and D. G. Nocera, Journal of the American Ceramic Society **127**, 13462 (2005).

[16] F. Bert, D. Bono, P. Mendels, F. Ladieu, F. Duc, J.-C. Trombe, and P. Millet, Physical Review Letters **95**, 087203 (2005).

[17] A. P. Ramirez, G. P. Espinosa, and A. S. Cooper, Physical Review Letters **64**, 2070 (1990).

[18] S. A. Baudron, P. Batail, C. Coulon, R. Clerac, E. Canadell, V. Laukhin, R. Melzi, P. Wzietek, D. Jerome, P. Auban-Senzier, and S. Ravy, Journal of the American Chemical Society **127**, 11785 (2005).

Project 8 Cold atomic gases as novel quantum simulators for condensed matter

Project leader: T. Giamarchi (UniGE)

Participating members: G. Blatter (ETHZ), T. Esslinger (ETHZ), T. Giamarchi (UniGE), V. Gritsev (UniFR), C. Kollath (UniGE), F. Mila (EPFL), M. Troyer (ETHZ)

Summary and highlights: The project continued to examine the physics of cold atomic gases, in connection with problems of condensed matter. It was mostly centered around three axes. i) The cold atomic systems could be used as quantum simulators, to create model systems. One of the most remarkable achievement in this direction is the realization of graphene-like structures. ii) In order to study these systems it is important to develop probes and thermometry adapted to such novel systems. This was the goal of the second direction of the project. Novel probes for magnetic order have been developed, and local imaging allows to probe for non-local order such as string order parameter. iii) Finally the cold atomic systems allow to treat unusual situations such as out of equilibrium ones, for which new concepts must be developed. This was the main focuss of the third research direction. Propagation of information, topological effects and thermalization effects were explored.

1 Model systems

The effort in realizing or analyzing via cold atoms model systems, in connection with condensed matter, has known important progress in several directions

1.1 Graphene-line structures *(T. Esslinger)*

Dirac points lie at the heart of many fascinating phenomena in condensed matter physics, from massless electrons in graphene to the emergence of conducting edge states in topological insulators. At a Dirac point, two energy bands intersect linearly and the particles behave as relativistic Dirac fermions. In solids, the rigid structure of the material sets the mass and velocity of the particles, as well as their interactions. A different, highly flexible approach is to create model systems using ultracold atoms trapped in the periodic potential of interfering laser beams [1]. The Esslinger group has realized Dirac points with adjustable properties in a tunable honeycomb optical lattice for ultracold fermions [2]. To create and manipulate such Dirac points, they have developed a two-dimensional optical lattice of adjustable geometry. It is formed by three retro-reflected laser beams, as depicted in Fig. 1. The honeycomb lattice consists of two sublattices A and B. Therefore, the wave functions are two-component spinors. Tunneling between the sublattices leads to the formation of two energy bands, which are well separated from the higher bands and have a conical intersection at two quasi-momentum points in the Brillouin zone — the Dirac points. These points are topological defects in the band structure, with an associated Berry phase of $\pm\pi$. The band structure for this lattice implementation is, in the two lowest bands, topologically equivalent to

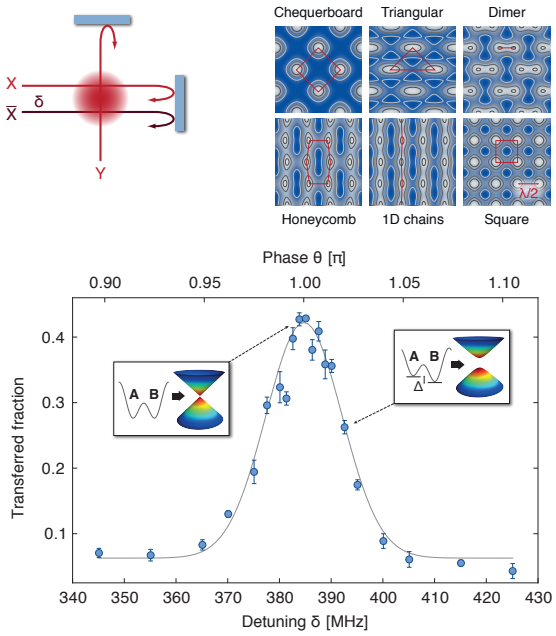

Figure 1: *Top: laser beams X and Y interfere and produce a checkerboard pattern, while $\overline{X}$ creates an independent standing wave. Their relative position is controlled by the detuning δ. Different lattice geometries can be realized. Bottom: dependence of the total fraction of atoms transferred to the second band on the detuning of the lattice beams δ, which controls the sublattice energy offset Δ. The maximum indicates the point of inversion symmetry.*

that of a hexagonal lattice with six-fold symmetry. For deep lattices both configurations then also map to the same tight-binding Hamiltonian. They have characterized the Dirac points by probing the energy splitting between the two lowest energy bands through interband transitions.

1.2 Quantum cavities *(G. Blatter, M. Troyer)*

Another system allowing for quantum simulation is provided by cavity quantum electrodynamics (QED) systems, reaching from quantum dots in photonic crystal cavities to superconducting qubits in transmission line resonators. One of the most spectacular consequences of strong light-matter interactions is the effect of photon blockade, where the presence of a single photon in a cavity prevents all other photons to enter, i.e. the realization of strong effective photon-photon interactions at the single-photon level.

In a recent theory-experiment collaboration together with Andrew Houck and Hakan Tureci at Princeton [3], the Blatter group demonstrated that photon blockade in an incoherently driven, dissipative cavity can be understood in perfect analogy to the Coulomb blockade in a gated quantum dot. Photon-photon interactions were realized experimentally in a superconducting coplanar waveguide cavity coupled to a superconducting charge qubit. When the cavity is pumped by varying the bandwidth of the incoming photons, interactions lead to quantized transmission of photons through the cavity. A measurement of the total transmitted power while increasing the incident photon bandwidth results in a transmission staircase (in analogy to Coulomb staircase), where each step indicates that an additional photon can be present in the cavity (Fig. 2). They have given a theoretical description of this highly non-Markovian process in terms of an effective master equation for the steady state density matrix of the system. The resulting transmission staircase qualitatively resembles the measured data and can be plotted in a way reminiscent of charge stability diagrams in electron transport through quantum dots.

With the experimental realization of strong light-matter interactions in a single cavity, a key challenge for further progress in the field is the study of coupled cavity systems [4] (for a review see [27]). Of particular interest is the realization of a possible superfluid (SF) Mott-insulator (MI) transition of polaritons in a coupled cavity-array as described by the Jaynes-

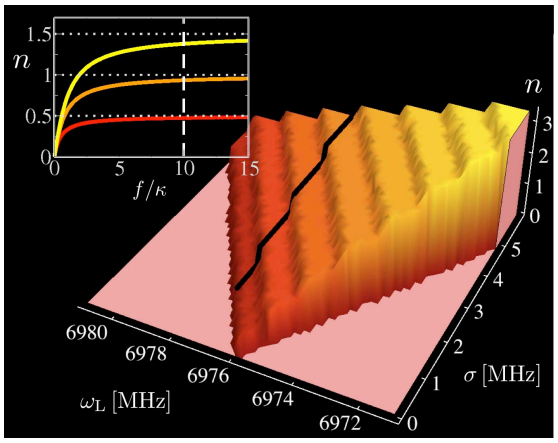

Figure 2: *Stability diagram for photon blockade showing the number photons in a cavity as a function of center frequency ω_L and bandwidth σ of the incident radiation. The center frequency, ω_L, can be changed to align the energy of incident photons with states of the cavity, much like the gate voltage in a quantum dot. The bandwidth of the incident photons, σ, controls the energy range of the photons in the system and can be increased to overcome photon blockade. Each step in the staircase indicates the contribution of an additional photon to the transmission through the cavity. The inset shows the number of photons as a function of the effective drive strength f/κ on the first step along the black line in the stability diagram.*

Cummings-Hubbard model (JCHM) [28]. In a previous work, the Blatter group provided the first analytic strong-coupling theory for the phase diagram and elementary excitations in the Mott-phase of the JCHM [5]. In a follow-up work, they have extended this theory using a slave-boson approach in order to describe the strongly correlated superfluid phase of lattice polaritons as well [6]. Recently, together with Lode Pollet and Martin Hohenadler, they performed large-scale quantum Monte Carlo simulations in order to investigate numerically the critical exponents of the JCHM, i.e. the critical behavior of the superfluid density and the compressibility [7]. In agreement with the previous analytical results, they showed that the SF-MI transition of polaritons falls in the 3D XY universality class, i.e. the same critical theory as for the Bose-Hubbard model describing ultracold atoms in an optical lattice.

Recently, they have also considered variants of the JCHM, taking into account next nearest neighbor, diagonal and long-range photon hopping in one and two dimensions [8]. These models are relevant for potential experimental realizations of polariton Mott-insulators based on trapped ions or circuit QED.

1.3 Impurities in bosonic gases *(T. Giamarchi)*

Impurities interacting with a quantum bath is a longstanding question with implementations such as X-ray edge of Kondo problems, but also mobile impurities in Helium. Recently cold atomic gases have provided remarkable way to study this problem. In connection with this problem, the Giamarchi group has pursued the theoretical study of mobile impurities in a one-dimensional interacting gas of bosons. These systems provide an ideal testbed for the study of a quantum mechanical impurity moving inside an interacting many-body one-dimensional system, which is hypothesized to form a new, non-Luttinger liquid type universality class of excitations (see previous MaNEP reports).
In particular they have analyzed the experiment performed in the group of F. Minardi (LENS, Italy), and provided some analysis of the observed behavior of the impurity in terms of polaronic processes [9]. Although they can understand some aspects of the experiments, a full description is still a challenging question.
They are also actively pursuing a numerical analysis, using density matrix renormalization group (DMRG) techniques to confirm the universality hypothesis (see previous reports). A first step has been the observation of the predicted timescales for subdiffusive and ballistic behavior of the impurity in low-order observables such as its time-dependent local density.

1.4 SU(4) Heisenberg model *(F. Mila)*

Cold atom provide a way to easily implement higher symmetries than the usual SU(2) one, since the role of spin is played by an internal isospin of the atom. The Mila group has studied such a problem for an insulating phase of fermions with SU(4) symmetry. Using infinite projected entangled pair states (iPEPS), exact diagonalization, and flavor wave theory [10], they have shown that the SU(4) Heisenberg model of the quarter-filled Mott-insulating phase of ultra-cold four-color fermionic atoms in an optical lattice undergoes a spontaneous dimerization on the square lattice (Fig. 3), in contrast to its SU(2) and SU(3) counterparts, which develop Néel and three-sublattice stripe-like long-range order. Since the ground state of a dimer is not a singlet for SU(4) but a six-dimensional irrep, this leaves the door open for further symmetry breaking. They have provided evidence that, unlike in SU(4) ladders, where dimers pair up to form singlet plaquettes, here the SU(4) symmetry is additionally broken, leading to a gapless spectrum in spite of the broken translational symmetry.

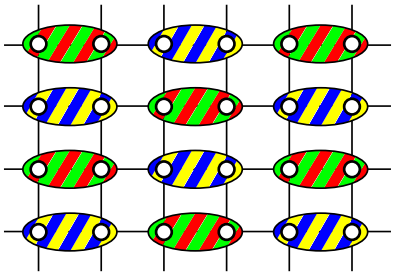

Figure 3: *Sketch of dimer and color order realized in the ground state of the SU(4) Heisenberg model on the square lattice.*

Using quantum Monte Carlo simulations for the 1D version of the SU(3) and SU(4) models, they have also investigated the temperature dependence of correlations. They have preliminary results indicating that signatures of the 3, respectively 4-sublattice algebraic ground state correlations start to be visible at an entropy per site of the order of $0.6 - 0.7\, k_B$, within the range of current state-of-the-art experimental setups.

1.5 Fermions at the unitary limit *(M. Troyer)*

The Troyer group has investigated the properties of the normal phase of a two-component Fermi gas with resonant interspecies interaction, which is realized at zero-temperature when the population imbalance is beyond the Chandrasekhar-Clogston limit where superfluid behavior disappears. From *in situ* density profiles of a deeply degenerate mixture of the two lowest internal states of Lithium-6 atoms, they measure the equation of state and the magnetic susceptibility across a Feshbach resonance. They compare the experimental data with quantum Monte Carlo results, finding excellent agreement [11]. Surprisingly, these results show that the resonant normal Fermi gas follows the paradigm of Landau Fermi liquid theory, with no indication of pseudo-gap physics.
In a related work [12], they present a cross validation between a new theoretical approach, bold diagrammatic Monte Carlo (BDMC), and precision experiments on ultra-cold atoms. Specifically, they compute and measure the normal state equation of state of the unitary gas, a prototypical example of a strongly correlated fermionic system, and find excellent agreement which demonstrates that a series of Feynman diagrams can be controllably resumed in a non-perturbative regime using BDMC.

2 Probes, thermometry and validation of quantum simulators

Various progress were also made in the way to probe the various physical phases that can be realized in cold atomic gases

2.1 Measure of spin fluctuations *(T. Esslinger)*

The subtle interplay between quantum-statistics and interactions is at the origin of many intriguing quantum phenomena connected to superfluidity and quantum magnetism. Current efforts in fermonic quantum gases are directed towards the identification of their magnetic properties [13], as well as the creation and detection of exotic quantum phases. Experiments studying density fluctuations have successfully demonstrated the potential of these techniques as a tool to study local thermodynamic properties of quantum gases [14][29]. The Esslinger group has recently demonstrated a shot-noise limited interferometer to directly measure the probability distribution of the local spin fluctuations in a two-component quantum degenerate Fermi gas. They obtained quantitative agreement with theory for a non-interacting Fermi gas. The interferometer is analogous to Young's double slit experiment. Two tightly focused beams, the probe and the local oscillator, are focused to separate points and overlap in the far field. Position and visibility of the resulting interference pattern are determined by changes in phase and amplitude of the probe beam, which passes through an atomic cloud, while the local oscillator does not. The analysis of the interference pattern thus allows the reconstruction of both quadratures of the probe beam, phase and amplitude, which carry information about the local properties of the atomic cloud.
From the measured values of the spin fluctuations they have determined the magnetic susceptibility χ via the fluctuation-dissipation theorem. Fig. 4 shows the column-integrated magnetic susceptibility per particle χ_{col}/n_{col} as a function of temperature. It relates the spin imbalance to the energy needed to create it. For high temperatures, the susceptibility decreases inversely proportional to the temperature, as expected. For low temperatures and with the onset of quantum degeneracy, the susceptibility saturates to a value depending on the trap details. The solid line shows theory for non-interacting fermions calculated for the trap parameters of the gas. The susceptibility for the strongly interacting gas of molecules is lower than for the weakly interacting gas.

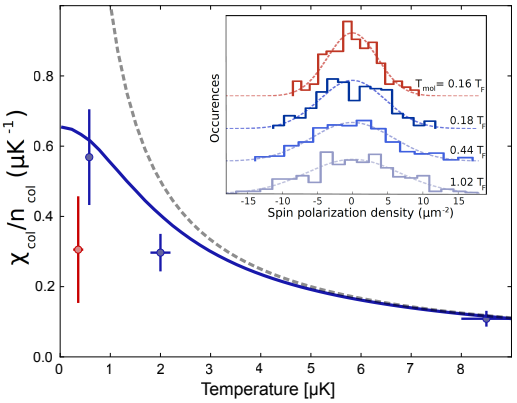

Figure 4: *Spin fluctuations in ultracold Fermi gases. Inset: normalized histograms for the measured spin polarization for weakly interacting gases as well as for a strongly interacting gas of molecules. Main graph: spin susceptibility per atom χ_{col}/n_{col} as a function of temperature for the weakly interacting gas (blue points) and the strongly interacting gas (see J. Meinecke* et al.*, submitted).*

2.2 Bosonic gases *(M. Troyer)*

Following a proposal of the Giamarchi group, in collaboration with E. Berg, E. Dalla Torre and E. Altman, of a string order parameter in the Mott-phase of a 1D bosonic system, the group of I. Bloch (Munich) used high-resolution imaging to probe for such a phase. The Troyer group has made a simulation of the corresponding low-dimensional Bose gases in optical lattices and compared to high-resolution imaging in the group of I. Bloch, validating the detection of string order in 1D quantum gas experiments [15].
To investigate conjectures by Phil Anderson about the absence of a Mott-transition in continuous space, the Troyer group has done direct continuous-space QMC simulations of bosons in an optical lattice [16]. The simulations clearly show the existence of a Mott-transition, but corrections to the one-band Hubbard model can be large when the lattice is not too deep. Using time-dependent DMRG they have calculated the response of a one-dimensional optical lattice of bosons to shaking, and investigated how this can be used to estimate the Hubbard U from such experiments [17].

3 Out of equilibrium physics

One of the interesting aspects of cold atomic gases is to allow an experimental study of out of equilibrium isolated quantum systems, and thus by comparison between theory and experiment to help us make progress in our understanding of this very complex question.

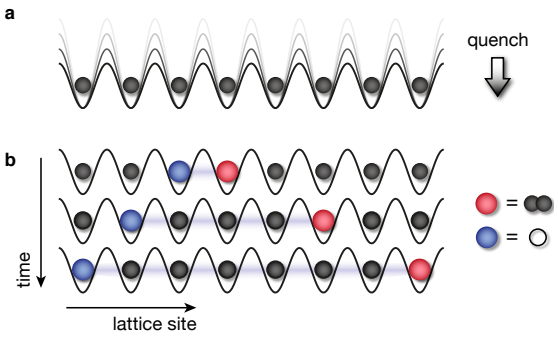

Figure 5: *Evolution of correlations in a gas of ultracold atoms in an optical lattice. a) Quench of the optical lattice potential. b) Quasi-particle picture of the spreading of correlations.*

3.1 Correlation dynamics in a gas of ultracold bosons in an optical lattice *(C. Kollath)*

How fast can correlations spread in a quantum many-body system as a solid? In contrast to relativistic quantum field theory, no "speed limit" exists in non-relativistic quantum mechanics, allowing in principle for the propagation of information over arbitrary distances in arbitrary short times. However, one could naively expect that, in real physical systems, short-range interactions allow information to propagate only with a finite velocity [30, 31, 32]. The Kollath group has detected the propagating correlations in an interacting quantum many-body system, an artificial solid. By lowering suddenly the amplitude of the optical lattice along a one-dimensional bosonic quantum gas, they reveal how quasi-particle pairs transport correlations with a finite velocity across the system, resulting in an effective light cone for the quantum dynamics (Fig. 5) [18]. To describe this phenomenon theoretically they developed a new analytical approach based on slave-fermionic systems. Additionally, they compare these analytical results to exact numerical simulations performed using the DMRG based on matrix product states. Following their proposal, their experimental collaborators at the MPQ Garching measured for the first time the spreading velocity of quantum correlations in this many-body system. Remarkable agreement was found supporting the theoretical description of the spreading by the formation of quasi-particle pairs.

3.2 Topology and out of equilibrium physics *(V. Gritsev)*

Geometric phases in quantum mechanics play an extraordinary role in broadening the understanding of fundamental significance of geometry in nature. One of the best known examples is the Berry phase [33] which naturally emerges in quantum adiabatic evolution. However, beyond the adiabatic limit, the influence of geometry and topology on dynamics in many-body quantum systems is not well understood. The Gritsev group analyzed this problem. They observe an interplay between dynamical and topological ingredients of quantum non-equilibrium dynamics revealed by the geometrical structure of the quantum space of states. The combined effects of dynamics, geometry and topology of quantum space of parameters are manyfold.

First, there is a natural interplay between dynamical and geometrical contributions to the phase of quantum systems acquired during their evolution when parameters of the Hamiltonian are changed in time. This interplay is a source of interesting quantum non-equilibrium phase transitions. As a primary example, Gritsev and coworkers use the anisotropic XY ring in a transverse magnetic field with an additional time-dependent flux. In particular, if the flux insertion is slow, non-adiabatic transitions in the dynamics are dominated by the dynamical phase. In the opposite limit, geometric phase strongly affects transition probabilities. They show that this interplay can lead to a non-equilibrium phase transition between these two regimes. They also analyze the effect of geometric phase on defect generation during crossing a quantum critical point. Similar results apply for non-equilibrium dynamics close to the phase transition in the Dicke model [19].

Second, it is important to elucidate how to observe the geometric and topological content of the quantum parameter space. This should enrich the insight into complexity of many-body systems. So far the applicability and measurements of the Berry (geometric) phase were mostly limited to systems of weakly interacting quasi-particles, where interference experiments are feasible. The Gritsev group shows however how one can go beyond this limitation and observe the Berry curvature, and hence the geometric phase, in generic systems as a non-adiabatic response of physical observables to the rate of change of an external parameter. These results can be interpreted as a dynamical quantum Hall effect in a parameter space. The conventional quantum Hall effect is a particular example of the general relation if one views the electric field as a rate of change of the vector potential. They illustrate their findings by analyzing the response of interacting spin chains to a rotating mag-

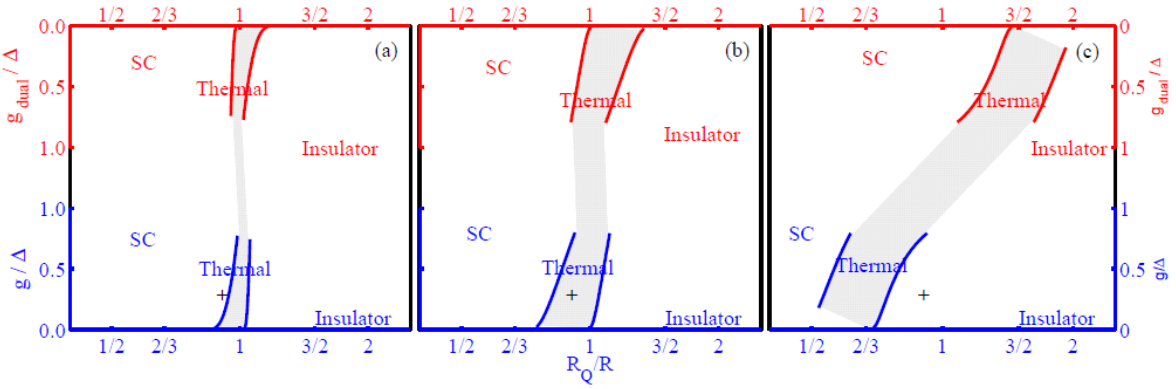

Figure 6: *An example of the generic out of equilibrium RG effects: phase diagram of a noisy Josephson junction subjected to a $1/f$ noise, as a function of the normalized resistance R of the junction and the normalized Josephson coupling g, for increasing noises. The noise both shifts the transition and also broadens it, because of the generated temperature. Similar effects occur for bosons in periodic potentials or ion chains.*

netic field. They observe the quantization of this response, which term the rotational quantum Hall effect. Therefore, topological quantization of the response of a system towards dynamical driving seems to be a very generic feature [20].

3.3 Quantum systems in presence of an out of equilibrium noise *(T. Giamarchi)*

The Giamarchi group has continued its efforts on the analysis on quantum system pushed out of equilibrium (see previous report). One important question is whether a system which has been quenched or is subjected to out of equilibrium noise can reach some form of thermodynamic equilibrium, and reach states that could be described for example by a thermal distribution.

In collaboration with A. Mitra (NYU, USA), they could develop using a Keldysh technique [21], a renormalization group (RG) analysis of a system that has undergone a quench and which contains some non-linear coupling modes terms. This is for example the case of bosons on a lattice, which is described by a sine-Gordon Hamiltonian. The renormalization procedure shows that the quench leads to two very different classes of effects. At the first order in the RG it renormalizes all the exponents that normally characterize an interacting one-dimensional system (Luttinger liquid exponents). At the second order, and in a very non-trivial way, the system develops dissipation and also a finite temperature. The former can be interpreted as a form of Landau damping. In order to confirm this point they also analyzed using a random phase approximation (RPA), another out-of equilibrium problem [22] and obtained similar effects. The generation of temperature is more subtle. It is important to note that this is only a true temperature for the low-energy modes of the system. Indeed the mechanism corresponds to exchange of energy between the low-energy modes and the high-energy ones, which act as a bath. This mechanism is reminiscent to some of the cascade mechanisms for turbulence. The consequences of the RG which have just started to be explored have been extended to the analysis of the transition itself [23].

Quite interestingly the mechanism also applies to systems subjected to the $1/f$ noise that were described in the previous report. They could thus extend, in collaboration with E. Dalla Torre, E. Altman (Weizmann Institute, Israel) and E. Demler (Harvard University, USA), the analysis for such systems [24]. They showed that here also the effect of the noise can be decomposed in two very different effects. The first one is to shift the phase transitions that existed in equilibrium. The second, which can be made parametrically small, is to generate a temperature that will broaden such transitions, as shown in Fig. 6.

4 Collaborative efforts

Various collaborations exist within the project. First there are of course constant interactions and discussions between the experimental group of T. Esslinger and the various theory groups of the project. Interactions within the theory groups also exist. The Giamarchi, Kollath, Mila and Troyer groups are linked together within the MAQUIS project to port the standard numerical tools to massively parallel architectures.

Across the projects many of the themes treated go beyond a project limited to cold atoms. This

is for example the case of the results and methods that can be used to deal with the Dirac points realized in the Esslinger group, given the importance of graphene in other MaNEP projects.
On the methodology level, some of the algorithmic developments made in the Troyer group are applicable to several projects as well. In particular, on the bosonic side, they built on the quantum Monte Carlo method to solve the bosonic DMFT equations [25] (see previous report). On the fermionic side, they have derived a new exchange-correlation density functional for contact rather than Coulomb interaction [26]. With this functional all tools of ground state, finite temperature, and time dependent density functional theory (DFT) are now available for the simulation of quantum gases. In addition to being directly useful for quantum gases, the comparison with experiments should allow to benchmark the approximations made, and thus benefit to the other DFT approximations in other contexts as well. Some of the methods used in the Kollath and Giamarchi group are directly relevant for quantum spin-systems, and have also been used in the Project 6.

MaNEP-related publications

[1] T. Esslinger, Annual Review of Condensed Matter Physics **1**, 129 (2010).

► [2] L. Tarruell, D. Greif, T. Uehlinger, G. Jotzu, and T. Esslinger, arXiv:1111.5020 (2011).

► [3] A. J. Hoffman, S. J. Srinivasan, S. Schmidt, L. Spietz, J. Aumentado, H. E. Türeci, and A. A. Houck, Physical Review Letters **107**, 053602 (2011).

[4] S. Schmidt, D. Gerace, A. A. Houck, G. Blatter, and H. E. Türeci, Physical Review B **82**, 100507(R) (2010).

[5] S. Schmidt and G. Blatter, Physical Review Letters **103**, 086403 (2009).

[6] S. Schmidt and G. Blatter, Physical Review Letters **104**, 216402 (2010).

[7] M. Hohenadler, M. Aichhorn, S. Schmidt, and L. Pollet, Physical Review A **84**, 041608(R) (2011).

[8] M. Hohenadler, M. Aichhorn, L. Pollet, and S. Schmidt, Physical Review A **85**, 013810 (2012).

► [9] J. Catani, G. Lamporesi, D. Naik, M. Gring, M. Inguscio, F. Minardi, A. Kantian, and T. Giamarchi, Physical Review A **85**, 023623 (2012).

► [10] P. Corboz, A. M. Läuchli, K. Penc, M. Troyer, and F. Mila, Physical Review Letters **107**, 215301 (2011).

► [11] S. Nascimbène, N. Navon, S. Pilati, F. Chevy, S. Giorgini, A. Georges, and C. Salomon, Physical Review Letters **106**, 215303 (2011).

► [12] K. Van Houcke, F. Werner, E. Kozik, N. Prokof'ev, B. Svistunov, M. J. H. Ku, A. T. Sommer, L. W. Cheuk, A. Schirotzek, and M. W. Zwierlein, Nature Physics (2012), doi:10.1038/nphys2273.

► [13] D. Greif, L. Tarruell, T. Uehlinger, R. Jördens, and T. Esslinger, Physical Review Letters **106**, 145302 (2011).

[14] T. Müller, B. Zimmermann, J. Meineke, J.-P. Brantut, T. Esslinger, and H. Moritz, Physical Review Letters **105**, 040401 (2010).

► [15] M. Endres, M. Cheneau, T. Fukuhara, C. Weitenberg, P. Schauß, C. Gross, L. Mazza, M. C. Bañuls, L. Pollet, I. Bloch, and S. Kuhr, Science **334**, 200 (2011).

[16] S. Pilati and M. Troyer, arXiv:1108.1408 (2011).

[17] J.-W. Huo, F.-C. Zhang, W. Chen, M. Troyer, and U. Schollwöck, Physical Review A **84**, 043608 (2011).

► [18] M. Cheneau, P. Barmettler, D. Poletti, M. Endres, P. Schauß, T. Fukuhara, C. Gross, I. Bloch, C. Kollath, and S. Kuhr, Nature **481**, 484 (2012).

► [19] M. Tomka, A. Polkovnikov, and V. Gritsev, Physical Review Letters **108**, 080404 (2012).

[20] V. Gritsev and A. Polkovnikov, arXiv:1109.6024 (2012).

► [21] A. Mitra and T. Giamarchi, Physical Review Letters **107**, 150602 (2011).

[22] J. Lancaster, T. Giamarchi, and A. Mitra, Physical Review B **84**, 075143 (2011).

► [23] A. Mitra and T. Giamarchi, Physical Review B **85**, 075117 (2012).

► [24] E. G. Dalla Torre, E. Demler, T. Giamarchi, and E. Altman, *to be published in* Physical Review B (2012), arXiv:1110.3678.

[25] P. Anders, E. Gull, L. Pollet, M. Troyer, and P. Werner, New Journal of Physics **13**, 075013 (2011).

[26] P.-N. Ma, S. Pilati, M. Troyer, and X. Dai, *submitted to* Nature Physics (2012).

Other references

[27] M. J. Hartmann, F. G. S. L. Brandão, and M. B. Plenio, Laser & Photonics Reviews **2**, 527 (2008).

[28] A. D. Greentree, C. Tahan, J. H. Cole, and L. C. L. Hollenberg, Nature Physics **2**, 856 (2006).

[29] C. Sanner, E. J. Su, A. Keshet, R. Gommers, Y.-i. Shin, W. Huang, and W. Ketterle, Physical Review Letters **105**, 040402 (2010).

[30] E. H. Lieb and D. W. Robinson, Communications in Mathematical Physics **28**, 251 (1972).

[31] P. Calabrese and J. Cardy, Physical Review Letters **96**, 136801 (2006).

[32] A. M. Läuchli and C. Kollath, Journal of Statistical Mechanics **P05018** (2008).

[33] M. V. Berry, Proceedings of the Royal Society A **392**, 45 (1984).

Techniques and know-how

Responsibles: Enrico Giannini (UniGE), Patrycja Paruch (UniGE), Ivan Maggio-Aprile (UniGE), Christof Niedermayer (PSI), Philipp Aebi (UniFR), Urs Staub (PSI), Leonardo Degiorgi (ETHZ), Matthias Troyer (ETHZ)

Summary: At the beginning of Phase III in 2009 the research projects of MaNEP were redefined around scientific themes and goals. Before this, in Phase II, two projects were focusing on methods to make new materials and methods to make single crystals. These cross-theme activities were an essential effort by MaNEP to develop new materials. With the redefinition of projects in Phase III focusing on scientific questions, we decided to establish the techniques and know-how activities to stimulate cross-disciplinary collaborations between groups having different scientific goals, but similar technical needs. We stress that the available finances for this activity is limited thus the proposed actions are carried out largely on a voluntary basis.

1 Crystal growth and bulk materials processing

Responsible: Enrico Giannini (UniGE)

Growing sizeable and high-quality crystals is a challenging endeavor of materials science. Understanding the physical properties of materials, as well as producing artificial novel materials predicted by theory and modeling, rely on the capability of mastering the processing and growth techniques. The broad know-how of the crystal growth community of MaNEP, and the richness and complementarity of the available techniques and facilities, make it possible to ensure an essential, quick and reliable support to the whole research activity of the present NCCR. The crystal growth activity of the MaNEP community during the last year has mainly focused on the recently discovered Fe-superconducting chalcogenides and pnictides, topological insulators, and magneto-electric materials. Processing of thermoelectric materials and catalysts for novel energy technologies has been successfully carried out as well during the last year. The overall activity of MaNEP members in this field has generated more that 80 publications, out of which about 60 directly related to MaNEP projects and 16 published in specialized crystal growth or physical chemistry journals. Numerous international collaborations have benefited from the novel materials processed by MaNEP scientists.

New facilities

The Czochralski crystal growth setup at UniGE has been successfully tested up to 2300°C under inert atmosphere. Operation under oxidizing atmosphere will soon be possible in the same temperature range by using Ir crucibles.

New materials

New nanoscale spinels have been discovered and successfully synthesized by G. Patzke at UniZH. Single crystals of the solid solution SmFe(As,P)O have been grown at the ETHZ by flux growth under high-pressure. Advances have been made in the field of ternary $A_{1-x}Fe_{2-y}Se_2$ (A = alkaline metals) superconductors and $Bi_2(Te_{1-x}Se_x)_3$ topological insulators at PSI and UniGE, respectively. The updated list of crystalline materials available within MaNEP can be found at the end of this chapter, p. 106.

Education and events

In the frame of tutorial satellites of the Swiss Workshop on Materials with Novel Electronic Properties (SWM 2011), focused on various topics in techniques and know-how, a crystal growth course has been given to young scientists coming from all the MaNEP member institutions. The course has been attended by about 30 PhD students and 10 postdoctoral fellows. The course began with a reminder of thermodynamics and phase diagrams in an introductory module, and covered the most common growth techniques in a second module, with emphasis on the most important materials treated in the SWM 2011 and the techniques used in MaNEP laboratories (Bridgman and related growth methods, Czochralski growth, floating zone, flux growth, hydrothermal/solvothermal techniques, physical vapor transport growth).
The Swiss Light Source (SLS) has organized a one-day symposium on "Crystal Growth and Characterization", at which the MaNEP mem-

bers from PSI and ETHZ have been invited to present the advances on crystal growth of novel materials.
A symposium on thermoelectric materials has been organized by EMPA within the *Troisième Cycle* seminars in Villars. This meeting has assembled scientists from various institutions and fields, working on all aspects of thermoelectric conversion technology.
A European Network on Crystal Growth (ENCG) is being created, under the coordination of Prof. Thierry Duffar from Grenoble, with the aim of gather together academic and industrial crystal growth laboratories in Europe: MaNEP laboratories on crystal growth have joined the ENCG. The MaNEP community of crystal growers will be present as well at next coming European Conference on Crystal Growth, to be held in Glasgow (UK) on June 17–20, 2012.

2 Thin film growth and characterization

Responsible: Patrycja Paruch (UniGE)

Thin films have continued to play an important role in MaNEP, with ongoing work on films, bilayers and superlattice structures from many different groups. The effort on chemical vapor deposition (CVD) graphene growth was continued by Dr. Ch. Caillier, who has now optimized the growth of large area polycrystalline single-layer graphene on copper, and its transfer to target oxide substrates. The effects of different dielectrics on mobility are currently explored.
A set of tutorials were offered as satellite courses associated with the Swiss Workshop on Materials with Novel Electronic Properties (SWM 2011) meeting at Les Diablerets in June 2011, one of which focused on thin film growth techniques. The course (attended by about 30 PhD students and 10 postdoctoral fellows) began with a review of the fundamental physics of thin films, in particular the important role of size effects, boundary conditions, and defects, and then presented different thin film growth techniques used in MaNEP laboratories, and the experimental and theoretical parameters guiding the choice of fabrication methods, substrates, and other aspects of the process.

4 Scanning local probes techniques

Responsible: Ivan Maggio-Aprile (UniGE)

In experimental condensed matter physics, it is nowadays quite common to implement local probes facilities dedicated to the investigation, characterization or manipulation of materials at the nanometer scale. This quite recent interest is mainly due to the fact that these powerful tools are relative easy to set up, and can be run without being necessarily an expert in the field. However, people which are confronted with local probes (as a user or having heard from these in reports or conferences) do not necessarily possess the required knowledge to catch up what can be really achieved using these techniques.
As tutorial satellites of the 2011 Swiss Workshop on Materials with Novel Electronic Properties, three courses focusing on techniques and know-how have been provided to graduate students (about 30 PhD students and 10 postdoctoral fellows). One of the courses was aimed to present a broad overview of the different scanning probe techniques which were developed subsequently to the invention of the STM in Zurich in 1981. In the first part of the course, various scanning probes have be presented in detail, focusing on technical aspects, their performances and possible applicability, as well as the problems associated with these sensitive techniques and the possible artifacts encountered in the measurements. In the second part, an emphasis was set on the interpretation of the data in scanning tunneling spectroscopy experiments, and the techniques of quantitative analysis of the spectra were described.

5 Neutron scattering and muon-spin resonance

Responsible: Christof Niedermayer (PSI)

Neutron scattering developments

The thermal triple axis instrument EIGER (Fig. 1) has been completed and commissioned in November 2011. EIGER consists of an in-pile section with a direct view of the thermal neutron source, a primary spectrometer optimized for high flux and low background and a

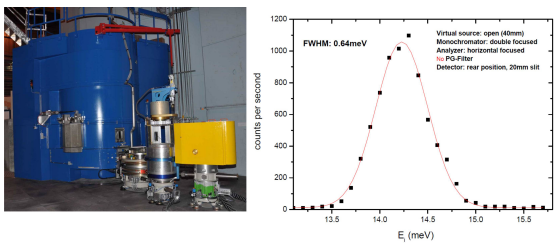

Figure 1: *Left: the new thermal triple axis instrument EIGER. Right: Vanadium scattering intensity measured at* $E_i = 14.6$ *meV.*

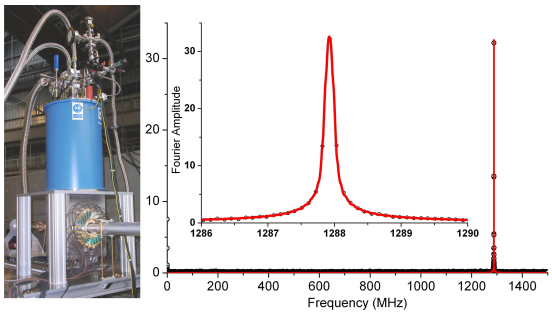

Figure 2: *Left: magnet with detector system. Right: Fourier transform of the first μSR spectrum obtained from a silver sample at 9.5 T. The narrow line demonstrates the excellent magnetic field homogeneity (better than 10 ppm).*

standard secondary spectrometer with a single detector. A multiplexing secondary spectrometer allowing significantly increased solid angle coverage without sacrificing momentum-resolution is planned for the future. The new spectrometer greatly enhances the available energy range for inelastic neutron scattering experiments.

Muon-spin spectroscopy (μSR) developments

Essential progress has been obtained towards the realization of the new high-field μSR instrument (Fig. 2). The main components of the high field μSR facility were installed towards the end of 2011. This world-wide unique instrument will allow studying a previously inaccessible range in the $B-T$ phase diagram of condensed matter ranging up to 9.5 T and down to about 20 mK. The spectrometer magnet is a custom high-homogeneity split pair recondensing system from Oxford Instruments. At 9.5 T the field homogeneity is better than 0.1 mT over a center volume of 10 mm diameter and 4 mm length. The detector system is based on direct readout of fast plastic scintillators by Hamamatsu Multipixel Photon counters and in-house developed front-end electronics. The overall time resolution is better than 80 ps.

6 Electron spectroscopies

Responsible: Philipp Aebi (UniFR)

MaNEP members are involved in several instrumental developments. First of all at the Swiss Light Source (SLS) at the Paul Scherrer Institute (PSI), the ADRESS beamline with its soft X-ray angle-resolved photoemission (ARPES) endstation has gone in user operation after several successful test experiments. The demand for beam time, as distributed by the SLS program review committee, monitors already strong overbooking.

The second development at the SLS concerns the PEARL beamline. PEARL stands for PhotoEmission and Atomic Resolution Laboratory and will be specialized for photoelectron diffraction experiments combined with STM/AFM on nanostructured surfaces of novel materials. Here, first light was obtained just before Christmas 2011. The endstation is ordered and the design is close to be completed.

Concerning developments in the home labs, the upgrade of the photoemission laboratory at UniFR is in progress. The new setup includes laser ARPES and a sample transfer system which is compatible with the STM and pulsed laser deposition system at UniFR and the PEARL endstation. The new components have been ordered except for the laser and the new design is close to be completed.

Finally, another edition of the "International Workshop on Strong Correlations and Angle-Resolved Photoemission Spectroscopy", CORPES11, has happened July 18–22, 2011 at Berkeley, California. It is organized with the contribution of members of MaNEP and the PSI. We had close to 100 participants with 55 talks and close to 60 posters, bringing together world leaders in photoemission and theorists working on correlated electron systems.

7 X-ray elastic and inelastic scattering

Responsible: Urs Staub (PSI)

Within this period, the beam quality to perform surface X-ray diffraction and X-ray powder diffraction experiments has been significantly improved at the Swiss Light Source (SLS). This is due to the upgrade of the Material Science beamline to keep the beamline on an internationally completive level. This upgrade included a change of the insertion device form a wiggler to an undulator, with significant increase of the X-ray brightness at the beamline. The beamline with its powder diffraction and the surface diffraction station are already back in the user operation mode in early 2012, with significantly improved experimental conditions.

To communicate the technical progress occurred on this beamline and the other absorption and resonant scattering beamlines at the SLS, a one-day workshop is planed for fall 2012. The idea is to follow up the successful one-day MaNEP workshop on resonant scattering and absorption in 2010. It is planed to

attract mainly researcher on the PhD and postdoc level, as it has been done very successfully in the last event. Communicating the new possibilities and improvements of these techniques, as well as informing young researcher on the many possibilities of this field at the SLS, will further improve the cross link between the dedicated large facility techniques within the MaNEP network.

8 Infrared spectroscopy

Responsible: Leonardo Degiorgi (ETHZ)

There is a broad know-how on optics within the Swiss scientific community, particularly as far as the infrared spectroscopy is concerned. Three research groups at UniGE (D. van der Marel), UniFR (Ch. Bernhard) and ETHZ (L. Degiorgi) exploit a wealth of optical techniques, like reflectivity and transmission measurements, broadband ellipsometry, time domain THz and Kerr-effect spectroscopy, as well as Raman- and IR-microscopy. These methods allow covering a rather broad energy interval from the THz up to the ultraviolet, which is the prerequisite for having access to all energy scales, relevant to the nowadays modern problems in condensed matter. Moreover, ellipsometry and time domain THz spectroscopy allow to measure simultaneously amplitude and phase reflection/transmission, which in turn provide the real and imaginary part of the optical constant. It is also worthwhile to emphasize the combination of those spectroscopies with externally tunable variables like temperature, magnetic and electric field, and also pressure. Needless to say that complex phase diagrams of novel materials, which are of relevance in the ongoing solid-state physics research, can be addressed with our experimental setups. There is furthermore an ongoing effort, in order to optimize the employment of this large variety of spectroscopic tools. In this respect, a relevant role is played by the infrared (IR) beamline at the Swiss Light Source (SLS). Several steps were taken in order to fully exploit the advantages of the synchrotron radiation (SR) source in the far-IR energy range. Also in the future, special efforts from the IR-community will be dedicated in order to boost possible improvements and equipment-developments of the IR-beamline at SLS. Special mention deserves the IR microspectrometer coupled to the SR source, which opens up new perspectives in fields like condensed and soft matter physics, chemistry and life science, to name just a few. The pressure dependent IR response of samples can be measured using the small spot offered by the SR source. Moreover, temperature dependent optical reflection and transmission as well as chemical mapping at the diffraction limit are possible. Recently, a pump-probe setup was installed. Samples are pumped with 100 ps (10 kHz repetition rate) long laser pulses and probed with 100 ps long broad band synchrotron pulses. The delay between pump and probe can be varied. There is room for a large variety of sample environment and a microfocusing unit is available as well. In addition to SLS, the three Swiss groups have very good connections to other synchrotron facilities at ANKA-Karlsruhe, Brookhaven and ELETTRA-Trieste. In summary, top-quality instrumentations will allow broad-band collaborations going well beyond the IR-community and involving other groups within the MaNEP program.

9 Theoretical and numerical methods

Responsible: Matthias Troyer (ETHZ)

Algorithmic developments

The main algorithmic development of the past year was a combination of diagrammatic quantum Monte Carlo (DiagMC) with dynamical mean field theory (DMFT), allowing to go beyond the local approximation in DMFT.
We have also written a review article about the recently developed continuous time quantum Monte Carlo algorithms for dynamical mean field theory which are currently being employed for simulating correlated materials and ultracold atomic gases.

High performance and high productivity computing

In collaboration with the Swiss high performance and high productivity computing (HP^2C) initiative, the groups of T. Giamarchi, C. Kollath, F. Mila and M. Troyer have continued the development of supercomputer simulation codes for exact diagonalization, density matrix renormalization group (DMRG), series expansions and quantum Monte Carlo methods (MAQUIS project). First codes, such as for exact diagonalization for frustrated magnets and high temperature series expansions are ready and the project is on track to finish all application codes by the end of the last year of MaNEP, which also coincide with the end of the HP^2C initiative. For the next period first application papers are expected.

	Material	Growth technique	Furnace	Conductor	Insulator	Magnetic	MaNEP Institution	Responsable
	Various elemental metals	Bridgman, Zone melting	RF Induction, Electronic bombardement	yes			UniGe	Giannini (022 3796076, enrico.giannini@unige.ch)
	Chalcogenides and pnictides							
	FeTe(1-x)Sex	self flux, TSFZ	1-zone vertical furnace, Mirror image furna	yes, superc. Tc<13K			UniGe	Giannini (022 3796076, enrico.giannini@unige.ch)
	FeTe(1-x)Sex	self flux	1-zone vertical furnace	yes, superc. Tc<13K			PSI	kazimierz.conder@psi.ch
NEW!	AFe2Se2 (A = K, Cs, Rb)	self flux	1-zone vertical furnace	yes, superc. Tc<30K			PSI	kazimierz.conder@psi.ch
NEW!	BeFe2Se3	self flux	1-zone vertical furnace	yes, superc. Tc<11K			PSI	kazimierz.conder@psi.ch
	LnFeAsO(1-x)Fx (Ln=La, Pr, Nd, Sm, Gd)	flux growth under HP	cubic anvil hot press	Yes superc. Tc = 20 - 55K			ETHZ	Karpinski(044 6332254, karpinski@phys.ethz.ch)
	Sm(Fe,Co)AsO(1-x)Fx	flux growth under HP	cubic anvil hot press	Yes superc. Tc = 20 - 55K			ETHZ	Karpinski(044 6332254, karpinski@phys.ethz.ch)
NEW!	SmFe(As,P)O	flux growth under HP	cubic anvil hot press	Yes superc. Tc < 23K			ETHZ	Karpinski(044 6332254, karpinski@phys.ethz.ch)
	CaFe(2-x)CoxAs2	flux growth		Yes superc. Tc = 20K			ETHZ	Karpinski(044 6332254, karpinski@phys.ethz.ch)
	EuFe(2-x)CoxAs2	flux growth		Yes superc. Tc = 20K			ETHZ	Karpinski(044 6332254, karpinski@phys.ethz.ch)
	Ba1-xRbxFe2As2	flux growth		Yes superc. Tc = 23K			ETHZ	Karpinski(044 6332254, karpinski@phys.ethz.ch)
	BiIn	self flux	1-zone vertical furnace	yes			UniGe	Giannini (022 3796076, enrico.giannini@unige.ch)
	Bi2Se3, Bi2Te3	self flux, TSFZ	1-zone furnace, Mirror image furnace	topological insulator	topological insulator		UniGe	Giannini (022 3796076, enrico.giannini@unige.ch)
NEW!	Bi2Te(1-x)Se(x)	self flux, TSFZ	1-zone furnace, Mirror image furnace	topological insulator	topological insulator		UniGe	Giannini (022 3796076, enrico.giannini@unige.ch)
	CuxBi2Se3, PdxBi2Te3	self flux, TSFZ	1-zone furnace, Mirror image furnace	yes, superc. Tc = 3 - 5 K			UniGe	Giannini (022 3796076, enrico.giannini@unige.ch)
NEW!	Bi2-xMxSe2 (M=transition metal)	self flux	1-zone vertical furnace				PSI	kazimierz.conder@psi.ch
	Bi(1-x)Sbx	Zone melting	Mirror image furnace	yes	yes (depending on x)		UniGe	Giannini (022 3796076, enrico.giannini@unige.ch)
	CoS2	CVT	2-zone furnace	Yes		ferromagnetic, Tc 121K	EPFL	Berger 021 693 4484, helmuth.berger@epfl.ch)
NEW!	Co0.33NbS2	CVT	2-zone furnace			frustrated magnet	EPFL	Berger 021 693 4484, helmuth.berger@epfl.ch)
	NbSe2	CVT	2-zone furnace	Yes Tc 7.2K			EPFL	Berger 021 693 4484, helmuth.berger@epfl.ch)
	NbTe2	CVT	2-zone furnace	Yes		ferromagnetic Tc= 86K	EPFL	Berger 021 693 4484, helmuth.berger@epfl.ch)
	TaS2	CVT	2-zone furnace					Berger 021 693 4484, helmuth.berger@epfl.ch)
	TaTe2	CVT	2-zone furnace	Yes		ferromagnetic Tc=130K	EPFL	Berger 021 693 4484, helmuth.berger@epfl.ch)
	TiTe2	CVT	2-zone furnace	Yes			EPFL	Berger 021 693 4484, helmuth.berger@epfl.ch)
	TiSe2	CVT	2-zone furnace	Yes				Berger 021 693 4484, helmuth.berger@epfl.ch)
	TiSe2	CVT	1-zone furnace with temp.gradient	Yes			UniGe	Giannini (022 3796076, enrico.giannini@unige.ch)
	ZrS3, ZrSe3, ZrTe3	CTV	2-zone furnace	No	Semiconductor		EPFL	Berger 021 693 4484, helmuth.berger@epfl.ch)
	HfS3, HfSe3, HfTe3	CTV	2-zone furnace	No	Semiconductor		EPFL	Berger 021 693 4484, helmuth.berger@epfl.ch)
	GaS, GaSe, GaTe	Bridgman	1-zone furnace with temp.gradient					Berger 021 693 4484, helmuth.berger@epfl.ch)
	BaVS3	Flux grown	1-zone furnace with temp.gradient	Yes	Insulator		EPFL	Berger 021 693 4484, helmuth.berger@epfl.ch)
	Pd3(PS4)2	CTV	2-zone furnace	No	Semiconductor	diamagnetic	EPFL	Berger 021 693 4484, helmuth.berger@epfl.ch)
	MnPS3	CTV	2-zone furnace	No	Semiconductor	magnetic properties	EPFL	Berger 021 693 4484, helmuth.berger@epfl.ch)
	MnPSe3	CTV	2-zone furnace	No	Semiconductor	magnetic properties	EPFL	Berger 021 693 4484, helmuth.berger@epfl.ch)
	NiPS3	CTV	2-zone furnace	No	Semiconductor	magnetic properties	EPFL	Berger 021 693 4484, helmuth.berger@epfl.ch)
	NiPSe3	CTV	2-zone furnace	No	Semiconductor	magnetic properties	EPFL	Berger 021 693 4484, helmuth.berger@epfl.ch)
	FePS3	CTV	2-zone furnace	No	Semiconductor	magnetic properties	EPFL	Berger 021 693 4484, helmuth.berger@epfl.ch)
	FePSe3	CTV	2-zone furnace	No	Semiconductor	magnetic properties	EPFL	Berger 021 693 4484, helmuth.berger@epfl.ch)
	CdCr2S4	CVT	2-zone furnace	Tc		ferromagnetic	EPFL	Berger 021 693 4484, helmuth.berger@epfl.ch)
	CdCr2Se4	CVT	2-zone furnace	Yes		ferromagnetic	EPFL	Berger 021 693 4484, helmuth.berger@epfl.ch)
	Cuprates							
	Sr14Cu24O41	TSFZ	Mirror image furnace	no	yes		UniGe	Giannini (022 3796076, enrico.giannini@unige.ch)
	(Sr,M1,M2)14Cu24O41-x (M1, M2 = Ca, Bi, Y…)	TSFZ	Mirror image furnace	no	yes		UniGe	Giannini (022 3796076, enrico.giannini@unige.ch)
	Sr(14-x)Ca(x)Cu24O41 (x up to 12.2)	high pressure TSFZ	Mirror image furnace				PSI	Kazimierz Conder/Ekaterina Pomjakushina
	Bi2Sr2Ca2Cu3O10 Bi-2223	TSFZ	Mirror image furnace	Yes, superc. Tc=110 K			UniGe	Giannini (022 3796076, enrico.giannini@unige.ch)
	Bi2-xPbxSr2Ca2Cu3O10+d Bi,Pb-2223	TSFZ	Mirror image furnace	Yes, superc. Tc=110 K			UniGe	Giannini (022 3796076, enrico.giannini@unige.ch)
	Bi2Sr2CaCu2O8 Bi-2212	TSFZ	Mirror image furnace	Yes, superc. Tc=91 K			UniGe	Giannini (022 3796076, enrico.giannini@unige.ch)
	Bi2-xPbxSr2CaCu2O8 Bi,Pb-2212	TSFZ, self flux	Mirror image furnace, 3-zone vertical	Yes, superc. Tc=93 K			UniGe	Giannini (022 3796076, enrico.giannini@unige.ch)
	Bi2Sr2CuO6 Bi-2201	TSFZ	Mirror image furnace	Yes,superc. Tc=15 K			UniGe	Giannini (022 3796076, enrico.giannini@unige.ch)
	Bi1.6Pb0.4Sr2CaCu2O8 Pr,Y doped Bi,Pb-2212	Flux grown	1-zone furnace with temp.gradient	Yes			EPFL	Berger 021 693 4484, helmuth.berger@epfl.ch)
	Bi1.6Pb0.4Sr2CaCu2O8 Bi,Pb-2212	Flux grown	1-zone furnace with temp.gradient	Yes			EPFL	Berger 021 693 4484, helmuth.berger@epfl.ch)
	Bi2Sr2CaCu2O8 Bi-2212	Flux grown	1-zone furnace with temp.gradient	Yes			EPFL	Berger 021 693 4484, helmuth.berger@epfl.ch)
	Bi2Sr2CaCu2O8 Ni, Co doped Bi-2212	Flux grown	1-zone furnace with temp.gradient	Yes			EPFL	Berger 021 693 4484, helmuth.berger@epfl.ch)
	REBa2Cu3O7	self flux	3-zone furnace, Top seeded growth	Yes,superc. Tc=92 K			UniGe	Giannini (022 3796076, enrico.giannini@unige.ch)
	YBa2Cu4O8	HP	high O2 pressure	yes, superc. Tc=80K			ETHZ	Karpinski(044 6332254, karpinski@phys.ethz.ch)
	YBa(2-x)SrxCu4O8	HP	high O2 pressure	yes, superc. Tc<80K			ETHZ	Karpinski(044 6332254, karpinski@phys.ethz.ch)
	YBa2Cu3O(6+x), x=0--1, 16O-18O	solid state synthesis		superconductor			PSI	Kazimierz Conder/Ekaterina Pomjakushina
	La(2-x)SrxCuO4	TSFZ	Mirror image furnace	superconductor			PSI	Kazimierz Conder/Ekaterina Pomjakushina
	La2CuO4	TSFZ	Mirror image furnace		AFM		PSI	Kazimierz Conder/Ekaterina Pomjakushina
	Ln(2-x)SrxCuO4, 16O-18O	solid state synthesis		superconductor			PSI	Kazimierz Conder/Ekaterina Pomjakushina
	Ca(2-x)NaxCuO2Cl2	HP	cubic anvil hot press	yes, superc. Tc=13-25K			ETHZ	Karpinski(044 6332254, karpinski@phys.ethz.ch)
	Other Transition Metal Oxides							
	KOs2O6	ampoule method	resistive furnace	yes, superc. Tc=9.6K			ETHZ	Karpinski(044 6332254, karpinski@phys.ethz.ch)
	Na2Os2O6.5	HP	cubic anvil hot press	no			ETHZ	Karpinski(044 6332254, karpinski@phys.ethz.ch)
	CaMn0.98Nb0.02O3	TSFZ	Mirror image furnace			yes	EMPA	Weidenkaff(044 8234131, Anke.Weidenkaff@empa.ch)
	CaMnO3	TSFZ	Mirror image furnace				EMPA	Weidenkaff(044 8234131, Anke.Weidenkaff@empa.ch)
	YMnO3	TSFZ	Mirror image furnace		stacked-triangular AF		PSI	Kazimierz Conder/Ekaterina Pomjakushina

	Material	Growth technique	Furnace	Conductor	Insulator	Magnetic	MaNEP Institution	Responsable
	DyMnO3	TSFZ	Mirror image furnace		AF Tn~40K, ferroelectric T<19K		PSI	Kazimierz Conder/Ekaterina Pomjakushina
	LaCoO3	TSFZ	Mirror image furnace		magnetic and spin state transitions		PSI	Kazimierz Conder/Ekaterina Pomjakushina
	La(1-x)SrxCoO3	TSFZ	Mirror image furnace		magnetic and spin state transitions		PSI	Kazimierz Conder/Ekaterina Pomjakushina
	SrCu2(BO3)2	TSFZ	Mirror image furnace			2D spin system	PSI	Kazimierz Conder/Ekaterina Pomjakushina
	LaFeO3	TSFZ	Mirror image furnace		magneto-optical Faraday effect		PSI	Kazimierz Conder/Ekaterina Pomjakushina
	La(1-x)SrxFeO3	TSFZ	Mirror image furnace		magneto-optical Faraday effect		PSI	Kazimierz Conder/Ekaterina Pomjakushina
	ErFeO3	TSFZ	Mirror image furnace		magneto-optical Faraday effect		PSI	Kazimierz Conder/Ekaterina Pomjakushina
	YFeO3	TSFZ	Mirror image furnace		magneto-optical Faraday effect		PSI	Kazimierz Conder/Ekaterina Pomjakushina
	TbBaCo2O(5+x)	TSFZ	Mirror image furnace		magnetic, metal-insulator, spin state transitions		PSI	Kazimierz Conder/Ekaterina Pomjakushina
	LuFe2O4	TSFZ	Mirror image furnace		ferroelectric, charge frustrated system		PSI	Kazimierz Conder/Ekaterina Pomjakushina
	NaxCoO2 (x=0.7, 0.75, 1)	TSFZ	Mirror image furnace		FM, AFM, MI transitions		PSI	Kazimierz Conder/Ekaterina Pomjakushina
	NdBaCo2O(5+x)	TSFZ	Mirror image furnace		magnetic, metal-insulator, spin state transitions		PSI	Kazimierz Conder/Ekaterina Pomjakushina
	Nd1/3Sr2/3FeO3	TSFZ	Mirror image furnace		AFM, charge disproportionation		PSI	Kazimierz Conder/Ekaterina Pomjakushina
	SmBaMn2O6	TSFZ	Mirror image furnace		charge ordering, orbital ordering		PSI	Kazimierz Conder/Ekaterina Pomjakushina
	LnBaCo2O5+x, x=0~1, 16O-18O	solid state synthesis			magnetic, metal-insulator, spin state transitions		PSI	Kazimierz Conder/Ekaterina Pomjakushina
	Na0.75CoO2	Flux grown	1-zone furnace with temp.gradient	Yes			EPFL	Berger 021 693 4484, helmuth.berger@epfl.ch)
	Na0.70CoO2	Flux grown	1-zone furnace with temp.gradient			magnetic properties	EPFL	Berger 021 693 4484, helmuth.berger@epfl.ch)
	Ca3Co2O6	Flux grown	1-zone furnace with temp.gradient			magnetic properties	EPFL	Berger 021 693 4484, helmuth.berger@epfl.ch)
	Ca3Co4O9	Flux grown	1-zone furnace with temp.gradient			magnetic properties	EPFL	Berger 021 693 4484, helmuth.berger@epfl.ch)
	(La(1-x)Prx)1-yCayMnO3, 16O-18O	solid state synthesis				AF, FM	PSI	Kazimierz Conder/Ekaterina Pomjakushina
	CaVO3	TSFZ	Mirror image furnace	metal below 1K			PSI	Kazimierz Conder/Ekaterina Pomjakushina
	Fe3O4	CVT	2-zone furnace	Yes		ferromagnetic, Tc 123K	EPFL	Berger 021 693 4484, helmuth.berger@epfl.ch)
	LiCu2O2	Flus grown	1-zone furnace with temp.gradient	No			EPFL	Berger 021 693 4484, helmuth.berger@epfl.ch)
	alpha TeVO4	CVT	2-zone furnace	No		magnetic properties	EPFL	Berger 021 693 4484, helmuth.berger@epfl.ch)
	beta TeVO4	CVT	2-zone furnace	No			EPFL	Berger 021 693 4484, helmuth.berger@epfl.ch)
	ZnO	CVT	2-zone furnace	No		magnetic properties	EPFL	Berger 021 693 4484, helmuth.berger@epfl.ch)
	CdRe2O7	CVT	2-zone furnace	Yes Tc=1k			EPFL	Berger 021 693 4484, helmuth.berger@epfl.ch)
	CuWO4	Flux grown and CVT	2-zone furnace	No		magnetic properties	EPFL	Berger 021 693 4484, helmuth.berger@epfl.ch)
	LiCu2O2	Flux grown	1-zone furnace with temp.gradient	No	Semiconductor	magnetic properties	EPFL	Berger 021 693 4484, helmuth.berger@epfl.ch)
NEW!	LiCu2O2	TSFZ	Mirror image furnace	No	Semiconductor	magnetic properties	UniGe	Giannini (022 3796076, enrico.giannini@unige.ch)
	Mo4O11, MoO3	CVT	2-zone furnace				EPFL	Berger 021 693 4484, helmuth.berger@epfl.ch)
	WO3	self-flux	1-zone furnace with temp.gradient				EPFL	Berger 021 693 4484, helmuth.berger@epfl.ch)
	Ca3Co4O9	TSFZ	Mirror image furnace				EMPA	Weidenkaff(044 8234131, Anke.Weidenkaff@empa.ch)
	Bi2(W,Mo)O6 nanomaterials	MW-HT	hydrothermal autoclave				UniZh	Patzke(044 63 54691, greta.patzke@aci.uzh.ch)
	Bi2WO6 nanomaterials	MW-HT	hydrothermal autoclave				UniZh	Patzke(044 63 54691, greta.patzke@aci.uzh.ch)
	Bi6S2O15 nanowires	MW-HT	hydrothermal autoclave				UniZh	Patzke(044 63 54691, greta.patzke@aci.uzh.ch)
NEW!	Dy1-xYxTi2O7	TSFZ	Mirror image furnace			spin-ice	PSI	Kazimierz Conder/Ekaterina Pomjakushina
NEW!	ZnM2O4 (M=Al,Ga) nanomaterials	MW-HT	hydrothermal autoclave				UniZh	Patzke(044 63 54691, greta.patzke@aci.uzh.ch)
NEW!	(Co,Mn)Ga2-xO4 nanomaterials	MW-HT	hydrothermal autoclave				UniZh	Patzke(044 63 54691, greta.patzke@aci.uzh.ch)
	EuTiO3	TSFZ	Mirror image furnace	yes	semiconductor	yes, antiferomagnetic Tc	EMPA	Weidenkaff(044 8234131, Anke.Weidenkaff@empa.ch)
	EuTi0.98Nb0.02O3	TSFZ	Mirror image furnace	yes	semiconductor	yes, antiferomagnetic Tc	EMPA	Weidenkaff(044 8234131, Anke.Weidenkaff@empa.ch)
	Eu0.5Ba0.5TiO3	TSFZ	Mirror image furnace				EMPA	Weidenkaff(044 8234131, Anke.Weidenkaff@empa.ch)
NEW!	CaMn0.97W0.03O3	TSFZ	Mirror image furnace		semiconductor	yes, antiferromagnetic	EMPA	Weidenkaff(044 8234131, Anke.Weidenkaff@empa.ch)
	Sr0.99Eu0.01Al2O4	TSFZ	Mirror image furnace				EMPA	Weidenkaff(044 8234131, Anke.Weidenkaff@empa.ch)
	Sr0.99Dy0.01Al2O4	TSFZ	Mirror image furnace				EMPA	Weidenkaff(044 8234131, Anke.Weidenkaff@empa.ch)
	Borides							
	MgB2	Mg-flux under HP	cubic anvil hot press	yes, superc. Tc=39K			UniGe	Giannini (022 3796076, enrico.giannini@unige.ch)
	MgB2	Mg-flux under HP	cubic anvil hot press	yes, superc. Tc=39K			ETHZ	Karpinski(044 6332254, karpinski@phys.ethz.ch)
	Mg(1-x)AlxB2	Mg-flux under HP	cubic anvil hot press	yes			ETHZ	Karpinski(044 6332254, karpinski@phys.ethz.ch)
	MgB2-xCx	Mg-flux under HP	cubic anvil hot press	yes			ETHZ	Karpinski(044 6332254, karpinski@phys.ethz.ch)
	Mg(1-x)MnxB2	Mg-flux under HP	cubic anvil hot press	yes			ETHZ	Karpinski(044 6332254, karpinski@phys.ethz.ch)
	Mn(1-x)FexB2	Mg-flux under HP	cubic anvil hot press	yes			ETHZ	Karpinski(044 6332254, karpinski@phys.ethz.ch)
	NdNi2B2C	arc melting		superconductor			PSI	Kazimierz Conder/Ekaterina Pomjakushina
	Chevrel phases							
	SnMo6S8	solid state synthesis		Yes superc. Tc = 14K			UniGe	Fischer (022 3796270, Oystein.Fischer@unige.ch)
	Sn(1-x)PbxMo6S8	solid state synthesis		Yes superc. Tc = 7-12K			UniGe	Fischer (022 3796270, Oystein.Fischer@unige.ch)
	LaMo6S8	solid state synthesis		Yes superc. Tc = 7K			UniGe	Fischer (022 3796270, Oystein.Fischer@unige.ch)
	Mo6Se8	solid state synthesis		Yes superc. Tc = 6K			UniGe	Fischer (022 3796270, Oystein.Fischer@unige.ch)
	Mo6S8	solid state synthesis		Yes superc. Tc = 1K			UniGe	Fischer (022 3796270, Oystein.Fischer@unige.ch)
	Mo6S6Br2	solid state synthesis		Yes superc. Tc = 13.5K			UniGe	Fischer (022 3796270, Oystein.Fischer@unige.ch)
	InMo6S8	solid state synthesis		Yes			UniGe	Fischer (022 3796270, Oystein.Fischer@unige.ch)
	Tl2Mo6Se6	solid state synthesis		Yes superc. Tc = 4.2K			UniGe	Fischer (022 3796270, Oystein.Fischer@unige.ch)
	In2Mo6Se6	solid state synthesis		Yes superc. Tc = 2.9K	Metal-Insulator		UniGe	Fischer (022 3796270, Oystein.Fischer@unige.ch)
	Na2Mo6Se6	solid state synthesis		No	Metal-Insulator		UniGe	Fischer (022 3796270, Oystein.Fischer@unige.ch)
	K2Mo6Se6	solid state synthesis		No	Metal-Insulator		UniGe	Fischer (022 3796270, Oystein.Fischer@unige.ch)
	Rb2Mo6Se6	solid state synthesis		No	Metal-Insulator		UniGe	Fischer (022 3796270, Oystein.Fischer@unige.ch)
	Cs2Mo6Se6	solid state synthesis		No			UniGe	Fischer (022 3796270, Oystein.Fischer@unige.ch)
	Mo6Se6	solid state synthesis		No			UniGe	Fischer (022 3796270, Oystein.Fischer@unige.ch)

	Material	Growth technique	Furnace	Conductor	Insulator	Magnetic	MaNEP Institution	Responsable
	CsMo12S14	solid state synthesis		Yes superc. Tc = 7K			UniGe	Fischer (022 3796270, Oystein.Fischer@unige.ch)
	Ba2Mo6S9	solid state synthesis		Yes superc. Tc = 5K			UniGe	Fischer (022 3796270, Oystein.Fischer@unige.ch)
	Rb(2n)Mo(6n+9)S(6n+13) (n = 1-4)	solid state synthesis		Yes superc. Tc = 4-10K			UniGe	Fischer (022 3796270, Oystein.Fischer@unige.ch)
	Silicides, Germanides, Carbides							
	TMSi (TM=Transition Metal: Co, Fe, Mn, …)	Czochralski, TSFZ	RF Induction, Mirror image furnace	yes/no		some	UniGe	Giannini (022 3796076, enrico.giannini@unige.ch)
	(TM',TM")Si solid solutions	Czochralski	RF Induction	yes/no		some	UniGe	Giannini (022 3796076, enrico.giannini@unige.ch)
	CeCoGe3	flux growth	1-zone vertical furnace	yes			UniGe	Giannini (022 3796076, enrico.giannini@unige.ch)
	EuNi2(Si(1-x)Gex)2	TSFZ	Mirror image furnace			valence transition in Eu-	PSI	Kazimierz Conder/Ekaterina Pomjakushina
	C-60	Sublimation	10-zone furnace	No	Insulator		EPFL	Berger 021 693 4484, helmuth.berger@epfl.ch)
NEW!	Ca3Ir4Sn13	flux growth	1-zone vertical furnace	Yes superc. Tc = 6.8K			PSI	Kazimierz Conder/Ekaterina Pomjakushina
	Chalcogenates, Phosphates, Oxo-Halides							
	Cu3TeO6	CVT and flux grown	2-zone furnace	No			EPFL	Berger 021 693 4484, helmuth.berger@epfl.ch)
	CuSb2O5	CVT	2-zone furnce	No			EPFL	Berger 021 693 4484, helmuth.berger@epfl.ch)
	Ni5(SeO3)4Cl2	CVT	2.zone furnace	No		magnetic properties	EPFL	Berger 021 693 4484, helmuth.berger@epfl.ch)
	Ni5(SeO3)4Br2	CVT	2-zone furnace	No		magnetic properties	EPFL	Berger 021 693 4484, helmuth.berger@epfl.ch)
	Cu5(SeO3)4Cl2	CVT	2-zone furnace	No		magnetic properties	EPFL	Berger 021 693 4484, helmuth.berger@epfl.ch)
	Cu2Te2O5Cl2	CTV	2-zone furnace	No		magnetic properties	EPFL	Berger 021 693 4484, helmuth.berger@epfl.ch)
	Cu2Te2O5Br2	CVT	2-zone furnace	No		magnetic properties	EPFL	Berger 021 693 4484, helmuth.berger@epfl.ch)
	Co6(TeO3)2(TeO6)Cl2	CVT	2-zone furnace	No		antiferromagnetic	EPFL	Berger 021 693 4484, helmuth.berger@epfl.ch)
	Co6(TeO3)2(TeO6)Br2	CVT	2-zone furnace	No		antiferromagnetic	EPFL	Berger 021 693 4484, helmuth.berger@epfl.ch)
	Co2TeO3Cl2	CVT	2-zone furnace	No		magnetic properties	EPFL	Berger 021 693 4484, helmuth.berger@epfl.ch)
	Co2TeO3Br2	CVT	2-zone furnace	No		magnetic properties	EPFL	Berger 021 693 4484, helmuth.berger@epfl.ch)
	Ni5(TeO3)4Cl2	CVT	2-zone furnace	No		magnetic properties	EPFL	Berger 021 693 4484, helmuth.berger@epfl.ch)
	Ni5(TeO3)4Br2	CVT	2-zone furnace	No		magnetic properties	EPFL	Berger 021 693 4484, helmuth.berger@epfl.ch)
	Ni5(TeO3)4Br2-xClx	CVT	2-zone furnace	No		magnetic properties	EPFL	Berger 021 693 4484, helmuth.berger@epfl.ch)
	Co7Te4O12Br6	CVT	2-zone furnace	No		magnetic properties	EPFL	Berger 021 693 4484, helmuth.berger@epfl.ch)
	CuSbTeO3Cl2	CVT	2-zone furnace	No	Insulator		EPFL	Berger 021 693 4484, helmuth.berger@epfl.ch)
	Cu3(SeO3)4Cl2	CTV	2-zone furnace	No		magnetic properties	EPFL	Berger 021 693 4484, helmuth.berger@epfl.ch)
	CuTe2O5	CVT	2-zone furnace	No		magnetic properties	EPFL	Berger 021 693 4484, helmuth.berger@epfl.ch)
	CuSe2O5	CVT	2-zone furnace	No			EPFL	Berger 021 693 4484, helmuth.berger@epfl.ch)
	FeTe2O5Cl	CTV	2-zone furnace	No	Insulator	magnetic properties	EPFL	Berger 021 693 4484, helmuth.berger@epfl.ch)
	FeTe2O5Br	CTV	2-zone furnace	No	Insulator	magnetic properties	EPFL	Berger 021 693 4484, helmuth.berger@epfl.ch)
	$NiSeO_3$	CTV	2-zone furnace	No	Insulator	magnetic properties	EPFL	Berger 021 693 4484, helmuth.berger@epfl.ch)
	TiOBr	CTV	2-zone furnace	No	Insulator	magnetic properties	EPFL	Berger 021 693 4484, helmuth.berger@epfl.ch)
	Ni3TeO6	CTV	2-zone furnace	No	Semiconductor	magnetic properties	EPFL	Berger 021 693 4484, helmuth.berger@epfl.ch)
	Co3TeO6	Flux grown	1-zone furnace with temp.gradient	No	Semiconductor	magnetic properties	EPFL	Berger 021 693 4484, helmuth.berger@epfl.ch)
	Cu_2CoTeO_6	Flux grown	1-zone furnace with temp.gradient	No	Semiconductor	magnetic properties	EPFL	Berger 021 693 4484, helmuth.berger@epfl.ch)
	Bi(Cu1-xZnx)2PO6 (x=0 - 0.05)	TSFZ	Mirror image furnace				PSI	ekaterina.pomjakushina@psi.ch
	Ca3Cu(3-x)Nix(PO4)4	solid state synthesis				quantum spin trimer	PSI	Kazimierz Conder/Ekaterina Pomjakushina
NEW!	Cu2OSeO3	CVT	2-zone furnace	No		magnetic properties	EPFL	Berger 021 693 4484, helmuth.berger@epfl.ch)
NEW!	Sr2CuO2Cl2	CVT	2-zone furnace	No	Insulator	magnetic properties	EPFL	Berger 021 693 4484, helmuth.berger@epfl.ch)
	Organics							
	Pentacene	CTV	2-zone furnace	No	Insulator		EPFL	Berger 021 693 4484, helmuth.berger@epfl.ch)
	Rubrene	CTV	2-zone furnace	No	Insulator		EPFL	Berger 021 693 4484, helmuth.berger@epfl.ch)
	Coronene	CTV	2-zone furnace	No	Insulator		EPFL	Berger 021 693 4484, helmuth.berger@epfl.ch)
	Tetracene	CTV	2-zone furnace	No	Insulator		EPFL	Berger 021 693 4484, helmuth.berger@epfl.ch)
	Anthracene	CTV	2-zone furnace	No	Insulator		EPFL	Berger 021 693 4484, helmuth.berger@epfl.ch)
	TCNQ	CTV	2-zone furnace	No	Insulator		EPFL	Berger 021 693 4484, helmuth.berger@epfl.ch)
	TTF-TCNQ	CTV	2-zone furnace	No	Organic Conductor		EPFL	Berger 021 693 4484, helmuth.berger@epfl.ch)
	Perylene	CTV	2-zone furnace	No	Insulator		EPFL	Berger 021 693 4484, helmuth.berger@epfl.ch)
	TCNQ-Perylene complexe	CTV	2-zone furnace	No			EPFL	Berger 021 693 4484, helmuth.berger@epfl.ch)
	Copper Pthalocyanine	CTV	2-zone furnace	No	p-type semiconductor		EPFL	Berger 021 693 4484, helmuth.berger@epfl.ch)
	In2VO5	CTV	2-zone furnace			magnetic properties	EPFL	Berger 021 693 4484, helmuth.berger@epfl.ch)
	$Co_5Te_4O_{11}Cl_4$.	CTV	2-zone furnace	No			EPFL	Berger 021 693 4484, helmuth.berger@epfl.ch)
	$Co_5(TeO_3)_4X_2$ (X = Cl, Br).	CTV	2-zone furnace	No	Insulator	magnetic properties	EPFL	Berger 021 693 4484, helmuth.berger@epfl.ch)
	$Co_5(SeO_3)_4X_2$ (X = Cl, Br).	CTV	2-zone furnace	No	Insulator	magnetic properties	EPFL	Berger 021 693 4484, helmuth.berger@epfl.ch)
	Other compounds							
	AlxGa1-xN	flux growth	high-pressure furnace		yes		ETHZ	Karpinski(044 6332254, karpinski@phys.ethz.ch)
	Cu:ZnGa2O4 nanomaterials	MW-HT	hydrothermal autoclave				UniZh	Patzke(044 63 54691, greta.patzke@aci.uzh.ch)
	Cu:Ga2O3 nanomaterials	MW-HT	hydrothermal autoclave				UniZh	Patzke(044 63 54691, greta.patzke@aci.uzh.ch)
NEW!	Ba2CuGe2O7	TSFZ	Mirror image furnace			magnetic properties	PSI	kazimierz.conder@psi.ch

3 Knowledge and technology transfer

The knowledge and technology transfer (KTT) activities of MaNEP have been intensified during the last period. Two main reasons have contributed to this progression. First, fundamental research from the previous years of MaNEP has generated consolidated expertise and know-how in fields of interest for industry. In particular, experimental capabilities related to microtechnology, microelectronics, materials synthesis and characterization have emerged as strategic by-products of basic research. Second, the lukewarm economic perspectives originated by the "strong Swiss Franc" have stimulated the industrial sector to search for innovative, commercially viable projects and technologies to be launched in a foreseeable future. MaNEP has consistently supported technology transfer by implementing applied research projects. Also, contacts with industry have been fostered through initiatives like the Geneva Creativity Center (GCC) and the presence in fairs. Several R&D projects have been launched in the framework of the Commission for Technology and Innovation (CTI) or as Swiss National Science Foundation (SNSF) *economic stimulus packages*. And a specialized, cross-disciplinary team with experience in pre-industrialization developments has successfully built prototypes and demonstrators.

3.1 Contacts with industry

The promotion of KTT

Effective technology transfer starts with the timely identification of needs and opportunities. This is exactly the mission of the Geneva Creativity Center (GCC), an initiative first elaborated by MaNEP and now largely supported by other organizations. The GCC was established as a collaboration between the University of Geneva, the university of applied sciences (HES-SO) in Geneva, the *Office de Promotion de l'Industrie et la Technologie* (OPI) and the *Union Industrielle Genevoise* (UIG) and was inaugurated on June 28, 2011. A formal agreement, implying a financial support from the Canton of Geneva for 2012 – 2013, has been signed, which allows the GCC to go forward. It has started activities by promoting contacts and exchanges between industry and research institutions. The vision of the GCC is to promote technology transfer by implementing special emphasis on the identification of the best opportunities and projects. By bringing together engineers and scientists from industry and academia, and by stimulating interactions (meetings, technical discussions) in a creative atmosphere, the GCC acts as a catalyst for technology transfer (Fig. 1).

Visibility is another important factor for the technology transfer process. One way to increase visibility is through an active presence at innovation fairs. The MaNEP *economic stimulus packages* have been presented at the Hannover Messe 2011 to an international audience (Fig. 2). Attending the Hannover Messe has been a very positive and useful experience. It has given practical insight into the marketing of applied research projects. Our industry partners have established concrete follow-ups for the presented *economic stimulus packages*. Also, the fair offered considerable opportunities to identify research partners in view of R&D projects at the European level, increasing

Figure 1: *Brainstorming session at the GCC. Topic: dc current distribution networks and the impact of new technologies.*

Figure 2: *Technology transfer: MaNEP presence at the Hannover Messe 2011.*

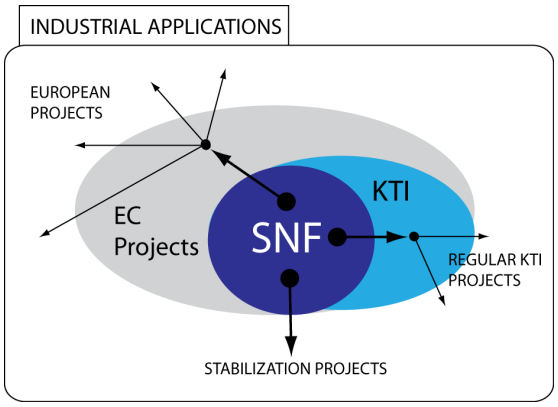

Figure 3: *The MaNEP developments: exposure to potential R&D partners at national and international levels. Stabilization projects concern for exemple the* economic stimulus packages *and EC Projects can be launched in the framework of structures as Euresearch Network.*

outreach beyond CTI projects (Fig. 3).
This increased promotion of KTT has led to a substantial progression of MaNEP's industrial contacts. Typical new initiatives are described here below.

Kugler BIMETAL SA

Encouraged and funded by the Geneva Creativity Center, a close collaboration was started in 2011 between Kugler BIMETAL SA and the University of Geneva with the aim of investigating and developing techniques and materials for the deposition of lead-free bronzes on steel, in response to the increasing regulatory pressure of eliminating lead from all applications.

Winterthur Instruments GmbH

Winterthur Instruments GmbH is a young Swiss company who has developed a new, innovative technology for the nondestructive testing of coatings. This original contact-less technology uses high-speed infrared sensors. A first early success was achieved by characterizing the thermal properties of coatings elaborated in the MaNEP "Cut-and- coat" *economic stimulus package*. MaNEP is particularly active in the fabrication and study of thin films and coatings in general. The synergy with Winterthur Instruments opens the way to the synthesis of functional surface alloys with tailored thermal properties (injection moulds, motor parts, cutting tools).

TIMELAB

TIMELAB is the Geneva Laboratory of horology and microengineering. TIMELAB activities are focused on the local watch industry. This institution controls and certifies the quality and precision of high-end watch movements. Moreover, TIMELAB delivers the "Hallmark of Geneva" ("*Poinçon de Genève*") certificate. This label or distinction is given to selected movements meeting strict requirements of precision and finishing. Initiated 125 years ago, the "Hallmark of Geneva" is engraved by stamping small watch parts. Today, MaNEP and TIMELAB are exploring ways to elaborate a new version of the "Hallmark of Geneva" incorporating features from modern metallurgy and nanoscience.

Sensorscope Sàrl

Sensorscope Sàrl is a spin-off company from the EPFL. This company provides flexible sensing systems designed to study environmental parameters. The measurement systems are based on multiple wireless stations. A dedicated website can be used as a central place to check real-time data. The Sensorscope modules have been designed for applications related to environmental parameters like humidity and temperature. However, following collaborative work with the MaNEP Development Lab, an interface between the Sensorscope modules and the oxygen sensor (see *economic stimulus package* "Electrochemical sensors with higher resolution") has been elaborated. Ubiquitous, wireless access to measurements performed by the newly developed sensor opens new possibilities for industrial applications requiring real-time monitoring of oxygen concentration.

Manufactures d'Outils Dumont SA

Manufactures d'Outils Dumont SA is a Swiss company specialized in precision tools and instruments for watchmaking, electronics, biology, and medical applications, among others. The Dumont precision tools made in fine steel-based alloys have gained worldwide reputation since several decades. Technologies and processes developed by MaNEP in surface treatments, in particular surface alloying applications have a big application potential for the Dumont products. Promising feasibility tests are in progress.

3.2 KTT Projects

Deposition of lead-free bronzes on steel, with Kugler BIMETAL SA

Kugler BIMETAL SA is specialized in the development of bronze alloys with particular antifriction properties. Since 1950, the company has exploited a patented technology based on the metallurgical "grafting" of lead-based bronze on steel. Such bi-metal structures are used in several applications where the mechanical and thermal environments are particularly harsh. Lead-based alloys are nowadays under strong regulatory pressure in the sense that lead is to be eliminated from applications. This is the case of the automotive industry for example. Under the umbrella of the GCC, Kugler and MaNEP have elaborated the CTI project "Lead-free antifriction copper alloys deposited on steel by surface coating techniques". This project has received CTI financial support in the frame of the measures to combat the "strong Swiss Franc". This project is based on the knowledge and skills accumulated by the group of applied superconductivity, led by C. Senatore, in material science in general and specifically in bronze metallurgy, powder metallurgy, microstructure analysis and wire fabrication. This project is of great strategic importance for Kugler, who benefits from the expertise and the equipment of UNIGE. And the academic partner is exposed to new challenges and perspectives. Kugler estimates that such collaborative efforts reduce at least by a factor of three the time needed to bring a specific R&D project to completion.

Cut-and-coat project with AgieCharmilles

AgieCharmilles +GF+ offers electrical discharge machining (EDM) machines and related

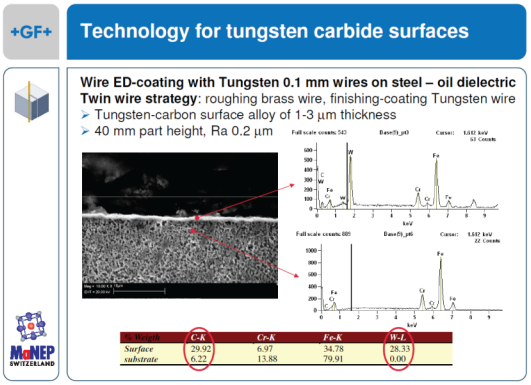

Figure 4: *Based on the results of the project, AgieCharmilles +GF+ is able to offer a tungsten-coating technology implemented on wire-cutting EDM machines.*

supplies in fast growing market segments of the tool and mould industries, and to manufacturers of precision components. This project started in 2010 as part of the SNSF supported *economic stimulus packages*. The general objective of the present project was to provide AgieCharmilles +GF+ with the technical and scientific support to enter the growing market of coated metal parts. This was achieved by modifying the traditional EDM setup. By changing the energy distribution of the machining sparks, and the metallurgical composition of the tool electrode, it has been possible to tune the physical process and to create surface alloys with controlled properties on the machined parts (Fig. 4).
The developed coating technology was successfully applied to the reinforcement of cutting dies manufactured by wire-EDM

Swatch Group R&D SA, Division Asulab

The goal of this project is the development of resistive hydrogen detectors based on materials undergoing metal-insulator transitions under hydrogen exposure. This CTI project is a MaNEP contribution to the hydrogen car initiative of Belenos Clean Power, a company member of the Swatch Group. Significant progress has been made by the team of the project under the supervision of K. Yvon, in collaboration with the group of J. Cors and Ø. Fischer. The continuation of the second phase of the three year project has received the green light from the CTI authorities. The scientific work is focused on the $LaMg_2Pd$-H system. Main achievements have been the following:

- the $LaMg_2Pd$-H system was successfully synthesized in the form of thin films; this

step was a critical milestone for the completion of the project;

- the hydrogen sensing properties of the $LaMg_2Pd$-H have been fully demonstrated and characterized;
- IP issues have been secured by a patent application;
- prototype thin film H_2 detectors have been mounted on standardized TO-5 holders.

Glass micromachining: INTERREG project with EREO SAS, France

The goal of this project is the development of a glass micromachining technology for microfluidics chips and general engraving applications. The working principle uses micropositioning and electronics know-how gathered from local probe microscopy and related technologies. A metal tip immersed in an electrolyte is brought at a very close distance of the glass surface. By applying a working voltage between the tip and a counterelectrode, a sparking process is initiated and glass can be removed from the surface (Fig. 5). Since glass micro-engraving covers a range of applications from microfluidics to decorations, we have received a grant from the INTERREG authorities to develop this technology. The innovative content of the project lies in the transposition of STM-like axis control of the sparking distance, and the simultaneous use of spectroscopic measurements to characterize and monitor the energy of the sparks. The industrial goal of the project is the construction of a prototype engraving machine.
Main achievements at midterm of this two-year project are the following:

- design and construction of the mechanical setup;

Figure 5: *The INTERREG project on glass micromachining.*

Figure 6: *The Sensorscope* Climaps *application interfaced to the MaNEP electrochemical sensor for remote control.*

- design and fabrication of the power electronics board;
- fabrication and optimization of the engraving electrodes.

Among the potential end users of the technology we have already identified glass laboratory equipment manufacturers, watchmakers, bio-chips applications and even glass cosmetics packaging manufacturers.

Electrochemical sensors with higher resolution

The goal of this project was to develop an electrochemical sensor of the Clark cell type with higher resolution than existing devices. The project started in 2010 as a *economic stimulus package* and it has now been completed. The most remarkable achievements have been the design and implementation of a new sensor head, and the design of a new complete electronics incorporating the latest sensing current amplification circuitry, largely inspired from STM electronics setups.
Moreover, in partnership with Sensorscope Sàrl, we have implemented a specific interface hardware that provides access to the GSM network, making possible the distance survey of the sensors through the Web (Fig. 6).

Marking technology for watch components

This project (partners: Vacheron Constantin and Phasis) is described in chapter 2, on Project 3. We point out here at least two emerging multiplier effects of the developments under way. The first new development con-

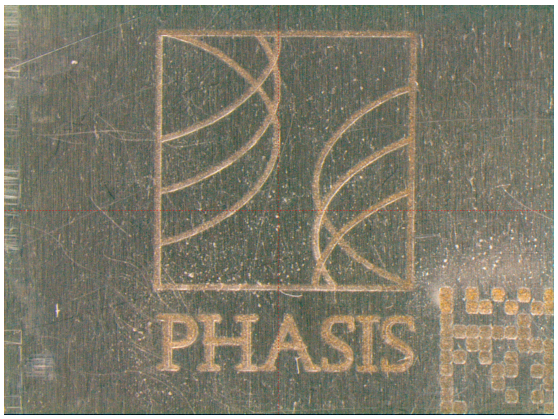

Figure 7: *Logos and data-matrix identification structures can be written on steels of medical quality.*

cerns the application of the marking technology for the implementation of secured certification hallmarks. Its feasibility is under way in coordination with TIMELAB. Another opportunity concerns the traceability of medical tools, the key point here is the extraordinary resistance of the marks to sterilization procedures. The new technology offers clear advantages when compared to laser or stamping marking techniques (Fig. 7). We are now implementing these new routes for technology transfer by identifying the most appropriate industrial partners.

SwissNeutronics

The *economic stimulus package* "Neutron optical devices for small samples" has been started in October 2009. The goal of the project was to develop elliptic guides/lenses for neutron beams to be focused on small samples with a height of $2-3$ mm. The project has included three main tasks:

- multichannel focusing guides/lens;
- adaptive focusing optics;
- reflectometer concept selene for tiny samples.

This project has been completed and has successfully reached all milestones included in the original proposal.

Bruker BioSpin AG

The *economic stimulus package* "Developments of MgB_2 wires with high critical current densities for economical NMR magnets at 4.2 K and 20 K" has also been started in October 2009. The purpose of the present project was to develop the cold high pressure densification (CHPD) technique, first introduced in Geneva (2 patents pending), up to the industrial level. This technique consists in pressing a MgB_2 wire simultaneously from all four sides, in order to get an enhanced mass density of the filament. So far, the efforts have been concentrated on *in situ* MgB_2 wires, where the initial cores consist of Mg and B, the MgB_2 phase being formed by a reaction at 650°C at the end of the deformation procedure. During this project, the high pressure was applied on monofilamentary tapes. Two important progress steps have been achieved in view of the application of this technique on industrial wire lengths: a) the technique was extended to multifilamentary MgB_2 wires, and b) a prototype machine was developed allowing for the first time the densification of long wire lengths at pressures exceeding 1 GPa. As a consequence of the enhancement of mass density on CHPD treated MgB_2 wires, a considerable increase of the critical current density was observed, not only for binary MgB_2 filaments, but also for filaments containing carbon impurities.

ABB

The collaboration between the University of Geneva and ABB to explore the properties of coated conductors for superconducting fault current limiters has been continued and new proposals for technical improvements have been elaborated.

3.3 Sustainable technology transfer

Technology transfer is a looping process (Fig. 8). Two conditions have to be met to

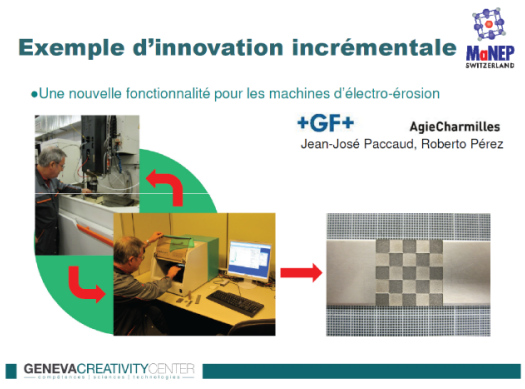

Figure 8: *A MaNEP incremental innovation project presented at the GCC.*

achieve a sustainable, creative interaction between industry and academia. First, the identification of ideas and opportunities has to be triggered in a dynamic way. Second, working prototypes and demonstrators have to be developed to sustain credibility and momentum in the exchange with industry. These two cornerstones of technology transfer, implemented through the MaNEP initiatives of the Geneva Creativity Center (GCC) and the MaNEP Development Lab (Fig. 9), have played a key role in the progression of our KTT activities. Success stories based on applied projects have had a catalytic effect for the implementation of new initiatives. Also, the timely availability of prototypes elaborated at the MaNEP Development Lab has facilitated the implementation of field tests and accelerated the learning process of pre-industrialization disciplines and methodologies.

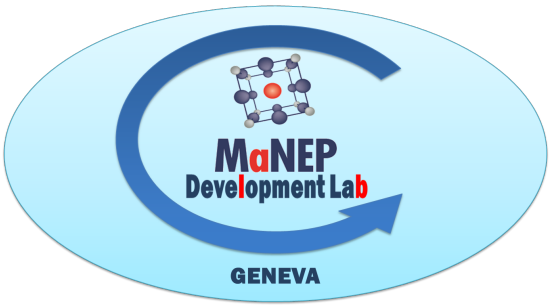

Figure 9: *Identity of the MaNEP Development Lab. These new MaNEP laboratories are located in the* Centre de Technologies Nouvelles *in a modern building of the industrial zone of Plan-les-Ouates.*

4 Education, training and advancement of women

4.1 Education and training

4.1.1 Doctoral school

In 2011, 25 PhD students were registered in the MaNEP-Geneva doctoral program. Only one of them defended his PhD during 2011, while three started their work during this same period. Among the 25 students, 25% have obtained their master degree from the University of Geneva, and 28% are women.

The Geneva students had an extensive doctoral training in 2011, for a total equivalent to 71 ECTS credits. This teaching was provided by international schools (34%), by the CUSO *Doctoral program in physics* (10%), and by the MaNEP-Geneva doctoral program (56%). The latter involved, in particular, the course of Antoine Georges, *Electronic Structure of Correlated Materials from a Dynamical Mean-Field Theory Viewpoint: Introduction, State of the Art and Perspectives*, as well as the course *Applications of the Many-Body Formalism in Condensed-Matter Physics* by Christophe Berthod, whose third part (spring 2011) was followed by 11 students, and first part (autumn 2011) by 14 students, among which 2 came from EPFL.

4.1.2 PhysiScope Genève

A fourth successful year

The PhysiScope is a public laboratory and science-theater operated since 2008, jointly by MaNEP and the Physics Section at the University of Geneva. Attendance has been steadily increasing to reach 4'200 in 2011. This is nearly as many as throughout the entire first three years of activity. Given that on average each group counts 17 visitors, the PhysiScope team has presented about 250 shows over one year in its setting at the University of Geneva. 60% of the students visiting the PhysiScope come from junior high school and 40% from high school. Like every year, the PhysiScope had again the pleasure to welcome a number of VIP guests and delegations, among them the strategic committee of UniGE, a delegation of alumni of UniGE, several official academic delegations from Russia, Canada and Australia, the outreach team of the NCCR MUST, 50 students from Slovenia, and many more.

In an effort to maintain an attractive and dynamic offer, new modules have been developed. Several novel experiments address different aspects of superconductivity (motivated by last year's celebrations), and a complete new show about pressure has been added.

Celebrating 100 years of superconductivity

The PhysiScope has been actively participating in the celebrations of the 100th anniversary of the discovery of superconductivity organized by MaNEP (see chapter 5.1). A total of 500 people enjoyed a special show on electricity and superconductivity (Fig. 1) during open days on April 8–20, 2011. The show was presented in the evening and during the weekend. About 1'500 visitors joined the Saturday for families *Fascinante supra* with several PhysiScope experiments on display among many other activities on September 17, 2011. The PhysiScope team further animated guided tours of the art & science exhibition SUPRA100 on display for two months at the University of Geneva. Finally, together with other MaNEP members, the PhysiScope has been collaborating with the French branch of the Swiss Radio and Television broadcasting company (*Radio Télévision Suisse*) to shoot short movies of several new experiments about superconductivity. These trailers can be viewed on www.rtsdecouverte.ch.

Figure 1: *Fascinating superconductivity.*

Outreach

The PhysiScope has extended its extramural activities, being invited to several events in Geneva and abroad. The PhysiScope entertained French school classes (primary, junior high school and high school) and the general public in the *Globe of Science and Innovation* at CERN during the European *"Fête de la science"*from 10 to 14 October, 2011. On October 14–16, 2011, the PhysiScope was invited by the *Cité des sciences et de l'industrie* in Paris. The focus of the event was on chemistry, the PhysiScope being the only invited physics show. This was a unique opportunity to be repeated with over 75'000 visitors. In November, the PhysiScope was invited to Leiden (NL) to perform a show as part of an exchange deal with the Dutch show *Rino*, who performed in Geneva and at PSI during the 100 years of superconductivity celebrations. The PhysiScope took part in the common show of the conference *ShowPhysics* organized each year by EuroPhysicsFun. In 2011 it was in Kharkiv, Ukraine, on April 7, and more than 4'000 visitors came to watch this one day show. Finally, the PhysiScope also took part in a number of annual events across Geneva, such as the *Futur en tous genres* open day for young children, the *Journée des collégiens*, as a showcase of the Physics Section for the potential future students, or the *Passeport Vacances* during the summer holidays.

Collaborations

The PhysiScope is co-applicant, with the Department of Astronomy of the University of Geneva and the University of Bern, of an Agora proposal that has been granted by the Swiss National Science Foundation to develop an original educational program centered on a remote controlled telescope stationed at the Gornergrat.
The PhysiScope has been collaborating with CERN on a novel initiative to acquaint 9 to 12 years old kids with the experimental approach. The project *Dans la peau d'un chercheur* (Fig. 2) proposes pupils from France and Geneva to discover what is hidden inside a small box they are not allowed to open. It turns the kids into researchers, making them think about some aspects of experimental research. What is a hypothesis? What are data? What is a proof? How to set up an experiment? The kids are brought to act as researchers, and finally share their results in a one day poster session and conference. Last year, 30 classes totalling 670 pupils did participate. This year 730 pupils in 33 classes will be challenged to uncover a different content of the box.
The ChimiScope, an endeavor inspired by the PhysiScope in the School of Chemistry and Biochemistry of UniGE has been inaugurated on November 24, 2011. The PhysiScope has collaborated in this new adventure, extensively sharing its experience and know-how. This is a first milestone towards extending the model to other scientific themes of the Faculties of Science and Medicine.

Figure 2: *Pupils discover optical spectroscopy during* Dans la peau d'un chercheur *collaboration with CERN.*

Acknowledgments

The PhysiScope thanks the foundation H. Dudley Wright for its continued financial support. We further acknowledge support from the University of Geneva, the Faculty of Science and the Geneva Department for Public Education.

The PhysiScope team 2011/2012

Prof. Michele Maggiore, new president of the Physics Section, is replacing Prof. Martin Pohl in the executive committee. Many thanks to M. Pohl for his enthusiastic participation over the past 5 years! **Executive committee:** Ch. Renner (president), Ø. Fischer, M. Pohl (until 30.06.2011), M. Maggiore (since 01.07.2011), J.-G. Bosch, O. Gaumer, A. Bonito Aleman. **Model maker:** C. Corthay. **Assistants and students:** A. Akrap, Ch. Cailler, F. Dufour, L. Favre-Quattropani, A. Fête, S. Gariglio (spring), F. Glass, C. Lichtensteiger (autumn), T. Magouroux, A. Michel, P. Sekatski. **Teachers:** R. Achimescu, A. Bardiot, D. Boehm and B. Gisin.

Further reading

www.physiscope.ch;
www.rtsdecouverte.ch;
cdsweb.cern.ch/record/1359921;
obswww.unige.ch/wordpress/gornergrat.

4.1.3 SWM 2011: Swiss Workshop on MaNEP in Les Diablerets

From June 29 till July 1, 2011, the MaNEP community met for the ninth edition of the Swiss Workshop on Materials with Novel Electronic Properties at the Eurotel in Les Diablerets. Over 192 registered MaNEP members and scientists from abroad, of those 80 PhD students from the different MaNEP partner institutes, have attended the workshop (Fig. 3). 10 invited speakers and 28 contributed talks did animate nine sessions covering most of the topics studied in the MaNEP network, from correlated oxides to cold atoms, including topological insulators, superconductivity, multiferroics, low dimensional and unconventional materials, interfaces and applications. 117 posters were on display for the entire duration of the workshop, providing ample opportunities for discussions.
Novel equipment and hardware could be discussed in a small technical exhibition. We thank Pfeiffer Vacuum, Teco René Koch and VG Scienta for their support and displays.

Figure 3: *SWM 2011 participants.*

This year, for the first time, a special tutorials day aimed at students was organized the day preceding the workshop in the frame of the techniques and know-how activity. In addition to learn about scientific topics, this day offered 32 MaNEP PhD students and 9 postdocs a unique opportunity to meet in a convivial setting. The tutorials covered three experimental topics: thin film synthesis, scanning probe microscopy and crystal growth. Many thanks to Patrycja Paruch, Ivan Maggio-Aprile and Enrico Giannini for their contributions and organization of these very well received tutorials.
During the traditional late evening meeting of the SWM steering committee, Christoph Renner was elected new chair, replacing Øystein Fischer who has been the conference chair for all of the nine SWM workshops to date.
Finally, many thanks to Marie Bagnoud, Greg Manfrini, Ivan Maggio-Aprile, Elizabeth Guéniat and Pascal Cugni for their efficient help with the organization of the meeting.

4.1.4 Topical meeting on Topological properties of electronic materials

The one-day topical meeting on *Topological properties of electronic materials* took place on May 6, 2011 in Geneva (organizers: A. Morpurgo (UniGE) and M. Sigrist (ETHZ)), to address the rapidly growing interest in this topic. The meeting intended to provide a pedagogical introduction to the concepts involved in the study of the topological properties that are relevant in new classes of materials, and to bring together Swiss researchers that are already active in this area. Two speakers from outside Switzerland were invited. P. W. Brouwer from the Freie Universität of Berlin explained the main concepts relevant to understand two-dimensional topological insulators; H. Buhmann from Wurzburg University presented work on HgTe/CdTe heterostruc-

tures, that are currently the best experimental realizations of 2D topological insulators. Other five talks from researchers at Swiss institutions completed the overview of research in this area, addressing angle-resolved photoemission spectroscopy and transport experiments on 3D topological insulators, the current situation in topological superconductors, and different theoretical aspects of topology in electronic systems. The meeting was attended by approximately 100 participants from all over Switzerland together with several researchers from Grenoble, who expressed great interest in the subjects covered and satisfaction for the initiative.

4.1.5 MaNEP Winter School 2013

The series of MaNEP summer and winter schools will be continued next year, and will take place from January 13 to 19, 2013 in Saas-Fee. A scientific committee led by Frédéric Mila (EPFL), and involving Christian Bernhard (UniFR), Dirk van der Marel (UniGE), Christian Rüegg (PSI), and Manfred Sigrist (ETHZ), is presently setting up the scientific program.

4.1.6 MaNEP participation to conferences

This report counts and lists all the presentations made by MaNEP members at conferences and fairs, as well as seminars or colloquia given in academic institutions. This list however does not contain the numerous posters also presented at conferences, mostly by young researchers. We want to point out that these poster presentations nevertheless represent a big part of the MaNEP scientific output. This is an essential part of the research made by young people and should also get recognition. A minimum of 500 posters per year can be estimated which are not counted in the statistical data of the report and do not appear in the lists generated by NIRA — balanced by about 500 oral contributions.

4.2 Advancement of women

4.2.1 Summer internships

For the eighth year, MaNEP summer internship program was organized for all women students working within the MaNEP network. In 2011, MaNEP supported seven candidates: 4 at UniGE, 2 at EPFL, 1 at UniFR. Five internships lasted one month, and two were extended over two months. All these internships were very successful. In addition to that, three exchange programs were launched for men students, one over one month, and two over two months.

4.2.2 Survey of the advancement of women activities

Introduction

Together with the Equality Office of the University of Geneva, we prepared a survey that was sent at the beginning of the summer 2010 to all women researchers in MaNEP. In this survey, we prepared questions to evaluate the current work and to see how to promote new activities devoted to the advancement of women (AOW). We considered three important points for the AOW program to follow and oriented the questions of the survey consequently. 1. More young women should be encouraged to choose science, particularly physics. This point was evaluated using the PhysiScope as an example of action. 2. Women physics students should be encouraged to continue their careers in research. This point was evaluated using the summer internships as an example of action. 3. The situation of women researchers (PhD students and postdocs, in particular) should be considered and they should be helped to combine professional and family life.

19 questionnaires out of a total of 31 were returned. Among them, 10 were filled by PhD students, born between 1981 and 1987, 3 by postdocs, born between 1979 and 1981, 4 by senior researchers, born between 1965 and 1978, and 2 by professors (one assistant professor born in 1974 and one associate professor born in 1977). One senior researcher is working in the industry (Bruker BioSpin). All other women are working in academic institutions members of MaNEP (UniGE, UniFR, UniZH, EPFL, ETHZ, PSI and Empa). 7 researchers did their latest degree in a foreign university, the 12 other did it in a Swiss academic institution. 2 had children.

Part of the analysis of the survey was carried out by Nalini Easwar (physics professor at the Smith College, in Northampton, MA, an undergraduate liberal arts college for women) during her two weeks stay in Geneva. The common interest theme for her visit was shar-

ing of ideas, in particular regarding advancement of women.

Summer internships for women

Among the women who filled the survey, 13 knew the MaNEP summer internships for women and 5 of them benefited from the internships. The reactions and the comments on these internships are unanimously positive. Thus, they are very important, *as an action that works very well at a very low cost*.
Almost all comments brought out the importance and positive impact of internships on training and the encouragement to continue for a PhD in physics.
However to the question "did MaNEP summer internships for women students have a positive impact on your CV?" 3 of the 5 women who participated do not have an opinion! This answer is surprising and shows an absence of valorization of one's know-how. The answer might be the same in case of men, however it has probably more consequences in the case of women, due to a certain self-restraint. This shows an absence of consciousness of their training evolution and weakens the insertion of women outside the academic world after their studies. They should be encouraged to learn to value what they do, their work, and not only their publications.

Needs for women researchers

The answers to the questions about their needs as women researchers indicate that if there are problems and needs, these are not women specific problems but structure problems (wish for less administrative work, for example).
The only real specific need that comes out of the survey is a help for combining professional and family life, in the presence of children (in the present or as a future concern). The comments were about:

- the lack of shared parental leave policies for both parents;
- the many issues for balancing profession and family were not seen as only a woman's problem, but needed by all parents.

This raises the question how to increase the flexibility of the work in the frame of research. Finding solutions for women today is anticipating solutions for equilibrate couples tomorrow. And solutions have to be found that will not consolidate the existing problems.

There is a lot of desire to get to an 80% format but not many are actually doing it for reasons that follow. The need to get a culture for recognizing the 80% work plan as professional and the recognition of the special demands of parents with kids, by others who do not have such demands. This needs to be noted and recognized. One can ask indeed why in research people (men and women) have to work more than elsewhere and why the request of working part-time (even at 80%) is perceived as a signal of being somebody who does not want to commit him/herself.

About the PhysiScope and the promotion of sciences for young people

The first part of the questionnaire, about the PhysiScope and the development of similar actions, mixed the question of the promotion of sciences for young people (men and women) and the question to show that physics is not a sexist science (reserved to men). We note however that the interest in physics may be hindered by three difficulties:

- a social obstacle (physics is difficult); as an example, we can cite this comment: "We have also to invite the whole families to the PhysiScope to change the perspective of physics and the image to stop the social discouragement to hard sciences";
- a teaching obstacle (the quality of the teachers — physics teachers have a great responsibility in the way physics will be perceived);
- a "political" obstacle (the way physics in integrated in the study plan).

Conclusions

MaNEP internships work very well for the women who do these internships and there are mentorship programs as well.
The support for the balance of family and profession is not just something for women, but also for men with young children. A factor is the acceptance of the culture of opting for the 80% work plan. While many express the desire and see how it will help, there are not many who are doing it. So, a survey for men and women, addressing specific questions about this, would be helpful. Of particular interest is the fact that there were just two women in the survey with children.

5 Communication

The superconductivity centennial stood out as the distinguishing event of 2011. This anniversary was a great opportunity to strengthen ties with a wide audience and particularly MaNEP research position both locally and nationally. Successful festive events were organized in collaboration with numerous academic, private and industrial partners. These novel events gave an unusual glimpse into a little known physics phenomenon, which will be an inescapable part of the future. They played a key role to connect science between MaNEP and the public. Thus, the public, school children, students, and of course the media were invited to discover superconductivity and physics. A special event was also organized for decision makers. A far-reaching communications strategy was developed using many tools to inform the public about all the events and above all promote the work of MaNEP.

5.1 Celebrating the superconductivity centennial

To celebrate the 100th anniversary of the discovery of superconductivity in 2011, MaNEP organized a wide range of events. Arrangements were successfully made for a rich and varied programme. More than 100 researchers, technicians, collaborators and students of MaNEP were involved in the organization of these events, which drew about 14'000 participants and visitors among which 1'500 scholars. MaNEP collaborated with the Swiss Physical Society, the Paul Scherrer Institute (PSI), the CERN, the University of Geneva and the PhysiScope, the Dutch show *Rino* from Leiden and the Geneva *La Bâtie Festival*. This vast programme found favor with various funding partners who provided generous support, namely the H. Dudley Wright Foundation, Vacheron Constantin, the Moser Foundation, Bruker Biospin AG and ABB.

Open days at the PhysiScope

To honor the day superconductivity was officially discovered, on April 8, 1911, the PhysiScope organized two weeks of open days, from April 8 to 20, 2011. The public discovered this amazing physics phenomenon with interactive and fun workshops (Fig. 1). Resulting in more than 500 people taking part and extra sessions being set up to meet public demand. This show was also presented to 550 students at the CERN's *Globe of Science and Innovation* during the French Science Festival in October and at the University of Leiden, cradle of superconductivity (see PhysiScope report on p. 115).

Figure 1: *People enjoying a fun demonstration at the PhysiScope.*

Superconductivity at the SPS

Last year, MaNEP did not participate to the Swiss Physical Society (SPS) annual meeting

Figure 2: *Five invited speakers and two Nobel Laureates during the SPS lively round table discussion.*

Figure 3: *SUPRA100 exhibition. (a) The free-standing structure called suprabox, composed by an artbox and a sciencebox at Uni Mail, UniGE. (b) Work of art, result of collaboration between Etienne Krähenbühl and technicians and scientists of MaNEP. (c) Illuminated panels presenting the secrets of superconductivity. (d) The demonstration on storage of energy, the flywheel.*

with its own session. However many MaNEP members were directly or indirectly active during the SPS meeting, which took place in Lausanne in June 2011 and which also celebrated this anniversary. A series of talks was given about the development of this exciting field in the past years, with a plenary talk by MaNEP's Director, Øystein Fischer, and two invited talks given by members of MaNEP, Dionys Baeriswyl (UniFR) and Andreas Schilling (UniZH). A lively round table chaired by Hugo Keller (UniZH), another member of MaNEP, was also organized, with five invited speakers and two Nobel laureates (Fig. 2). Roughly 200 scientists attended this session (about 650 in total). The MaNEP Mix&Remix exhibition on superconductivity was displayed in the hall, promoting both superconductivity and MaNEP.

SUPRA100 exhibition

In Geneva, the festivities continued into autumn. Firstly, with the SUPRA100 exhibition that was held in the building of Uni Mail, from September 14 to November 12, 2011 (Fig. 3a). This art & science exhibition is the result of a collaboration that began in 2007 between MaNEP researchers and technicians and the Swiss artist Etienne Krähenbühl. The world première of a sculpture that flirts with superconductivity was revealed by the Swiss artist, well known for his work that mixes novel and surprising materials. In the artbox, a large sphere hovers over a flat square surface. It moves randomly. The surface slopes at an angle so the sphere should drop, but remains suspended in the air. This is the magic of superconductivity that plunges the spectator into a parallel universe where superconducting wires float like clouds (Fig. 3b).

Visitors moved on to the sciencebox where a scientific presentation complemented the artistic part of the exhibition revealing the secrets of superconductivity on illuminated panels (Fig. 3c). While mirroring this unusual work of art, its current applications were illustrated, and those of the future which may transform and revolutionize our daily lives. Two demonstrations showed superconductivity in action (Fig. 3d). Visitors enjoyed an interactive, entertaining and instructive visit.

Special events were organized for young audiences. Accompanied by a qualified guide,

1000 primary school children were able to discover the secrets of superconductivity. These lively activities were more than just the passing on of scientific knowledge; they were an opportunity for children to enjoy science as a creative and dynamic activity. One hour visits conducted by specialists from the PhysiScope and the Physics Section of UniGE were also offered to secondary school students as well as to the general public.
About 9'500 visitors, including many school classes visited this exhibition.
This exhibition presented on the one hand an underrated but essential physics phenomenon in an original way for the future, and on the other hand played an important part in bringing researchers and the public together.
SUPRA100 may be able to travel.

A documentary between art and science

A film *SUPRA100, Le temps suspendu* (Fig. 4) was made, showing the incredible adventure and encounter between MaNEP technicians and scientists and the artist Etienne Krähenbühl. Several shootings took place between 2008 and 2011 and the result is not only an opportunity to discover superconductivity from a hitherto unexplored perspective but also a wonderful and useful tool of communication for MaNEP.

Figure 4: *Cover of the DVD* SUPRA100, Le temps suspendu, *a documentary projected during the exhibition and showing the surprising encounter between art and science.*

Levitarium Museum with Exos

As part of the *Bâtie Festival* of Geneva, a partnership was arranged to set up a show with the theatrical company EXOS. EXOS has been collaborating with MaNEP since 2007 to create surprising superconductivity effects. This company which is at the cross roads between theater, movement, dance and circus, has joined forces with physicists to offer a show which demonstrates magic and levitation, mixing superconductivity and visual effects. The *Levitarium Museum* performance was played eight times to a full house and to critical acclaim from September 14 to 17, 2011.

Saturday for families

Another of the successes was *Fascinante supra*, a Saturday for families event (Fig. 5) organized in collaboration with the PhysiScope and EurophysicsFun on September 17. For five hours, more than 1200 people turned up to join in with the many workshops and demonstrations organized by the University of Geneva, and by more than 100 MaNEP collaborators and stu-

Figure 5: *Saturday for families. Top: the very successful* Rino-Leiden *show. Bottom: People discovering advantages of superconductivity in transports.*

dents who worked together to guarantee the success of this great event. Enigmas, mini-conferences, all sorts of experiments, laboratory visits were proposed in the afternoon's programme including a fun introduction to superconductivity.

Conference on superconductivity and energies of the future

At the beginning of the academic semester of the University of Geneva, on September 20, MaNEP invited the President of the Japanese Agency for Science and Technology, Professor Koichi Kitazawa. As an international expert, K. Kitazawa discussed the major role that high temperature superconductors can play with the energies of the future (Fig. 6). 450 people attended this most rewarding conference that raised many questions to solve energy problems.

Figure 6: *International expert Koichi Kitazawa was invited by MaNEP for a grand conference on energies of the future.*

SupraLunch

The cultural activities of the University of Geneva together with MaNEP offered five SupraLunches around the theme of superconductivity, every Thursday from October 6 to November 3, 2011. Guided tours and conferences allowed students of all faculties to get together around the theme of superconductivity to achieve a better understanding of this phenomenon.

Superconductivity at PSI

During the PSI Open House day, on October 16, 2011, about 900 visitors discovered the mysteries of superconductivity (about 10'000 visitors in total). Old pictures from the archives of the Kamerlingh Onnes Lab (superconductivity discoverer) were displayed in the neutron hall (Fig. 7), surrounded by instruments and movies of Leiden at the beginning of the last century. At various times of the day scientists gave a presentation on the importance of superconductivity mixed with "tricks" by the *Rino* show from Leiden . The public also enjoyed the superconducting train of the University of Zurich.

Figure 7: *Presentation on superconductivity at the PSI open day.*

And more...

MaNEP was also present at the Daniel Dautreppe workshop on *Current challenges of superconductivity* organized by the French Society of Physics (section of the Alps) from 21 to 25 November 2011, in Grenoble. This workshop compiled a vast panorama of the advances in basic and applied research in this area based on a series of courses as well as presentations at the forefront of current research by well-known experts, including members of MaNEP.

The outcome of all the events about superconductivity was very positive. A broad audience, as well as major media coverage, illustrated the value of the work carried out, as much regarding superconductivity as well as more globally regarding electronic materials. Important events that brought together the world of research and the public contributed to ensuring important internal communications and strengthening ties between MaNEP's collaborators.

Figure 8: *Superconductivity centennial events were very well covered by the media.*

Figure 9: *Information booth on thermoelectrics at* Scientifica*, Zurich*

Superconductivity and media

MaNEP and the University of Geneva held two press conferences, one on April 7 (Fig. 8) and the other on September 14. The first one was given jointly with the CERN. More than ten articles were published in newspapers in Switzerland — namely *Bilan*, *Le Temps*, *Tribune de Genève*, *Entreprises romandes*, *Revue Technique Suisse*, *Les Clés de l'école*, etc. — targeting industry, schools as well as the general public. Nine radio broadcasts on the *Radio Télévision Suisse* and six televisions broadcasts on *Radiotelevisione svizzera*, *Radio Télévision Suisse* and *Léman Bleu* also strongly promoted all these events, as well as the MaNEP trademark. A special partnership with the (*Radio Télévision Suisse*) was set up and 13 short films were shot on superconductivity. These trailers, which show some experiments carried out in the PhysiScope as well as interviews with scientists, can be found on www.rts.ch/decouverte/dossiers/2011/supraconductivite/.
The press review of events can be viewed on www.manep.ch/en/supra/#supramedia.

5.2 Scientifica, science days in Zurich

The *Scientifica* science days took place in ETHZ and the University of Zurich from 26 to 28 August, 2011. Starting with robots over geothermal energy and metabolites, nearly all topics of current research were covered. The laboratory of solid-state chemistry and catalysis led by Anke Weidenkaff (Empa) and the working groups of Bertram Batlogg (ETHZ) and Manfred Sigrist (ETHZ) installed an information booth on thermoelectrics (Fig. 9). On the stand with the slogan *How does heat convert into electricity?* an overview was given about the theory of thermoelectrics as well as insights into current research projects. With the aid of small, vivid experiments and demonstrations, a bridge from theory to practice was built. This was fascinating to both young and old. While children were captivated by the hands-on experiments, the older audience's thirst for knowledge concerning this relatively unknown field of research was also satisfied. The *Scientifica* was a great success as ongoing research was presented not only to specialists but to the public as well.

5.3 MaNEP in the media

Three discoveries were the subject of press releases in January and February 2012, informing the media about MaNEP's innovative developments. The first two, "Oxides prepare their revolution" and "Quantum computer: a theoretical Genevese model validated by a German experiment", published respectively in *Nature Materials* and in *Nature*, were observed at the University of Geneva. The third one "It works: Ultrafast magnetic processes observed 'live' using an X-ray laser" was made at PSI. These discoveries were reported in the media. Last spring the PSI also published two press releases "The electron torus can help us to understand high temperature" and "Der Unterschied zwischen dünn und sehr dünn".
Moreover, MaNEP strengthened its visibility in the private sector with a special article published in the Geneva Chamber of Commerce's journal, *CCIGinfo*, with a vivid description of its innovative activities.

5.4 Several other outreach activities in year 11

MaNEP researchers continued to be active with many different audiences. On the occasion of the superconductivity centennial, many scientists were invited to give talks at scientific conferences but also to the public, in Geneva, Switzerland and elsewhere. MaNEP experts were also invited to deliver conferences on other topics, like Joël Mesot "From fundamental research to applications, examples from the PSI" at the *Austrian academy of sciences* in October 2011, "Quelle est l'importance de la recherche fondamentale pour notre société ?" at the *Club des quatre saisons* in Zurich in April 2011, or "The status and perspectives of collaborations between the PSI and the Chinese academy of sciences" at the *7th Chinese association of science and technology in Switzerland general assembly* in September 2011. Christoph Renner also gave a talk in May 2011 at *les Causeries du Rotary* in Geneva entitled "Les nanotechnologies, promesses ou menaces". On March 12, 2012, Joël Mesot and Øystein Fischer participated in the third conference of the cycle *Vers un accès durable à l'énergie ? Le regard des scientifiques* organised by the Institut National Genevois and the Faculty of Science of UniGE. Their talks were entitled "Le PSI : une expertise au profit des énergies du futur " and "Supraconductivité et défis énergétiques : un avenir à portée de main", respectively.
The website and the e-newsletter are still playing a key role in disseminating information to various MaNEP audiences and its Forum.

6 Structural aspects

MaNEP quickly approaches the end of the 12-year finance period foreseen by the SNSF NCCR concept. We are therefore now actively preparing the continuation of MaNEP's activities after the end of this period. As described in detail in the last report, the future of MaNEP will follow two different routes: a) the stabilization of MaNEP Geneva, and b) an effort to maintain the MaNEP national network.

6.1 The stabilization of MaNEP Geneva

Since the beginning of MaNEP, the University of Geneva and the cantonal authorities have taken measures to support MaNEP after the NCCR period, preparing thus the terrain for a strong activity in the field of MaNEP after the final deadline of the federally financed NCCR MaNEP in 2013.

Financial aspects

MaNEP has by now received an annual budget from the University of Geneva amounting to a total of 3'850'000 CHF of which 1'495'00 comes from the *Convention d'objectifs* 2009 - 2011. We are in addition in the process of establishing an additional budget of 500'000 CHF for MaNEP, coming from the budget of the first year of the *Convention d'objectifs* 2012 - 2015. The appointment of personnel on this budget is presently underway. At the end of this process, the University shall have established a yearly budget for continuing the activities of MaNEP of 4'350'000 CHF, in agreement with the engagement taken by the University on March 30, 2009.

Human resources, professor positions

In addition to the professor appointments already made during MaNEP existence (Thierry Giamarchi, Dirk van der Marel, Christoph Renner, Patrycja Paruch, Alberto Morpurgo, Corinna Kollath), this year has seen the appointment of Antoine Georges as full professor who will spend 20% of his time in Geneva. Radovan Černý was appointed as associate professor responsible for the crystallography laboratory. Furthermore, as announced earlier, the succession of Prof. Klaus Yvon has been oriented in the direction of MaNEP. The opening of a position has been announced and the selection process is now in its final stages. This appointment is carried out in close collaboration with the Paul Scherrer Institute (PSI) and the result may be a split appointment of two professors between the two institutions.

Institutional stabilization of MaNEP Geneva

As explained in last year's report, MaNEP has been the initiator and the cornerstone of the development of a project to establish a new Center for astronomical, physical and mathematical sciences in Geneva. One key element of this new center is to integrate scientifically these activities in order to stimulate synergies between units that do not have a tradition to interact. This center shall thus build on the very strong activities in Geneva these various fields to establish an even higher scientific level. For MaNEP this means to be reinforced even more, and thus to guaranty the establishment of a long-term activity based on the past 12 years of federal support. This new center shall also have a strong new outreach center called "ScienScope" and a "Laboratory of advanced technology" for applied projects between the University of Geneva, the university of applied sciences (HES-SO) in Geneva and industry. This must be seen as a result, a continuation and a reinforcement of MaNEP's success in the field of "other activities".

To achieve these goals a new building is being planned. This part of the project has been elaborated based on a convention between the Canton of Geneva, the Foundation Hans Wils-

dorf, Rolex SA, the University of Geneva, and the university of applied sciences (HES-SO) in Geneva. This project proposes to use the present military exercise grounds at les Vernets to install the new center in addition to the construction of 1000 apartments, which Geneva needs strongly. The project was presented to the Geneva government on January 31, 2012 and presently discussions are underway to see how and if this project can be implemented on this site.

Concerning MaNEP, and as a first step imposed by the date of 30 June 2013 when the federal support of MaNEP ends, a project of institutionalizing MaNEP is in preparation. The main concern is to define how MaNEP will continue in Geneva in the coming years, before entering the new center, and how its institutional base shall be defined with respect to the present Department of Condensed Matter Physics, MaNEP's leading house. The plan is to clarify this question during the coming months and then to carry out the formal steps during the academic year 2012 – 2013.

6.2 The MaNEP network

In the report last year, we described the efforts we have deployed to establish a network research program to follow MaNEP. The proposal NEXT was submitted to the Swiss National Science Foundation on March 5, 2011, by the NCCR Climate and the NCCR MaNEP. A roundtable discussion then took place on May 3, 2011 between representatives of MaNEP and the NCCR Climate on the one hand, and representatives of Division 4 of SNSF on the other. Following this the SNSF examined these proposals, but decided not to enter into a real consideration of these requests, based on the policy that it is not the role of SNSF to follow up the continuation of the NCCR after the 12 years period. Instead it was proposed that another national institution, the Swiss university conference (SUK·CUS), could take up the challenge to finance this type of projects. Unfortunately, for the next federal budgetary period 2013 – 2016, it was too late to seriously consider this possibility. We suggest, however, that the SNSF enters rapidly into preliminary discussions on this topic for the next fiscal period 2017 – 2020. The absence of a policy on the federal level to support the very best national networks is clearly an important aspect that is missing from the otherwise successful NCCR program.

Faced with the situation that no federal institution is presently ready to finance excellence networks beyond the NCCR, MaNEP is presently preparing for the establishment of an association of institutions and/or individual researchers in the field of MaNEP. The MaNEP Forum approved the principle of such an association on January 11, 2012 and the scientific committee is now working on the practical realization of such a structure. This association will be financed by its members, especially on the institutional level, and shall have the task to organize conferences, workshops, winter/summer schools, summer internships, and other events earlier organized by MaNEP. It will also constitute a Forum to discuss and coordinate various initiatives to financially support the research in the field of MaNEP in the future. The association shall in one way or another carry the name of MaNEP in order to benefit from the trademark established now over 11 years.

Since the new call for NCCR projects explicitly excludes the possibility of continuing MaNEP, we have renounced to submit such a proposal. However several new proposals, not based on MaNEP but nevertheless implying some of its members, have been submitted.

7 Management

7.1 Activities

Throughout year 11 MaNEP's management has been active in every aspect of its operations on the one hand, and has been increasingly involved in preparing the future of MaNEP after 2013, on the other hand.

MaNEP management in 2011

As of August 1, 2011, Edward Coutureau has been employed full time with MaNEP to assist in the development of the plans for the continuation of MaNEP after 2013. MaNEP management is very grateful to Michel Decroux for presiding over the advancement of women program and the summer/winter schools. In January 2012 he handed over the responsibility of these two projects to Lidia Favre-Quattropani and Christophe Berthod, respectively.

During the superconductivity centennial events, Lidia Favre-Quattropani's employment was temporarily increased to 60% from April 1, 2011 to January 31, 2012. David Parietti who assisted Adriana Bonito Aleman in the communications department during the superconductivity centennial festivities left MaNEP as planned at the end of January 2012. From February 1, 2012 he was replaced by Mehregan Joseph who will be helping with communication issues related to the official end of the NCCR.

MaNEP has invited Professors Vladimir Falko (Lancaster University) and Stewart Barnes (University of Miami) for the summer semester 2012. The crystallography laboratory is currently being integrated into MaNEP. The MaNEP administration has been involved in the process of recruiting the successor of Prof. Klaus Yvon. Radovan Černý, who has been running the laboratory since the retirement of Prof. Yvon, has been promoted to associate professor. He is now a full member of MaNEP and has been appointed to Project 3 "Electronic materials for energy systems and other application" lead by Øystein Fischer.

Stabilizing MaNEP after 2013 — what this will mean for the management?

The project for a new Center for astronomical, physical and mathematical sciences in Geneva is the brainchild of MaNEP to ensure that the 12-year investment of the SNSF continues to have an impact on the research field of MaNEP. As mentioned in last year's report, the future of MaNEP in Geneva will be achieved by reinforcing the fields of astronomy, physics and mathematics. Prof. Øystein Fischer is responsible for the new budget for the target agreement COB (*Convention d'objectifs sciences physiques et mathématiques*). Marie Bagnoud, as administrator of MaNEP, will oversee the administration of the budget. The first COB 2009 – 2011 is now complete and we are presently working on the second COB 2012 – 2015. Prof. Fischer has been commissioned by the *Rectorat* to elaborate plans for the new Center for astronomical, physical and mathematical sciences. MaNEP administration has also been highly active in this process.

MaNEP has been provided with an excellent opportunity to be involved in the *economic stimulus packages* introduced by the SNSF, albeit considerably increasing the workload. The integration process has been very successful and actually increased the KTT activity for this period. MaNEP management was also involved in compiling and ranking the proposals for the new SNSF *transfer projects 2012*. Six *transfer projects* were submitted to the SNSF on February 15, 2012.

The KTT activity has led to several CTI projects and the MaNEP management is taking care of the administration of these funds.

As we approach the end of MaNEP there is increased pressure on the financial situation which has also resulted in an increase of the workload for the MaNEP administration. We have to keep track on the detailed financial situation of the large number of financial projects to assure that they all tally on June 30, 2013.
Whereas the science projects will continue after June 30, 2013, this date marks a discontinuity for the MaNEP management. We are presently working on how we can make use of the high competence of the MaNEP management, developed over the 12 years, in a constructive and dynamic way after the end of the NCCR MaNEP.

Events organized by MaNEP management

The **Swiss Workshop on Materials with Novel Electronic Properties (SWM 2011)**, basic research and applications, was held at Les Diablerets from June 29 to July 1, 2011. Of the 192 participants, 80 were PhD students. New to this edition were tutorial courses aimed at PhD students that took place the day before the workshop on scanning probes, single crystal growth and thin films in the frame of the techniques and know-how activity. 41 participants attended the tutorial sessions of whom 32 were PhD students and 9 were postdocs. These meetings were entirely organized by the MaNEP management.
The **Scientific Committee** was held on December 22, 2011 in Berne and a second meeting is planned for April 2012. The committee is composed of the director, two deputy directors, the project leaders plus two additional members appointed by the director, namely: Leonardo Degiorgi (ETHZ), Øystein Fischer (UniGE), director, László Forró (EPFL), Thierry Giamarchi (UniGE), Dirk van der Marel (UniGE), deputy director, Frédéric Mila (EPFL), Alberto Morpurgo (UniGE), Christoph Renner (UniGE), deputy director, Manfred Sigrist (ETHZ), Jean-Marc Triscone (UniGE), Urs Staub (PSI), Andrey Zheludev (ETHZ). The main topic of these meetings is the preparation of a new association to continue the MaNEP network.
There was an excellent turnout of MaNEP Forum members for the **MaNEP Forum** held in Neuchâtel on January 11, 2012. Radovan Černý (UniGE), Manfred Fiebig (ETHZ), Corinna Kollath (UniGE), Christian Rüegg (PSI), Nicola Spaldin (ETHZ), Philipp Werner (UniFR) joined the MaNEP Forum as full members and Carmine Senatore (UniGE) as associate member. The principle of establishing an association to continue the MaNEP network was approved.
The MaNEP **Internal Workshops** took place in Neuchâtel on January 10, 11, 12 and 19, 2012. The eight MaNEP scientific projects, as well as the collaborative projects, were discussed among the main participants of each project. This resulted in lively and stimulating discussions during the whole workshops. These meetings are the basis for the elaboration of the scientific report, which each MaNEP member had to send in by January 27, 2012.
In order to elaborate the scientific basis for the new Center for astronomical, physical and mathematical sciences in Geneva a retreat took place in les Diablerets from March 31 until April 2, 2011 with all the professors concerned with this project. As MaNEP has the lead in this development the MaNEP management was directly involved in its organization. An important issue at this meeting was to discuss new perspectives as to how MaNEP Geneva may continue after 2013, and how this initiative may support national networks in the respective field, in particular the MaNEP network.
The **fifth MaNEP Winter School 2013** will take place from January 13 to 19, 2013 in Saas-Fee. A scientific committee has been set up to organize the program and MaNEP management is preparing the administrative and logistic organization.
The **MaNEP Management Committee** meets once a month to discuss and monitor the evolution of MaNEP's daily activities: events, meetings, newsletters, accounting, KTT, education, doctoral school, advancement of women, communications, etc. These meetings are essential to keep the vast MaNEP organization informed.

Events and meetings co-organized by MaNEP management

MaNEP and the University of Geneva celebrated the **100th anniversary of the discovery of superconductivity**. From April to September 2011, MaNEP management was actively involved with the University of Geneva and CERN in all events as well as the organization of the SUPRA100 exhibition including the world première of a work of art by sculptor Etienne Krähenbühl displaying superconducting levitation.
The **Topical meeting** on *Topological properties of electronic materials* took place on May 6, 2011 at the University of Geneva. This meeting was co-organized with MaNEP management and

ETHZ.
The **Review Panel** met in Geneva on May 30–31, 2011. The meeting was organized by the Swiss National Science Foundation as a collaboration between Dr. Stefan Bachmann and the management team of MaNEP.
The MaNEP advancement of woman **summer internship program** and the **student exchange program** awarded 10 new fellowships last summer. The emphasis is on training and encouraging students to advance towards a PhD in physics. MaNEP management oversees every aspect of this program.

The **Swiss Physical Society (SPS) annual meeting** will take place on June 21–22, 2012 in the University of Basel. Every other year MaNEP is present and this year will organize a special session with its own invited speakers. There will be a large number of participants and poster talks.
The *Nuit de la Science* will take place in Geneva on July 7–8, 2012. MaNEP management, the Physics Section and the PhysiScope will join forces with enthusiasm to develop this great event and continue to promote physics in Geneva.

7.2 Experiences, recommendations to the SNSF

MaNEP management's workload increased enormously to prepare the home institution reporting for the SNSF financial accounting audit on November 24, 2011 in Geneva. NIRA 2.0 is an improvement from the previous version but the system remains globally too slow when executing recordings of its various features.

8 Reactions to the recommendations of the Review Panel

The comments of the Review Panel after the last meeting were overwhelmingly positive and MaNEP and its members are of course extremely pleased hearing these constructive and encouraging comments. The MaNEP director and all the members of MaNEP would like here to express their appreciation of the thorough and thoughtful advice that has come from the members of the Review Panel over the soon 12 years of service.

The Review Panel gave advice on one aspect this time, which is on the procedure of how to proceed to continue the network. We shall here explain what we have done.

After the NEXT proposal was turned down by the SNSF (they clearly did not listen to the advice of the Review Panel), we did first explore the proposed approach consisting of sending in a proposal to SUK/CUS. The problem here was that for sending in such a proposal, the institutions participating in MaNEP would have to commit in writing considerable funds. Within the limited time available, such an action had no chance to succeed. However, the approach we have chosen, i.e. to establish an association, will allow having a Forum where a proposal to the Swiss university conference (SUK·CUS) can be prepared well in time for the next federal fiscal period 2017 – 2020. Since the new call for NCCR projects explicitly excludes the possibility of continuing MaNEP, we have renounced to submit such a proposal. However several new proposals, not based on MaNEP but nevertheless implying some of its members, have been submitted. Since these proposals are indeed different from MaNEP, we do not describe them in this report.

There is no contradiction between the establishment of the association and the possibility of some of these new NCCR to be accepted. If this situation should materialize, synergies between the association and the NCCR would be developed, as common conferences, education initiatives, etc. This would thus allow to have focused NCCR projects and, at the same time, a broad network, which is essential to the field to be able to pick up changes in the scientific development.

And we promise to try hard to keep up the good work!

9 Lists

9.3 Publications over the last period

The following lists cover the period from April 1st, 2011 to March 31st, 2012:

1. Scientific articles in journals with peer review
2. Scientific articles in journals without peer review
3. Scientific articles in anthologies
4. Publications from lists 1 and 2 involving several groups

The fist two lists are sorted by the name of the group leaders. The most important publications are outlined by a red mark.

9.3.1 Scientific articles in journals with peer review

Group of Ph. Aebi

▶ C. Monney, C. Battaglia, H. Cercellier, P. Aebi, and H. Beck
Exciton Condensation Driving the Periodic Lattice Distortion of 1T-$TiSe_2$
Physical Review Letters **106**, 106404 (2011).
Group(s): Aebi / Project(s): 7

E. F. Schwier, C. Monney, N. Mariotti, Z. Vydrovà, M. García-Fernández, C. Didiot, G. M. G., and P. Aebi
Influence of elastic scattering on the measurement of core-level binding energy dispersion in X-ray photoemission spectroscopy
The European Physical Journal B **81**, 399 (2011).
Group(s): Aebi / Project(s): 7

C. Battaglia, E. F. Schwier, C. Monney, C. Didiot, N. Mariotti, K. Gaál-Nagy, G. Onida, M. Garnier Gunnar, and P. Aebi
Valence band structure of the Si(331)-(12 × 1) surface reconstruction
Journal of Physics: Condensed Matter **23**, 135003 (2011).
Group(s): Aebi / Project(s): 7

Group of D. Baeriswyl

D. Baeriswyl
Adiabatic continuity and broken symmetry in many-electron systems: A variational perspective
Annalen der Physik (Leipzig) **523**, 724 (2011).
Group(s): Baeriswyl / Project(s): 4

D. Baeriswyl
Superconductivity in the Repulsive Hubbard Model
Journal of Superconductivity and Novel Magnetism **24**, 1157 (2011).
Group(s): Baeriswyl / Project(s): 4

Group of B. Batlogg

▶ R. Häusermann and B. Batlogg
Gate bias stress in pentacene field-effect-transistors: Charge trapping in the dielectric or semiconductor
Applied Physics Letters **99**, 083303 (2011).
Group(s): Batlogg / Project(s): 2

N. D. Zhigadlo, S. Katrych, M. Bendele, P. J. W. Moll, M. Tortello, S. Weyeneth, V. Y. Pomjakushin, J. Kanter, R. Puzniak, Z. Bukowski, H. Keller, R. S. Gonnelli,

R. KHASANOV, J. KARPINSKI, AND B. BATLOGG
Interplay of composition, structure, magnetism, and superconductivity in $SmFeAs_{1-x}P_xO_{1-y}$
Physical Review B **84**, 134526 (2011).
Group(s): Batlogg, Karpinski, Keller / Project(s): 4

P. J. W. MOLL, J. KANTER, R. D. MCDONALD, F. BALAKIREV, P. BLAHA, K. SCHWARZ, Z. BUKOWSKI, N. D. ZHIGADLO, S. KATRYCH, K. MATTENBERGER, J. KARPINSKI, AND B. BATLOGG
Quantum oscillations of the superconductor $LaRu_2P_2$: Comparable mass enhancement $\lambda \approx 1$ in Ru and Fe phosphides
Physical Review B **84**, 224507 (2011).
Group(s): Batlogg, Karpinski / Project(s): 4

S. WEYENETH, P. J. W. MOLL, R. PUZNIAK, K. NINIOS, F. F. BALAKIREV, R. D. MCDONALD, H. B. CHAN, N. D. ZHIGADLO, S. KATRYCH, Z. BUKOWSKI, J. KARPINSKI, H. KELLER, B. BATLOGG, AND L. BALICAS
Rearrangement of the antiferromagnetic ordering at high magnetic fields in SmFeAsO and $SmFeAsO_{0.9}F_{0.1}$ single crystals
Physical Review B **83**, 134503 (2011).
Group(s): Batlogg, Karpinski, Keller / Project(s): 4

P. H. TOBASH, F. RONNING, J. D. THOMPSON, B. L. SCOTT, P. J. W. MOLL, B. BATLOGG, AND E. D. BAUER
Single crystal study of the heavy-fermion antiferromagnet $CePt_2In_7$
Journal of Physics: Condensed Matter **24**, 015601 (2012).
Group(s): Batlogg / Project(s): 4

J. ZHANG, A. BELOUSOV, J. KARPIŃSKI, B. BATLOGG, G. WICKS, AND R. SOBOLEWSKI
Time-resolved femtosecond optical characterization of multi-photon absorption in high-pressure-grown $Al_{0.86}Ga_{0.14}N$ single crystals
Journal of Applied Physics **110**, 113112 (2011).
Group(s): Batlogg, Karpinski / Project(s): 4

Group of Ch. Bernhard

P. D. ROGERS, Y. J. CHOI, E. C. STANDARD, T. D. KANG, K. H. AHN, A. DUBROKA, P. MARSIK, C. WANG, C. BERNHARD, S. PARK, S.-W. CHEONG, M. KOTELYANSKII, AND A. A. SIRENKO
Adjusted oscillator strength matching for hybrid magnetic and electric excitations in $Dy_3Fe_5O_{12}$ garnet
Physical Review B **83**, 174407 (2011).
Group(s): Bernhard / Project(s): 1

▶ A. V. BORIS, Y. MATIKS, E. BENCKISER, A. FRANO, P. POPOVICH, V. HINKOV, P. WOCHNER, M. CASTRO-COLIN, E. DETEMPLE, V. K. MALIK, C. BERNHARD, T. PROKSCHA, A. SUTER, Z. SALMAN, E. MORENZONI, G. CRISTIANI, H.-U. HABERMEIER, AND B. KEIMER
Dimensionality Control of Electronic Phase Transitions in Nickel-Oxide Superlattices
Science **332**, 937 (2011).
Group(s): Bernhard, Morenzoni / Project(s): 1

▶ A. DUBROKA, M. RÖSSLE, K. W. KIM, V. K. MALIK, D. MUNZAR, D. N. BASOV, A. A. SCHAFGANS, S. J. MOON, C. T. LIN, D. HAUG, V. HINKOV, B. KEIMER, T. WOLF, J. G. STOREY, J. L. TALLON, AND C. BERNHARD
Evidence of a Precursor Superconducting Phase at Temperatures as High as 180 K in $RBa_2Cu_3O_{7-\delta}$ (R = Y, Gd, Eu) Superconducting Crystals from Infrared Spectroscopy
Physical Review Letters **106**, 047006 (2011).
Group(s): Bernhard / Project(s): 1

F. J. OWENS, L. GLADCZUK, R. SZYMCZAK, P. DLUZEWSKI, A. WISNIEWSKI, H. SZYMCZAK, A. GOLNIK, C. BERNHARD, AND C. NIEDERMAYER
High temperature magnetic order in zinc sulfide doped with copper
Journal of the Physics and Chemistry of Solids **72**, 648 (2011).
Group(s): Bernhard, Niedermayer / Project(s): 1

▶ L. SCHULZ, M. WILLIS, L. NUCCIO, P. SHUSHAROV, S. FRATINI, F. L. PRATT, W. P. GILLIN, T. KREOUZIS, M. HEENEY, N. STINGELIN, C. A. STAFFORD, D. J. BEESLEY, C. BERNHARD, J. E. ANTHONY, I. MCKENZIE, J. S. LORD, AND A. J. DREW
Importance of intramolecular electron spin relaxation in small molecule semiconductors
Physical Review B **84**, 085209 (2011).
Group(s): Bernhard / Project(s): 1

B. M. WOJEK, E. MORENZONI, D. G. ESHCHENKO, A. SUTER, T. PROKSCHA, H. KELLER, E. KOLLER, Ø. FISCHER, V. K. MALIK, C. BERNHARD, AND M. DÖBELI
Magnetism, superconductivity, and coupling in cuprate heterostructures probed by low-energy muon-spin rotation
Physical Review B **85**, 024505 (2012).
Group(s): Bernhard, Fischer, Keller, Morenzoni / Project(s): 1, 4

Group of G. Blatter

- A. J. Hoffman, S. J. Srinivasan, S. Schmidt, L. Spietz, J. Aumentado, H. E. Türeci, and A. A. Houck
  Dispersive Photon Blockade in a Superconducting Circuit
  Physical Review Letters **107**, 053602 (2011).
  Group(s): Blatter / Project(s): 8

M. Hohenadler, M. Aichhorn, S. Schmidt, and L. Pollet
Dynamical critical exponent of the Jaynes-Cummings-Hubbard model
Physical Review A **84**, 041608(R) (2011).
Group(s): Blatter, Troyer / Project(s): 8

M. Hohenadler, M. Aichhorn, L. Pollet, and S. Schmidt
Polariton Mott insulator with trapped ions or circuit QED
Physical Review A **85**, 013810 (2012).
Group(s): Blatter, Troyer / Project(s): 8

Group of M. Büttiker

- J. Li, I. Martin, M. Büttiker, and A. F. Morpurgo
  Marginal topological properties of graphene: a comparison with topological insulators
  Physica Scripta **T146**, 014021 (2012).
  Group(s): Büttiker, Morpurgo / Project(s): 2

Group of M. Decroux

- L. Antognazza, M. Decroux, M. Therasse, and M. Abplanalp
  Heat Propagation Velocities in Coated Conductors for Fault Current Limiter Applications.
  IEEE Transactions on Applied Superconductivity **21**, 1213 (2011).
  Group(s): Abplanalp, Decroux / Project(s): 3

Group of L. Degiorgi

- A. Dusza, A. Lucarelli, F. Pfuner, J.-H. Chu, I. R. Fisher, and L. Degiorgi
  Anisotropic charge dynamics in detwinned $Ba(Fe_{1-x}Co_x)_2As_2$
  Europhysics Letters **93**, 37002 (2011).
  Group(s): Degiorgi / Project(s): 4

- A. Dusza, A. Lucarelli, A. Sanna, S. Massidda, J.-H. Chu, I. R. Fisher, and L. Degiorgi
  Anisotropic in-plane optical conductivity in detwinned $Ba(Fe_{1-x}Co_x)_2As_2$
  New Journal of Physics **14**, 023020 (2012).
  Group(s): Degiorgi / Project(s): 4

L. Degiorgi
Electronic correlations in iron-pnictide superconductors and beyond: lessons learned from optics
New Journal of Physics **13**, 023011 (2011).
Group(s): Degiorgi / Project(s): 4

F. Pfuner, S. N. Gvasaliya, O. Zaharko, L. Keller, J. Mesot, V. Pomjakushin, J.-H. Chu, I. R. Fisher, and L. Degiorgi
Incommensurate magnetic order in $TbTe_3$
Journal of Physics: Condensed Matter **24**, 036001 (2012).
Group(s): Degiorgi, Mesot / Project(s): 7

I. R. Fisher, L. Degiorgi, and Z. X. Shen
In-plane electronic anisotropy of underdoped '122' Fe-arsenide superconductors revealed by measurements of detwinned single crystals
Reports on Progress in Physics **74**, 124506 (2011).
Group(s): Degiorgi / Project(s): 4

A. Sanna, F. Bernardini, G. Profeta, S. Sharma, J. K. Dewhurst, A. Lucarelli, L. Degiorgi, E. K. U. Gross, and S. Massidda
Theoretical investigation of optical conductivity in $Ba(Fe_{1-x}Co_x)_2As_2$
Physical Review B **83**, 054502 (2011).
Group(s): Degiorgi / Project(s): 4

Group of T. Esslinger

- D. Greif, L. Tarruell, T. Uehlinger, R. Jördens, and T. Esslinger
  Probing Nearest-Neighbor Correlations of Ultracold Fermions in an Optical Lattice
  Physical Review Letters **106**, 145302 (2011).
  Group(s): Esslinger / Project(s): 8

Group of Ø. Fischer

- A. Piriou, N. Jenkins, C. Berthod, I. Maggio-Aprile, and Ø. Fischer
  First direct observation of the Van Hove singularity in the tunneling spectra of cuprates
  Nature Communications **2**, 221 (2011).
  Group(s): Fischer, Giamarchi / Project(s): 4

B. M. Wojek, E. Morenzoni, D. G. Eshchenko, A. Suter, T. Prokscha, H. Keller, E. Koller, Ø. Fischer, V. K. Malik, C. Bernhard, and M. Döbeli

Magnetism, superconductivity, and coupling in cuprate heterostructures probed by low-energy muon-spin rotation

Physical Review B **85**, 024505 (2012).
Group(s): Bernhard, Fischer, Keller, Morenzoni / Project(s): 1, 4

Group of R. Flükiger and C. Senatore

R. Flükiger, M. S. A. Hossain, C. Senatore, F. Buta, and M. Rindfleisch
A New Generation of In Situ MgB_2 Wires With Improved J_c and B_{irr} Values Obtained by Cold Densification (CHPD)
IEEE Transactions on Applied Superconductivity **21**, 2649 (2011).
Group(s): Flükiger/Senatore / Project(s): 3

C. Scheuerlein, M. Di Michiel, G. Arnau, R. Flükiger, F. Buta, I. Pong, L. Oberli, and L. Bottura
Coarse Nb_3Sn Grain Formation and Phase Evolution During the Reaction of a High Sn Content Internal Tin Strand
IEEE Transactions on Applied Superconductivity **21**, 2554 (2011).
Group(s): Flükiger/Senatore / Project(s): 3

J. Viljamaa, M. Kulich, P. Kováč, T. Melišek, and M. Reissner
Comparison on Effects of B_4C, Al_2O_3, and SiC Doping on Performance of MgB_2 Conductors
IEEE Transactions on Applied Superconductivity **21**, 2659 (2011).
Group(s): Flükiger/Senatore / Project(s): 3

L. Muzzi, V. Corato, A. della Corte, G. De Marzi, T. Spina, J. Daniels, M. Di Michiel, F. Buta, G. Mondonico, B. Seeber, R. Flükiger, and C. Senatore
Direct observation of Nb_3Sn lattice deformation by high-energy X-ray diffraction in internal-tin Nb_3Sn wires subject
to be published in Superconductor Science & Technology (2012).
Group(s): Flükiger/Senatore / Project(s): 3

C. Senatore, M. S. A. Hossain, and R. Flükiger
Enhanced Connectivity and Percolation in Binary and Doped In Situ MgB_2 Wires After Cold High Pressure Densification
IEEE Transactions on Applied Superconductivity **21**, 2680 (2011).
Group(s): Flükiger/Senatore / Project(s): 3

B. Bordini, L. Bottura, G. Mondonico, L. Oberli, D. Richter, B. Seeber, C. Senatore, E. Takala, and D. Valentinis
Extensive Characterization of the 1 mm PIT Nb_3Sn strand for the 13-T FRESCA2 Magnet
IEEE Transactions on Applied Superconductivity (2012), doi:10.1109/TASC.2011.2178217.
Group(s): Flükiger/Senatore / Project(s): 3

R. Flükiger, M. S. A. Hossain, C. Senatore, and M. A. Rindfleisch
Improved transport properties and connectivity of in situ MgB_2 wires obtained by Cold High Pressure Densification (CHPD)
Physica C **471**, 1119 (2011).
Group(s): Flükiger/Senatore / Project(s): 3

▶ M. S. A. Hossain, C. Senatore, M. A. Rindfleisch, and R. Flükiger
Improvement of J_c by cold high pressure densification of binary, 18-filament in situ MgB_2 wires
Superconductor Science & Technology **24**, 075013 (2011).
Group(s): Flükiger/Senatore / Project(s): 3

T. Miyatake, Y. Murakami, H. Kurahashi, S. Hayashi, K. Zaitsu, B. Seeber, G. Mondonico, and N. Yoshihiro
Influence of wire parameters on critical current vs. strain characteristics of bronze processed Nb_3Sn superconducting wires
IEEE Transactions on Applied Superconductivity (2012), doi:10.1109/TASC.2011.2179697.
Group(s): Flükiger/Senatore / Project(s): 3

B. Seeber, A. Ferreira, G. Mondonico, F. Buta, C. Senatore, R. Flükiger, and T. Takeuchi
Low Critical Current Sensitivity of RHQT Nb_3Al Wires Under Transverse Compressive Stress Up to 300 MPa
IEEE Transactions on Applied Superconductivity **21**, 2593 (2011).
Group(s): Flükiger/Senatore / Project(s): 3

B. Bordini, D. Bessette, L. Bottura, A. Devred, M. Jewell, D. Richter, and C. Senatore
Magnetization and Inter-Filament Contact in HEP and ITER Bronze-Route Nb_3Sn Wires
IEEE Transactions on Applied Superconductivity **21**, 3373 (2011).
Group(s): Flükiger/Senatore / Project(s): 3

▶ C. Senatore, G. Mondonico, F. Buta, B. Seeber, R. Flükiger, B. Bordini, P. Alknes, and L. Bottura
Phase formation, composition and T_c distribution of binary and Ta-alloyed Nb_3Sn wires produced by various techniques
IEEE Transactions on Applied Superconductiv-

ity (2012), doi:10.1109/TASC.2011.2178992.
Group(s): Flükiger/Senatore / Project(s): 3

G. De Marzi, V. Corato, L. Muzzi, A. della Corte, G. Mondonico, B. Seeber, and C. Senatore
Reversible stress-induced anomalies in the strain function of Nb_3Sn wires
Superconductor Science & Technology **25**, 025015 (2012).
Group(s): Flükiger/Senatore / Project(s): 3

M. Kulich, P. Kováč, H. W. Weber, and W. Hässler
SiC doped MgB_2 wires in a Ti sheath prepared by stage formation
Superconductor Science & Technology **24**, 065025 (2011).
Group(s): Flükiger/Senatore / Project(s): 3

B. Seeber, G. Mondonico, and C. Senatore
Toward a standard for critical current vs. axial strain measurements of Nb_3Sn
to be published in Superconductor Science & Technology (2012).
Group(s): Flükiger/Senatore / Project(s): 3

Group of L. Forró

V. Ilakovac, N. B. Brookes, J. C. Cezar, P. Thakur, V. Bisogni, C. Dallera, G. Ghiringhelli, L. Braicovich, S. Bernu, H. Berger, L. Forró, A. Akrap, and C. F. Hague
$BaVS_3$ probed by V L edge x-ray absorption spectroscopy
Journal of Physics: Condensed Matter **24**, 045503 (2012).
Group(s): Forró / Project(s): 7

N. Barišić, I. Smiljanić, P. Popčević, A. Bilušić, E. Tutiš, A. Smontara, H. Berger, J. Jaćimović, O. Yuli, and L. Forró
High-pressure study of transport properties in $Co_{0.33}NbS_2$
Physical Review B **84**, 075157 (2011).
Group(s): Forró / Project(s): 7

R. A. de Souza, U. Staub, V. Scagnoli, M. Garganourakis, Y. Bodenthin, and H. Berger
Origin of the anomalous low-temperature phase transition in $BaVS_3$
Physical Review B **84**, 014409 (2011).
Group(s): Forró, Staub / Project(s): 6

Á. Antal, T. Fehér, E. Tátrai-Szekeres, F. Fülöp, B. Náfrádi, L. Forró, and A. Jánossy
Pressure and temperature dependence of interlayer spin diffusion and electrical conductivity in the layered organic conductors κ-(BEDT-TTF)$_2$Cu[N(CN)$_2$]X (X = Cl, Br)
Physical Review B **84**, 075124 (2011).
Group(s): Forró / Project(s): 7

S. Arsenijević, R. Gaál, A. S. Sefat, M. A. McGuire, B. C. Sales, D. Mandrus, and L. Forró
Pressure effects on the transport coefficients of $Ba(Fe_{1-x}Co_x)_2As_2$
Physical Review B **84**, 075148 (2011).
Group(s): Forró / Project(s): 7

Group of A. Georges

▶ S. Nascimbène, N. Navon, S. Pilati, F. Chevy, S. Giorgini, A. Georges, and C. Salomon
Fermi-Liquid Behavior of the Normal Phase of a Strongly Interacting Gas of Cold Atoms
Physical Review Letters **106**, 215303 (2011).
Group(s): Georges, Troyer / Project(s): 8

▶ M. Aichhorn, L. Pourovskii, and A. Georges
Importance of electronic correlations for structural and magnetic properties of the iron pnictide superconductor LaFeAsO
Physical Review B **84**, 054529 (2011).
Group(s): Georges / Project(s): 4, 5

▶ L. de' Medici, J. Mravlje, and A. Georges
Janus-Faced Influence of Hund's Rule Coupling in Strongly Correlated Materials
Physical Review Letters **107**, 256401 (2011).
Group(s): Georges / Project(s): 4, 5

▶ G. Seyfarth, A.-S. Rüetschi, K. Sengupta, A. Georges, S. Watanabe, A. Miyake, and D. Jaccard
Multiprobe Signatures of the Valence Crossover in Heavy Fermion Superconductor $CeCu_2Si_2$ Under High Pressure
to be published in Journal of the Physical Society of Japan (2012).
Group(s): Georges, Jaccard / Project(s): 5

▶ O. E. Peil, A. Georges, and F. Lechermann
Strong Correlations Enhanced by Charge Ordering in Highly Doped Cobaltates
Physical Review Letters **107**, 236404 (2011).
Group(s): Georges / Project(s): 4, 5

Group of T. Giamarchi

- T. Jarlborg
  A model of the T-dependent pseudogap and its competition with superconductivity in copper oxides
  Solid State Communications **151**, 639 (2011).
  Group(s): Giamarchi / Project(s): 4

- T. Jarlborg
  Bands, spin-fluctuations and traces of Fermi surfaces in angle-resolved photoemission intensities for high-T_C cuprates
  Physical Review B **84**, 064506 (2011).
  Group(s): Giamarchi / Project(s): 4

  P. Chudzinski and T. Giamarchi
  Collective excitations and low-temperature transport properties of bismuth
  Physical Review B **84**, 125105 (2011).
  Group(s): Giamarchi / Project(s): 4

- E. G. Dalla Torre, E. Demler, T. Giamarchi, and E. Altman
  Dynamics and universality in noise driven dissipative systems
  to be published in Physical Review B (2012), arXiv:1110.3678.
  Group(s): Giamarchi / Project(s): 8

- S. C. Furuya, P. Bouillot, C. Kollath, M. Oshikawa, and T. Giamarchi
  Electron Spin Resonance Shift in Spin Ladder Compounds
  Physical Review Letters **108**, 037204 (2012).
  Group(s): Giamarchi, Kollath / Project(s): 6

- A. Piriou, N. Jenkins, C. Berthod, I. Maggio-Aprile, and Ø. Fischer
  First direct observation of the Van Hove singularity in the tunneling spectra of cuprates
  Nature Communications **2**, 221 (2011).
  Group(s): Fischer, Giamarchi / Project(s): 4

- A. Mitra and T. Giamarchi
  Mode-Coupling-Induced Dissipative and Thermal Effects at Long Times after a Quantum Quench
  Physical Review Letters **107**, 150602 (2011).
  Group(s): Giamarchi / Project(s): 8

- M. A. Cazalilla, R. Citro, T. Giamarchi, E. Orignac, and M. Rigol
  One dimensional bosons: From condensed matter systems to ultracold gases
  Reviews of Modern Physics **83**, 1405 (2011).
  Group(s): Giamarchi / Project(s): 8

- J. Catani, G. Lamporesi, D. Naik, M. Gring, M. Inguscio, F. Minardi, A. Kantian, and T. Giamarchi
  Quantum dynamics of impurities in a one-dimensional Bose gas
  Physical Review A **85**, 023623 (2012).
  Group(s): Giamarchi / Project(s): 8

  J. Lancaster, T. Giamarchi, and A. Mitra
  Random phase approximation study of one-dimensional fermions after a quantum quench
  Physical Review B **84**, 075143 (2011).
  Group(s): Giamarchi / Project(s): 8

- T. Jarlborg, B. Barbiellini, H. Lin, R. S. Markiewicz, and A. Bansil
  Renormalization of $\int$ levels away from the Fermi energy in electron excitation spectroscopies: Density-functional results for $Nd_{2-x}Ce_xCuO_4$
  Physical Review B **84**, 045109 (2011).
  Group(s): Giamarchi / Project(s): 4

- A. Tokuno and T. Giamarchi
  Spectroscopy for Cold Atom Gases in Periodically Phase-Modulated Optical Lattices
  Physical Review Letters **106**, 205301 (2011).
  Group(s): Giamarchi / Project(s): 8

- P. Bouillot, K. Corinna, A. M. Läuchli, M. Zvonarev, B. Thielemann, C. Rüegg, E. Orignac, R. Citro, M. Horvatić, C. Berthier, M. Klanjšek, , and T. Giamarchi
  Statics and dynamics of weakly coupled antiferromagnetic spin-1/2 ladders in a magnetic field
  Physical Review B **83**, 054407 (2011).
  Group(s): Giamarchi, Kollath / Project(s): 6

- A. M. Lobos and T. Giamarchi
  Superconductor-to-insulator transition in linear arrays of Josephson junctions capacitively coupled to metallic films
  Physical Review B **84**, 024523 (2011).
  Group(s): Giamarchi / Project(s): 2

- A. Mitra and T. Giamarchi
  Thermalization and dissipation in out-of-equilibrium quantum systems: A perturbative renormalization group approach
  Physical Review B **85**, 075117 (2012).
  Group(s): Giamarchi / Project(s): 8

  C. Berthod and T. Giamarchi
  Tunneling conductance and local density of states in tight-binding junctions
  Physical Review B **84**, 155414 (2011).
  Group(s): Giamarchi / Project(s): 4, 7

Group of E. Giannini

- B. Sacépé, J. B. Oostinga, J. Li, A. Ubaldini, N. J. G. Couto, E. Giannini, and A. F. Morpurgo
  Gate-tuned normal and superconducting transport at the surface of a topological insulator
  Nature Communications **2**, 575 (2011).
  Group(s): Giannini, Morpurgo / Project(s): 2

J. Teyssier, R. Viennois, E. Giannini, R. M. Eremina, A. Günther, J. Deisenhofer, M. V. Eremin, and D. van der Marel
Optical study of phonons and electronic excitations in tetragonal Sr_2VO_4
Physical Review B **84**, 205130 (2011).
Group(s): Giannini, van der Marel / Project(s): 4

- Z.-H. Zhu, G. Levy, B. Ludbrook, C. N. Veenstra, J. A. Rosen, R. Comin, D. Wong, P. Dosanjh, A. Ubaldini, P. Syers, N. P. Butch, J. Paglione, I. S. Elfimov, and A. Damascelli
  Rashba Spin-Splitting Control at the Surface of the Topological Insulator Bi_2Se_3
  Physical Review Letters **107**, 186405 (2011).
  Group(s): Giannini / Project(s): 5

Y. Talanov, L. Salakhutdinov, E. Giannini, and R. Khasanov
Vortex Excitations Above T_c in the Cuprate Superconductor $Bi_2Sr_2Ca_2Cu_3O_{10}$ as Revealed by ESR
Applied Magnetic Resonance **40**, 37 (2011).
Group(s): Giannini / Project(s): 4

Group of M. Grioni

E. Frantzeskakis, S. Pons, A. Crepaldi, H. Brune, K. Kern, and M. Grioni
Ag-coverage-dependent symmetry of the electronic states of the Pt(111)-Ag-Bi interface : The ARPES view of a structural transition
Physical Review B **84**, 245443 (2011).
Group(s): Grioni / Project(s): 7

A. Crepaldi, S. Pons, E. Frantzeskakis, K. Kern, and M. Grioni
Anisotropic spin gaps in $BiAg_2$-Ag/Si(111)
Physical Review B **85**, 075411 (2012).
Group(s): Grioni / Project(s): 7

- E. Frantzeskakis and M. Grioni
  Anisotropy effects on Rashba and topological insulator spin-polarized surface states : A unified phenomenological description
  Physical Review B **84**, 155453 (2011).
  Group(s): Grioni / Project(s): 7

M. F. Beaux II, T. Durakiewicz, L. Moreschini, M. Grioni, F. Offi, G. Monaco, G. Panaccione, J. J. Joyce, E. D. Bauer, J. L. Sarrao, M. T. Butterfield, and E. Guziewicz
Electronic structure of single crystal UPd_3, UGe_2 and USb_2 from hard x-ray and angle-resolved photoelectron spectroscopy
Journal of Electron Spectroscopy and Related Phenomena **184**, 517 (2011).
Group(s): Grioni / Project(s): 7

M. Moretti Sala, V. Bisogni, C. Aruta, G. Balestrino, H. Berger, N. B. Brookes, G. M. de Luca, D. Di Castro, M. Grioni, M. Guarise, P. G. Medaglia, F. Miletto Granozio, M. Minola, P. Perna, M. Radovic, M. Salluzzo, T. Schmitt, K. J. Zhou, L. Braicovich, and G. Ghiringhelli
Energy and symmetry of dd excitations in undoped layered cuprates measured by Cu L3 resonantinelastic x-ray scattering
New Journal of Physics **13**, 043026 (2011).
Group(s): Grioni / Project(s): 7

Group of V. Gritsev

- M. Tomka, A. Polkovnikov, and V. Gritsev
  Geometric phase contribution to quantum nonequilibrium many-body dynamics
  Physical Review Letters **108**, 080404 (2012).
  Group(s): Gritsev / Project(s): 8

Group of D. Jaccard

- G. Seyfarth, A.-S. Rüetschi, K. Sengupta, A. Georges, S. Watanabe, A. Miyake, and D. Jaccard
  Multiprobe Signatures of the Valence Crossover in Heavy Fermion Superconductor $CeCu_2Si_2$ Under High Pressure
  to be published in Journal of the Physical Society of Japan (2012).
  Group(s): Georges, Jaccard / Project(s): 5

- A.-S. Rüetschi, K. Sengupta, G. Seyfarth, and D. Jaccard
  Nernst effect in $CeCu_2Si_2$
  Journal of Physics: Conference Series **273**, 012052 (2011).
  Group(s): Jaccard / Project(s): 5

Group of J. Karpinski

Z. Guguchia, S. Bosma, S. Weyeneth, A. Shengelaya, R. Puzniak, Z. Bukowski, J. Karpinski, and H. Keller
Anisotropic magnetic order of the Eu sublattice in single crystals of $EuFe_{2-x}Co_xAs_2$ ($x = 0, 0.2$) studied by means of magnetization and magnetic torque
Physical Review B **84**, 144506 (2011).
Group(s): Karpinski, Keller / Project(s): 4

U. Welp, C. Chaparro, A. E. Koshelev, W. K. Kwok, A. Rydh, N. D. Zhigadlo, J. Karpinski, and S. Weyeneth
Anisotropic phase diagram and superconducting fluctuations of single-crystalline $SmFeAsO_{0.85}F_{0.15}$
Physical Review B **83**, 100513 (2011).
Group(s): Karpinski / Project(s): 4

M. Matusiak, Z. Bukowski, and J. Karpinski
Doping dependence of the Nernst effect in $Eu(Fe_{1-x}Co_x)_2As_2$: Departure from Dirac-fermion physics
Physical Review B **83**, 224505 (2011).
Group(s): Karpinski / Project(s): 4

M. Ciszek, K. Rogacki, and J. Karpiński
Effect of carbon substitution on low magnetic field AC losses in MgB_2 single crystals
Physica C **471**, 794 (2011).
Group(s): Karpinski / Project(s): 4

A. Alfonsov, F. Murányi, V. Kataev, G. Lang, N. Leps, L. Wang, R. Klingeler, A. Kondrat, C. Hess, S. Wurmehl, A. Köhler, G. Behr, S. Hampel, M. Deutschmann, S. Katrych, N. D. Zhigadlo, Z. Bukowski, J. Karpinski, and B. Büchner
High-field electron spin resonance spectroscopy study of $GdFeAsO_{1-x}F_x$ superconductors
Physical Review B **83**, 094526 (2011).
Group(s): Karpinski / Project(s): 4

J. C. Loudon, C. J. Bowell, N. D. Zhigadlo, J. Karpinski, and P. A. Midgley
Imaging flux vortices in MgB_2 using transmission electron microscopy
Physica C **474**, 18 (2012).
Group(s): Karpinski / Project(s): 4

A.Błachowski, K. Ruebenbauer, J. Żukrowski, Z. Bukowski, K. Rogacki, P. Moll, and J. Karpinski
Interplay between magnetism and superconductivity in $EuFe_{2-x}Co_xAs_2$ studied by ^{57}Fe and ^{151}Eu Mössbauer spectroscopy
Physical Review B **84**, 174503 (2011).
Group(s): Karpinski / Project(s): 4

N. D. Zhigadlo, S. Katrych, M. Bendele, P. J. W. Moll, M. Tortello, S. Weyeneth, V. Y. Pomjakushin, J. Kanter, R. Puzniak, Z. Bukowski, H. Keller, R. S. Gonnelli, R. Khasanov, J. Karpinski, and B. Batlogg
Interplay of composition, structure, magnetism, and superconductivity in $SmFeAs_{1-x}P_xO_{1-y}$
Physical Review B **84**, 134526 (2011).
Group(s): Batlogg, Karpinski, Keller / Project(s): 4

G. Li, G. Grissonnanche, A. Gurevich, N. D. Zhigadlo, S. Katrych, Z. Bukowski, J. Karpinski, and L. Balicas
Multiband superconductivity in $LaFeAsO_{0.9}F_{0.1}$ single crystals probed by high-field vortex torque magnetometry
Physical Review B **83**, 214505 (2011).
Group(s): Karpinski / Project(s): 4

Z. Guguchia, Z. Shermadini, A. Amato, A. Maisuradze, A. Shengelaya, Z. Bukowski, H. Luetkens, R. Khasanov, J. Karpinski, and H. Keller
Muon-spin rotation measurements of the magnetic penetration depth in the iron-based superconductor $Ba_{1-x}Rb_xFe_2As_2$
Physical Review B **84**, 094513 (2011).
Group(s): Karpinski, Keller / Project(s): 4

P. J. W. Moll, J. Kanter, R. D. McDonald, F. Balakirev, P. Blaha, K. Schwarz, Z. Bukowski, N. D. Zhigadlo, S. Katrych, K. Mattenberger, J. Karpinski, and B. Batlogg
Quantum oscillations of the superconductor $LaRu_2P_2$: Comparable mass enhancement $\lambda \approx 1$ in Ru and Fe phosphides
Physical Review B **84**, 224507 (2011).
Group(s): Batlogg, Karpinski / Project(s): 4

S. Weyeneth, P. J. W. Moll, R. Puzniak, K. Ninios, F. F. Balakirev, R. D. McDonald, H. B. Chan, N. D. Zhigadlo, S. Katrych, Z. Bukowski, J. Karpinski, H. Keller, B. Batlogg, and L. Balicas
Rearrangement of the antiferromagnetic ordering at high magnetic fields in SmFeAsO and $SmFeAsO_{0.9}F_{0.1}$ single crystals
Physical Review B **83**, 134503 (2011).
Group(s): Batlogg, Karpinski, Keller / Project(s): 4

A. Blachowski, K. Ruebenbauer, J. Zukrowski, K. Rogacki, Z. Bukowski, and J. Karpinski

Shape of spin density wave versus temperature in AFe_2As_2 (A = Ca, Ba, Eu): A Mössbauer study

Physical Review B **83**, 134410 (2011).

Group(s): Karpinski / Project(s): 4

Z. Guguchia, J. Roos, A. Shengelaya, S. Katrych, Z. Bukowski, S. Weyeneth, F. Murányi, S. Strässle, A. Maisuradze, J. Karpinski, and H. Keller

Strong coupling between Eu^{2+} spins and Fe_2As_2 layers in $EuFe_{1.9}Co_{0.1}As_2$ observed with NMR

Physical Review B **83**, 144516 (2011).

Group(s): Karpinski, Keller / Project(s): 4

J. Zhang, A. Belousov, J. Karpiński, B. Batlogg, G. Wicks, and R. Sobolewski

Time-resolved femtosecond optical characterization of multi-photon absorption in high-pressure-grown $Al_{0.86}Ga_{0.14}N$ single crystals

Journal of Applied Physics **110**, 113112 (2011).

Group(s): Batlogg, Karpinski / Project(s): 4

R. Khasanov, S. Sanna, G. Prando, Z. Shermadini, M. Bendele, A. Amato, P. Carretta, R. De Renzi, J. Karpinski, S. Katrych, H. Luetkens, and N. D. Zhigadlo

Tuning of competing magnetic and superconducting phase volumes in $LaFeAsO_{0.945}F_{0.055}$ by hydrostatic pressure

Physical Review B **84**, 100501 (2011).

Group(s): Karpinski / Project(s): 4

Group of H. Keller

▶ S. Strässle, B. Graneli, M. Mali, J. Roos, and H. Keller

Absence of Orbital Currents in Superconducting $YBa_2Cu_4O_8$ Using a Zeeman-Perturbed Nuclear-Quadrupole-Resonance Technique

Physical Review Letters **106**, 097003 (2011).

Group(s): Keller / Project(s): 4

Z. Guguchia, S. Bosma, S. Weyeneth, A. Shengelaya, R. Puzniak, Z. Bukowski, J. Karpinski, and H. Keller

Anisotropic magnetic order of the Eu sublattice in single crystals of $EuFe_{2-x}Co_xAs_2$ (x = 0, 0.2) studied by means of magnetization and magnetic torque

Physical Review B **84**, 144506 (2011).

Group(s): Karpinski, Keller / Project(s): 4

▶ A. Bussmann-Holder, A. Simon, H. Keller, and A. R. Bishop

Identifying the Pairing Mechanism in Fe-As Based Superconductors: Gaps and Isotope Effects

Journal of Superconductivity and Novel Magnetism **24**, 1099 (2011).

Group(s): Keller / Project(s): 4

N. D. Zhigadlo, S. Katrych, M. Bendele, P. J. W. Moll, M. Tortello, S. Weyeneth, V. Y. Pomjakushin, J. Kanter, R. Puzniak, Z. Bukowski, H. Keller, R. S. Gonnelli, R. Khasanov, J. Karpinski, and B. Batlogg

Interplay of composition, structure, magnetism, and superconductivity in $SmFeAs_{1-x}P_xO_{1-y}$

Physical Review B **84**, 134526 (2011).

Group(s): Batlogg, Karpinski, Keller / Project(s): 4

▶ A. Bussmann-Holder, H. Keller, R. Khasanov, A. Simon, A. Bianconi, and A. R. Bishop

Isotope and interband effects in a multi-band model of superconductivity

New Journal of Physics **13**, 093009 (2011).

Group(s): Keller / Project(s): 4

S. Bosma, S. Weyeneth, R. Puzniak, A. Erb, A. Schilling, and H. Keller

Magnetic torque study of the temperature-dependent anisotropy parameter in overdoped superconducting single-crystal $YBa_2Cu_3O_7$

Physical Review B **84**, 024514 (2011).

Group(s): Keller / Project(s): 4

B. M. Wojek, E. Morenzoni, D. G. Eshchenko, A. Suter, T. Prokscha, H. Keller, E. Koller, Ø. Fischer, V. K. Malik, C. Bernhard, and M. Döbeli

Magnetism, superconductivity, and coupling in cuprate heterostructures probed by low-energy muon-spin rotation

Physical Review B **85**, 024505 (2012).

Group(s): Bernhard, Fischer, Keller, Morenzoni / Project(s): 1, 4

▶ A. Maisuradze, A. Shengelaya, A. Amato, E. Pomjakushina, and H. Keller

Muon spin rotation investigation of the pressure effect on the magnetic penetration depth in $YBa_2Cu_3O_x$

Physical Review B **84**, 184523 (2011).

Group(s): Keller / Project(s): 4

Z. Guguchia, Z. Shermadini, A. Amato, A. Maisuradze, A. Shengelaya, Z. Bukowski, H. Luetkens, R. Khasanov, J. Karpinski, and H. Keller

Muon-spin rotation measurements of the magnetic penetration depth in the iron-based superconductor $Ba_{1-x}Rb_xFe_2As_2$

Physical Review B **84**, 094513 (2011).
Group(s): Karpinski, Keller / Project(s): 4

A. Maisuradze, Z. Guguchia, B. Graneli, H. M. Rønnow, H. Berger, and H. Keller
μSR investigation of magnetism and magnetoelectric coupling in Cu_2OSeO_3
Physical Review B **84**, 064433 (2011).
Group(s): Keller, Rønnow / Project(s): 4, 6

C. M. Bonilla, N. Marcano, J. Herrero-Albillos, A. Maisuradze, L. M. García, and F. Bartolomé
μSR study of short-range magnetic order in the paramagnetic regime of $ErCo_2$
Physical Review B **84**, 184425 (2011).
Group(s): Keller / Project(s): 4

B. Maroni, D. Di Castro, M. Hanfland, J. Boby, C. Vercesi, M. C. Mozzati, S. Weyeneth, H. Keller, R. Khasanov, C. Drathen, P. Dore, P. Postorino, and L. Malavasi
Pressure Effects in the Isoelectronic $REFe_{0.85}Ir_{0.15}AsO$ System
Journal of the American Chemical Society **133**, 3252 (2011).
Group(s): Keller / Project(s): 4

S. Weyeneth, P. J. W. Moll, R. Puzniak, K. Ninios, F. F. Balakirev, R. D. McDonald, H. B. Chan, N. D. Zhigadlo, S. Katrych, Z. Bukowski, J. Karpinski, H. Keller, B. Batlogg, and L. Balicas
Rearrangement of the antiferromagnetic ordering at high magnetic fields in SmFeAsO and $SmFeAsO_{0.9}F_{0.1}$ single crystals
Physical Review B **83**, 134503 (2011).
Group(s): Batlogg, Karpinski, Keller / Project(s): 4

Z. Guguchia, J. Roos, A. Shengelaya, S. Katrych, Z. Bukowski, S. Weyeneth, F. Murányi, S. Strässle, A. Maisuradze, J. Karpinski, and H. Keller
Strong coupling between Eu^{2+} spins and Fe_2As_2 layers in $EuFe_{1.9}Co_{0.1}As_2$ observed with NMR
Physical Review B **83**, 144516 (2011).
Group(s): Karpinski, Keller / Project(s): 4

Group of M. Kenzelmann

▶ J. S. White, T. Honda, K. Kimura, T. Kimura, C. Niedermayer, O. Zaharko, A. Poole, B. Roessli, and M. Kenzelmann
Coupling of magnetic and ferroelectric hysteresis by a multicomponent magnetic structure in Mn_2GeO_4
Physical Review Letters **108**, 077204 (2012).
Group(s): Kenzelmann, Niedermayer / Project(s): 6

R. Toft-Petersen, J. Jensen, T. B. S. Jensen, N. H. Andersen, N. B. Christensen, C. Niedermayer, M. Kenzelmann, M. Skoulatos, M. D. Le, K. Lefmann, S. R. Hansen, J. Li, J. L. Zarestky, and D. Vaknin
High-field magnetic phase transitions and spin excitations in magnetoelectric $LiNiPO_4$
Physical Review B **84**, 054408 (2011).
Group(s): Kenzelmann, Niedermayer / Project(s): 4

▶ Y. Hu, M. Bator, M. Kenzelmann, T. Lippert, C. Niedermayer, C. W. Schneider, and A. Wokaun
Strain and lattice distortion in (1 1 0)-epitaxial orthorhombic $TbMnO_3$ multiferroic thin films grown by pulsed laser deposition
Applied Surface Science (2011), doi:10.1016/j.apsusc.2011.10.082.
Group(s): Kenzelmann, Niedermayer / Project(s): 1

Group of C. Kollath

▶ P. Barmettler and C. Kollath
Controllable manipulation and detection of local densities and bipartite entanglement in a quantum gas by a dissipative defect
Physical Review A **84**, 041606 (2011).
Group(s): Kollath / Project(s): 8

▶ S. C. Furuya, P. Bouillot, C. Kollath, M. Oshikawa, and T. Giamarchi
Electron Spin Resonance Shift in Spin Ladder Compounds
Physical Review Letters **108**, 037204 (2012).
Group(s): Giamarchi, Kollath / Project(s): 6

▶ M. Cheneau, P. Barmettler, D. Poletti, M. Endres, P. Schauss, T. Fukuhara, C. Gross, I. Bloch, C. Kollath, and S. Kuhr
Light-cone-like spreading of correlations in a quantum many-body system
Nature **481**, 484 (2012).
Group(s): Kollath / Project(s): 8

▶ J.-S. Bernier, G. Roux, and C. Kollath
Slow Quench Dynamics of a One-Dimensional Bose Gas Confined to an Optical Lattice
Physical Review Letters **106**, 200601 (2011).
Group(s): Kollath / Project(s): 8

D. Poletti and C. Kollath
Slow quench dynamics of periodically driven quantum gases

Physical Review A **84**, 013615 (2011).
Group(s): Kollath / Project(s): 8

- P. Bouillot, K. Corinna, A. M. Läuchli, M. Zvonarev, B. Thielemann, C. Rüegg, E. Orignac, R. Citro, M. Horvatić, C. Berthier, M. Klanjšek, , and T. Giamarchi
  Statics and dynamics of weakly coupled antiferromagnetic spin-1/2 ladders in a magnetic field
  Physical Review B **83**, 054407 (2011).
  Group(s): Giamarchi, Kollath / Project(s): 6

Group of D. van de Marel

D. van der Marel, J. L. M. van Mechelen, and I. I. Mazin
Common Fermi-liquid origin of T^2 resistivity and superconductivity in n-type $SrTiO_3$
Physical Review B **84**, 205111 (2011).
Group(s): van der Marel / Project(s): 4

- S. Dal Conte, C. Giannetti, G. Coslovich, F. Cilento, D. Bossini, T. Abebaw, F. Banfi, G. Ferrini, H. Eisaki, M. Greven, A. Damascelli, D. van der Marel, and F. Parmigiani
  Disentangling the electronic and phononic glue in a high-T_c superconductor
  to be published in Science (2012), arXiv:1203.0588.
  Group(s): van der Marel / Project(s): 4

- D. N. Basov, R. D. Averitt, D. van der Marel, M. Dressel, and K. Haule
  Electrodynamics of correlated electron materials
  Reviews of Modern Physics **83**, 471 (2011).
  Group(s): van der Marel / Project(s): 4, 5

- I. Crassee, J. Levallois, A. L. Walter, M. Ostler, A. Bostwick, E. Rotenberg, T. Seyller, D. van der Marel, and A. B. Kuzmenko
  Giant Faraday rotation in single- and multilayer graphene
  Nature Physics **7**, 48 (2011).
  Group(s): van der Marel / Project(s): 2, 5

- J. Levallois, F. Lévy-Bertrand, M. K. Tran, D. Stricker, J. A. Mydosh, Y.-K. Huang, and D. van der Marel
  Hybridization gap and anisotropic far-infrared optical conductivity of URu_2Si_2
  Physical Review B **84**, 184420 (2011).
  Group(s): van der Marel / Project(s): 5

- I. Crassee, J. Levallois, D. van der Marel, A. L. Walter, T. Seyller, and A. B. Kuzmenko
  Multicomponent magneto-optical conductivity of multilayer graphene on SiC
  Physical Review B **84**, 035103 (2011).
  Group(s): van der Marel / Project(s): 2

J. F. DiTusa, V. Guritanu, S. Guo, D. P. Young, P. W. Adams, R. G. Goodrich, J. Y. Chan, and D. van der Marel
Optical conductivity and superconductivity in $LaSb_2$
Journal of Physics: Conference Series **273**, 012151 (2011).
Group(s): van der Marel / Project(s): 5

J. Teyssier, R. Viennois, E. Giannini, R. M. Eremina, A. Günther, J. Deisenhofer, M. V. Eremin, and D. van der Marel
Optical study of phonons and electronic excitations in tetragonal Sr_2VO_4
Physical Review B **84**, 205130 (2011).
Group(s): Giannini, van der Marel / Project(s): 4

- C. Giannetti, F. Cilento, S. Dal Conte, G. Coslovich, G. Ferrini, H. Molegraaf, M. Raichle, R. Liang, H. Eisaki, M. Greven, A. Damascelli, D. van der Marel, and F. Parmigiani
  Revealing the high-energy electronic excitations underlying the onset of high-temperature superconductivity in cuprates.
  Nature Communications **2**, 353 (2011).
  Group(s): van der Marel / Project(s): 4

- J. L. M. van Mechelen, D. van der Marel, I. Crassee, and T. Kolodiazhnyi
  Spin Resonance in $EuTiO_3$ Probed by Time-Domain Gigahertz Ellipsometry
  Physical Review Letters **106**, 217601 (2011).
  Group(s): van der Marel / Project(s): 4

- D. van der Marel and M. Golden
  Superconductivity: Heike's heritage
  Nature Physics **7**, 377 (2011).
  Group(s): van der Marel / Project(s): 4

- J. N. Hancock, J. L. M. van Mechelen, A. B. Kuzmenko, D. van der Marel, C. Brüne, E. G. Novik, G. V. Astakhov, H. Buhmann, and L. W. Molenkamp
  Surface State Charge Dynamics of a High-Mobility Three-Dimensional Topological Insulator
  Physical Review Letters **107**, 136803 (2011).
  Group(s): van der Marel / Project(s): 5

D. van der Marel and J. N. Hancock
Susceptible to Pairing
Physics **4**, 89 (2011).
Group(s): van der Marel / Project(s): 4

Group of J. Mesot

- T. Shiroka, F. Casola, V. Glazkov, A. Zheludev, K. Prša, H.-R. Ott, and J. Mesot
  Distribution of NMR Relaxations in a Random Heisenberg Chain
  Physical Review Letters **106**, 137202 (2011).
  Group(s): Mesot, Ott, Zheludev / Project(s): 6

F. Pfuner, S. N. Gvasaliya, O. Zaharko, L. Keller, J. Mesot, V. Pomjakushin, J.-H. Chu, I. R. Fisher, and L. Degiorgi
Incommensurate magnetic order in $TbTe_3$
Journal of Physics: Condensed Matter **24**, 036001 (2012).
Group(s): Degiorgi, Mesot / Project(s): 7

K.-J. Zhou, M. Radovic, J. Schlappa, V. Strocov, R. Frison, J. Mesot, L. Patthey, and T. Schmitt
Localized and delocalized Ti 3d carriers in $LaAlO_3/SrTiO_3$ superlattices revealed by resonant inelastic x-ray scattering
Physical Review B **83**, 201402 (2011).
Group(s): Mesot, Staub / Project(s): 6

Group of F. Mila

- F. Michaud, F. Vernay, S. Manmana, and F. Mila
  Antiferromagnetic spin-S chains with exactly dimerized ground states
  Physical Review Letters **108**, 127202 (2012).
  Group(s): Mila / Project(s): 6

- N. Laflorencie and F. Mila
  Condensate-Free Superfluid Induced by the Frustrated Proximity Effect
  Physical Review Letters **107**, 037203 (2011).
  Group(s): Mila / Project(s): 6

Z. Hao, Y. Wan, I. Rousochatzakis, J. Wildeboer, A. Seidel, F. Mila, and O. Tchernyshyov
Destruction of valence-bond order in a $S = \frac{1}{2}$ sawtooth chain with a Dzyaloshinskii-Moriya term
Physical Review B **84**, 094452 (2011).
Group(s): Mila / Project(s): 6

M. Moliner, I. Rousochatzakis, and F. Mila
Emergence of one-dimensional physics from the distorted Shastry-Sutherland lattice
Physical Review B **83**, 140414 (2011).
Group(s): Mila / Project(s): 6

S. R. Manmana, A. M. Läuchli, F. H. L. Essler, and F. Mila
Phase diagram and continuous pair-unbinding transition of the bilinear-biquadratic $S = 1$ Heisenberg chain in a magnetic field
Physical Review B **83**, 184433 (2011).
Group(s): Mila / Project(s): 6

- T. Coletta, J.-D. Picon, S. Korshunov, and F. Mila
  Phase diagram of the fully frustrated transverse-field Ising model on the honeycomb lattice
  Physical Review B **83**, 054402 (2011).
  Group(s): Mila / Project(s): 6

A. F. Albuquerque, N. Laflorencie, J.-D. Picon, and F. Mila
Phase separation versus supersolid behavior in frustrated antiferromagnets
Physical Review B **83**, 174421 (2011).
Group(s): Mila / Project(s): 6

- P. Corboz, A. M. Läuchli, K. Penc, M. Troyer, and F. Mila
  Simultaneous Dimerization and SU(4) Symmetry Breaking of 4-Color Fermions on the Square Lattice
  Physical Review Letters **107**, 215301 (2011).
  Group(s): Mila, Troyer / Project(s): 6, 8

- F. Michaud, F. Vernay, and F. Mila
  Theory of inelastic light scattering in spin-1 systems: Resonant regimes and detection of quadrupolar order
  Physical Review B **84**, 184424 (2011).
  Group(s): Mila / Project(s): 6

B. Bauer, P. Corboz, A. M. Läuchli, L. Messio, K. Penc, M. Troyer, and F. Mila
Three-sublattice order in the SU(3) Heisenberg model on the square and triangular lattice
Physical Review B **85**, 125116 (2012).
Group(s): Mila, Troyer / Project(s): 6

S. R. Manmana, J.-D. Picon, K. P. Schmidt, and F. Mila
Unconventional magnetization plateaus in a Shastry-Sutherland spin tube
Europhysics Letters **94**, 67004 (2011).
Group(s): Mila / Project(s): 6

Group of E. Morenzoni

Q. Song, K. H. Chow, Z. Salman, H. Saadaoui, M. D. Hossain, R. F. Kiefl, G. D. Morris, C. D. P. Levy, M. R. Pearson, T. J. Parolin, I. Fan, T. A. Keeler,

M. Smadella, D. Wang, K. M. Yu, X. Liu, J. K. Furdyna, and W. A. MacFarlane
β-detected NMR of Li in $Ga_{1-x}Mn_xAs$
Physical Review B **84**, 054414 (2011).
Group(s): Morenzoni / Project(s): 1

Z. Salman, M. Smadella, W. A. MacFarlane, B. D. Patterson, P. R. Willmott, K. H. Chow, M. D. Hossain, H. Saadaoui, D. Wang, and R. F. Kiefl
Depth dependence of the structural phase transition of $SrTiO_3$ studied with β-NMR and grazing incidence x-ray diffraction
Physical Review B **83**, 224112 (2011).
Group(s): Morenzoni, Willmott / Project(s): 1

▶ A. V. Boris, Y. Matiks, E. Benckiser, A. Frano, P. Popovich, V. Hinkov, P. Wochner, M. Castro-Colin, E. Detemple, V. K. Malik, C. Bernhard, T. Prokscha, A. Suter, Z. Salman, E. Morenzoni, G. Cristiani, H.-U. Habermeier, and B. Keimer
Dimensionality Control of Electronic Phase Transitions in Nickel-Oxide Superlattices
Science **332**, 937 (2011).
Group(s): Bernhard, Morenzoni / Project(s): 1

B. M. Wojek, E. Morenzoni, D. G. Eshchenko, A. Suter, T. Prokscha, H. Keller, E. Koller, Ø. Fischer, V. K. Malik, C. Bernhard, and M. Döbeli
Magnetism, superconductivity, and coupling in cuprate heterostructures probed by low-energy muon-spin rotation
Physical Review B **85**, 024505 (2012).
Group(s): Bernhard, Fischer, Keller, Morenzoni / Project(s): 1, 4

▶ E. Morenzoni, B. M. Wojek, A. Suter, T. Prokscha, G. Logvenov, and I. Božović
The Meissner effect in a strongly underdoped cuprate above its critical temperature
Nature Communications **2**, 272 (2011).
Group(s): Morenzoni / Project(s): 1

▶ A. Suter, E. Morenzoni, T. Prokscha, B. M. Wojek, H. Luetkens, G. Nieuwenhuys, A. Gozar, G. Logvenov, and I. Božović
Two-Dimensional Magnetic and Superconducting Phases in Metal-Insulator $La_{2-x}Sr_xCuO_4$ Superlattices Measured by Muon-Spin Rotation
Physical Review Letters **106**, 237003 (2011).
Group(s): Morenzoni / Project(s): 1

H. Saadaoui, Z. Salman, T. Prokscha, A. Suter, B. M. Wojek, and E. Morenzoni
Zero-field spin depolarization of low-energy muons in ferromagnetic nickel and silver metal
to be published in Physica B (2012).
Group(s): Morenzoni / Project(s): 1

Group of A. Morpurgo

▶ J. Ye, M. F. Craciun, M. Koshino, S. Russo, S. Inoue, H. Yuan, H. Shimotani, A. F. Morpurgo, and Y. Iwasa
Accessing the transport properties of graphene and its multilayers at high carrier density
Proceedings of the National Academy of Science of the USA **108**, 13002 (2011).
Group(s): Morpurgo / Project(s): 2

▶ N. A. Minder, S. Ono, Z. Chen, A. Facchetti, and A. F. Morpurgo
Band-Like Electron Transport in Organic Transistors and Implication of the Molecular Structure for Performance Optimization
Advanced Materials **24**, 503 (2012).
Group(s): Morpurgo / Project(s): 1, 2

▶ B. Sacépé, J. B. Oostinga, J. Li, A. Ubaldini, N. J. G. Couto, E. Giannini, and A. F. Morpurgo
Gate-tuned normal and superconducting transport at the surface of a topological insulator
Nature Communications **2**, 575 (2011).
Group(s): Giannini, Morpurgo / Project(s): 2

▶ J. Li, I. Martin, M. Büttiker, and A. F. Morpurgo
Marginal topological properties of graphene: a comparison with topological insulators
Physica Scripta **T146**, 014021 (2012).
Group(s): Büttiker, Morpurgo / Project(s): 2

▶ N. J. G. Couto, B. Sacépé, and A. F. Morpurgo
Transport through Graphene on $SrTiO_3$
Physical Review Letters **107**, 225501 (2011).
Group(s): Morpurgo / Project(s): 2

Group of Ch. Niedermayer

L. Udby, P. K. Willendrup, E. Knudsen, C. Niedermayer, U. Filges, N. B. Christensen, E. Farhi, B. O. Wells, and K. Lefmann
Analysing neutron scattering data using McStas virtual experiments
Nuclear Instruments and Methods in Physics Research A **634**, S138 (2011).
Group(s): Niedermayer / Project(s): 4

- J. S. White, T. Honda, K. Kimura, T. Kimura, C. Niedermayer, O. Zaharko, A. Poole, B. Roessli, and M. Kenzelmann
  Coupling of magnetic and ferroelectric hysteresis by a multicomponent magnetic structure in Mn_2GeO_4
  Physical Review Letters **108**, 077204 (2012).
  Group(s): Kenzelmann, Niedermayer / Project(s): 6

F. J. Owens, L. Gladczuk, R. Szymczak, P. Dluzewski, A. Wisniewski, H. Szymczak, A. Golnik, C. Bernhard, and C. Niedermayer
High temperature magnetic order in zinc sulfide doped with copper
Journal of the Physics and Chemistry of Solids **72**, 648 (2011).
Group(s): Bernhard, Niedermayer / Project(s): 1

R. Toft-Petersen, J. Jensen, T. B. S. Jensen, N. H. Andersen, N. B. Christensen, C. Niedermayer, M. Kenzelmann, M. Skoulatos, M. D. Le, K. Lefmann, S. R. Hansen, J. Li, J. L. Zarestky, and D. Vaknin
High-field magnetic phase transitions and spin excitations in magnetoelectric $LiNiPO_4$
Physical Review B **84**, 054408 (2011).
Group(s): Kenzelmann, Niedermayer / Project(s): 4

P. G. Freeman, D. Prabhakaran, K. Nakajima, A. Stunault, M. Enderle, C. Niedermayer, C. D. Frost, K. Yamada, and A. T. Boothroyd
Low-energy quasi-one-dimensional spin dynamics in charge-ordered $La_{2-x}Sr_xNiO_4$
Physical Review B **83**, 094414 (2011).
Group(s): Niedermayer / Project(s): 4

- Y. Hu, M. Bator, M. Kenzelmann, T. Lippert, C. Niedermayer, C. W. Schneider, and A. Wokaun
  Strain and lattice distortion in (1 1 0)-epitaxial orthorhombic $TbMnO_3$ multiferroic thin films grown by pulsed laser deposition
  Applied Surface Science (2011), doi:10.1016/j.apsusc.2011.10.082.
  Group(s): Kenzelmann, Niedermayer / Project(s): 1

Group of H.-R. Ott

Z. Salman, M. Smadella, W. A. MacFarlane, B. D. Patterson, P. R. Willmott, K. H. Chow, M. D. Hossain, H. Saadaoui, D. Wang, and R. F. Kiefl
Depth dependence of the structural phase transition of $SrTiO_3$ studied with β-NMR and grazing incidence x-ray diffraction
Physical Review B **83**, 224112 (2011).
Group(s): Morenzoni, Willmott / Project(s): 1

- T. Shiroka, F. Casola, V. Glazkov, A. Zheludev, K. Prša, H.-R. Ott, and J. Mesot
  Distribution of NMR Relaxations in a Random Heisenberg Chain
  Physical Review Letters **106**, 137202 (2011).
  Group(s): Mesot, Ott, Zheludev / Project(s): 6

- C. Cancellieri, D. Fontaine, S. Gariglio, N. Reyren, A. D. Caviglia, A. Fête, S. J. Leake, S. A. Pauli, P. R. Willmott, M. Stengel, P. Ghosez, and J.-M. Triscone
  Electrostriction at the $LaAlO_3/SrTiO_3$ Interface
  Physical Review Letters **107**, 056102 (2011).
  Group(s): Triscone (JM), Willmott / Project(s): 1

- S. A. Pauli, S. J. Leake, B. Delley, M. Björck, C. W. Schneider, C. M. Schlepütz, D. Martoccia, S. Paetel, J. Mannhart, and P. R. Willmott
  Evolution of the Interfacial Structure of $LaAlO_3$ on $SrTiO_3$
  Physical Review Letters **106**, 036101 (2011).
  Group(s): Willmott / Project(s): 1

Group of P. Paruch

- J. Guyonnet, I. Gaponenko, S. Gariglio, and P. Paruch
  Conduction at Domain Walls in Insulating $Pb(Zr_{0.2}Ti_{0.8})O_3$ Thin Films
  Advanced Materials **23**, 5377 (2011).
  Group(s): Paruch, Triscone / Project(s): 1

Group of G. Patzke

Y. Zhou and G. R. Patzke
Bi_2O_3 or $Bi_6S_2O_{15}$ nanowires? The role of templating inorganic additives in nanomaterials formation
CrystEngComm **14**, 1161 (2012).
Group(s): Patzke / Project(s): 3

Y. Zhou, E. Antonova, Y. Lin, J.-D. Grunwaldt, W. Bensch, and G. R. Patzke
In Situ X-ray Absorption Spectroscopy/Energy-Dispersive X-ray Diffraction Studies on the Hydrothermal Formation of $Bi_2W_{1-x}Mo_xO_6$ Nanomaterials
European Journal of Inorganic Chemistry **2012**, 783 (2012).
Group(s): Patzke / Project(s): 3

F. Conrad, C. Massue, S. Kühl, E. Kunkes, F. Girgsdies, I. Kasatkin, B. Zhang, M. Friedrich, Y. Luo, M. Armbrüster, G. R. Patzke, and M. Behrens
Microwave-hydrothermal synthesis and characterization of nanostructured copper substituted ZnM_2O_4 (M = Al, Ga) spinels as precursors for thermally stable Cu catalysts
Nanoscale **4**, 2018 (2012).
Group(s): Patzke / Project(s): 3

F. Conrad, M. Bauer, D. Sheptyakov, S. Weyeneth, D. Jaeger, K. Hametner, P.-E. Car, J. Patscheider, D. Günther, and G. R. Patzke
New spinel oxide catalysts for visible-light-driven water oxidation
RSC Advances **2**, 3076 (2012).
Group(s): Patzke / Project(s): 3

R. Kontic and G. R. Patzke
Synthetic trends for $BiVO_4$ photocatalysts: Molybdenum substitution vs. TiO_2 and SnO_2 heterojunctions
Journal of Solid State Chemistry (2012), doi:10.1016/j.jssc.2011.11.050.
Group(s): Patzke / Project(s): 3

▶ Y. Zhou, K. Zheng, J.-D. Grunwaldt, T. Fox, L. Gu, X. Mo, G. Chen, and G. R. Patzke
W/Mo-Oxide Nanomaterials: Structure-Property Relationships and Ammonia-Sensing Studies
The Journal of Physical Chemistry C **115**, 1134 (2011).
Group(s): Patzke / Project(s): 3

Group of Ch. Renner

▶ K. C. Rahnejat, C. A. Howard, N. E. Shuttleworth, S. R. Schofield, K. Iwaya, C. F. Hirjibehedin, C. Renner, G. Aeppli, and M. Ellerby
Charge density waves in the graphene sheets of the superconductor CaC_6
Nature Communications **2**, 558 (2011).
Group(s): Renner / Project(s): 2

H. J. Liu, J. H. G. Owen, and K. Miki
Degenerate electronic structure of reconstructed $MnSi_{1.7}$ nanowires on Si(001)
Journal of Physics: Condensed Matter **24**, 095005 (2012).
Group(s): Renner / Project(s): 7

F. Bianco, J. H. G. Owen, S. A. Köster, D. Mazur, C. Renner, and D. R. Bowler
Endotaxial Si nanolines in Si(001):H
Physical Review B **84**, 035328 (2011).
Group(s): Renner / Project(s): 7

▶ B. Bryant, C. Renner, Y. Tokunaga, Y. Tokura, and G. Aeppli
Imaging oxygen defects and their motion at a manganite surface
Nature Communications **2**, 212 (2011).
Group(s): Renner / Project(s): 6

H. J. Liu, J. H. G. Owen, K. Miki, and C. Renner
Manganese silicide nanowires on Si(001)
Journal of Physics: Condensed Matter **23**, 172001 (2011).
Group(s): Renner / Project(s): 7

Group of T. M. Rice

▶ T. M. Rice, K.-Y. Yang, and F. C. Zhang
A phenomenological theory of the anomalous pseudogap phase in underdoped cuprates
Reports on Progress in Physics **75**, 016502 (2012).
Group(s): Rice, Sigrist / Project(s): 4

D. Müller, S. Pilgram, T. M. Rice, and M. Sigrist
Extending the Gutzwiller approximation for liquid ^{3}He by including intersite correlations
Annalen der Physik **523**, 732 (2011).
Group(s): Rice, Sigrist / Project(s): 5

K.-Y. Yang, Y. Yamashita, A. M. Läuchli, M. Sigrist, and T. M. Rice
Microscopic model for the semiconductor-to-ferromagnetic-metal transition in $FeSi_{1-x}Ge_x$ Alloys
Europhysics Letters **95**, 47007 (2011).
Group(s): Rice, Sigrist / Project(s): 5

Group of N. de Rooij

▶ P. Janphuang, D. Isarakorn, D. Briand, and N. F. de Rooij
Energy harvesting from a rotating gear using an impact type piezoelectric MEMS scavenger
in *Proceedings of the 16th International Conference on Solid-State Sensors, Actuators and Microsystems (TRANSDUCERS'11)* (2011), p. 735.
Group(s): de Rooij / Project(s): 3

▶ A. Sambri, D. Isarakorn, A. Torres-Pardo, S. Gariglio, J. M. Triscone, P. Janphuang, D. Briand, N. F. de Rooij, O. Stephan, J. W. Reiner, and C. H. Ahn

Epi-Piezo Pb(ZrO:2TiO:8)O_3 thin film on silicon for energy harvesting devices

to be published in Smart Materials Research – Special Issue (2012).

Group(s): de Rooij, Triscone (JM) / Project(s): 3

▶ D. Isarakorn, D. Briand, A. Sambri, S. Gariglio, J.-M. Triscone, F. Guy, J. W. Reiner, C. H. Ahn, and N. F. de Rooij

Finite element analysis and experiments on a silicon membrane actuated by an epitaxial PZT thin film for localized-mass sensing applications

Sensors and Actuators B: Chemical **153**, 54 (2011).

Group(s): de Rooij, Triscone (JM) / Project(s): 3

D. Isarakorn, D. Briand, P. Janphuang, A. Sambri, S. Gariglio, J.-M. Triscone, F. Guy, J. W. Reiner, C. H. Ahn, and N. F. de Rooij

The realization and performance of vibration energy harvesting MEMS devices based on an epitaxial piezoelectric thin film

Smart Materials and Structures **20**, 025015 (2011).

Group(s): de Rooij, Triscone (JM) / Project(s): 3

Group of H. M. Rønnow

S. Fallahi, M. Mazaheri, N. Nikseresht, H. M. Rønnow, and M. Akhavan

Effect of Ca substitution on crystal structure and superconducting properties of ferromagnetic superconductor $RuSr_{2-x}Ca_xGd_{1.4}Ce_{0.6}Cu_2O_{10-\delta}$

Journal of Magnetism and Magnetic Materials **324**, 949 (2012).

Group(s): Rønnow / Project(s): 6

A. Maisuradze, Z. Guguchia, B. Graneli, H. M. Rønnow, H. Berger, and H. Keller

μSR investigation of magnetism and magnetoelectric coupling in Cu_2OSeO_3

Physical Review B **84**, 064433 (2011).

Group(s): Keller, Rønnow / Project(s): 4, 6

G. J. Nilsen, F. C. Coomer, M. A. de Vries, J. R. Stewart, P. P. Deen, A. Harrison, and H. M. Rønnow

Pair correlations, short-range order, and dispersive excitations in the quasi-kagome quantum magnet volborthite

Physical Review B **84**, 172401 (2011).

Group(s): Rønnow / Project(s): 6

▶ J. D. Thompson, P. A. McClarty, H. M. Rønnow, L. P. Regnault, A. Sorge, and M. J. P. Gingras

Rods of Neutron Scattering Intensity in $Yb_2Ti_2O_7$: Compelling Evidence for Significant Anisotropic Exchange in a Magnetic Pyrochlore Oxide

Physical Review Letters **106**, 187202 (2011).

Group(s): Rønnow / Project(s): 6

T. Fennell, J. O. Piatek, R. A. Stephenson, G. J. Nilsen, and H. M. Rønnow

Spangolite: an s = 1/2 maple leaf lattice antiferromagnet?

Journal of Physics: Condensed Matter **23**, 164201 (2011).

Group(s): Rønnow / Project(s): 6

E. A. Goremychkin, R. Osborn, C. H. Wang, M. D. Lumsden, M. A. McGuire, A. S. Sefat, B. C. Sales, D. Mandrus, H. M. Rønnow, Y. Su, and A. D. Christianson

Spatial inhomogeneity in $RFeAsO_{1-x}F_x$ (R = Pr, Nd) determined from rare-earth crystal-field excitations

Physical Review B **83**, 212505 (2011).

Group(s): Rønnow / Project(s): 6

▶ J. Schlappa, K. Wohlfeld, K. J. Zhou, M. Mourigal, M. W. Haverkort, V. N. Strocov, L. Hozoi, C. Monney, S. Nishimoto, S. Singh, A. Revcolevschi, J.-S. Caux, L. Patthey, H. M. Rønnow, J. van den Brink, and T. Schmitt

Spin-Orbital Separation in the quasi 1D Mott-insulator Sr_2CuO_3

to be published in Nature (2012).

Group(s): Rønnow, Staub / Project(s): 6

S. Nandi, Y. Su, Y. Xiao, S. Price, X. F. Wang, X. H. Chen, J. Herrero-Martín, C. Mazzoli, H. C. Walker, L. Paolasini, S. Francoual, D. K. Shukla, J. Strempfer, T. Chatterji, C. M. N. Kumar, R. Mittal, H. M. Rønnow, C. Rüegg, D. F. McMorrow, and T. Brückel

Strong coupling of Sm and Fe magnetism in SmFeAsO as revealed by magnetic x-ray scattering

Physical Review B **84**, 054419 (2011).

Group(s): Rønnow / Project(s): 6

Group of M. Sigrist

▶ T. M. Rice, K.-Y. Yang, and F. C. Zhang

A phenomenological theory of the anomalous pseudogap phase in underdoped cuprates

Reports on Progress in Physics **75**, 016502 (2012).

Group(s): Rice, Sigrist / Project(s): 4

T. Neupert and M. Sigrist
Coexistence of Ferromagnetism and Superconductivity in Noncentrosymmetric Materials with Cubic Symmetry
Journal of the Physical Society of Japan **80**, 114712 (2011).
Group(s): Sigrist / Project(s): 5

D. Müller, S. Pilgram, T. M. Rice, and M. Sigrist
Extending the Gutzwiller approximation for liquid ^{3}He by including intersite correlations
Annalen der Physik **523**, 732 (2011).
Group(s): Rice, Sigrist / Project(s): 5

Y. Yanase and M. Sigrist
Ginzburg-Landau Analysis for the Antiferromagnetic Order in the Fulde-Ferrell-Larkin-Ovchinnikov Superconductor
Journal of the Physical Society of Japan **80**, 094702 (2011).
Group(s): Sigrist / Project(s): 5

D. Maruyama, M. Sigrist, and Y. Yanase
Locally Non-centrosymmetric Superconductivity in Multilayer Systems
Journal of the Physical Society of Japan **81**, 034702 (2012).
Group(s): Sigrist / Project(s): 5

K.-Y. Yang, Y. Yamashita, A. M. Läuchli, M. Sigrist, and T. M. Rice
Microscopic model for the semiconductor-to-ferromagnetic-metal transition in $FeSi_{1-x}Ge_x$ Alloys
Europhysics Letters **95**, 47007 (2011).
Group(s): Rice, Sigrist / Project(s): 5

▶ M. H. Fischer, F. Loder, and M. Sigrist
Superconductivity and local noncentrosymmetricity in crystal lattices
Physical Review B **84**, 184533 (2011).
Group(s): Sigrist / Project(s): 5

T. Nakamura, R. Nakagawa, T. Yamagishi, T. Terashima, S. Yonezawa, M. Sigrist, and Y. Maeno
Topological competition of superconductivity in $Pb/Ru/Sr_2RuO_4$ junctions
Physical Review B **84**, 060512 (2011).
Group(s): Sigrist / Project(s): 5

Group of U. Staub

▶ J. de Groot, K. Marty, M. D. Lumsden, A. D. Christianson, S. E. Nagler, S. Adiga, W. J. H. Borghols, K. Schmalzl, Z. Yamani, S. R. Bland, R. de Souza, U. Staub, W. Schweika, Y. Su, and M. Angst
Competing Ferri- and Antiferromagnetic Phases in Geometrically Frustrated $LuFe_2O_4$
Physical Review Letters **108**, 037206 (2012).
Group(s): Staub / Project(s): 6

▶ S. L. Johnson, R. A. de Souza, U. Staub, P. Beaud, E. Möhr-Vorobeva, G. Ingold, A. Caviezel, V. Scagnoli, W. F. Schlotter, J. J. Turner, O. Krupin, W.-S. Lee, Y.-D. Chuang, L. Patthey, R. G. Moore, D. Lu, M. Yi, P. S. Kirchmann, M. Trigo, P. Denes, D. Doering, Z. Hussain, Z.-X. Shen, D. Prabhakaran, and A. T. Boothroyd
Femtosecond Dynamics of the Collinear-to-Spiral Antiferromagnetic Phase Transition in CuO
Physical Review Letters **108**, 037203 (2012).
Group(s): Staub / Project(s): 6

▶ M. Le Tacon, G. Ghiringhelli, J. Chaloupka, M. Moretti Sala, V. Hinkov, M. W. Haverkort, M. Minola, M. Bakr, K. J. Zhou, S. Blanco-Canosa, C. Monney, Y. T. Song, G. L. Sun, C. T. Lin, G. M. De Luca, M. Salluzzo, G. Khaliullin, T. Schmitt, L. Braicovitch, and B. Keimer
Intense paramagnon excitations in a large family of high-temperature superconductors
Nature Physics **7**, 725 (2011).
Group(s): Staub / Project(s): 6

K.-J. Zhou, M. Radovic, J. Schlappa, V. Strocov, R. Frison, J. Mesot, L. Patthey, and T. Schmitt
Localized and delocalized Ti 3d carriers in $LaAlO_3/SrTiO_3$ superlattices revealed by resonant inelastic x-ray scattering
Physical Review B **83**, 201402 (2011).
Group(s): Mesot, Staub / Project(s): 6

R. A. de Souza, U. Staub, V. Scagnoli, M. Garganourakis, Y. Bodenthin, S.-W. Huang, M. García-Fernández, S. Ji, S.-H. Lee, S. Park, and S.-W. Cheong
Magnetic structure and electric field effects in multiferroic YMn_2O_5
Physical Review B **84**, 104416 (2011).
Group(s): Staub / Project(s): 6

▶ E. Möhr-Vorobeva, S. L. Johnson, P. Beaud, U. Staub, R. De Souza, C. Milne, G. Ingold, J. Demsar, H. Schaefer, and A. Titov
Nonthermal Melting of a Charge Density Wave in $TiSe_2$
Physical Review Letters **107**, 036403 (2011).

Group(s): Staub / Project(s): 6

- V. Scagnoli, U. Staub, Y. Bodenthin, R. A. de Souza, M. García-Fernández, M. Garganourakis, A. T. Boothroyd, D. Prabhakaran, and S. W. Lovesey
  Observation of Orbital Currents in CuO
  Science **332**, 696 (2011).
  Group(s): Staub / Project(s): 6

R. A. de Souza, U. Staub, V. Scagnoli, M. Garganourakis, Y. Bodenthin, and H. Berger
Origin of the anomalous low-temperature phase transition in $BaVS_3$
Physical Review B **84**, 014409 (2011).
Group(s): Forró, Staub / Project(s): 6

- H. Wadati, J. Okamoto, M. Garganourakis, V. Scagnoli, U. Staub, Y. Yamasaki, H. Nakao, Y. Murakami, M. Mochizuki, M. Nakamura, M. Kawasaki, and Y. Tokura
  Origin of the Large Polarization in Multiferroic $YMnO_3$ Thin Films Revealed by Soft- and Hard-X-Ray Diffraction
  Physical Review Letters **108**, 047203 (2012).
  Group(s): Staub / Project(s): 6

- J. Schlappa, K. Wohlfeld, K. J. Zhou, M. Mourigal, M. W. Haverkort, V. N. Strocov, L. Hozoi, C. Monney, S. Nishimoto, S. Singh, A. Revcolevschi, J.-S. Caux, L. Patthey, H. M. Rønnow, J. van den Brink, and T. Schmitt
  Spin-Orbital Separation in the quasi 1D Mott-insulator Sr_2CuO_3
  to be published in Nature (2012).
  Group(s): Rønnow, Staub / Project(s): 6

A. J. Princep, A. M. Mulders, U. Staub, V. Scagnoli, T. Nakamura, A. Kikkawa, S. W. Lovesey, and E. Balcar
Triakontadipole and high-order dysprosium multipoles in the antiferromagnetic phase of DyB_2C_2
Journal of Physics: Condensed Matter **23**, 266002 (2011).
Group(s): Staub / Project(s): 6

- S. Glawion, J. Heidler, M. W. Haverkort, L. C. Duda, T. Schmitt, V. N. Strocov, C. Monney, K. J. Zhou, A. Ruff, M. Sing, and R. Claessen
  Two-Spinon and Orbital Excitations of the Spin-Peierls System TiOCl
  Physical Review Letters **107**, 107402 (2011).
  Group(s): Staub / Project(s): 6

Group of J.-M. Triscone

- C. Cancellieri, D. Fontaine, S. Gariglio, N. Reyren, A. D. Caviglia, A. Fête, S. J. Leake, S. A. Pauli, P. R. Willmott, M. Stengel, P. Ghosez, and J.-M. Triscone
  Electrostriction at the $LaAlO_3/SrTiO_3$ Interface
  Physical Review Letters **107**, 056102 (2011).
  Group(s): Triscone (JM), Willmott / Project(s): 1

- A. Sambri, D. Isarakorn, A. Torres-Pardo, S. Gariglio, J. M. Triscone, P. Janphuang, D. Briand, N. F. de Rooij, O. Stephan, J. W. Reiner, and C. H. Ahn
  Epi-Piezo Pb(ZrO:2TiO:8)O_3 thin film on silicon for energy harvesting devices
  to be published in Smart Materials Research – Special Issue (2012).
  Group(s): de Rooij, Triscone (JM) / Project(s): 3

- M. Gibert, P. Zubko, R. Scherwitzl, J. Íñiguez, and J.-M. Triscone
  Exchange bias in $LaNiO_3$–$LaMnO_3$ superlattices
  Nature Materials **11**, 195 (2012).
  Group(s): Triscone (JM) / Project(s): 1

F. Le Marrec, H. Toupet, C. Lichtensteiger, B. Dkhil, and M. G. Karkut
Ferroic phase transition sequence in epitaxial $BiFeO_3$ thin films
Phase Transitions **84**, 453 (2011).
Group(s): Triscone (JM) / Project(s): 1

- D. Isarakorn, D. Briand, A. Sambri, S. Gariglio, J.-M. Triscone, F. Guy, J. W. Reiner, C. H. Ahn, and N. F. de Rooij
  Finite element analysis and experiments on a silicon membrane actuated by an epitaxial PZT thin film for localized-mass sensing applications
  Sensors and Actuators B: Chemical **153**, 54 (2011).
  Group(s): de Rooij, Triscone (JM) / Project(s): 3

P. Zubko, S. Gariglio, M. Gabay, P. Ghosez, and J.-M. Triscone
Interface Physics in Complex Oxide Heterostructures
Annual Review of Condensed Matter Physics **2**, 141 (2011).
Group(s): Triscone (JM) / Project(s): 1

- R. Scherwitzl, S. Gariglio, M. Gabay, P. Zubko, M. Gibert, and J.-M. Triscone
  Metal-Insulator Transition in Ultrathin $LaNiO_3$ Films
  Physical Review Letters **106**, 246403 (2011).
  Group(s): Triscone (JM) / Project(s): 1

S. Gariglio and J.-M. Triscone
Oxide interface superconductivity
Comptes Rendus de Physique **12**, 591 (2011).
Group(s): Triscone (JM) / Project(s): 1

A. Torres-Pardo, A. Gloter, P. Zubko, N. Jecklin, C. Lichtensteiger, C. Colliex, J.-M. Triscone, and O. Stéphan
Spectroscopic mapping of local structural distortions in ferroelectric $PbTiO_3/SrTiO_3$ superlattices at the unit-cell scale
Physical Review B **84**, 220102 (2011).
Group(s): Triscone (JM) / Project(s): 1

S. Gariglio, J.-M. Triscone, and A. Cavigliа
Superconductivity and magnetism living apart together?
Physics **4**, 59 (2011).
Group(s): Triscone (JM) / Project(s): 1

D. Isarakorn, D. Briand, P. Janphuang, A. Sambri, S. Gariglio, J.-M. Triscone, F. Guy, J. W. Reiner, C. H. Ahn, and N. F. de Rooij
The realization and performance of vibration energy harvesting MEMS devices based on an epitaxial piezoelectric thin film
Smart Materials and Structures **20**, 025015 (2011).
Group(s): de Rooij, Triscone (JM) / Project(s): 3

Group of M. Troyer

▶ E. Gull, A. J. Millis, A. I. Lichtenstein, A. N. Rubtsov, M. Troyer, and P. Werner
Continuous-time Monte Carlo methods for quantum impurity models
Reviews of Modern Physics **83**, 349 (2011).
Group(s): Troyer / Project(s): 5, 8

K.-Y. Yang, E. Kozik, X. Wang, and M. Troyer
Diagrammatic quantum Monte Carlo solution of the two-dimensional cooperon-fermion model
Physical Review B **83**, 214516 (2011).
Group(s): Troyer / Project(s): 5

M. Hohenadler, M. Aichhorn, S. Schmidt, and L. Pollet
Dynamical critical exponent of the Jaynes-Cummings-Hubbard model
Physical Review A **84**, 041608(R) (2011).
Group(s): Blatter, Troyer / Project(s): 8

P. Anders, E. Gull, L. Pollet, M. Troyer, and P. Werner
Dynamical mean-field theory for bosons
New Journal of Physics **13**, 075013 (2011).
Group(s): Troyer / Project(s): 8

S. V. Isakov, P. Fendley, A. W. W. Ludwig, S. Trebst, and M. Troyer
Dynamics at and near conformal quantum critical points
Physical Review B **83**, 125114 (2011).
Group(s): Troyer / Project(s): 6

▶ S. Nascimbène, N. Navon, S. Pilati, F. Chevy, S. Giorgini, A. Georges, and C. Salomon
Fermi-Liquid Behavior of the Normal Phase of a Strongly Interacting Gas of Cold Atoms
Physical Review Letters **106**, 215303 (2011).
Group(s): Georges, Troyer / Project(s): 8

▶ K. Van Houcke, F. Werner, E. Kozik, N. Prokof'ev, B. Svistunov, M. J. H. Ku, A. T. Sommer, L. W. Cheuk, A. Schirotzek, and M. W. Zwierlein
Feynman diagrams versus Fermi-gas Feynman emulator
Nature Physics (2012), doi:10.1038/nphys2273.
Group(s): Troyer / Project(s): 8

M. H. Freedman, J. Gukelberger, M. B. Hastings, S. Trebst, M. Troyer, and Z. Wang
Galois conjugates of topological phases
Physical Review B **85**, 045414 (2012).
Group(s): Troyer / Project(s): 5

L. Pollet, N. V. Prokof'ev, and B. V. Svistunov
Incorporating dynamic mean-field theory into diagrammatic Monte Carlo
Physical Review B **83**, 161103 (2011).
Group(s): Troyer / Project(s): 5

E. Ardonne, J. Gukelberger, A. W. W. Ludwig, S. Trebst, and M. Troyer
Microscopic models of interacting Yang-Lee anyons
New Journal of Physics **13**, 045006 (2011).
Group(s): Troyer / Project(s): 5

B. Surer, M. Troyer, P. Werner, A. M. Läuchli, T. O. Wehling, A. Wilhelm, and A. I. Lichtenstein
Multi-orbital Kondo physics of Co in Cu hosts
Physical Review B **85**, 085114 (2011).
Group(s): Troyer / Project(s): 5

R. Ganesh, S. V. Isakov, and A. Paramekanti

Néel to dimer transition in spin-S antiferromagnets: Comparing bond operator theory with quantum Monte Carlo simulations for bilayer Heisenberg models

Physical Review B **84**, 214412 (2011).

Group(s): Troyer / Project(s): 6

▶ M. Endres, M. Cheneau, T. Fukuhara, C. Weitenberg, P. Schauss, C. Gross, L. Mazza, M. C. Bañuls, L. Pollet, I. Bloch, and S. Kuhr

Observation of Correlated Particle-Hole Pairs and String Order in Low-Dimensional Mott Insulators

Science **334**, 200 (2011).

Group(s): Troyer / Project(s): 8

M. Hohenadler, M. Aichhorn, L. Pollet, and S. Schmidt

Polariton Mott insulator with trapped ions or circuit QED

Physical Review A **85**, 013810 (2012).

Group(s): Blatter, Troyer / Project(s): 8

D. Poilblanc, A. W. W. Ludwig, S. Trebst, and M. Troyer

Quantum spin ladders of non-Abelian anyons

Physical Review B **83**, 134439 (2011).

Group(s): Troyer / Project(s): 5

▶ P. Corboz, A. M. Läuchli, K. Penc, M. Troyer, and F. Mila

Simultaneous Dimerization and SU(4) Symmetry Breaking of 4-Color Fermions on the Square Lattice

Physical Review Letters **107**, 215301 (2011).

Group(s): Mila, Troyer / Project(s): 6, 8

S. Fuchs, E. Gull, M. Troyer, M. Jarrell, and T. Pruschke

Spectral properties of the three-dimensional Hubbard model

Physical Review B **83**, 235113 (2011).

Group(s): Troyer / Project(s): 5, 8

▶ P. Corboz, S. R. White, G. Vidal, and M. Troyer

Stripes in the two-dimensional $t - J$ model with infinite projected entangled-pair states

Physical Review B **84**, 041108 (2011).

Group(s): Troyer / Project(s): 5

▶ B. Bauer, L. D. Carr, H. G. Evertz, A. Feiguin, J. Freire, S. Fuchs, L. Gamper, J. Gukelberger, E. Gull, S. Guertler, A. Hehn, R. Igarashi, S. V. Isakov, D. Koop, P. N. Ma, P. Mates, H. Matsuo, O. Parcollet, G. Pawlowski, J. D. Picon, L. Pollet, E. Santos, V. W. Scarola, U. Schollwöck, C. Silva, B. Surer, S. Todo, S. Trebst, M. Troyer, M. L. Wall, P. Werner, and S. Wessel

The ALPS project release 2.0: open source software for strongly correlated systems

Journal of Statistical Mechanics **2011**, P05001 (2011).

Group(s): Troyer / Project(s): 5, 6, 8

B. Bauer, P. Corboz, A. M. Läuchli, L. Messio, K. Penc, M. Troyer, and F. Mila

Three-sublattice order in the SU(3) Heisenberg model on the square and triangular lattice

Physical Review B **85**, 125116 (2012).

Group(s): Mila, Troyer / Project(s): 6

▶ S. V. Isakov, M. B. Hastings, and R. G. Melko

Topological entanglement entropy of a Bose-Hubbard spin liquid

Nature Physics **7**, 772 (2011).

Group(s): Troyer / Project(s): 5,6

M. H. Freedman, L. Gamper, C. Gils, S. V. Isakov, S. Trebst, and M. Troyer

Topological phases: An expedition off lattice

Annals of Physics (N.Y.) **326**, 2108 (2011).

Group(s): Troyer / Project(s): 5

J.-W. Huo, F.-C. Zhang, W. Chen, M. Troyer, and U. Schollwöck

Trapped ultracold bosons in periodically modulated lattices

Physical Review A **84**, 043608 (2011).

Group(s): Troyer / Project(s): 8

A. W. W. Ludwig, D. Poilblanc, S. Trebst, and M. Troyer

Two-dimensional quantum liquids from interacting non-Abelian anyons

New Journal of Physics **13**, 045014 (2011).

Group(s): Troyer / Project(s): 5

▶ S. V. Isakov, R. G. Melko, and M. B. Hastings

Universal Signatures of Fractionalized Quantum Critical Points

Science **335**, 193 (2012).

Group(s): Troyer / Project(s): 5, 6

Group of A. Weidenkaff

D. Moser, L. Karvonen, S. Populoh, M. Trottmann, and A. Weidenkaff

Influence of the oxygen content on thermoelectric propertiesof $Ca_{3-x}Bi_xCo_4O_{9+\delta}$ system

Solid State Sciences **13**, 2160 (2011).

Group(s): Weidenkaff / Project(s): 3

Group of Ph. Willmott

Z. Salman, M. Smadella, W. A. MacFarlane, B. D. Patterson, P. R. Willmott, K. H. Chow, M. D. Hossain, H. Saadaoui, D. Wang, and R. F. Kiefl
Depth dependence of the structural phase transition of $SrTiO_3$ studied with β-NMR and grazing incidence x-ray diffraction
Physical Review B **83**, 224112 (2011).
Group(s): Morenzoni, Willmott / Project(s): 1

▶ C. Cancellieri, D. Fontaine, S. Gariglio, N. Reyren, A. D. Caviglia, A. Fête, S. J. Leake, S. A. Pauli, P. R. Willmott, M. Stengel, P. Ghosez, and J.-M. Triscone
Electrostriction at the $LaAlO_3/SrTiO_3$ Interface
Physical Review Letters **107**, 056102 (2011).
Group(s): Triscone (JM), Willmott / Project(s): 1

▶ S. A. Pauli, S. J. Leake, B. Delley, M. Björck, C. W. Schneider, C. M. Schlepütz, D. Martoccia, S. Paetel, J. Mannhart, and P. R. Willmott
Evolution of the Interfacial Structure of $LaAlO_3$ on $SrTiO_3$
Physical Review Letters **106**, 036101 (2011).
Group(s): Willmott / Project(s): 1

Group of K. Yvon

G. Schöllhammer, P. Herzig, W. Wolf, P. Vajda, and K. Yvon
First-principles study of the solid solution of hydrogen in lanthanum
Physical Review B **84**, 094122 (2011).
Group(s): Yvon / Project(s): 3

Group of A. Zheludev

A. Zheludev and D. Hüvonen
Comment on "Transition from Bose glass to a condensate of triplons in $Tl_{1-x}K_xCuCl_3$"
Physical Review B **83**, 216401 (2011).
Group(s): Zheludev / Project(s): 6

I. A. Zaliznyak, Z. J. Xu, J. S. Wen, J. M. Tranquada, G. D. Gu, V. Solovyov, V. N. Glazkov, A. I. Zheludev, V. O. Garlea, and M. B. Stone
Continuous magnetic and structural phase transitions in $Fe_{1+y}Te$
Physical Review B **85**, 085105 (2012).
Group(s): Zheludev / Project(s): 6

▶ E. Wulf, S. Mühlbauer, T. Yankova, and A. Zheludev
Disorder instability of the magnon condensate in a frustrated spin ladder
Physical Review B **84**, 174414 (2011).
Group(s): Zheludev / Project(s): 6

▶ T. Shiroka, F. Casola, V. Glazkov, A. Zheludev, K. Prša, H.-R. Ott, and J. Mesot
Distribution of NMR Relaxations in a Random Heisenberg Chain
Physical Review Letters **106**, 137202 (2011).
Group(s): Mesot, Ott, Zheludev / Project(s): 6

▶ S. Mühlbauer, S. N. Gvasaliya, E. Pomjakushina, and A. Zheludev
Double-k phase of the Dzyaloshinskii-Moriya helimagnet $Ba_2CuGe_2O_7$
Physical Review B **84**, 180406 (2011).
Group(s): Zheludev / Project(s): 6

V. N. Glazkov, T. S. Yankova, J. Sichelschmidt, D. Hüvonen, and A. Zheludev
Electron spin resonance study of anisotropic interactions in a two-dimensional spin-gap magnet $(C_4H_{12}N_2)(Cu_2Cl_6)$
Physical Review B **85**, 054415 (2012).
Group(s): Zheludev / Project(s): 6

D. Schmidiger, S. Mühlbauer, S. N. Gvasaliya, T. Yankova, and A. Zheludev
Long-lived magnons throughout the Brillouin zone of the strong-leg spin ladder $(C_7H_{10}N)_2CuBr_4$
Physical Review B **84**, 144421 (2011).
Group(s): Zheludev / Project(s): 6

▶ B. Náfrádi, T. Keller, H. Manaka, A. Zheludev, and B. Keimer
Low-Temperature Dynamics of Magnons in a Spin-1/2 Ladder Compound
Physical Review Letters **106**, 177202 (2011).
Group(s): Zheludev / Project(s): 6

A. A. Bush, V. N. Glazkov, M. Hagiwara, T. Kashiwagi, S. Kimura, K. Omura, L. A. Prozorova, L. E. Svistov, A. M. Vasiliev, and A. Zheludev
Magnetic phase diagram of the frustrated $S = \frac{1}{2}$ chain magnet $LiCu_2O_2$
Physical Review B **85**, 054421 (2012).
Group(s): Zheludev / Project(s): 6

▶ V. N. Glazkov, G. Dhalenne, A. Revcolevschi, and A. Zheludev
Multiple spin-flop phase diagram of $BaCu_2Si_2O_7$
Journal of Physics: Condensed Matter **23**, 086003 (2011).
Group(s): Zheludev / Project(s): 6

B. C. KEITH, F. XIAO, C. P. LANDEE, M. M. TURNBULL, AND A. ZHELUDEV

Random exchange in the spin ladder Cu(quinoxaline)X_2 (X = Cl, Br)

Polyhedron **30**, 3006 (2012).

Group(s): Zheludev / Project(s): 6

9.3.2 Scientific articles in journals without peer review

Group of C. Bernhard

- D. K. Satapathy, M. A. Uribe-Laverde, I. Marozau, V. K. Malik, S. Das, T. Wagner, C. Marcelot, J. Stahn, S. Brück, A. Rühm, S. Macke, T. Tietze, E. Goering, F. A., J. H. Kim, M. Wu, E. Benckiser, B. Keimer, A. Devishvili, B. P. Toperverg, M. Merz, P. Nagel, S. Schuppler, and C. Bernhard
  Magnetic proximity effect in $YBa_2Cu_3O_7/La_{1-x}Ca_xMnO_3$ superlattices
  arXiv:1111.5772 (2011).
  Group(s): Bernhard / Project(s): 1

- V. K. Malik, I. Marozau, S. Das, B. Doggett, D. K. Satapathy, M. A. Uribe-Laverde, N. Biskup, M. Varela, C. W. Schneider, C. Marcelot, J. Stahn, and C. Bernhard
  Pulsed laser deposition growth of heteroepitaxial $YBa_2Cu_3O_7/La_{0.67}Ca_{0.33}MnO_3$ superlattices on $NdGaO_3$ and $Sr_{0.7}La_{0.3}Al_{0.65}Ta_{0.35}O_3$ substrates
  arXiv:1110.4173 (2011).
  Group(s): Bernhard / Project(s): 1

Group of G. Blatter

- A. U. Thomann, V. B. Geshkenbein, and G. Blatter
  Dynamic Aspects of Strong Pinning
  arXiv:1110.4247 (2011).
  Group(s): Blatter / Project(s): 5

Group of M. Büttiker

- J. Li, G. Fleury, and M. Büttiker
  Scattering theory of chiral Majorana fermion interferometry
  arXiv:1202.1018 (2012).
  Group(s): Büttiker / Project(s): 2

Group of T. Esslinger

- L. Tarruell, D. Greif, T. Uehlinger, G. Jotzu, and T. Esslinger
  Creating, moving and merging Dirac points with a Fermi gas in a tunable honeycomb lattice
  arXiv:1111.5020 (2011).
  Group(s): Esslinger / Project(s): 8

Group of A. Georges

- X. Deng, M. Ferrero, J. Mravlje, M. Aichhorn, and A. Georges
  Hallmark of strong electronic correlations in $LaNiO_3$: photoemission kink and broadening of fully occupied bands
  arXiv:1107.5920 (2011).
  Group(s): Georges / Project(s): 4, 5

- J. Mravlje, M. Aichhorn, and A. Georges
  Origin of the high Néel temperature in $SrTcO_3$
  arXiv:1108.1168 (2011).
  Group(s): Georges / Project(s): 4, 5

- G. Seyfarth, A.-S. Rüetschi, K. Sengupta, A. Georges, and D. Jaccard
  Heavy Fermion superconductor $CeCu_2Si_2$ under high pressure: multiprobing the valence crossover
  arXiv:1111.4873 (2011).
  Group(s): Georges, Jaccard / Project(s): 5

Group of T. Giamarchi

- E. Agoritsas, V. Lecomte, and T. Giamarchi
  Disordered elastic systems and one-dimensional interfaces
  Physica B (2012), doi:10.1016/j.physb.2012.01.017.
  Group(s): Giamarchi / Project(s): 1

  A. Tokuno, E. Demler, and T. Giamarchi
  Doublon production rate in modulated optical lattices
  arXiv:1106.1333 (2011).
  Group(s): Giamarchi / Project(s): 8

- S. E. Barnes, J.-P. Eckmann, T. Giamarchi, and V. Lecomte
  Noise and Topology in Driven Systems - and Application to Interface Dynamics
  arxiv:1105.2219 (2011).
  Group(s): Giamarchi / Project(s): 1

- D. Schmidiger, P. Bouillot, S. Mühlbauer, S. Gvasaliya, C. Kollath, T. Giamarchi, and A. Zheludev
  Spectral and thermodynamic properties of a strong-leg quantum spin ladder
  arXiv:1112.4307 (2011).
  Group(s): Giamarchi, Kollath, Zheludev / Project(s): 6

Group of V. Gritsev

V. Gritsev and A. Polkovnikov
Dynamical Quantum Hall Effect in the Parameter Space
arXiv:1109.6024 (2012).
Group(s): Gritsev / Project(s): 8

Group of D. Jaccard

▶ G. Seyfarth, A.-S. Rüetschi, K. Sengupta, A. Georges, and D. Jaccard
Heavy Fermion superconductor $CeCu_2Si_2$ under high pressure: multiprobing the valence crossover
arXiv:1111.4873 (2011).
Group(s): Georges, Jaccard / Project(s): 5

Group of C. Kollath

J.-S. Bernier, D. Poletti, P. Barmettler, G. Roux, and C. Kollath
Slow quench dynamics of Mott-insulating regions in a trapped Bose-gas
arXiv:1111.4214 (2011).
Group(s): Kollath / Project(s): 8

▶ D. Schmidiger, P. Bouillot, S. Mühlbauer, S. Gvasaliya, C. Kollath, T. Giamarchi, and A. Zheludev
Spectral and thermodynamic properties of a strong-leg quantum spin ladder
arXiv:1112.4307 (2011).
Group(s): Giamarchi, Kollath, Zheludev / Project(s): 6

Group of D. van der Marel

▶ J. Levallois, M. Tran, and A. B. Kuzmenko
Decrypting the cyclotron effect in graphite using Kerr rotation spectroscopy
arXiv:1110.2754 (2011).
Group(s): van der Marel / Project(s): 2

D. van der Marel
Superconductivity: Beware of the pseudogap
Nature Physics **7**, 10 (2011).
Group(s): van der Marel / Project(s): 4

Group of A. Morpurgo

I. Martin and A. F. Morpurgo
Majorana fermions in superconducting helical magnets
arXiv:1110.5637 (2011).
Group(s): Morpurgo / Project(s): 2

Group of C. Niedermayer

▶ D. Hüvonen, S. Zhao, M. Månsson, T. Yankova, E. Ressouche, C. Niedermayer, M. Laver, S. Gvasaliya, and A. Zheludev
Field-induced criticality in a gapped quantum magnet with bond disorder
arXiv:1201.6143 (2012).
Group(s): Niedermayer, Zheludev / Project(s): 6

Group of T. M. Rice

A. J. A. James, R. M. Konik, and T. M. Rice
Magnetic Response in the Underdoped Cuprates
arXiv:1112.2676 (2011).
Group(s): Rice, Sigrist / Project(s): 4

Group of N. de Rooij

A. V. Quintero, D. Briand, P. Janphuang, J. J. Ruan, R. Lockhart, and N. F. de Rooij
Vibration energy harvesters on plastic foil by lamination of PZT thick sheets
in *to be published in Proceedings of the 25th International Conference on Micro Electro Mechanical Systems (IEEE MEMS 2012)* (2012).
Group(s): de Rooij / Project(s): 3

Group of M. Sigrist

Y. Yanase and M. Sigrist
Antiferromagnetic Phases in the Fulde-Ferrell-Larkin-Ovchinnikov State of $CeCoIn_5$
arXiv:1104.2670 (2011).
Group(s): Sigrist / Project(s): 5

S. Youn, M. H. Fischer, S. H. Rhim, M. Sigrist, and D. F. Agterberg
Hexagonal pnictide SrPtAs: superconductivity with locally broken inversion symmetry
arXiv:1111.5058 (2011).
Group(s): Sigrist / Project(s): 5

D. Maruyama, M. Sigrist, and Y. Yanase
Superconductivity without Local Inversion Symmetry; Multi-layer Systems
arXiv:1110.6000 (2011).
Group(s): Sigrist / Project(s): 5

A. J. A. James, R. M. Konik, and T. M. Rice
Magnetic Response in the Underdoped Cuprates
arXiv:1112.2676 (2011).
Group(s): Rice, Sigrist / Project(s): 4

Group of J.-M. Triscone

P. Ghosez and J.-M. Triscone
Multiferroics: Coupling of three lattice instabilities
Nature Materials **10**, 269 (2011).
Group(s): Triscone (JM) / Project(s): 1

M. Gabay and J.-M. Triscone
Superconductors: Terahertz superconducting switch
Nature Photonics **5**, 447 (2011).
Group(s): Triscone (JM) / Project(s): 1

▶ M. L. Reinle-Schmitt, C. Cancellieri, D. Li, D. Fontaine, M. Medarde, E. Pomjakushina, C. W. Schneider, S. Gariglio, P. Ghosez, J.-M. Triscone, and P. R. Willmott
Intrinsic origin of the two-dimensional electron gas at polar oxide interfaces
arXiv:1112.3532 (2011).
Group(s): Triscone (JM), Willmott / Project(s): 1

Group of M. Troyer

D. Poilblanc, M. Troyer, E. Ardonne, and P. Bonderson
Fractionalization of itinerant anyons in one dimensional chains
arXiv:1112.5950 (2011).
Group(s): Troyer / Project(s): 5

S. V. Streltsov, E. Gull, A. O. Shorikov, M. Troyer, V. I. Anisimov, and P. Werner
Magnetic susceptibility of Ce: an LDA+DMFT study
arXiv:1106.3470 (2011).
Group(s): Troyer / Project(s): 5

S. Pilati and M. Troyer
The bosonic superfluid-insulator transition in continuous space
arXiv:1108.1408 (2011).
Group(s): Troyer / Project(s): 8

Group of A. Weidenkaff

L. Karvonen, Tomeš, and A. Weidenkaff
Thermoelectric Performance of Perovskite-type Oxide Materials
Material Matters **6**, 92 (2011).
Group(s): Weidenkaff / Project(s): 3

Group of Ph. Willmott

▶ M. L. Reinle-Schmitt, C. Cancellieri, D. Li, D. Fontaine, M. Medarde, E. Pomjakushina, C. W. Schneider, S. Gariglio, P. Ghosez, J.-M. Triscone, and P. R. Willmott
Intrinsic origin of the two-dimensional electron gas at polar oxide interfaces
arXiv:1112.3532 (2011).
Group(s): Triscone (JM), Willmott / Project(s): 1

Group of A. Zheludev

T. Yankova, D. Hüvonen, S. Mühlbauer, D. Schmidiger, E. Wulf, S. Zhao, A. Zheludev, T. Hong, V. O. Garlea, R. Custelcean, and G. Ehlers
Crystals for neutron scattering studies of quantum magnetism
arXiv:1110.6375 (2011).
Group(s): Zheludev / Project(s): 6

▶ D. Schmidiger, P. Bouillot, S. Mühlbauer, S. Gvasaliya, C. Kollath, T. Giamarchi, and A. Zheludev
Spectral and thermodynamic properties of a strong-leg quantum spin ladder
arXiv:1112.4307 (2011).
Group(s): Giamarchi, Kollath, Zheludev / Project(s): 6

▶ D. Hüvonen, S. Zhao, M. Månsson, T. Yankova, E. Ressouche, C. Niedermayer, M. Laver, S. Gvasaliya, and A. Zheludev
Field-induced criticality in a gapped quantum magnet with bond disorder
arXiv:1201.6143 (2012).
Group(s): Niedermayer, Zheludev / Project(s): 6

9.3.3 Scientific articles in anthologies

Group of R. Flükiger and C. Senatore

R. Flükiger and H. Kumakura
The MgB_2 conductor story
in *100 Years of Superconductivity*, H. Rogalla and P. Kes, eds. (Taylor and Francis, London, 2011).
Group(s): Flükiger/Senatore / Project(s): 3

Group of T. Giamarchi

L. Benfatto, C. Castellani, and T. Giamarchi
Beresinskii-Kosterlitz-Thouless transition within the sine-Gordon approach: the role of the vortex-core energy
in *to be published in Berezinskii-Kosterlitz-Thouless Transition*, J. V. José, ed. (World Scientific, 2012), arXiv:1201.2307.
Group(s): Giamarchi / Project(s): 1, 4

Group of J.-M. Triscone

J.-M. Triscone and M. Gabay
Electric Field Effect Tuning of Superconductivity
in *100 Years of Superconductivity*, H. Rogalla and P. Kes, eds. (Taylor and Francis, London, 2011).
Group(s): Triscone (JM) / Project(s): 1

C. Lichtensteiger, P. Zubko, M. Stengel, P. Aguado-Puente, J.-M. Triscone, P. Ghosez, and J. Junquera
Ferroelectricity in ultrathin-film capacitors
in *Oxide ultrathin films: science and technology*, G. Pacchioni and S. Valeri, eds. (Wiley, 2011), chap. 12.
Group(s): Triscone (JM) / Project(s): 1

9.3.4 Publications involving several groups

L. ANTOGNAZZA, M. DECROUX, M. THERASSE, AND M. ABPLANALP
Heat Propagation Velocities in Coated Conductors for Fault Current Limiter Applications.
IEEE Transactions on Applied Superconductivity **21**, 1213 (2011).
Group(s): Abplanalp, Decroux / Project(s): 3

P. J. W. MOLL, J. KANTER, R. D. MCDONALD, F. BALAKIREV, P. BLAHA, K. SCHWARZ, Z. BUKOWSKI, N. D. ZHIGADLO, S. KATRYCH, K. MATTENBERGER, J. KARPINSKI, AND B. BATLOGG
Quantum oscillations of the superconductor $LaRu_2P_2$: Comparable mass enhancement $\lambda \approx 1$ in Ru and Fe phosphides
Physical Review B **84**, 224507 (2011).
Group(s): Batlogg, Karpinski / Project(s): 4

J. ZHANG, A. BELOUSOV, J. KARPIŃSKI, B. BATLOGG, G. WICKS, AND R. SOBOLEWSKI
Time-resolved femtosecond optical characterization of multi-photon absorption in high-pressure-grown $Al_{0.86}Ga_{0.14}N$ single crystals
Journal of Applied Physics **110**, 113112 (2011).
Group(s): Batlogg, Karpinski / Project(s): 4

N. D. ZHIGADLO, S. KATRYCH, M. BENDELE, P. J. W. MOLL, M. TORTELLO, S. WEYENETH, V. Y. POMJAKUSHIN, J. KANTER, R. PUZNIAK, Z. BUKOWSKI, H. KELLER, R. S. GONNELLI, R. KHASANOV, J. KARPINSKI, AND B. BATLOGG
Interplay of composition, structure, magnetism, and superconductivity in $SmFeAs_{1-x}P_xO_{1-y}$
Physical Review B **84**, 134526 (2011).
Group(s): Batlogg, Karpinski, Keller / Project(s): 4

S. WEYENETH, P. J. W. MOLL, R. PUZNIAK, K. NINIOS, F. F. BALAKIREV, R. D. MCDONALD, H. B. CHAN, N. D. ZHIGADLO, S. KATRYCH, Z. BUKOWSKI, J. KARPINSKI, H. KELLER, B. BATLOGG, AND L. BALICAS
Rearrangement of the antiferromagnetic ordering at high magnetic fields in SmFeAsO and $SmFeAsO_{0.9}F_{0.1}$ single crystals
Physical Review B **83**, 134503 (2011).
Group(s): Batlogg, Karpinski, Keller / Project(s): 4

B. M. WOJEK, E. MORENZONI, D. G. ESHCHENKO, A. SUTER, T. PROKSCHA, H. KELLER, E. KOLLER, Ø. FISCHER, V. K. MALIK, C. BERNHARD, AND M. DÖBELI
Magnetism, superconductivity, and coupling in cuprate heterostructures probed by low-energy muon-spin rotation
Physical Review B **85**, 024505 (2012).
Group(s): Bernhard, Fischer, Keller, Morenzoni / Project(s): 1, 4

A. V. BORIS, Y. MATIKS, E. BENCKISER, A. FRANO, P. POPOVICH, V. HINKOV, P. WOCHNER, M. CASTRO-COLIN, E. DETEMPLE, V. K. MALIK, C. BERNHARD, T. PROKSCHA, A. SUTER, Z. SALMAN, E. MORENZONI, G. CRISTIANI, H.-U. HABERMEIER, AND B. KEIMER
Dimensionality Control of Electronic Phase Transitions in Nickel-Oxide Superlattices
Science **332**, 937 (2011).
Group(s): Bernhard, Morenzoni / Project(s): 1

F. J. OWENS, L. GLADCZUK, R. SZYMCZAK, P. DLUZEWSKI, A. WISNIEWSKI, H. SZYMCZAK, A. GOLNIK, C. BERNHARD, AND C. NIEDERMAYER
High temperature magnetic order in zinc sulfide doped with copper
Journal of the Physics and Chemistry of Solids **72**, 648 (2011).
Group(s): Bernhard, Niedermayer / Project(s): 1

M. HOHENADLER, M. AICHHORN, S. SCHMIDT, AND L. POLLET
Dynamical critical exponent of the Jaynes-Cummings-Hubbard model
Physical Review A **84**, 041608(R) (2011).
Group(s): Blatter, Troyer / Project(s): 8

M. HOHENADLER, M. AICHHORN, L. POLLET, AND S. SCHMIDT
Polariton Mott insulator with trapped ions or circuit QED
Physical Review A **85**, 013810 (2012).
Group(s): Blatter, Troyer / Project(s): 8

J. LI, I. MARTIN, M. BÜTTIKER, AND A. F. MORPURGO
Marginal topological properties of graphene: a comparison with topological insulators
Physica Scripta **T146**, 014021 (2012).
Group(s): Büttiker, Morpurgo / Project(s): 2

F. PFUNER, S. N. GVASALIYA, O. ZAHARKO, L. KELLER, J. MESOT, V. POMJAKUSHIN, J.-H. CHU, I. R. FISHER, AND L. DEGIORGI
Incommensurate magnetic order in $TbTe_3$
Journal of Physics: Condensed Matter **24**,

036001 (2012).
Group(s): Degiorgi, Mesot / Project(s): 7

- A. Sambri, D. Isarakorn, A. Torres-Pardo, S. Gariglio, J. M. Triscone, P. Janphuang, D. Briand, N. F. de Rooij, O. Stephan, J. W. Reiner, and C. H. Ahn
  Epi-Piezo Pb(ZrO:2TiO:8)O_3 thin film on silicon for energy harvesting devices
  to be published in Smart Materials Research – Special Issue (2012).
  Group(s): de Rooij, Triscone (JM) / Project(s): 3

- D. Isarakorn, D. Briand, A. Sambri, S. Gariglio, J.-M. Triscone, F. Guy, J. W. Reiner, C. H. Ahn, and N. F. de Rooij
  Finite element analysis and experiments on a silicon membrane actuated by an epitaxial PZT thin film for localized-mass sensing applications
  Sensors and Actuators B: Chemical **153**, 54 (2011).
  Group(s): de Rooij, Triscone (JM) / Project(s): 3

  D. Isarakorn, D. Briand, P. Janphuang, A. Sambri, S. Gariglio, J.-M. Triscone, F. Guy, J. W. Reiner, C. H. Ahn, and N. F. de Rooij
  The realization and performance of vibration energy harvesting MEMS devices based on an epitaxial piezoelectric thin film
  Smart Materials and Structures **20**, 025015 (2011).
  Group(s): de Rooij, Triscone (JM) / Project(s): 3

- A. Piriou, N. Jenkins, C. Berthod, I. Maggio-Aprile, and Ø. Fischer
  First direct observation of the Van Hove singularity in the tunneling spectra of cuprates
  Nature Communications **2**, 221 (2011).
  Group(s): Fischer, Giamarchi / Project(s): 4

  R. A. de Souza, U. Staub, V. Scagnoli, M. Garganourakis, Y. Bodenthin, and H. Berger
  Origin of the anomalous low-temperature phase transition in $BaVS_3$
  Physical Review B **84**, 014409 (2011).
  Group(s): Forró, Staub / Project(s): 6

- G. Seyfarth, A.-S. Rüetschi, K. Sengupta, A. Georges, S. Watanabe, A. Miyake, and D. Jaccard
  Multiprobe Signatures of the Valence Crossover in Heavy Fermion Superconductor $CeCu_2Si_2$ Under High Pressure
  to be published in Journal of the Physical Society of Japan (2012).
  Group(s): Georges, Jaccard / Project(s): 5

- S. Nascimbène, N. Navon, S. Pilati, F. Chevy, S. Giorgini, A. Georges, and C. Salomon
  Fermi-Liquid Behavior of the Normal Phase of a Strongly Interacting Gas of Cold Atoms
  Physical Review Letters **106**, 215303 (2011).
  Group(s): Georges, Troyer / Project(s): 8

- S. C. Furuya, P. Bouillot, C. Kollath, M. Oshikawa, and T. Giamarchi
  Electron Spin Resonance Shift in Spin Ladder Compounds
  Physical Review Letters **108**, 037204 (2012).
  Group(s): Giamarchi, Kollath / Project(s): 6

- P. Bouillot, K. Corinna, A. M. Läuchli, M. Zvonarev, B. Thielemann, C. Rüegg, E. Orignac, R. Citro, M. Horvatić, C. Berthier, M. Klanjšek, , and T. Giamarchi
  Statics and dynamics of weakly coupled antiferromagnetic spin-1/2 ladders in a magnetic field
  Physical Review B **83**, 054407 (2011).
  Group(s): Giamarchi, Kollath / Project(s): 6

- B. Sacépé, J. B. Oostinga, J. Li, A. Ubaldini, N. J. G. Couto, E. Giannini, and A. F. Morpurgo
  Gate-tuned normal and superconducting transport at the surface of a topological insulator
  Nature Communications **2**, 575 (2011).
  Group(s): Giannini, Morpurgo / Project(s): 2

  J. Teyssier, R. Viennois, E. Giannini, R. M. Eremina, A. Günther, J. Deisenhofer, M. V. Eremin, and D. van der Marel
  Optical study of phonons and electronic excitations in tetragonal Sr_2VO_4
  Physical Review B **84**, 205130 (2011).
  Group(s): Giannini, van der Marel / Project(s): 4

  Z. Guguchia, S. Bosma, S. Weyeneth, A. Shengelaya, R. Puzniak, Z. Bukowski, J. Karpinski, and H. Keller
  Anisotropic magnetic order of the Eu sublattice in single crystals of $EuFe_{2-x}Co_xAs_2$ ($x = 0, 0.2$) studied by means of magnetization and magnetic torque
  Physical Review B **84**, 144506 (2011).
  Group(s): Karpinski, Keller / Project(s): 4

  Z. Guguchia, Z. Shermadini, A. Amato, A. Maisuradze, A. Shengelaya, Z. Bukowski, H. Luetkens, R. Khasanov, J. Karpinski, and H. Keller
  Muon-spin rotation measurements of the magnetic penetration depth in the iron-based superconductor $Ba_{1-x}Rb_xFe_2As_2$
  Physical Review B **84**, 094513 (2011).

Group(s): Karpinski, Keller / Project(s): 4

Z. Guguchia, J. Roos, A. Shengelaya, S. Katrych, Z. Bukowski, S. Weyeneth, F. Murányi, S. Strässle, A. Maisuradze, J. Karpinski, and H. Keller
Strong coupling between Eu^{2+} spins and Fe_2As_2 layers in $EuFe_{1.9}Co_{0.1}As_2$ observed with NMR
Physical Review B **83**, 144516 (2011).
Group(s): Karpinski, Keller / Project(s): 4

A. Maisuradze, Z. Guguchia, B. Graneli, H. M. Rønnow, H. Berger, and H. Keller
μSR investigation of magnetism and magnetoelectric coupling in Cu_2OSeO_3
Physical Review B **84**, 064433 (2011).
Group(s): Keller, Rønnow / Project(s): 4, 6

▶ J. S. White, T. Honda, K. Kimura, T. Kimura, C. Niedermayer, O. Zaharko, A. Poole, B. Roessli, and M. Kenzelmann
Coupling of magnetic and ferroelectric hysteresis by a multicomponent magnetic structure in Mn_2GeO_4
Physical Review Letters **108**, 077204 (2012).
Group(s): Kenzelmann, Niedermayer / Project(s): 6

R. Toft-Petersen, J. Jensen, T. B. S. Jensen, N. H. Andersen, N. B. Christensen, C. Niedermayer, M. Kenzelmann, M. Skoulatos, M. D. Le, K. Lefmann, S. R. Hansen, J. Li, J. L. Zarestky, and D. Vaknin
High-field magnetic phase transitions and spin excitations in magnetoelectric $LiNiPO_4$
Physical Review B **84**, 054408 (2011).
Group(s): Kenzelmann, Niedermayer / Project(s): 4

▶ Y. Hu, M. Bator, M. Kenzelmann, T. Lippert, C. Niedermayer, C. W. Schneider, and A. Wokaun
Strain and lattice distortion in (1 1 0)-epitaxial orthorhombic $TbMnO_3$ multiferroic thin films grown by pulsed laser deposition
Applied Surface Science (2011), doi:10.1016/j.apsusc.2011.10.082.
Group(s): Kenzelmann, Niedermayer / Project(s): 1

▶ T. Shiroka, F. Casola, V. Glazkov, A. Zheludev, K. Prša, H.-R. Ott, and J. Mesot
Distribution of NMR Relaxations in a Random Heisenberg Chain
Physical Review Letters **106**, 137202 (2011).
Group(s): Mesot, Ott, Zheludev / Project(s): 6

K.-J. Zhou, M. Radovic, J. Schlappa, V. Strocov, R. Frison, J. Mesot, L. Patthey, and T. Schmitt
Localized and delocalized Ti 3d carriers in $LaAlO_3/SrTiO_3$ superlattices revealed by resonant inelastic x-ray scattering
Physical Review B **83**, 201402 (2011).
Group(s): Mesot, Staub / Project(s): 6

▶ P. Corboz, A. M. Läuchli, K. Penc, M. Troyer, and F. Mila
Simultaneous Dimerization and SU(4) Symmetry Breaking of 4-Color Fermions on the Square Lattice
Physical Review Letters **107**, 215301 (2011).
Group(s): Mila, Troyer / Project(s): 6, 8

B. Bauer, P. Corboz, A. M. Läuchli, L. Messio, K. Penc, M. Troyer, and F. Mila
Three-sublattice order in the SU(3) Heisenberg model on the square and triangular lattice
Physical Review B **85**, 125116 (2012).
Group(s): Mila, Troyer / Project(s): 6

Z. Salman, M. Smadella, W. A. MacFarlane, B. D. Patterson, P. R. Willmott, K. H. Chow, M. D. Hossain, H. Saadaoui, D. Wang, and R. F. Kiefl
Depth dependence of the structural phase transition of $SrTiO_3$ studied with β-NMR and grazing incidence x-ray diffraction
Physical Review B **83**, 224112 (2011).
Group(s): Morenzoni, Willmott / Project(s): 1

▶ J. Guyonnet, I. Gaponenko, S. Gariglio, and P. Paruch
Conduction at Domain Walls in Insulating $Pb(Zr_{0.2}Ti_{0.8})O_3$ Thin Films
Advanced Materials **23**, 5377 (2011).
Group(s): Paruch, Triscone / Project(s): 1

▶ T. M. Rice, K.-Y. Yang, and F. C. Zhang
A phenomenological theory of the anomalous pseudogap phase in underdoped cuprates
Reports on Progress in Physics **75**, 016502 (2012).
Group(s): Rice, Sigrist / Project(s): 4

D. Müller, S. Pilgram, T. M. Rice, and M. Sigrist
Extending the Gutzwiller approximation for liquid ^3He by including intersite correlations
Annalen der Physik **523**, 732 (2011).
Group(s): Rice, Sigrist / Project(s): 5

K.-Y. Yang, Y. Yamashita, A. M. Läuchli, M. Sigrist, and T. M. Rice
Microscopic model for the semiconductor-to-ferromagnetic-metal transition in $FeSi_{1-x}Ge_x$ Alloys

Europhysics Letters **95**, 47007 (2011).

Group(s): Rice, Sigrist / Project(s): 5

- J. SCHLAPPA, K. WOHLFELD, K. J. ZHOU, M. MOURIGAL, M. W. HAVERKORT, V. N. STROCOV, L. HOZOI, C. MONNEY, S. NISHIMOTO, S. SINGH, A. REVCOLEVSCHI, J.-S. CAUX, L. PATTHEY, H. M. RØNNOW, J. VAN DEN BRINK, AND T. SCHMITT

  Spin-Orbital Separation in the quasi 1D Mott-insulator Sr_2CuO_3

  to be published in Nature (2012).

Group(s): Rønnow, Staub / Project(s): 6

- C. CANCELLIERI, D. FONTAINE, S. GARIGLIO, N. REYREN, A. D. CAVIGLIA, A. FÊTE, S. J. LEAKE, S. A. PAULI, P. R. WILLMOTT, M. STENGEL, P. GHOSEZ, AND J.-M. TRISCONE

  Electrostriction at the $LaAlO_3/SrTiO_3$ Interface

  Physical Review Letters **107**, 056102 (2011).

Group(s): Triscone (JM), Willmott / Project(s): 1

11 Finance

Contents

NCCR:	**MaNEP**	Report:	**Year 11 Intermediate Report**
Director:	**Fischer Oystein**	Period:	01.07.2009 - 30.06.2013
Home Institution:	**Université de Genève - GE**	Year:	**9 - 12**
Start Date:	**01.07.2001**	Status:	**in preparation**

FNSNF SWISS NATIONAL SCIENCE FOUNDATION

Criteria:

Finance NCCR Overview

Project leader	Institution	Project title	Group leader	Start of project	Duration	Total SNSF-funding	Total other funding	Total
Management						**1'954'453**	**4'392'008**	**6'346'462**
Bagnoud Marie	Université de Genève	Office		01.07.2001	156	906'071	1'801'969	2'708'040
Decroux Michel	Université de Genève	Education / Women		01.07.2001	156	285'624	905'391	1'191'015
Bonito Aleman Adriana	Université de Genève	Knowledge and Technology Transfer		01.07.2001	156	530'152	730'261	1'260'413
Bonito Aleman Adriana	Université de Genève	Communication		01.07.2001	156	232'606	954'388	1'186'993
Reserve						**4'364'855**	**0**	**4'364'855**
		Fischer Øystein				4'364'855	0	4'364'855
Project(s) without workpackage						**6'666'344**	**69'041'576**	**75'707'920**
Fischer Øystein	Université de Genève	Balance Phase II		01.07.2009	48	128'003	22'500	150'503
Fischer Øystein	Université de Genève	Fischer Oystein, Ph3, GCC		01.07.2010	36	0	57'526	57'526
Triscone Jean-Marc	Université de Genève	Project 1 - Novel phenomena at interfaces and in superlattices		01.07.2009	48	355'940	7'012'695	7'368'636
Morpurgo Alberto	Université de Genève	Project 2 - Materials for future electronics		01.07.2009	48	248'236	7'403'681	7'651'918

Signature of NCCR Director:.....

Project leader	Institution	Project title	Group leader	Start of project	Duration	Total SNSF-funding	Total other funding	Total
Fischer Øystein	Université de Genève	Project 3 - Electronic materials for energy systems and other applications		01.07.2009	48	938'635	14'373'303	15'311'939
Van der Marel Dirk	Université de Genève	Project 4 - Electronic properties of oxide superconductors and related materials		01.07.2009	48	761'630	11'130'657	11'892'287
Sigrist Manfred	ETH Zürich	Project 5 - Novel electronic phases in strongly correlated electron systems		01.07.2009	48	379'411	5'591'095	5'970'506
Mila Frederic	EPF Lausanne	Project 6 - Magnetism and competing interactions in bulk materials		01.07.2009	48	593'878	6'813'836	7'407'714
Forro Laszlo	EPF Lausanne	Project 7 - Electronic materials with reduced dimensionality		01.07.2009	48	561'899	5'692'875	6'254'774
Giamarchi Thierry	Université de Genève	Project 8 - Cold atomic gases as novel quantum simulators for condensed matter		01.07.2009	48	386'984	5'928'114	6'315'099
Cors Jorge	Université de Genève	Economic stimulus package - Cut-and-coat process by wire-EDM		01.11.2009	36	497'432	532'928	1'030'361
Flükiger Rene	Université de Genève	Economic stimulus package - Development of MgB2 wires		01.10.2009	36	336'252	274'478	610'730
Cors Jorge	Université de Genève	Economic stimulus package - Electrochemical sensors with higher resolution		01.10.2009	36	295'804	151'192	446'996
Kenzelmann Michel	PSI	Economic stimulus package - Neutron optical devices for small samples		01.10.2009	36	278'217	247'184	525'401
Fischer Øystein	Université de Genève	Equipment Geneva		01.07.2001	144	143'997	995'394	1'139'391

Project leader	Institution	Project title	Group leader	Start of project	Duration	Total SNSF-funding	Total other funding	Total
Fischer Øystein	Université de Genève	Collaborations		01.02.2010	29	614'197	806'809	1'421'006
Fischer Øystein	Université de Genève	Techniques Know-How		01.07.2009	48	145'830	2'007'307	2'153'137
					Total:	**12'985'653**	**73'433'584**	**86'419'237**

NCCR:	**MaNEP**	Report:	**Year 11 Intermediate Report**
Director:	**Fischer Oystein**	Period:	01.07.2009 - 30.06.2013
Home Institution:	**Université de Genève - GE**	Year:	**9 - 12**
Start Date:	**01.07.2001**	Status:	**in preparation**

Criteria:

Funding sources

Funding source		Year 9	Year 10	Year 11	Year 12	Total Cash Total in Kind	% %	Reserve	Total	%
SNSF-funding	Cash	2'770'798	3'099'539	2'039'012	711'448	8'620'798	36.4	4'364'855	12'985'653	15.0
	in Kind	0	0	0	0	0	0.0			
Self-funding from Home Institution	Cash	2'883'030	3'245'903	3'064'344	5'889'072	15'082'349	63.6	0	15'082'349	17.5
	in Kind	0	0	0	0	0	0.0			
Self-funding from groups	Cash	0	0	0	0	0	0.0	0	51'050'313	59.1
	in Kind	14'302'737	14'648'455	13'299'771	8'799'350	51'050'313	87.5			
Self-funding other	Cash	0	0	0	0	0	0.0	0	2'640'708	3.1
	in Kind	849'091	951'379	769'038	71'200	2'640'708	4.5			
3rd party-funding	Cash	0	0	0	0	0	0.0	0	4'660'214	5.4
	in Kind	1'198'607	2'104'952	298'450	1'058'205	4'660'214	8.0			
Total:	Cash	**5'653'828**	**6'345'443**	**5'103'357**	**6'600'520**	**23'703'147**		**4'364'855**	**86'419'237**	**100.0**
	in Kind	**16'350'434**	**17'704'786**	**14'367'259**	**9'928'755**	**58'351'235**				

Signature of NCCR Director:.....

NCCR:	**MaNEP**	Report:	**Year 11 Intermediate Report**
Director:	**Fischer Oystein**	Period:	01.07.2009 - 30.06.2013
Home Institution:	**Université de Genève - GE**	Year:	**9 - 12**
Start Date:	**01.07.2001**	Status:	**in preparation**

Criteria:

Allocation to projects

Project leader	Project title	Relation % P.I- WP		Year 9	Year 10	Year 11	Year 12	Total SNSF Funded	Total Not SNSF Funded	Total	%
Management				**1'456'601**	**1'620'377**	**1'605'110**	**1'664'373**	**1'954'453**	**4'392'008**	**6'346'462**	**7.3**
Bagnoud Marie	Office		Cash	577'817	662'491	685'765	441'967	906'071	1'461'969	2'708'040	3.1
			in Kind	105'000	105'000	130'000	0	0	340'000		
Decroux Michel	Education / Women		Cash	170'726	233'314	163'222	418'030	285'624	699'668	1'191'015	1.4
			in Kind	50'000	80'723	75'000	0	0	205'723		
Bonito Aleman Adriana	Knowledge and Technology Transfer		Cash	280'077	222'340	340'474	361'568	530'152	674'306	1'260'413	1.5
			in Kind	43'529	12'426	0	0	0	55'954		
Bonito Aleman Adriana	Communication		Cash	194'453	298'361	210'649	442'808	232'606	913'665	1'186'993	1.4
			in Kind	35'000	5'723	0	0	0	40'723		
Reserve								**4'364'855**	**0**	**4'364'855**	**5.1**
Fischer Øystein			Cash					4'364'855	0	4'364'855	5.1
Project(s) without workpackage				**20'547'661**	**22'429'852**	**17'865'505**	**14'864'902**	**6'666'344**	**69'041'576**	**75'707'920**	**87.6**
Fischer Øystein	Balance Phase II		Cash	133'302	-5'300	0	0	128'003	0	150'503	0.2
			in Kind	7'500	7'500	7'500	0	0	22'500		
Fischer Øystein	Fischer Oystein, Ph3, GCC		Cash	0	42'526	0	0	0	42'526	57'526	0.1
			in Kind	0	7'500	7'500	0	0	15'000		

Signature of NCCR Director:.....

Project leader	Project title	Relation % P.I- WP	Year 9	Year 10	Year 11	Year 12	Total SNSF Funded	Total Not SNSF Funded	Total	%
Triscone Jean-Marc	Project 1 - Novel phenomena at	Cash	320'711	484'358	515'384	410'149	355'940	1'374'662	7'368'636	8.5
		in Kind	1'591'373	1'851'415	1'437'646	757'600	0	5'638'034		
Morpurgo Alberto	Project 2 - Materials for future electronics	Cash	142'575	68'118	72'483	607'569	248'236	642'509	7'651'918	8.9
		in Kind	1'915'756	2'166'717	1'376'000	1'302'700	0	6'761'172		
Fischer Øystein	Project 3 - Electronic materials for energy	Cash	1'179'815	938'668	1'113'785	1'012'838	938'635	3'306'471	15'311'939	17.7
		in Kind	3'141'045	3'379'057	2'391'350	2'155'380	0	11'066'832		
Van der Marel Dirk	Project 4 - Electronic properties of oxide	Cash	636'026	733'026	635'931	645'121	761'630	1'888'474	11'892'287	13.8
		in Kind	3'358'247	2'521'020	1'819'667	1'543'250	0	9'242'183		
Sigrist Manfred	Project 5 - Novel electronic phases in	Cash	258'810	211'476	180'978	30'000	379'411	301'852	5'970'506	6.9
		in Kind	1'580'600	1'357'501	1'668'542	682'600	0	5'289'243		
Mila Frederic	Project 6 - Magnetism and competing	Cash	118'775	174'670	227'133	73'300	593'878	0	7'407'714	8.6
		in Kind	1'630'207	2'247'997	2'019'232	916'400	0	6'813'836		
Forro Laszlo	Project 7 - Electronic materials with	Cash	267'851	217'694	120'606	75'000	561'899	119'252	6'254'774	7.2
		in Kind	1'268'472	1'366'950	1'145'000	1'793'200	0	5'573'622		
Giamarchi Thierry	Project 8 - Cold atomic gases as novel	Cash	286'637	333'998	105'034	204'743	386'984	543'428	6'315'099	7.3
		in Kind	1'459'353	1'587'500	1'560'208	777'625	0	5'384'687		
Cors Jorge	Economic stimulus package -	Cash	165'743	338'608	71'731	0	497'432	78'649	1'030'361	1.2
		in Kind	0	376'000	78'280	0	0	454'280		
Flükiger Rene	Economic stimulus package -	Cash	62'184	210'589	111'706	0	336'252	48'228	610'730	0.7
		in Kind	7'500	77'500	141'250	0	0	226'250		

Project leader	Project title	Relation % P.I- WP	Year 9	Year 10	Year 11	Year 12	Total SNSF Funded	Total Not SNSF Funded	Total	%
Cors Jorge	Economic stimulus package -	Cash	56'656	173'547	99'590	0	295'804	33'989	446'996	0.5
		in Kind	28'533	50'000	38'670	0	0	117'203		
Kenzelmann Michel	Economic stimulus package - Neutron	Cash	79'122	57'319	141'776	0	278'217	0	525'401	0.6
		in Kind	72'500	165'074	9'610	0	0	247'184		
Fischer Øystein	Equipment Geneva	Cash	323'238	243'653	0	550'000	143'997	972'894	1'139'391	1.3
		in Kind	7'500	7'500	7'500	0	0	22'500		
Fischer Øystein	Collaborations	Cash	36'271	366'872	211'054	0	614'197	0	1'421'006	1.6
		in Kind	40'819	319'184	446'805	0	0	806'809		
Fischer Øystein	Techniques Know-How	Cash	363'038	339'116	96'057	1'327'427	145'830	1'979'807	2'153'137	2.5
		in Kind	7'500	12'500	7'500	0	0	27'500		
Total			**22'004'262.25**	**24'050'229.00**	**19'470'615.27**	**16'529'275.00**	**12'985'653**	**73'433'584**	**86'419'237**	**100.0**

NCCR:	**MaNEP**	Report:	**Year 11 Intermediate Report**
Director:	**Fischer Oystein**	Period:	01.07.2009 - 30.06.2013
Home Institution:	**Université de Genève - GE**	Year:	**9 - 12**
Start Date:	**01.07.2001**	Status:	**in preparation**

FNSNF SWISS NATIONAL SCIENCE FOUNDATION

Criteria:

Expenditures

Project	Project leader		Gross salaries	Social charges	Equipment	Consumables	Travel	Miscellaneou	Credit	Total Cash Total in Kind	Total
Management			**4'398'667.08**	**729'863.68**	**38'709.93**	**345'093.42**	**121'404.07**	**712'723.45**	**0.00**		**6'346'461.63**
Office	Bagnoud Marie	Cash	1'673'979.18	306'705.22	102.00	95'571.40	36'850.25	254'832.28	0.00	2'368'040.33	2'708'040.33
		in Kind	315'000.00	0.00	0.00	0.00	0.00	25'000.00		340'000.00	
Education / Women	Decroux Michel	Cash	605'846.17	118'707.25	0.00	51'584.73	70'527.42	138'626.90	0.00	985'292.47	1'191'015.22
		in Kind	155'722.75	0.00	0.00	0.00	0.00	50'000.00		205'722.75	
Knowledge and Technology Transfer	Bonito Aleman Adriana	Cash	878'243.55	163'222.12	15'087.91	99'287.97	2'918.50	45'698.61	0.00	1'204'458.66	1'260'412.92
		in Kind	0.00	0.00	0.00	0.00	0.00	55'954.26		55'954.26	
Communication	Bonito Aleman Adriana	Cash	729'152.68	141'229.09	23'520.02	98'649.32	11'107.90	142'611.40	0.00	1'146'270.41	1'186'993.16
		in Kind	40'722.75	0.00	0.00	0.00	0.00	0.00		40'722.75	
Reserve											**4'364'855.49**
	Fischer Øystein	Cash									4'364'855.49
Project(s) without workpackage			**63'080'796.08**	**2'257'888.01**	**4'114'086.26**	**2'392'014.05**	**758'407.09**	**3'142'262.53**	**-37'534.13**		**75'707'919.89**
Balance Phase II	Fischer Øystein	Cash	39'230.05	7'946.55	62'505.70	62.75	17'882.50	23'577.60	-23'202.50	128'002.65	150'502.65
		in Kind	22'500.00	0.00	0.00	0.00	0.00	0.00		22'500.00	
Fischer Oystein, Ph3, GCC	Fischer Øystein	Cash	36'209.80	6'316.10	0.00	0.00	0.00	0.00	0.00	42'525.90	57'525.90
		in Kind	15'000.00	0.00	0.00	0.00	0.00	0.00		15'000.00	

Signature of NCCR Director:.....

Project	Project leader		Gross salaries	Social charges	Equipment	Consumables	Travel	Miscellaneou	Credit	Total Cash Total in Kind	Total
Project 1 - Novel phenomena at interfaces and in superlattices	Triscone Jean-Marc	Cash	1'324'082.23	254'722.10	935.80	51'374.85	50'648.23	48'838.74	0.00	1'730'601.95	7'368'635.64
		in Kind	5'260'933.69	0.00	181'500.00	95'000.00	53'600.00	47'000.00		5'638'033.69	
Project 2 - Materials for future electronics	Morpurgo Alberto	Cash	560'607.70	110'913.35	18'478.65	137'407.69	24'884.90	38'452.87	0.00	890'745.16	7'651'917.50
		in Kind	5'563'372.34	0.00	796'800.00	287'000.00	64'000.00	50'000.00		6'761'172.34	
Project 3 - Electronic materials for energy systems and other applications	Fischer Øystein	Cash	3'259'419.43	619'807.68	43'713.75	197'642.81	39'229.07	85'422.74	-129.08	4'245'106.40	15'311'938.55
		in Kind	8'640'944.10	0.00	235'150.00	243'081.25	29'196.00	1'918'460.80		11'066'832.15	
Project 4 - Electronic properties of oxide superconductors and related materials	Van der Marel Dirk	Cash	2'014'833.85	374'162.28	18'382.78	139'894.99	24'002.84	83'910.99	-5'084.15	2'650'103.58	11'892'286.56
		in Kind	8'678'426.18	0.00	118'500.00	227'890.00	82'340.80	135'026.00		9'242'182.98	
Project 5 - Novel electronic phases in strongly correlated electron systems	Sigrist Manfred	Cash	426'734.87	84'219.32	84'205.23	50'193.07	31'833.93	13'195.18	-9'118.40	681'263.20	5'970'505.85
		in Kind	5'101'262.65	0.00	87'000.00	56'420.00	44'560.00	0.00		5'289'242.65	
Project 6 - Magnetism and competing interactions in bulk materials	Mila Frederic	Cash	478'612.30	69'345.94	0.00	14'819.35	9'600.40	21'500.00	0.00	593'877.99	7'407'714.22
		in Kind	6'537'490.78	0.00	15'000.00	52'065.05	70'590.20	138'690.20		6'813'836.23	
Project 7 - Electronic materials with reduced dimensionality	Forro Laszlo	Cash	500'131.98	76'415.80	20'428.66	67'338.07	9'633.30	7'203.40	0.00	681'151.21	6'254'773.55
		in Kind	4'626'322.34	0.00	625'000.00	224'000.00	64'600.00	33'700.00		5'573'622.34	
Project 8 - Cold atomic gases as novel quantum simulators for condensed matter	Giamarchi Thierry	Cash	662'649.70	144'483.20	18'841.73	52'758.33	35'892.05	15'786.95	0.00	930'411.96	6'315'098.63
		in Kind	5'209'686.67	0.00	50'000.00	60'000.00	65'000.00	0.00		5'384'686.67	

Project	Project leader		Gross salaries	Social charges	Equipment	Consumables	Travel	Miscellaneou	Credit	Total Cash Total in Kind	Total
Economic stimulus package - Cut-and-coat process by wire-EDM	Cors Jorge	Cash	328'459.22	59'247.43	125'997.55	48'590.42	13'779.61	7.00	0.00	576'081.23	1'030'360.78
		in Kind	92'679.55	0.00	111'000.00	83'000.00	2'600.00	165'000.00		454'279.55	
Economic stimulus package - Development of MgB2 wires	Flükiger Rene	Cash	178'139.10	35'484.55	133'648.10	23'380.44	13'827.46	0.00	0.00	384'479.65	610'729.65
		in Kind	226'250.00	0.00	0.00	0.00	0.00	0.00		226'250.00	
Economic stimulus package - Neutron optical devices for small samples	Kenzelmann Michel	Cash	96'968.05	12'858.35	25'287.60	108'243.26	0.00	34'859.50	0.00	278'216.76	525'400.76
		in Kind	162'110.00	0.00	23'000.00	26'754.00	2'300.00	33'020.00		247'184.00	
Economic stimulus package - Electrochemical sensors with higher resolution	Cors Jorge	Cash	163'261.37	31'427.78	83'684.65	33'146.98	225.50	18'046.21	0.00	329'792.49	446'995.67
		in Kind	51'203.18	0.00	20'000.00	39'000.00	4'600.00	2'400.00		117'203.18	
Equipment Geneva	Fischer Øystein	Cash	0.00	0.00	1'116'890.81	0.00	0.00	0.00	0.00	1'116'890.81	1'139'390.81
		in Kind	22'500.00	0.00	0.00	0.00	0.00	0.00		22'500.00	
Collaborations	Fischer Øystein	Cash	433'677.90	70'955.60	88'782.65	20'351.65	429.00	0.00	0.00	614'196.80	1'421'005.88
		in Kind	800'983.53	0.00	5'700.00	125.55	0.00	0.00		806'809.08	
Techniques Know-How	Fischer Øystein	Cash	1'543'613.52	299'581.98	3'652.60	47'473.54	3'151.30	228'164.35	0.00	2'125'637.29	2'153'137.29
		in Kind	22'500.00	0.00	0.00	5'000.00	0.00	0.00		27'500.00	
Total			**67'479'463.16**	**2'987'751.69**	**4'152'796.19**	**2'737'107.47**	**879'811.16**	**3'854'985.98**	**-37'534.13**		**86'419'237.01**

11.5 Comments on finances

NIRA 2.0 is a highly performing instrument but continues to impose a heavy workload on our management team.

Explanations to the reserve

The "reserve" which appears in the NIRA summary is 4'364'855 CHF. This corresponds on the one hand to about 1'400'000 CHF of equipment and consumables already paid in year 11 or projected until the end of year 11, but not yet registered in NIRA. The remaining amount of about 2'900'000 CHF is to a very large extent already allocated and represents the budget for year 12. The initial budget for year 12 was planned as very low with the anticipation that there would be a delay in the expenses so that a reasonable budget for year 12 would emerge from the transfers from years 9 – 11. This is what has happened and corresponds to the above-mentioned budget.
The main elements of the budget are (this is a global budget and do not correspond to the exact allocation):

1. For the 41 groups active since the beginning of Phase III, estimated transfer of budget years 9 – 11 to year 12: **1'300'000 CHF**

   Together with the budget for year 12 this amounts on the average to about 37'000 CHF per group for one year, which is a low but reasonable amount that the groups will have no problem in using.

2. Budget allocated to the new members from the reserve; 7 new members (period January 1, 2012 – June 30, 2013): **450'000 CHF**

3. Equipment for the professor presently being appointed: **500'000 CHF**

   The attraction of a top scientist to MaNEP Geneva will be a major asset for the continued activity after the end of the NCCR MaNEP and justifies the use of MaNEP funds to that effect.

4. A new SQUID already ordered; contribution from MaNEP: **150'000 CHF**

5. Contribution to the new He-liquefactor for MaNEP Geneva: **200'000 CHF**

   The continuation of MaNEP after 2013 will depend critically on the availability of enough liquid helium. Thus the new liquefactor is essential for the maintaining the activities of MaNEP.

6. In agreement with the recommendations of the Review Panel, we have increased our effort in technology transfer by allocating for the last year approximately: **300'000 CHF**

Comment to the amounts available under management

At the beginning of Phase III we set aside relatively large amounts as reserve for education, KTT and communication, amounts taken from the *solde Phase II*. Of these we have not used the total amount set aside for education since we did receive 100'000 CHF from EPFL for this purpose. For KTT our effort will be larger than anticipated and a transfer from communication and/or education of 300'000 CHF will be necessary. For communication the amounts foreseen was planned to cover the expenses for the large SUPRA100 event in 2011. As explained in the report of last year, we were able to attract over 350'000 CHF from private sponsors. Thus we did not use the total amount transferred. The remaining funds on management will be used to cover the expenses as explained above.

12 Appendix: milestones of the MaNEP projects

The tables of milestones allow one to follow the time evolution of MaNEP scientific activities. The tables below are drawn from the situation at the end of the previous reporting period (year 10) and displays the changes for year 11.

Color code

Milestones unchanged since the Proposal	
Milestones added this year	
Milestones suppressed this year	

Project 1: Novel phenomena at interfaces and in superlattices

	Milestones	Year 9	Year 10	Year 11	Year 12
1.	**Conducting interfaces**				
	Growth and characterization of oxide interfaces ($LaAlO_3/SrTiO_3$) [*J.-M. Triscone, Willmott, Niedermayer*]				
	Study of the electronic properties of conducting oxide interface systems (transport properties) [*Jaccard, J.-M. Triscone, van der Marel*]				
	Structure of LAO/STO interface [*Willmott*]				
	Control of interface mobility at the LAO/STO interface [*J.-M. Triscone, Willmott*]				
	Fabrication of novel 2D electron gases not based on $SrTiO_3$ [*J.-M. Triscone, Willmott*]				
	Structural studies using SXRD on the SC interface between under- and overdoped LSCO [*Willmott*]				
	Optical probes of metallic interface states in oxide heterostructures [*Bernhard, van der Marel*]				

	Milestones (Project 1, continued)	Year 9	Year 10	Year 11	Year 12
	Oxygen diffusion studies in thin films [*Niedermayer*]				
	Electronic properties of ^{18}O exchanged interfaces [*Niedermayer*]				
	Resistivity and Hall effect of the LAO/STO interface in pressurized liquid [*Jaccard, J.-M. Triscone*]				
	Multi-probe investigation of the LAO/STO interface in various pressure media [*Jaccard, J.-M. Triscone*]				
	Aspects of mechanisms [*Sigrist*]				
	Aspects of non-centrosymmetricity [*Sigrist*]				
	Investigate the atomic environment at surfaces and interfaces close to the surface [*Aebi, J.-M. Triscone*]				
	PES/ARPES of oxide films and oxide interfaces [*Aebi, J.-M. Triscone*]				
	RIXS of interfaces and superlattices [*J.-M. Triscone*]				
	Spectroscopic studies (Raman, optical studies) [*Niedermayer, Bernhard*]				
	Magneto-transmission in the THz range [*van der Marel, J.-M. Triscone*]				
2.	**Coupling of instabilities at insulating interfaces**				
	Growth and characterization of oxide interfaces ($PbTiO_3/SrTiO_3$ and novel systems) [*Aebi, Paruch J.-M. Triscone*]				
	Structural studies using SXRD of improper FE lattices [*J.-M. Triscone, Willmott*]				
	XPD measurement of tetragonality in ultra-thin PTO films as a function of temperature [*Aebi, J.-M. Triscone*]				
	Investigate the atomic environment at surfaces and interfaces close to the surface [*Aebi, J.-M. Triscone*]				
	Study of the electronic properties of insulating oxide systems (dielectric, ferroelectric, multiferroic) [*Paruch, J.-M. Triscone*]				

	Milestones (Project 1, continued)	Year 9	Year 10	Year 11	Year 12
3.	**Magnetic/superconducting interfaces**				
	μSR and optical experiments on Y123/Pr123 [*Fischer, Morenzoni, Bernhard, Keller*]				
	μSR experiments in 214 superlattices (Interface superconductivity and magnetism) [*Morenzoni, Keller, Bernhard*]				
	Experiments on LSCO tri- and bilayers (study of proximity effects in UD and OD layers) [*Morenzoni, Keller, Bernhard*]				
	Spectroscopic studies (Raman, optical studies) [*Niedermayer, Bernhard*]				
	Study electronic properties at magnetic/superconducting interfaces close to the surface [*Aebi, Bernhard*]				
	Superconductivity induced changes in magnetic states of high-T_c-manganite multilayers [*Bernhard, Niedermayer*]				
	Magnetism control by electric fields [*Morenzoni, J.-M. Triscone*]				
4.	**Electronic properties of organic charge transfer interfaces**				
	Identification of new materials for charge-transfer interfaces [*Morpurgo*]				
	Magneto-transmission in the THz range [*Morpurgo, van der Marel*]				
	Low-temperature transport through metallic charge transfer interfaces [*Morpurgo*]				
5.	**Domain walls in ferroelectrics/multiferroics: a model interface system**				
	Domains with internal degrees of freedom [*Giamarchi, Paruch*]				
	Response to oscillatory fields [*Giamarchi, Paruch*]				
	AFM studies of magnetoelectric coupling in nanocomposite multiferroic materials [*Paruch*]				
	Nanoscale variable temperature studies of ferroelectric domain walls in $PbZr_{0.2}Ti_{0.8}O_3$ [*Paruch*]				

	Milestones (Project 1, continued)	Year 9	Year 10	Year 11	Year 12
	Variable temperature studies of ferroelectric domains in complex oxide systems [*Paruch, J.-M. Triscone*]				
	Nanoscale variable temperature studies of ferroelectric domain walls in $BiFeO_3$ [*Paruch*]				
	Effects of atmosphere and surface chemical modification on ferroelectric polarization [*Paruch*]				
6.	**Crystal growth of new substrates with tuned structural and physical properties**				
	Preliminary growth experiments of $SrTiO_3$ crystals with the existing equipment [*Giannini*]				
	Growth of various oxide substrates with the improved Czocharlski technique [*Giannini*]				
	Development of new substrates with tuned structural and electronic properties [*Giannini*]				

Project 2: Materials for future electronics

	Milestones	Year 9	Year 10	Year 11	Year 12
1.	**Oxide heterostructures**				
	Nano-patterned top gates on $LaAlO_3/SrTiO_3$ heterostructures [*J.-M. Triscone, Morpurgo*]				
	Electrostatically controlled Josephson junctions [*J.-M. Triscone, Morpurgo*]				
	Interplay of superconductivity and confinement in $LaAlO_3/SrTiO_3$ heterostructures [*J.-M. Triscone, Morpurgo*]				
	Nanostructures for the investigation of spin-orbit interaction [*J.-M. Triscone, Morpurgo*]				
	Atomic force microscopy writing of nanostructures at the $LaAlO_3/SrTiO_3$ interface [*Paruch, J.-M. Triscone*]				
	Atomic force microscopy reading (conducting AFM and capacitive) of nanostructures at the $LaAlO_3/SrTiO_3$ interface [*Paruch, J.-M. Triscone*]				

	Milestones (Project 2, continued)	Year 9	Year 10	Year 11	Year 12
	Transport properties of AFM written nanostructures at the $LaAlO_3/SrTiO_3$ interface at room temperature [*Paruch, J.-M. Triscone*]				
	Low temperature invesigations of AFM written nanostructures at the $LaAlO_3/SrTiO_3$ interface [*Paruch, J.-M. Triscone*]				
2.	**Carbon based materials**				
2.1	**Graphene**				
	Optimization of sample preparation and atomic scale imaging of single layer and bilayer graphene [*Renner*]				
	Implementation of combined AFM/STM imaging/spectroscopy on graphene [*Renner*]				
	Structural and spectroscopic characterisation of few-layer graphene [*Renner*]				
	Spectroscopy on doped/intercalated few-layer graphene devices [*Renner*]				
	Edge-state tunneling spectroscopy of single layer graphene [*Renner*]				
	Spin dependent tunneling spectroscopy of graphene [*Renner*]				
	Nature of transport gap in graphene nano-ribbons [*Morpurgo*]				
	Magnetoresistance of graphene nano-ribbons [*Morpurgo*]				
	Comparison of transport in few-layer graphene of different thickness [*Morpurgo*]				
	Transport through suspended graphene [*Morpurgo*]				
	Magnetotransport in high-mobility graphene [*Morpurgo*]				
	Transport through graphene on high-k dielectrics or ferroelectric substrates [*Paruch, Morpurgo, J.-M. Triscone*]				
	Gate-dependent spectroscopy of bi-layer graphene [*van der Marel*]				

	Milestones (Project 2, continued)	Year 9	Year 10	Year 11	Year 12
	Spectroscopy of few-layer graphene in different dielectric environments [*van der Marel*]				
	Magneto-optical spectroscopy of epitaxial graphene [*van der Marel*]				
	ESR on exfoliated graphene [*Forró*]				
2.2	**Carbon Nanotubes**				
	Ferroelectric field-effect modulation of carbon nanotube resistivity [*Paruch*]				
	Controlled manipulation of carbon nanotubes on ferroelectric substrates [*Paruch*]				
	Fonctionalized carbon nanotubes AFM tips for multiferroic studies [*Paruch*]				
	Non-destructive AFM measurements of polarization around carbon nanotubes [*Paruch*]				
	Mechanism of domain switching and growth using carbon nanotubes [*Paruch*]				
2.3	**Organic semiconductors**				
	New molecular materials for the study of intrinsic transport [*Morpurgo*]				
	Mechanisms of threshold voltage shift and drift [*Morpurgo*]				
	Low-temperature transport measurements [*Morpurgo*]				
	Comparison of intrinsic transport properties in different organic semiconductors [*Morpurgo*]				
	Infrared spectroscopy of organic semiconductor interfaces [*van der Marel*]				
3.	**Theory**				
	Aharonov-Bohm effect in topological insulators [*Büttiker*]				
	Edge conductance in gapped bilayer graphene [*Büttiker*]				

	Milestones (Project 2, continued)	Year 9	Year 10	Year 11	Year 12
	Topological properties of gapped bilayer graphene [*Büttiker*]				
	Shot-noise and pre-formed pairs: Analysis of shot noise [*Büttiker*]				
	Effect of electron-phonon coupling on transport through graphene nano-ribbons [*Sigrist*]				
	Ordered phases in heterostructures of correlated electrons [*Sigrist*]				
	Transport properties of heterostructures of correlated electrons [*Sigrist*]				
	Luttinger liquids with an external bath [*Giamarchi*]				
4.	**Topolgical properties of electronic materials**				
	Study of surface states in devices of 3D topological insulators [*Morpurgo, Giannini*]				
	Surface states charge dynamics of topological insulators [*van der Marel*]				
	Edge states in chiral p-wave superconductors [*Sigrist*]				

Project 3: Electronic materials for energy systems and other applications

	Milestones	Year 9	Year 10	Year 11	Year 12
1.	**Applied superconductivity**				
	Development of a new method to fabricate MgB_2 wires with higher critical current [*Flükiger/Senatore*]				
	Development of long lengths of MgB_2 wires [*Flükiger/Senatore*]				
	Investigation of relaxation in inhomogenous YBCO [*Flükiger/Senatore*]				
	Study of contact resistance between coated conductors and other superconductors [*Flükiger/Senatore, Bruker*]				

	Milestones (Project 3, continued)	Year 9	Year 10	Year 11	Year 12
	Development and calibration of an experimental setup for the measurement of thermal conductivity of coated conductors [*Decroux*]				
	Thermal conductance of interfaces in coated conductors [*Decroux*]				
	Measurement of propagation velocities on coated conductors [*Decroux*]				
2.	**Oxides for energy harvesting**				
	Optimization and full characterization of ultra-thin $SrTiO_3$ epitaxial buffer layers on silicon [*J.-M. Triscone, G. Triscone*]				
	Growth of epitaxial Pb(Zr,Ti)O_3, 50/50, with high piezoelectric coefficient on silicon with metallic oxide electrodes [*J.-M. Triscone, G. Triscone*]				
	Growth of epitaxial PMN-PT on silicon with giant piezoelectric response [*J.-M. Triscone, G. Triscone*]				
	Realization and mechanical and electrical characterization of membranes based on fully epitaxial oxide materials [*J.-M. Triscone, de Rooij*]				
	Realization of an energy harvesting demonstrator based on piezoelectric materials [*J.-M. Triscone, de Rooij*]				
	Investigation of the thermoelectric properties of the 2-DEG electron gas at the $LaAlO_3/SrTiO_3$ interface [*J.-M. Triscone*]				
	Investigation of the thermoelectric properties of $LaAlO_3/SrTiO_3$ superlattices [*J.-M. Triscone*]				
	Investigation of the thermoelectric properties of thin doped $SrTiO_3$ layers on silicon [*J.-M. Triscone, Weidenkaff*]				
	Identification of new promising thermoelectric oxides and Heusler compounds and synthesis of performing polycrystalline thermoelectric materials of a new generation [*Weidenkaff*]				
	Modeling of energy conversion based on data from the material specification [*Weidenkaff*]				

	Milestones (Project 3, continued)	Year 9	Year 10	Year 11	Year 12
	Synthesis of single crystalline materials [*Weidenkaff*]				
	Evaluation of candidate materials and decision about which to use for the p and n type legs of a ceramic and Heusler converter [*Weidenkaff*]				
	Assembling of a first generation oxide thermoelectric converter based on the news materials [*Weidenkaff*]				
	Second generation thermoelectric convertor as demonstrator [*Weidenkaff*]				
3.	**Application of artificial superlattices**				
	Investigation of the growth process of Ni/Ti layers to achieve lower roughness as well as an improved homogeneity of the layers [*Kenzelmann*]				
	Systematic characterization of various substrate materials in order to find a tool for selecting substrates experiencing the required surface quality [*Kenzelmann*]				
	Developing polishing processes to manufacture metal substrates with a very low roughness [*Kenzelmann*]				
	Improvement of polarizing supermirrors, i.e. extending the critical angle of reflection [*Kenzelmann*]				
	Development of adaptive neutron optics [*Kenzelmann*]				
4.	**Hydrogen detectors and other sensors**				
	Setup of experimental tools for conductance measurements in H_2 atmosphere [*Yvon, Fischer/Cors*]				
	Identification of hydrogen sensitive intermetallic compounds, fabrication of thin films [*Yvon, Fischer/Cors*]				
	Performance validation [*Asulab, Yvon, Fischer/Cors*]				
	Design of the resistive detector electronics layout and fabrication of first prototype devices [*Asulab, Yvon, Fischer/Cors*]				

	Milestones (Project 3, continued)	Year 9	Year 10	Year 11	Year 12
	Benchmarking against the performance of commercial devices [*Asulab, Yvon, Fischer/Cors*]				
	Fine tuning of device design [*Asulab*]				
	Fabrication of a large number of devices and testing/homologisation at sensor performance facility (NL) [*Asulab, Yvon, Fischer/Cors*]				
	Technology transfer to industrial partners [*Asulab, Yvon, Fischer/Cors*]				
	Study and optimization of cantilever surface passivation for optimal piezo-resistive effect. Functional cantilever using piezo-resistive deflection readout for AFM [*Renner*]				
	Deflection and torsion mode AFM cantilever using non-optical readout [*Renner*]				
	Development and optimization of one-step hydrothermal approaches to functionalized oxidic nanorods and nanowires for sensor applications: W/Mo-oxide nanorods and Bi-based nanooxides as major preparative targets [*Patzke*]				
	Setup of gas sensor construction [*Patzke, Phasis, Fischer/Cors*]				
	Preparative exploration of advanced ternary and higher oxide systems with sensor activity, e.g. targeted modification of Mo-oxides sensors [*Patzke, Phasis, Fischer/Cors*]				
	Fabrication of portable gas-sensors based on oxidic nanomaterials for CTI applications [*Patzke, Phasis, Fischer/Cors*]				
	Development of market-ready gas phase sensors with special emphasis on new portable devices for environmental applications and industrial process control [*Patzke, Phasis, Fischer/Cors*]				
	Proposal for a CTI project [*Patzke, Phasis, Fischer/Cors*]				
	Industrial implementation and marketing optimization of the gas sensor devices [*Patzke, Phasis, Fischer/Cors*]				

	Milestones (Project 3, continued)	Year 9	Year 10	Year 11	Year 12
5.	**New surface treatments for microcomponents**				
	Experimental investigation of compounds suitable for chemical marking on stainless steel, brass, gold and platinum [*Fischer/Cors, Phasis, Vacheron Constantin*]				
	Definition of the identification tools for reliable identification of the microscopic marks [*Fischer/Cors, Phasis, Vacheron Constantin*]				
	Design and construction of an automatic marking prototype [*Fischer/Cors, Phasis, Vacheron Constantin*]				
	Experimental validation of the ability to mark 20'000 parts/year [*Fischer/Cors, Phasis, Vacheron Constantin*]				
	Research of visually attractive surface effects using the marking technology at a macroscopic scale [*Fischer/Cors, Phasis*]				
	Selective coating of watch cases and other parts with transition metal carbides and nitrides. [*Fischer/Cors, Phasis*]				
	Implementation and measurement of tribological nanomaterial-based coatings on selected substrates [*Fischer/Cors, Phasis*]				

Project 4: Electronic properties of oxide superconductors and related materials

	Milestones	Year 9	Year 10	Year 11	Year 12
1.	**Optical conductivity, ARPES, RIXS, STM, muons, neutrons studies of cuprate superconductors**				
1.1	**What is the nature of the pseudogap?**				
	ARPES studies of SC and pseudogaps in $(La,Nd)_{2-x}Sr_xCuO_4$ [*Mesot*]				
	Muon spectroscopy and influence of isotope substitution on the gap in cuprate high-T_c [*Keller*]				
1.2	**How does the spectrum of collective spin excitations evolve from anti-ferromagnetic state to the high-T_c phase?**				
	STM studies of strongly overdoped Bi2201 [*Fischer*]				

	Milestones (Project 4, continued)	Year 9	Year 10	Year 11	Year 12
	STM studies of strongly overdoped Bi2212 and Bi2223 [*Fischer*]				
	STM studies of tunneling asymmetry in $Y_{1-x}Pr_xBa_2Cu_3O_7$ [*Fischer*]				
	Resonant inelastic soft X-ray scattering (RIXS) at the SLS [*Grioni*]				
1.3	**What is the mechanism of superconductivity pairing in the cuprates: is there a pairing glue?**				
	The interplay between superconductivity and magnetism [*Mesot*]				
	Electron-boson scattering in optical- and single particle spectral functions [*van der Marel*]				
2.	**New materials and crystal growth**				
2.1	**Iron pnictide high-T_c superconductors**				
	STM studies of iron-pnictides [*Fischer*]				
	ARPES studies of pnictides [*Mesot*]				
	Processing and crystal growth of Sb-based ternary and quaternary pnictides [*Giannini*]				
	Crystal growth of superconducting Fe-chalchogenides and related materials [*Giannini*]				
	Processing and growth of new binary pnictides with a tetrahedral structure [*Giannini*]				
	Crystal growth of $LnFeAsO$ and $A(Me)As_2Fe_2$ [*Karpinski*]				
	Substitutions in $LnFeAsO$ and $A(Me)As_2Fe_2$ [*Karpinski*]				
	Muon spectroscopy of the multiple-gap behavior in pnictide superconductors [*Morenzoni, Keller*]				
	Optical investigations of pnictides [*van der Marel*]				

	Milestones (Project 4, continued)	Year 9	Year 10	Year 11	Year 12
	Study of the coexistence and competition of antiferromagnetism and superconductivity in $Ba(Fe_{1-x}Co_x)_2As_2$ [*Niedermayer*]				
	Pressure effect studies of iron-based superconductors [*Keller, Morenzoni*]				
2.2	**Other non-cuprate high-T_c superconductors**				
	Development of hydrothermal growth technique and application to the Sr_2VO_4 system [*Giannini*]				
	Searching for new superconductors [*Karpinski*]				
	Optical investigations of Sr_2VO_4 [*van der Marel*]				
2.3	**Cuprate high-T_c superconductors**				
	Cuprates with reduced lattice parameter [*Jaccard*]				
	investigations on the 122 FeAs compounds [*Degiorgi*]				
	Interaction of localized f electrons with superconductivity [*Morenzoni*]				
	Pressure effect studies of cuprate superconductors [*Keller, Morenzoni*]				
3.	**Microscopic theories for cuprate superconductivity and novel superconductors**				
3.1	**Variational many-body wavefunctions**				
	Coexistence of hot spots and superconductivity [*Baeriswyl*]				
	Superconductivity and ferromagnetism (multilayers), superfluid density [*Baeriswyl*]				
	Superconductivity and antiferromagnetism [*Baeriswyl*]				
	Broken symmetry and long-range order [*Baeriswyl*]				

	Milestones (Project 4, continued)	Year 9	Year 10	Year 11	Year 12
3.2	**The chiral *p*-wave (spin triplet) state of Sr_2RuO_4**				
	study of the 3K phase in Sr_2RuO_4 [*Sigrist*]				
	study of Josephson effect in Sr_2RuO_4 [*Sigrist*]				
	study of Sr_2RuO_4 in magnetic field [*Sigrist*]				
	study of exotic vortices in Sr_2RuO_4 [*Sigrist*]				

Project 5: Novel electronic phases in strongly correlated electron systems

	Milestones	Year 9	Year 10	Year 11	Year 12
1.	**Unconventional superconductivity in heavy fermion metals**				
1.1	**Superconductivity and magnetism**				
	Study of influence of FFLO phase of $CeCoIn_5$ on flux lattice of fields along *c*-axis [*Kenzelmann*]				
	Symmetry of flux lattice in CeCoIn5 for fields in basal plane (in Q-phase) [*Kenzelmann*]				
	Form factor of flux lattice in $CeCoIn_5$ for fields in the basal plane [*Kenzelmann*]				
	Microscopic measurements of magnetism in superconducting phase [*Kenzelmann*]				
	Temperature dependence of the flux lattice in $CeCoIn_5$ for fields in the basal plane [*Kenzelmann*]				
	Theoretical discussion of Q-phase of CeCoIn5 [*Sigrist*]				
	Investigation of $CeRhIn_5$ [*Jaccard, Morenzoni*]				
1.2	**Superconductivity and valence fluctuations**				
	Hall and Nernst effect in $CeCu_2Si_2$ [*Jaccard*]				
	Investigation of $CeNi_2Ge_2$ [*Jaccard*]				

	Milestones (Project 5, continued)	Year 9	Year 10	Year 11	Year 12
1.3	**Non-centrosymmetric superconductors**				
	Phenomenology and microscopic theory [*Sigrist*]				
	Processing of polycrystal and crystal growth of $CeCo(Ge,Si)_3$ [*Giannini*]				
1.4	**Vortex matter in superconductors**				
	Study of pinning-depinning transition [*Blatter*]				
	Geometric barriers in superconductors with complex shape [*Blatter*]				
2.	**Novel quantum phases and phase transitions in $4f$- and $5f$-electron systems**				
	NMR under pressure and at low temperatures on Ce intermetallics [*Ott*]				
	Optical studies of (Eu,Ba)Si [*Degiorgi*]				
	Optical studies on the hidden phase of URu_2Si_2 [*van der Marel*]				
3.	**Magnetic, optical and transport properties in TM Si/Ge and Bi**				
	Optical studies of Co-doped $FeSb_2$ [*Degiorgi*]				
	Growth of $3d$- and $4d$-TM silicides [*Giannini*]				
	High-pressure synthesis of TM germanides [*Giannini*]				
	Optical and transport studies of TM silicides [*van der Marel*]				
	Optical studies of TM germanides [*van der Marel*]				
	Theoretical discussion of transition metal silicides/germanides [*Sigrist*]				
	Sb-tuning in Bi_2Se_3 crystals and related materials [*Giannini*]				
	Optical studies of topological band-edge insulators [*van der Marel*]				

	Milestones (Project 5, continued)	Year 9	Year 10	Year 11	Year 12
4.	**Theoretical and computational developments for strongly correlated electrons**				
	Characterization of crossover phenomena [*Baeriswyl*]				
	Competition between (positional) disorder and (electron-electron) interaction [*Gritsev*]				
	Development of new QMC algorithms [*Troyer*]				

Project 6: Magnetism and competing interactions in bulk materials

	Milestones	Year 9	Year 10	Year 11	Year 12
1.	**Spin chains and ladders**				
	Excitations experimental [*Rønnow, Mesot, Ott, Zheludev, Rüegg*]				
	NMR/NQR on low-dimensional systems [*Mesot, Ott*]				
	Theoretical [*Giamarchi, Troyer, Mila, Kollath*]				
	Quenched disorder [*Zheludev, Ott, Rüegg*]				
	μSR [*Morenzoni, Zheludev*]				
	1D spin chains ($KTi(SO_4)H_2O$, NaV_2O_4) [*Degiorgi, Rønnow*]				
2.	**Spin-dimer physics**				
	Exotic phases in Shastry-Sutherland model [*Mila, Troyer*]				
	High-pressure studies of $SrCu_2(BO_3)_2$ [*Rønnow, Rüegg*]				
	Frustration effects in Han Purple [*Mila, Rønnow, Rüegg*]				
3.	**Spin-liquids**				
	Quadrupolar order in $NiGaS_4$ [*Mila*]				

	Milestones (Project 6, continued)	Year 9	Year 10	Year 11	Year 12
	Kagome spin-1/2 theory [*Mila*]				
	Kagome spin-1/2 experimental realizations [*Rønnow*]				
4.	**Multiferroics and helimagnets**				
	Resonant X-ray diffraction [*Staub*]				
	Magnetic structures in multiferroic and magneto-electric model materials [*Kenzelmann, Staub, Zheludev*]				
	Topological phases in helimagnets [*Zheludev*]				
	Microscopic studies of magneto-electric materials [*Forró, Keller*]				
5.	**Magneto-resistive materials**				
	STM on perovskite manganites [*Fischer*]				
	Spin-polarized STM on bi-layer manganites [*Renner*]				
6.	**Resonant inelastic X-ray scattering**				
	Theory of light scattering in frustrated magnets [*Mila*]				
	Experiments on collective excitations [*Rønnow, Schmitt*]				

Project 7: Electronic materials with reduced dimensionality

	Milestones	Year 9	Year 10	Year 11	Year 12
1.	**Investigation of the electronic properties of $TiSe_2$ and related dichalcogenides**				
	T dependence of ARPES in $TiSe_2$ [*Aebi*]				
	ARPES study of intercalated $TiSe_2$ [*Aebi*]				
	STM on copper intercalated $TiSe_2$ [*Renner*]				

	Milestones (Project 7, continued)	Year 9	Year 10	Year 11	Year 12
	High pressure study of $TiSe_2$ and related compounds [*Forró*]				
	High pressure study of $Co_{1/3}NbS_2$ [*Forró, Rønnow*]				
2.	**Spectroscopic and structural investigation of RTe_3**				
	Optical spectroscopy of RTe_3 [*Degiorgi*]				
	X-ray and neutron scattering measurements of rare-earth tritellurides [*Rønnow*]				
3.	**ESR, ARPES and transport study of organic charge transfer salts**				
	ESR and transport study of ET-based salts [*Forró, Grioni*]				
4.	**Study of quasi-1D vanadates**				
	ARPES and RIXS of $BaVS_3$ [*Grioni*]				
	Magnetic measurements of $BaVS_3$ [*Forró, Ott*]				
5.	**Study of other low-dimensional materials**				
	ESR study of quasi 1-D organic conductors [*Forró, Giamarchi*]				
	Transport and STM study of Chevrel phases [*Fischer*]				
	Spin and charge degrees of freedom in $Sr_{14}Cu_{24}O_{41}$ [*Rønnow, Mila, Giannini, Degiorgi, Conder*]				

Project 8: Cold atomic gases as novel quantum simulators for condensed matter

	Milestones	Year 9	Year 10	Year 11	Year 12
1.	**Model Systems and novel phases**				
	Strongly correlated quantum states of cold atoms and light [*Gritsev*]				

	Milestones (Project 8, continued)	Year 9	Year 10	Year 11	Year 12
	Phase diagram of two-dimensional dipolar gases on a square- lattice substrate potential [*Blatter*]				
	Observation of anti-ferromagnetic order in an optical lattice [*Esslinger*]				
	Quantitative comparison between experiment and theory on spin ordering [*Esslinger*]				
	Study of the two-dimensional Hubbard model in the low entropy regime [*Esslinger*]				
	Numerical simulations of cold atomic systems [*Troyer, Kollath*]				
	Equation of state of 3D Fermi gases [*Troyer*]				
	Equation of state of 2D Fermi gases [*Troyer*]				
	Density functional theory for cold gases [*Troyer*]				
	Mott transition and antiferromagnetism in cold atomic gases [*Giamarchi*]				
	Bose mixture [*Giamarchi, Kollath*]				
	Multi-flavor cold atoms in optical lattices [*Mila*]				
2.	**Probe and Thermometry**				
	Validation of cold atomic systems [*Troyer, Esslinger*]				
	Spectroscopy [*Giamarchi*]				
3.	**Dynamics and novel Phases**				
	Nonequilibrium dynamics [*Gritsev*]				
	Dynamics and strong correlation of condensates for precision measurements [*Gritsev*]				

	Milestones (Project 8, continued)	Year 9	Year 10	Year 11	Year 12
	Quantum phase transition and non-equilibrium dynamics of polaritons in an array of coupled QED cavities [*Blatter*]				
	Non-equilibrium physics in the Mott-insulating phase [*Esslinger*]				
	Disordered Bosonic and Fermionic systems [*Giamarchi*]				